UNIVERSITY OF KWAZULU-NATAL

CORRELATION OF RAIN DROPSIZE DISTRIBUTION WITH RAIN RATE DERIVED FROM DISDROMETERS AND RAIN GAUGE NETWORKS IN SOUTHERN AFRICA

AKINTUNDE A. ALONGE

December 2011

CORRELATION OF RAIN DROPSIZE DISTRIBUTION WITH RAIN RATE DERIVED FROM DISDROMETERS AND RAIN GAUGE NETWORKS IN SOUTHERN AFRICA

AKINTUNDE AYODEJI ALONGE

In fulfillment of the degree of Master of Science in Engineering in the School of Electrical, Electronics and Computer Engineering from the University of KwaZulu-Natal, Durban, South Africa

DECEMBER 2011

Supervisor:

Professor Thomas J. Afullo

As the candidate's Supervisor, I agree/do not agree to the submission of this dissertation

Professor T.J. Afullo _____

Date _____

Declaration

I, ..., with Student Number ..... , with the dissertation entitled **Correlation of Rain Drop-size Distribution with Rain Rate Derived from Disdrometers and Rain Gauge Networks in Southern Africa** hereby declare that:

(i) The research reported in this dissertation, except where otherwise indicated, is my original work.

(ii) This dissertation has not been submitted for any degree or examination at any other university.

(iii) This dissertation does not contain other persons' data, pictures, graphs or other information, unless specifically acknowledged as being sourced from other persons.

(iv) This dissertation does not contain other persons' writing, unless specifically acknowledged as being sourced from other researchers. Where other written sources have been quoted, then:

a) their words have been re-written but the general information attributed to them has been referenced;

b) where their exact words have been used, their writing has been placed inside quotation marks, and referenced.

(v) Where I have reproduced a publication of which I am an author, co-author or editor, I have indicated in detail which part of the publication was actually written by myself alone and have fully referenced such publications.

(vi) This dissertation does not contain text, graphics or tables copied and pasted from the Internet, unless specifically acknowledged, and the source being detailed in the dissertation and in the References sections.

Name: _____

Signed: _____

Date: _____

Acknowledgements

My deepest and sincere appreciation goes to my supervisor, Professor Thomas J. Afullo for His time, patience, understanding and the provision of available resources to undertake this research.

My gratitude also goes to the Head of School of Electrical, Electronics and Computer Engineering, University of KwaZulu-Natal, Durban and other members of staff who have contributed in no small measure to this success of this research.

To my postgraduate colleagues and friends, Mr. Ilesanmi Oluwafemi, Mr. Stephen Chabalala, Mr. Gbolahan Aiyetoro, Mr. Peter Akuon , Mr. Mike Asiyo, Miss Nomfanelo Dlamini and Mr. Chrispin Mulangu, I say thank you all. I specially acknowledge the efforts of Dr. Pius Owolawi for his contributions at several stages of this work.

Special thank goes to my parents, Mr. and Mrs. Olufemi Alonge, for their unrelenting moral and financial support throughout this programme; many special thanks to my siblings too.

Finally, I give all glory and honour to Almighty God for His infinite grace and strength I acquired to complete this work.

Abstract

Natural phenomena such as rainfall are responsible for communication service disruption, leading to severe outages and bandwidth inefficiency in both terrestrial and satellite systems, especially above 10 GHz. Rainfall attenuation is a source of concern to radio engineers in link budgeting and is primarily related to the rainfall mechanism of absorption and scattering of millimetric signal energy. Therefore, the study of rainfall microstructure can serve as a veritable means of optimizing network parameters for the design and deployment of millimetric and microwave links. Rainfall rate and rainfall drop-size are two microstructural parameters essential for the appropriate estimation of local rainfall attenuation. There are several existing analytical and empirical models for the prediction of rainfall attenuation and their performances largely depend on regional and climatic characteristics of interest. In this study, the thrust is to establish the most appropriate models in South African areas for rainfall rate and rainfall drop-size.

Statistical analysis is derived from disdrometer measurements sampled at one-minute interval over a period of two years in Durban, a subtropical site in South Africa. The measurements are further categorized according to temporal rainfall regimes: drizzle, widespread, shower and thunderstorm. The analysis is modified to develop statistical and empirical models for rainfall rate using gamma, lognormal, Moupfouma and other ITU-R compliant models for the control site.

Additionally, rain drop-size distribution (DSD) parameters are developed from the modified gamma, lognormal, negative exponential and Weibull models. The spherical droplet assumption is used to estimate the scattering parameters for frequencies between 2 GHz and 1000 GHz using the disdrometer diameter ranges. The resulting proposed DSD models are used, alongside the scattering parameters, for the prediction and estimation of rainfall attenuation.

Finally, the study employs correlation and regression techniques to extend the results to other locations in South Africa. The cumulative density function analysis of rainfall parameters is applied for the selected locations to obtain their equivalent models for rainfall rate and rainfall DSD required for the estimation of rainfall attenuation.

TABLE OF CONTENT

Chapter Three

Rainfall Rate Modelling and Analysis

LIST OF FIGURES

LIST OF TABLES

LIST OF ABBREVIATIONS

CDF Cumulative Distribution Function

CHI Chi Square Error

DSD Drop-Size Distribution

ECS Extinction Cross Section

GM Gamma model

ITU-R International Telecommunications Union-Radiocommunication sector

LGN Lognormal model

LOS Line Of Sight

LWC Liquid Water Content

MGM Modified gamma model

MM Method of Moments

MML Method of Maximum Likelihood

MPN Marshall-Palmer negative exponential model

PDF Probability Distribution Function

QoS Quality of Service

RF Radio Frequency

RMS Root Mean Square

SAWS South African Weather Service

WBL Weibull model

CHAPTER ONE

General Introduction

1.1 Introduction

Communication is one of the most progressive and dynamic aspects of human life. It encompasses the act of sharing certain aspects of human life which entails thoughts, ideas, emotions and of course, information. Information is perhaps the only factor distinguishable in every sphere of human life that summarizes these aspects in form of communication. Therefore, communication is a viable medium for the transference of information from one point to another. In transferring information, methods and systems have emerged throughout the history of man, some of which have served its purposes and have invariably outlived its usefulness due to progressing technologies. In other words, communication systems have emerged and evolved over time.

Today, one of the most important features of an ideal communication system is its ability to deliver information from one point to another with correctness and precision. The real life situation, is however different, because our environment itself is modelled with many parametric variables some of which are random and dynamic. Therefore, no ideal communication system exists in the actual sense.

While modern communication systems have evolved over time, the basic principles of signal propagation remain the same. Signal propagation in modern communication systems can be achieved in two ways: guided and unguided communication systems. In a typical setting, a communication system is made up of three basic components: the sender (transmitter), the medium (channel) and the receiver. In a guided system, the channel or medium component is usually a modelled waveguide or cable whose properties depend on the characteristics of the medium itself. The performance of the system is exponentially dependent on the attenuation constant and distance of propagation [*Pozar*, 1998]. Therefore, the noisy or attenuating part of the information or signal depends on the distance and the structural properties of the guided medium. Interestingly, in an unguided system, the channel or medium is completely dependent on the characteristics of the atmosphere [*Crane*, 1996; *Crane*, 2003]. Atmospheric parameters such as temperature, humidity, pressure and of course, gaseous concentrations play a huge role in ensuring that the medium is stochastic and therefore, probabilistic. The inverse-square law, however, holds true in propagation

theories that affect unguided media i.e. the received signal continually deteriorates proportionally to the inverse of the square of the distance. Invariably, in comparing the two types of medium, the unguided medium provides a preferable method of propagation in the absence of the atmospheric effects responsible for variable path losses [*Pozar*, 1998].

Previously, traditional communication systems rarely needed large bandwidth to perform basic services like telegraphy, telephony and facsimile services. They were mostly developed based on moderate Public Switched Telephone Network (PSTN) architectures. Provision of wireless network services at higher frequency spectra, particularly for metropolitan area networks (MAN) and wide area networks (WAN), require acceptable quality-of-service (QoS) indices irrespective of the prevailing natural phenomena**.** More recently, high-speed and bandwidth driven communication services are increasingly constituting a huge demand on already constrained network capacities of service providers. The result of which has lead to continuous transition from lower order frequency spectra (smaller bandwidths) to higher order frequency spectra (larger bandwidth). The rapid development and successes recorded in advanced computing are believed to have changed the scope of services offered by communication networks with more emphasis on data-centric services, trailed behind by video and multimedia services. This development led to bandwidth "hungry" systems and consequently, huge demands of RF and microwave frequencies. However, this came as a challenge to wireless and unguided systems where the channel and propagation efficiencies largely depend on atmospheric effects and climatic factors.

The useful bandwidths needed to achieve these downstream services include the very high frequency (VHF) and ultra high frequency (UHF) bands, microwave bands and millimeter wave bands all of which vary from a range of 30 MHz to about 1000 GHz. However, atmospheric effects that lead to signal degradation and distortion affect these bands. The atmospheric effects mainly consists of condensates in form of hydrometeors i.e. rain, snow, fog, and hail. Dust particles are also prominent in regions such as deserts. Hydrometeors are capable of affecting signal reliability through phenomena such as scintillations and rain fading (either long or short). Rain fading is responsible for signal attenuation and outages in most microwave and satellite links, which uses S, C, Ku, K and Ka bands [*Crane*, 1996; *Crane*, 2003]. Millimetric bands are much more susceptible to rain fading and can result in long duration of outages, which can lead to total signal degradation.

The extent to which rain fading, rain attenuation, signal depolarization and other forms of hydrometeor phenomena affect signal propagation can be investigated empirically or physically

[*Rogers et al.*, 1997; *Ojo et al.*, 2008]. The empirical method is usually ideal because all the necessary parameters have been derived, accounted for and are readily available. In using the empirical method, meteorological data is collected and statistically analyzed to set model parameters that can be reused [*Crane*, 2003; *Emiliani et al.*, 2009]. The physical method involves real life experimentation with the motive of generating parameters from observed readings, which encourage the use of equipment for testing and taking measurements during experimental observations.

The importance of hydrometeors in signal impairment evaluation requires the development of radiometeorological relationships and parameters. However, because of the variability of the atmosphere, atmospheric measurements involving rainfall rate and rainfall drop-size have been found to be useful in the modelling and prediction of rain attenuation, attenuation distribution and other parameters. Extensive research have been carried out on the determination and prediction of rain attenuation due to rainfall rate distribution and rainfall drop size distribution (DSD) over the years [*Rogers et al.*, 1997; *Maitra*, 2004; *Fashuyi et al.*, 2006; *Ojo et al.*, 2008]. However, there is still lack of available working knowledge and data in establishing the correlation between the two parameters for different climatic zones as well as localized regions. The correlation can also provide parameteric and geographic statistics for the accurate prediction of rainfall attenuation. This dissertation is geared towards developing appropriate models, which consider the influence of both the rainfall rate and the rainfall DSD on microwave signal propagation as proposed by the pioneer work of *Olsen et. al.* [1978], *Crane* [1980], *Ajayi and Ofoche* [1983], *Moupfouma* [1984; 1987; 1993]. More recently, we have the research works of *Maitra* [2004], *Fashuyi et al.* [2006], *Odedina and Afullo* [2008; 2009a; 2010], *Owolawi et al.* [2008], *Mulangu and Afullo* [2009], *Owolawi* [2011a; 2011b], *Afullo* [2011]. The South African area is being proposed as the focal point of this research work. This research is expected to propose a new level of understanding of radiometeorological parameters and its effect on signal propagation at South African locations.

1.2 Motivation

The presence of hydrometeors in signal propagation has been identified as a universal problem encountered by microwave and millimetric links in networks. With increasing demand for high-speed data and multimedia services in Africa, most especially in South Africa, there is a need to adequately provide optimized wireless services. Optimized services need be ensured irrespective of hostile atmospheric conditions such as rainfall. Rainfall, a form of hydrometeor has been identified

as a major setback in signal propagation; it can intermittently or even abruptly disrupt transmission links during a downpour, resulting in fading and attenuation to wireless communication systems.

Meanwhile, studies involving rainfall parameters in South Africa and its surrounding region have mainly been approached using rainfall rate statistics [*Fashuyi et. al.*, 2006; *Odedina and Afullo*, 2008; *Owolawi et al.,* 2008; *Owolawi and Afullo*, 2008; *Odedina and Afullo*, 2009a]. Rainfall rate is only one of the microstructural properties of rainfall. Rainfall drop-size distribution (DSD) is another parameter important in studies involving rainfall attenuation estimation and prediction. However, appreciable measurement from rainfall DSD in South Africa is scarce and rare.

Interestingly, the statistics of rainfall DSD of a region, if available, can broaden the knowledge of rainfall attenuation and prediction. The combination of independent rainfall DSD and rainfall rate statistics can benefit long-term research knowledge in satellite and microwave studies in the Southern African region. ITU-R recommendations related to precipitation [*ITU-R P.838-3*, 2005; *ITU-R P.837-5*, 2008; *ITU-R P.530-13*, 2009; *ITU-R P.618-10*, 2009] have equally proved very useful in these studies. However, It has been acknowledged by researchers that these models sometime fail to estimate the exact localized rainfall pattern in some regions as witnessed in the reclassification of ITU-R climatic zones in South Africa by *Fashuyi et al.* in 2006.

Globally, several rainfall rate and rain DSD models have been developed, as a solution to solving the inherent localized problems, which are intrinsic and distinct to rainfall and radio-meteorological features of that region. In some tropical countries in Africa and Latin America, the modified Moupfouma model has been adapted as the standard. However, for the Southern African region, approximate models for both rain rate and rain DSD are almost non-existent. The non-existence of approximate models for the analysis of rainfall rate and rain DSD has raised some problems concerning the spatial and distinct relationship between the two variables. Establishing suitable models for the two microstructural properties of rainfall can assist in ascertaining:

(i) The type of existing relationship(s) in South African regions, between rainfall rate and rain DSD.

(ii) The importance of this relationship to fading and link outages in microwave and satellite communication within this region.

1.3 Objectives of Research

The objectives of this research are to:

(1) Determine the rainfall rate distribution in Durban using measurements from the RD-80 Joss-Waldvogel disdrometer.

(2) Determine the monthly, seasonal, and annual DSD in Durban using data from the RD-80 Joss-Waldvogel impact disdrometer.

(3) Determine the correlation between rainfall drop-size and rainfall rate distributions, while establishing a basis for regional correlation.

(4) Utilize both distributions to predict the LOS rain attenuation over a Ka-band millimetric path.

1.4 Dissertation Overview

Chapter one presents the introduction to the research work being undertaken. The sections in this chapter are: motivation for research, objectives of research, the thesis overview, original contributions from research and the description of research publications.

Chapter two gives a description of the research background with emphasis on the physics of rainfall microstructures. The discussions are mainly focused on the mechanics of rainfall rate and rainfall drop-size, as well as, research progress so far. A brief discussion is also undertaken on the progress of rainfall campaigns in the region of interest.

Chapter three investigates the rainfall rate distribution models for the city of Durban in South Africa. Comparisons are made among existing empirical and statistical rainfall rate models using their probability distribution statistics.

Chapter four discusses the subject of rainfall drop-size distribution modelling. In this chapter, empirical rainfall DSD models are developed for Durban using known statistical models. This is achieved by applying a point estimation technique from two-year point rainfall data in Durban using one minute sampled data. Different rainfall DSD models are obtained using four distinct rainfall classifications. The rainfall classification is applied to determine the performances of the proposed models at the prescribed percentage of time rainfall is exceeded. In addition, the avenue for determining the best model(s) is explored by comparing the different performances of the proposed models.

In Chapter five, the study on rainfall attenuation in Durban is approached using results from the previous chapter. Rainfall attenuation is dependent on the availability of the extinction cross section and rainfall DSD. Therefore, a scattering technique is applied based on the prevailing climatic conditions in Durban from which new power-law models are proposed for frequencies up to 1 THz. The scattering parameters developed, are used alongside the empirical rainfall DSD models, to predict rainfall attenuation in Durban. The related rainfall classification earlier proposed is investigated to understand the dynamics of rainfall attenuation in Durban. An attempt is also made in this chapter, to compare the empirical results with the microwave link measurements, undertaken in Durban at 19.5 GHz.

Chapter six gives a detailed approach to utilizing statistical tools in the correlation and determination of microwave properties between rainfall parameters and other South African areas. In this chapter, the rainfall microstructural parameters are completely described by their point distribution functions using one-minute rainfall rate conversion, and, the definition is used to describe prevailing conditions elsewhere. The parameters of rainfall rate and rain drop-size are adequately discussed in this chapter with respect to their effects on microwave communication at selected locations in South Africa.

Chapter seven is mainly concerned with the general summary obtained from the research and conclusions are drawn from the results. The future related works are also discussed in this chapter.

1.5 Original Contributions

- Development of four distinct rainfall DSD models, for rainfall rates up to 120 mm/h, for the city of Durban. The proposed empirical models are based on the monthly, seasonal, regime and annual analysis of rainfall conditions in Durban. The investigations arising from these proposed models reveal that DSD peaks do not depend only on high values of rainfall rate exceedence probability at 1% (or $R_{0.01}$), but also on the water volume present in the collection of rainfall events.

- Development of power-law models for the extinction cross section in Durban for microwave and millimeter frequency ranges between 2 GHz and 1000 GHz at 20^{o}C ambient temperature. The spherical droplet assumption was adopted for the proposed models with droplet diameter unit scale of the order of 10^{-3} m. The proposed models are

used for the estimation of the rainfall attenuation for distinct rainfall classification. Results from the predicted specific attenuation show that the contributions from rainfall water volume, rather than the higher values of $R_{0.01}$, play a greater role in the monthly, seasonal and regime variation of rainfall attenuation in Durban.

- A proposition for the formulation of empirical distribution functions for seven other locations in South Africa for rainfall DSD. The concept of this method is derived from point rainfall measurements in Durban and can be extended to derive distribution functions required for the prediction of rainfall attenuation for other locations in South Africa and other parts of the world.

1.6 Publications in Journals and Conference Proceedings

1. **A.A. Alonge** and T.J. Afullo, "Estimation of Parameters for Lognormal Rainfall DSD Model for Various Rainfall Types in Durban," *Presented at the Southern African Telecommunications Networks Conference (SATNAC)*, East London, South Africa; ISBN: 978-0-620-50893-3, September 4-7, 2011.
2. **A.A. Alonge** and T.J. Afullo, "Rainfall Rate Modeling for Various Rainfall Types in South Africa," *Presented at the AFRICON IEEE conference*, Livingstone, Zambia; ISBN: 978-1-61284-991-1, September 12-15, 2011.
3. **A.A. Alonge** and T.J. Afullo, "Rainfall Drop-Size Estimators for Weibull Probability distribution using Method of Moments Technique," *Submitted to the African Research Journal, Quarterly Publication of the South African Institute of Electrical Engineers*. [Accepted].
4. **A.A. Alonge** and T.J. Afullo, "Regime Analysis of Rainfall Drop-Size Distribution Models for Microwave Terrestrial Networks," *Submitted to the Journal of the Institution of Electrical Technology*; London, United Kingdom.[Accepted].
5. **A.A. Alonge** and T.J. Afullo, "A Semi-Empirical Comparison of Rainfall Attenuation in Durban at 19.5 GHz," submitted as a conference paper to the Radio Africa Conference, National University of Rwanda. [Conference paper under review].
6. **A.A. Alonge** and T.J. Afullo, "Seasonal Analysis and Prediction of Rainfall Effects in Eastern South Africa at Microwave Frequencies", *Submitted to the Progress in Electromagnetics Research Journal* (PIER Online). [Under Review]

CHAPTER TWO

Signal Propagation and Rainfall Studies

2.1 Introduction

Prediction of rainfall attenuation requires a proper understanding of the dynamics of the rainfall phenomenon. Researchers have identified that rainfall attenuation, the consequence of dynamic change in rainfall microstructural parameters primarily occurs within the troposphere, and, is influential to signal losses in microwave terrestrial and satellite communication systems. Rainfall rate and rainfall drop-size have been identified as the two major parameters, that explain the microphysics of rainfall, and can be utilized for the prediction of rainfall attenuation [*Ajayi et al.*, 1996; *Crane*, 1996]. The rainfall microphysics are characterized by the dynamics of rainfall types, rainfall rate, rainfall cellular distribution and rainfall DSD, all of which contribute to the problem of signal impairment in microwave propagation.

In this chapter, a review of past and recent contributions of different researchers on rainfall analysis, with respect to rainfall modelling and prediction, is examined. Statistical models employed as a representation of the rainfall microstructure related to rainfall rate and rainfall DSD are explored. The inherent attenuation losses encountered in microwave and millimetric link systems are discussed, and then, the larger contribution of rainfall attenuation to microwave and millimeter wave communication is later explored. The chapter is concluded by examining the recent rainfall campaigns undertaken in South Africa toward solving the problem of rainfall attenuation.

2.2 Layers of the Atmosphere

A terrestrial wireless communication system utilizes the troposphere for transmission and reception of electromagnetic (EM) waves from one point to another. The underlying principle in propagating in this medium is related to the radioclimatological properties in these regions. Broadly speaking, the regions, which are most important for signal propagation in wireless communication, are:

(1) Ionosphere: This is the region where the composites of the atmosphere are mainly made up of ionized or charged particles known as *plasma*. This region is a conducting layer which is useful for 'bouncing' back signals at low and moderate frequencies such as LHF, MHF and HF all in the range of 30 KHz to 30 MHz. This region is sensitive to cosmic radiation and astrophysical activities. It has a range of 500 km above the earth just above

the stratosphere [*Crane*, 2003]. The average plasma frequency value in this region is about 8 MHz [*Pozar*, 1998].

(2) Troposphere: This is the region in space where high frequency signal propagation is mainly achieved; It is also called the *free space* region. Some authors also call it the *non-conducting* region because of the low activities of electrons in the belt. Broadband communication systems, which employ the use of satellite and microwave links, use this region for propagation. It is located about 17 km from the earth in the equator and 9 km from the earth at the poles [*Crane*, 2003].

(3) Satellite Orbits: Beyond the above-mentioned layers *i.e.* above 500 km, we have regions, which are useful for satellite and interplanetary communication. Presently, ITU-R has four specified satellite orbits for satellite communication for C-band, Ku-band frequencies and above. *Seybold* [2005] listed the orbits as thus:

- Low Earth Orbit **(**LEO) located between 500 km and 2000 km above the earth.
- Medium Earth Orbit (MEO) located between 5,000km and 12,000 km from the earth.
- Geostationary Earth Orbit (GEO) located approximately about 36,000 km from the earth.
- High Earth Orbit (HEO) is the orbital above GEO i.e. over 36,000 km

The troposphere will be the main area of concern for this research work. This is because it is a region of high radio-meteorological turbulences due to its ground proximity and the unfettered influences of the natural environment on wave propagation in its domain.

2.3 RF and Microwave Communication in the Troposphere

Radio Frequency (RF) and Microwave communication systems have traditionally relied on the tropospheric layer of the atmosphere to propagate signals. The preference of this layer over other layers is mainly due to its ground proximity, which makes it suitable for line-of-sight propagation (LoS), especially at high frequency spectrum. However, the troposphere is also a region of radio-meteorological turbulences involving independent natural parameters such as pressure (P), water vapour pressure (ρ), atmospheric refraction and temperature (T). These variables affect the speed and orientation at which electromagnetic waves travel in the atmosphere. The radio refractivity (N), an important function related to these three parameters, is defined from [*Crane*, 2003] as:

$$N = \frac{77.6\,P}{T} + \frac{3.73\ \times\ 10^5\,\rho}{T^2} \tag{2.1}$$

Usually, these variables in one way or the other contribute to the prevalence of instability credited to the tropospheric region. For example, an event of low pressure evenly spread over a region could sometimes indicate the likelihood of rainfall or even heavy thunderstorms, which are both deleterious to propagation. Hence, the variability of these parameters contributes to the random behaviour of the tropospheric layer.

In utilising the troposphere for RF and microwave propagation, a clear line-of-sight distance must be established between the receiver and transmitter as shown in Figure 2-1. In adopting LoS principle, it must be noted that obstacles between the transmitter and receiver do not diffract the propagation path in order to avoid *multipath fading* (also known as signal ghosting). Designing an unobstructed microwave link requires the use of Fresnel principle for the calculation of minimum clearance [*Crane*, 2003]. The LoS is dependent, in principle, on the Fresnel ellipsoidal zone, F_n, given by:

$$F_n = \sqrt{\frac{n\lambda\, D_1 D_2}{(D_1 + D_2)}} \tag{2.2}$$

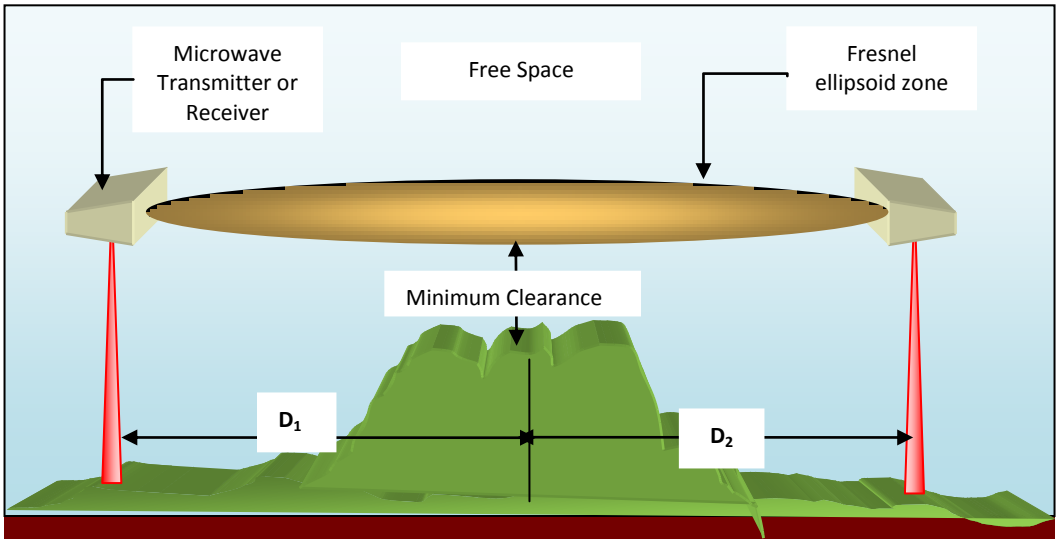

Figure 2-1: The Line-of-Sight (LoS) link between the receiver and transmitter

where n is the number of the ellipsoids required, D_1 and D_2 are the distances from the obstacle for both the transmitter and the receiver, λ is the wavelength of the center frequency of transmission.

Usually a simplified form of the equation, which includes the frequency (MHz) and a constant for the velocity, C, is also given as:

$$F_n = 17.3\sqrt{\frac{nCD_1D_2}{F_{MHz}(D_1 + D_2)}} \tag{2.3}$$

The Fresnel equation allows for calculation of the LoS distance for maximum clearance from the nearest obstacle. The obstacles may be hills, buildings and any other object capable of causing obstruction to the LOS path.

Most importantly, setting up a link requires making adequate consideration for worst scenarios of signal losses; this known as *link budget*. These scenarios can arise from multipath propagation, diffraction fading, rainfall path attenuation, path losses and antenna inadequacies such as polarization mismatch, pointing errors and antenna inefficiencies. The line-of-sight is usually classified into two types: optical line-of-sight and the radio line-of-sight. In the optical LOS, the farthest point is usually that which the eyes can see. However, the radio LOS is considered to be longer than that of optical LOS because of the curvature and sphericity of the earth. In calculating the radius of the earth, an adjustment is normally made as a correction for earth sphericity:

$$R' = kR \tag{2.4}$$

where $k = 1.33$ for the average correction due to the earth curvature in temperate regions and R = 6370 km. Invariably, the adjusted earth radius for design purposes, for example, is about 8300 km for temperate regions.

The frequency of transmission used for the design of RF and microwave links is ranged between 30 MHz to about 300 GHz. Appendix A-1 summarizes typical frequency bands useful for RF and microwave propagation

2.3.1 Limitations of RF and Microwave Communication in the Troposphere

The massive deployment of RF and microwave links for wireless communication around the world testifies to its popularity and preference as communication system designers' choice. Notwithstanding its popular use in electronic communication, it has quite a number of disadvantages: the first disadvantage is largely a drawback from the system (medium) itself. Generally, all communication systems experience a type of system loss in the form of *free space attenuation*. Free space attenuation is the loss that accompanies the use of the free space or atmosphere (troposphere included) for radio and microwave propagation. It is often calculated as a loss between the transmitter and receiver and it is extensively included in system design.

The power received by a receiver from a transmitter is taken as [*Seybold*, 2005]:

$$P_{Rx} = P_{Tx} G_{Rx} G_{Tx} \left(\frac{\lambda}{4\pi R}\right)^2 \tag{2.5}$$

where P_{RX} is the received power level in dB, P_{TX} is the transmitted power level in dB, G_{RX} and G_{TX} both represent the antenna gains at the receiver and transmitter respectively.

This expression is usually summarized in a logarithmic form by assuming that $G_{Rx}G_{Tx}$ = 1 and deriving free space loss as the ratio of P_{Rx} and P_{Tx}. Thus,

$$\text{Free Space Loss FSL} = 10\, Log_{10}\left(\frac{P_{Rx}}{P_{Tx}}\right) = 10\, Log_{10}\left(\frac{\lambda}{4\pi R}\right)^2 \tag{2.6}$$

By summary, the above equation can be written in a much more canonical form as recommended by ITU-R known as the *Friis transmission equation*:

$$FSL = 32.4 + 20\, \log_{10} R_{km} + 20\, \log_{10} F_{MHz} \tag{2.7}$$

where R_{km} is the distance in kilometers between the transmitter and receiver, F_{MHz} is the frequency of transmission in MHz.

This expression indicates that signal attenuation and its consequent losses are both frequency dependent and distance dependent. From (2.6) and (2.7), it is noticed that radio transmission at

higher frequencies such as those at microwave and millimeter bands are much more susceptible to free space loss at the receiving end.

The second disadvantage is based on signal losses, efficiency and availability, which are caused by the presence of hydrometeors and concentration of gaseous particles. Signal transmission in the troposphere at microwave frequencies above 10 GHz, hydrometeors and gaseous concentrations affect the link destructively resulting in attenuation, scattering, absorption and signal impairment as indicated by *Banjo et al.* [1986].

The most common of such destructive features are scintillation, which is notorious in satellite broadcast, while multipath fading and rain fading are common in terrestrial microwave communication [*Banjo et al*., 1986; *Crane*, 2003]. They are both due to the influence of *hydrometeors*. The mechanism behind this can be plainly observed when a link is set-up and closely monitored during transmission in the presence of the atmospheric conditions. Hydrometeors are believed to be responsible for most of the signal impairments especially in tropical, sub-tropical and equatorial climatic regions [*Ajayi et al.* 1996].

Hydrometeors can be classified into three major groups: clouds, solid precipitates and rain [*Crane*, 1996]. Clouds (fog and dew also included) may affect high frequency radio link resulting to an increase in the intensity of scintillation particularly in paths with cumulus clouds [*Savvaris et al.*, 2004]. This is possible in links at high elevation in the atmosphere, which is generally prone to scattering effects from the water droplets in fogs and clouds. Solid precipitates on the other hand cause reflection and scattering of transmitted waves, which is enough to cause significant attenuation in the level of the propagated signal [*Crane*, 1996]. These precipitates include snow, hail, sleet and every frozen element of precipitation. They are products of near-zero and sub-zero temperature in the ambient atmospheric conditions, which are often features of geographic areas such as temperate regions, arid and tropical areas.

The most important of all these hydrometeors is rainfall. Rainfall is prevalent in almost every geographical location although the distribution often varies with latitude. Rainfall structure is characterized by its drop size, rate, volume density, shape, elevation, temperature, terminal speed and distribution all of which play a significant role in the determination and prediction of signal attenuation and degradation [*Salema*, 2003; *Seybold*, 2005]. The effects of rainfall are a potential source of problem in the design of radio and microwave links because of its degrading effect on

communication. At frequencies above 6 GHz, rainfall could be destructive to signals and very destructive above 20 GHz based on the link distance and geographical location [*Crane,* 2003; *Seybold*, 2005]. The path loss experienced from rainfall is known as *rain loss*. Rain losses often result in signal deterioration in the form of fading, to a more extreme form of path loss, known as *rain fade* [*Seybold*, 2005] which can result in link outage during signal transmission.

Dust particles in the atmosphere are known for disrupting the polarization mechanism in transmitted signals i.e. it causes depolarization and cross-polarization [*Srivastava and Vishwakarma*, 2003]. This also depends on frequency of transmission and visibility of the environment. The millimeter wave spectrum is adversely affected by dust particles, a feature of terrestrial communication in desert regions.

Gaseous components of the atmosphere that induce attenuation include oxygen, water vapour and carbon-dioxide. Their presence in the atmosphere result in a form of path loss called *atmospheric loss*; it is usually of more importance to signal transmission between the frequencies at 2 GHz and 100 GHz [*Crane*, 2003]. The attenuation ($A_{gaseous}$) due to gaseous concentration in the atmosphere is proportional to the specific attenuation. On a terrestrial path, this is calculated from *ITU-R P.530-13* [2009]:

$$A_{gaseous} = \gamma_a \, d \qquad dB \tag{2.9}$$

$$\gamma_a = \gamma_o + \gamma_w \tag{2.10}$$

where γ_a is the specific attenuation of the atmosphere in dB/km, d is the LoS distance in km, while, γ_o and γ_w are the specific attenuations of oxygen and water vapour respectively.

Figure 2-2 shows the contribution of different atmospheric influences at different frequencies while Table 2-1 shows a summary of the types of path losses that accompanies propagation in wireless communication.

In summary, signal propagation in wireless communication (RF and microwave) in the troposphere is both frequency dependent and distance dependent. In addition, signal susceptibility at high frequencies is mainly associated with hydrometeors and atmospheric gases.

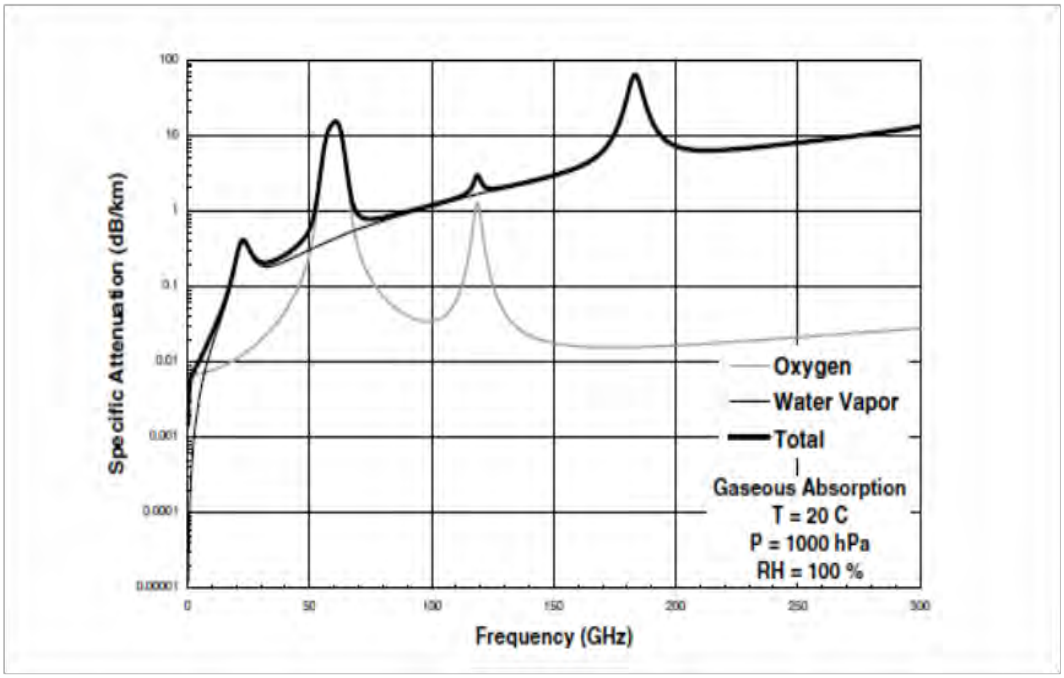

Figure 2-2: Specific attenuation from the effects of oxygen and water vapour at microwave and millimeter wave frequencies [*Crane*, 2003]

Table 2-1: Path Losses in Wireless Communication systems [*Seybold*, 2005]

TYPE OF LOSSES	LIKELY CAUSES
FREE SPACE LOSS	Spatial loss due to transmission media
TRANSMITTER POINTING ERROR	Non-precise orientation of transmitter and receiver for line-of-sight transmission
RAIN LOSS	High and low intensity rainfall rates during transmission
MULTIPATH LOSS	Multiple reflections from hard surfaces during propagation
ATMOSPHERIC LOSS	Presence of gaseous constituents in the atmosphere
DIFFRACTION LOSS	Variation in the refractivity gradient, dN/dh, between the transmitter and Receiver

2.4 Rainfall in RF and Microwave Communication

Rainfall parameters are used in the design of microwave links. Rainfall is responsible for the absorption, scattering and depolarization of radio waves [*Salema*, 2003; *Seybold*, 2005] and, these effects result in *rain fade*. Rain fade duration coincides with the duration of a rainfall event. A rainfall event is characterised by increasing and decreasing rainfall rates intensities depending on the rainfall structure. The acceptable percentage of time for which rainfall rate is exceeded in a wet spell (otherwise known as $R_{0.01}$) is of major interest to researchers. Figure 2-3 shows the concept of rainfall and rainfall attenuation concerning communication systems.

$R_{0.01}$ is a local phenomenon, which varies from region to region based on latitudinal coordinates as shown in *ITU-R P.837-5* [2008]. It varies with the elevation and wind current system of a particular location. It is also subject to monthly variations based on seasonal changes and yearly variations based on global parameters. Over the years, studies on rainfall and its effect on wave propagation have increased tremendously. This is mainly ascribed to the improvements in rainfall data harvesting campaigns and consequent development of empirical and statistical methods of rainfall analysis.

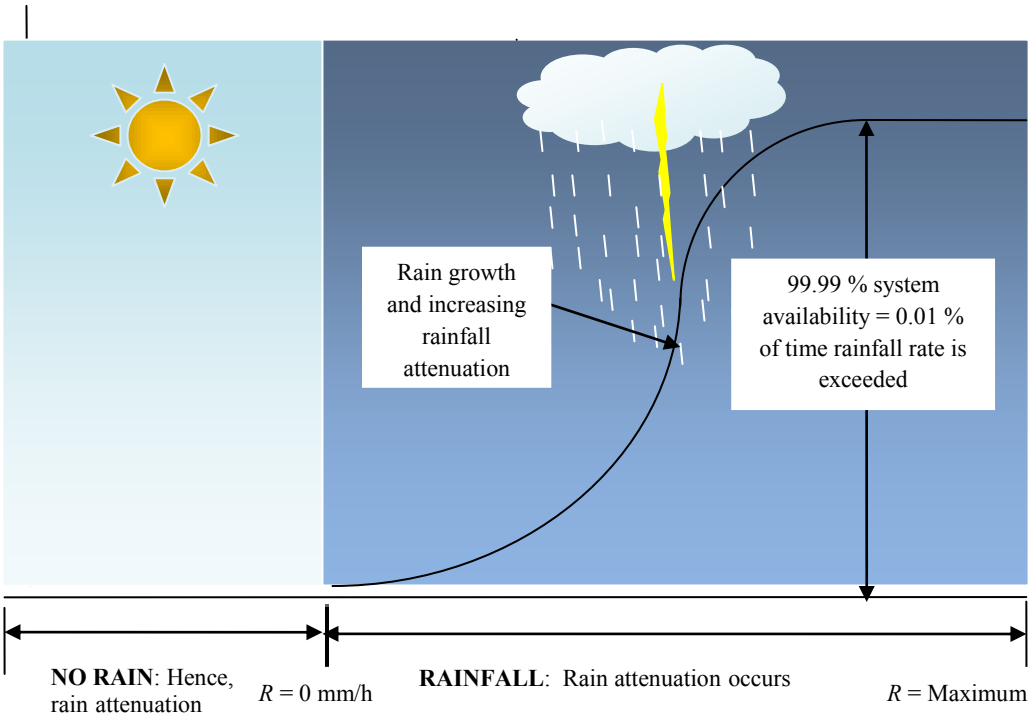

Figure 2-3: The concept of rainfall exceeded and rainfall attenuation

However, it has also been identified that majority of global rainfalls are a combination of convective and stratified types [*Ajayi et al*., 1996]. Many rain models for the prediction of attenuation have also emerged [*Moupfouma*, 1984; *Crane*, 1996; *Crane*, 2003; *Maitra*, 2004; *Fashuyi et al.*, 2006; *Ojo et al.*, 2008]. These models which are generated from experimental rainfall data, and some analytically, all have inputs related to the microstructural properties of rainfall.

These properties are given in *Ajayi et al.* [1996] and *Seybold* [2005] as:

(i) Rainfall rate
(ii) Rainfall-drop size
(iii) Rainfall volume density
(iv) Rainfall drop-shape
(v) Rainfall elevation

In this research, consideration will be given to two important parameters (rainfall rate and rainfall drop-size) which have been used by contemporary researchers in this field for estimation of rain attenuation. The aim of using these parameters is to obtain empirically or statistically the localized radioclimatological conditions available over a defined geographical area. Contemporary research by [*Maitra*, 2004; *Fashuyi et al.*, 2006; *Ojo et al.*, 2008; *Emiliani et al*., 2009] have also shown that these parameters are important in the modelling of appropriate prediction techniques necessary for the design of a viable radio link with minimal and acceptable rain attenuation margin.

Microwave and millimeter wave communication particularly at frequencies above 2 GHz have particularly been of interest to broadband stakeholders in the satellite systems and mobile telephony systems. Interestingly, the quantum leap in personal, mobile and commercial communication systems is gradually approaching a state where the demand for broadband services in most conventional microwave bands outstrips supply. These bands such as C-band (4 - 8 GHz), X- band (8 - 12 GHz) and Ku-band (12 - 18 GHz) which have traditionally satisfied the large array of communication operation are becoming congested. This has resulted in migration to the use of higher sub-bands levels such as K-bands (18 - 26.5 GHz) and above. Signal propagation in these bands is adversely affected by rain attenuation, especially at higher frequencies. To successfully transmit signals at these bands, exhaustive modelling and prediction techniques are required to determine the acceptable level of rain attenuation.

2.5 Rainfall Microstructure and Mechanics

2.5.1 Types of Rainfall

Generally, rainfall types can be generally classified into four distinct groups based on spatial distribution of rainfall [*Ajayi et al.*, 1996; *Salema*, 2003] :

(a) Stratified Rain: This type of rainfall occurs at low rain rates up to about 25 mm/h, and, usually has widespread rain cell during rainfall duration. It is also known as *stratiforms* [*Ajayi et al.*, 1996] because it is associated with the fusion of small ice particles into larger particles during the build-up to rainfall.

(b) Convective Rain: These mainly occur at localized areas with relatively high rain distribution coupled with wind currents. They have a short duration of fall (about tens of minutes) with smaller rain cells and are prominent in tropical regions.

(c) Monsoon Rain: This is usually a cumulative sequencing of convective rain cells followed by bursts of stratified rainfall. They have large widths and can span hundreds of kilometres. They have longer duration than convective rain types.

(d) Tropical Storm Rain: These intense rainfall patterns span larger dimensions in hundreds of kilometers. The peripheral regions around the location of rainfall may experience a mild monsoon or convective rainfall.

2.5.2 Rainfall Drop-Shape Profile

Raindrops are believed to have varying shape profile which depends on rainfall rate, cloud proximity to the ground, rainfall type, terminal velocity, ambient temperature *e.t.c.* [*Pruppacher and Pitter*, 1971; *Li et al.*, 1995; *Jiang et al.*, 1997; *Li et al.*, 2000]. As a result, researchers have suggested three basic drop shapes: spherical, spheroidal and oblate-spheroidal [*Pruppacher and Pitter*, 1971; *Oguchi*, 1973; *Nader*, 1998; *Li et al.*, 2000; *Amarjit and Gangwar*, 2009].

Pruppacher and Pitter [1971] earlier described the shape forming mechanics of raindrops as a combination of internal and external forces around the drops leading to deformation with rainfall rate. In addition, *Jiang et al.* [1997] identified the raindrop growth as useful in playing an important role in the determination of larger drop densities. Based on this knowledge of rainfall dynamics, a functional analytical model, which is a summation of cosine series, was developed [*Pruppacher and Pitter*, 1971; *Oguchi*, 1977] to cater for the shape deformation.

The spherical drop-shape has no deformation; hence, the radius of the raindrops is constant. The

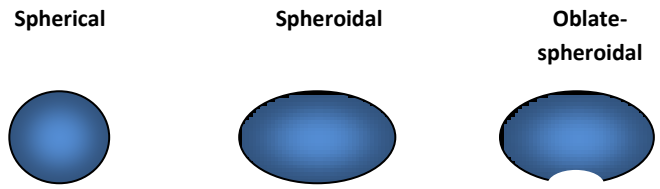

Figure 2-4: Types of rainfall drop shapes

spheroidal and oblate-spheroidal shape both consider the axial influences on rainfall drops and hence, provide good estimation for polarized waves. However, their estimation involves much more rigorous mathematical computations to implement the raindrop energy scattering mechanism.

2.5.3 Rainfall Cells

Rain cells are generally described as the *mapped–out* areas influenced by the effects of rainfall during a single or multiple rain events. A rain cell is generally dynamic as rainfall is assumed to be influenced by wind speeds and the cloud drift. *Pastoriza et al.* [2010] describes a rain cell as a defined region where the rainfall intensity is assumed to be greater or equal to an assumed threshold. Generally, the concept of rain cells is greatly affected by the types of rainfall. A convective rain cell, for example, is usually mapped, as a smaller rainfall cell diameter at higher rainfall rate intensities, while a stratiform rain cell is of larger rainfall cell diameter and lower rainfall intensities [*Mandeep and Allnut*, 2007; *Ramachandran et al.*, 2007; *Pastoriza et al.*, 2010]. A rain cell is assumed to have the highest rainfall intensity at the centre and decays rapidly towards the edges of the mapped area. *Capsoni et al.* [1987] in Figure 2-5 depicted the variation in rainfall intensities in the EXCELL model for rain cells.

Therefore, a transmitted signal travelling through several overlapping rain cells will suffer greatly from the effects of rainfall attenuation. With variation in the rain-cell volume distribution, the conditions of rainfall attenuation will therefore depend on the climatic and geographic pattern of a locality.

2.5.4 Physics of Rainfall Rate

The rainfall rate is defined as the diameter integral of the rainfall drop size distribution and is related to the fall velocity and volumetric property of the rainfall droplets. This is mathematically

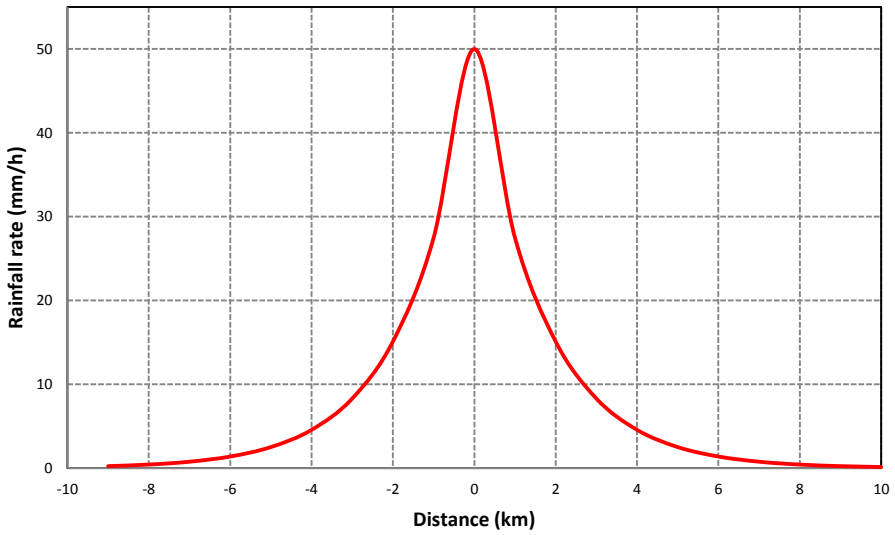

Figure 2-5: Variation of rainfall in a typical EXCELL rainfall cell [*Pastoriza*, 2010]

described in *Sadiku* [2000] and *Owolawi* [2010]:

$$R(D) = \int_0^\infty v_t(D)N(D)V(D)\,dD \quad [mm/h] \tag{2.11}$$

where $v_t(D)$ is the terminal or fall velocity of the rainfall drops in m/s, $N(D)$ is the rainfall drop-size distribution in m^{-3} mm^{-1} and $V(D)$ is the volume of rain droplets in mm^{-3}.

With a general spherical assumption for the raindrop shape, the volume of an assumed raindrop sphere for a diameter, D, in mm is given as:

$$V(D) = \frac{4\pi}{3}\left(\frac{D}{2}\right)^3 \tag{2.12}$$

thus,

$$R(D) = \frac{\pi}{6}\int_0^\infty v_t(D)N(D)D^3dD \quad [m/s] \tag{2.13}$$

By adopting the conversion of the rainfall rate unit from m/s to mm/h and balancing the excess physical units, equation (2.13) becomes a model describing rainfall rate as a function of the third moment of the rainfall drop-size distribution. Thus, the new equation is:

$$R(D) = 6\pi \times 10^{-4} \int_0^{\infty} v_t(D) N(D) D^3 dD \quad [mm/h] \tag{2.14}$$

For discrete values of rainfall rate where D_k is the mid-value of a diameter class with an interval such that, $\left(D_k - \frac{\Delta D_k}{2}\right) \leq D_k \leq \left(D_k + \frac{\Delta D_k}{2}\right)$. The rainfall rate equation in (2.14) can be approximated for B_n discrete classes such that:

$$R(D) \approx 6\pi \times 10^{-4} \sum_{k=1}^{B_n} v_t(D_k) N(D_k) {D_k}^3 \Delta D_k \quad [mm/h] \tag{2.15}$$

where all the parameters have usual meaning as defined in equation (2.11) above.

2.5.5 Rainfall Drop-Size Distribution (DSD) Physics

The rainfall DSD is a *scaled* probability density function of the drop sizes. It is mainly concerned with the spatial distribution of rain droplets within a designated rainfall cell [*Crane*, 1996]. A typical rainfall event exists as a single or multiple cells undergoing a temporal static or dynamic velocity according to the cloud and wind movement. It is usual for raindrops of different diameters to exist within a rain cell, although, this is defined by the type of rainfall being experienced [*Ajayi et al.*, 1996]. The rainfall DSD is assumed as probabilistic dependent on the number of droplets per unit volume present such that [*Ulbrich*, 1983; *Marzuki et al.*, 2010]:

$$N(D) = N_T \times f^*(D) \quad [m^{-3} mm^{-1}] \tag{2.16}$$

where $f^*(D)$ is the probability density function of the rain drop-sizes. By definition, the concentration of rain drops is the diameter integral of the raindrops from zero to infinity. Thus, the concentration N_T is given as:

$$N_T = \int_0^{\infty} N(D)\, dD \approx \sum_{k=1}^{B_n} N(D_k) \Delta D_k \approx \sum_{k=1}^{B_n} \frac{C_k}{A \times T \times v_t(D_k)} \quad [m^{-3}] \tag{2.17}$$

The sampling area of the observation point being A m^2, which specifies the maximum number of rainfall drops, C_k, captured in a volumetric sweep of the rain cell with B_n number of grouped observations. T is the sampling time undertaken for the selection of a discrete number of rainfall

drops. Substituting N_T in place of the diameter integral of $N(D)$ in (2.15), the new equation becomes:

$$R(D) = \frac{6\pi \times 10^{-4}}{A \times T} \sum_{k=1}^{B_n} \left[C_k {D_k}^3\right] \quad [mm/h] \tag{2.18}$$

where B_n represents the total number of grouped diameter sizes or classes describing the population of rain drops sampled at T seconds within a rain event.

Sadiku [2000] gives the relationship between rainfall rate and rain drop-size distribution which has been modified for kth diameter as:

$$N(D_k) = \frac{R(D_k)}{6\pi v_t(D_k) {D_k}^3} \times 10^4 \quad [m^{-3}mm^{-1}] \tag{2.19}$$

for,

$$R(D) = \sum_{k=1}^{B_n} R(D_k) \tag{2.19b}$$

substituting the expression for $R(D)$ in (2.18) into (2.19), for a single kth diameter rain drop, a new expression for rainfall DSD is derived such that:

$$N(D_K) = \frac{C_K}{A \times T \times v_t(D_K) \times \Delta D_K} \quad [m^{-3}mm^{-1}] \tag{2.20}$$

Therefore, having the knowledge of the parameters C_k, A, T, $v_t(D_k$ and ΔD_k is sufficient to determine the rainfall DSD of any grouped rain drop-size class of mean diameter D_k.

2.6 Rainfall Measurement for Parameter Modelling

Rainfall modelling has remained very mandatory in the planning and design of radio and microwave links. The influence of rainfall on signal transmission is responsible for significant loss of transmitted energy in a typical LoS path. It is often desired as part of link budgeting that a compromise transmitted power level be reached to compensate for the effects of rain fading and

rain attenuation [*Seybold*, 2005]. The compensation must not be over-estimated as this can lead to increased system complexity and high cost of installation and maintenance; under-estimation, on the hand, leads to poor performance of the overall system as the likely effects of rain fading may be present [*Seybold*, 2005].

Rainfall modelling majorly considers two microstructural properties of rainfall: rain rate and rain drop-size. Measurements of rainfall rate and rain drop-size distribution are usually part of the modelling procedure that requires accuracy and precision. Measurement is an integral tool that used for recording, comparing, validating, and calibrating useful information obtained through stand-alone devices or network of devices. The measurement of these parameters can be undertaken using any of the instruments listed by [*Ajayi et al.*, 1996; *Crane*, 2003]:

(a) Rain gauge
(b) Radiometer
(c) Radar
(d) Disdrometer

Of the three above-mentioned instruments, the radar has been described as the best in terms of proper estimation of attenuation and profiling of rain microstructure along a propagation path. The radar uses reflected wave energy; its deployment is however costly and calibration difficult [*Ajayi et al.*, 1996]. The radiometer is used for the simulation of slant path attenuation.

The rain gauge, on the other hand, is the most popular and widely used in rain attenuation studies and is being used in large numbers to constitute a *rain gauge network* for simultaneous rainfall data collection at several locations [*Ajayi et al.*, 1996]. There are two popular types of rain gauges: tipping bucket rain gauge and capacitor rain gauge [*Crane*, 2003]. However, the tipping bucket rain gauge has remained far more popular because of its precision and accurate measurement [*Emiliani et al.*, 2009]. The *integration time* is a quantity often derived from the tipping bucket rain gauge based on the interval of tips *i.e.* the number of times the gauge empties water accumulation to start another reading. It is also described as the time resolution of rainfall rate. A lower the integration time yields a more accurate and precise rainfall rate information. As result, there is a need to convert larger integration time to smaller integration time *e.g.* 60-minute to 1-minute.

The disdrometer is mainly used for the precise measurement of rainfall drops, rainfall rate and sometimes shape profile along a propagation path. There are three major types of disdrometers:

impact disdrometer, video disdrometer and optical disdrometer [*Ajayi et al.*, 1996; *Bartholomew*, 2009; *Zhang et al.*, 2008; *Saikia et al.*, 2009]. The impact disdrometer makes use of pressure-based transducers to measure raindrop impact on its uppermost cone (its working operation is discussed in section 3.3.1). The video disdrometer utilizes the motion detection features of video technology to 'count' the number of rainfall drops, while, the optical disdrometer makes use the "make-and break" action of laser spectrum by rainfall drops [*Zhang et al.*, 2008; *Saikia et al.*, 2009].

In computing appropriate statistical results from rain models, independent distribution models need to be established from the rain rate data and rain-drop size data. Research over the years especially from the works of *Law and Parsons* [1943], *Olsen et al.* [1978], *Crane* [1980], *Ajayi and Ofoche* [1983], *Moupfouma* [1984], *Ajayi et. al.* [1996], *Maitra* [2004] have provided appreciable results responsible for various regions of the world. The ITU-R recommendations [*ITU-R P.838-3*, 2005; *ITU-R P.530-13*, 2009] have also contributed in appropriating different parts of the world as fixed climatic zones with their respective rainfall rates and rain-drop size effects.

2.7 Statistical Theory of Rainfall rate

Rainfall is a random event of probability, wherein the statistical properties are readily measurable as a function of statistical distributions, qualitatively and quantitatively. As a discretized function with a constant sampling rate or integration time, the probability density function (PDF) can completely describe its characteristics. Mathematically, researchers have observed the rainfall rate process as a right-sided normal distribution whose PDF can be represented as $f(r)$. *Soong* [2004] gives the cumulative distribution function (CDF), $F(r)$, derived from the PDF, $f(r)$, as:

$$F(r) = \int_{-\infty}^{r} f(s)ds \tag{2.21}$$

where s is a dummy variable defined by the rainfall rate bounded for an interval of $-\infty \leq s \leq r$.
Following this statistical validity of rainfall rate, the concept of rainfall rate exceeded follows from the idea of the complementary function of the CDF. This leads to the concept of non-availability of the cumulative function which *Moupfouma* [1987a] and *Ojo et al.* [2008] describes the exceedence function of rainfall rate as, $P(R \geq r)$, as:

$$P(R \geq r) + F(r) = 1 \tag{2.22}$$

where,

$$F(r) = P(R < r) \tag{2.22a}$$

so that,

$$P(R \geq r) = 1 - F(r) \tag{2.23}$$

where $P(R \geq r)$ is the probability that rainfall rate is exceeded at a particular time. The concept of this function is useful especially when $r = R_{0.01}$ when the maximum CDF is 99.99 % available. $R_{0.01}$ is used for the threshold prediction the worst level of attenuation expected at a locality [*Crane*, 1996; *Crane*, 2003; *Seybold*, 2005; *ITU-R P.837-5*, 2008; *Ojo et al.*, 2008]. Therefore, the $R_{0.01}$ parameter varies universally and is a function of the climatic variability of a location.

2.7.1 Rain Rate Distribution Models

Rainfall rate is a parameter measured in terms of its intensity per time scale with a unit of measurement in millimeters per hour (mm/h). Modelling of rain rate for communication systems requires the collection of necessary data from rain gauges, or better still, rain gauge networks. As rainfall within a localized region could vary in a typical intense rainfall scenario so that rain cells are formed, it is often necessary to use the rain gauge network approach for solving multiple distribution points for moving rain cells. The rain gauge is used for the measurement of point rainfall rate *i.e.* rainfall along a propagation path profile.

Conversion of rainfall integration time obtained from tipping bucket rain gauge to suitable integration time is often necessary. *Crane* [1996] and *Emiliani et al.* [2009] suggested 30-seconds and one-minute integration time of rain data as suitable conversion values from the standard 60-minutes integration time. Also, *Ajayi and Ofoche* [1983] supported the use of the one-minute integration time as the best in line with rainfall attenuation determination in microwave link designs.

Over the years, several rain rate models have emerged and have been found useful in solving both localized and regional problems associated with rainfall attenuation. The area of interest of researchers is to utilize a statistical application of *cumulative distribution function* (CDF) and *probability distribution function* (PDF) to investigate rainfall. The use of CDFs and PDFs in rainfall rate modelling lies in its use for obtaining values either by interpolating or extrapolating at points

within the function. In addition, the amount of time rainfall is exceeded for 0.01% of the time also known as $R_{0.01}$ can be obtained from the CDF. This value is used in the design of fade probability in a microwave link [*Ajayi et al.*, 1996].

There are different rain rate models [*ITU-R P.837-1,2*, 1994; *Ajayi et al.*, 1996; *Crane*, 1996; *Seybold*, 2005] which are used for microwave and millimeter link design. The most popular models include:

(a) The ITU-R P.837 rainfall rate model

(b) The Global Crane rainfall rate model

(c) Moupfouma I and Moupfouma II rain rate models

(d) Gamma rainfall rate model

(e) Lognormal rainfall rate model

2.7.1.1 The ITU-R P.837 Rain Rate Model

The ITU-R model partitions the worldwide rain rate distribution into 15 regions namely: A, B, C, D, E, F, G, H, J, K, L, M, N, P and Q. The ITU-R model is basically derived from ITU-R recommendation P. 837-1 to P. 837-4 [*ITU-R P.837-1*, 2, 3, 4,5, 2008]. Table 2-2 and Figure 2-6 show the proposed rainfall rates suggested by ITU-R for different zones.

The model employs equations from ITU-R recommendation P.838 in the calculation of rainfall attenuation values. The ITU-R P.837-5 coutour maps for $R_{0.01}$ gives their geographic values at different locations. This map showing the worldwide variation is provided in Appendix C-1.

Table 2-2: ITU-R Model values for the 15 different rain zones around the World [*ITU-R Rec PN. 837-1/2,* 1992/1994]

Percentage of Time	A	B	C	D	E	F	G	H	J	K	L	M	N	P	Q
1	1	0.5	0.7	2.1	0.6	1.7	3	2	8	1.5	2	4	5	12	24
0.3	0.8	2	2.8	4.5	2.4	4.5	7	4	13	4.2	7	11	15	34	49
0.1	2	3	5	8	6	8	12	10	20	12	15	22	35	65	72
0.03	5	6	9	13	12	15	20	18	28	23	33	40	65	105	96
0.01	8	12	15	19	22	28	30	32	35	42	60	63	95	145	115
0.003	14	21	26	29	41	54	45	55	45	70	105	95	140	200	142
0.001	22	32	42	42	70	78	65	83	55	100	150	120	180	250	170

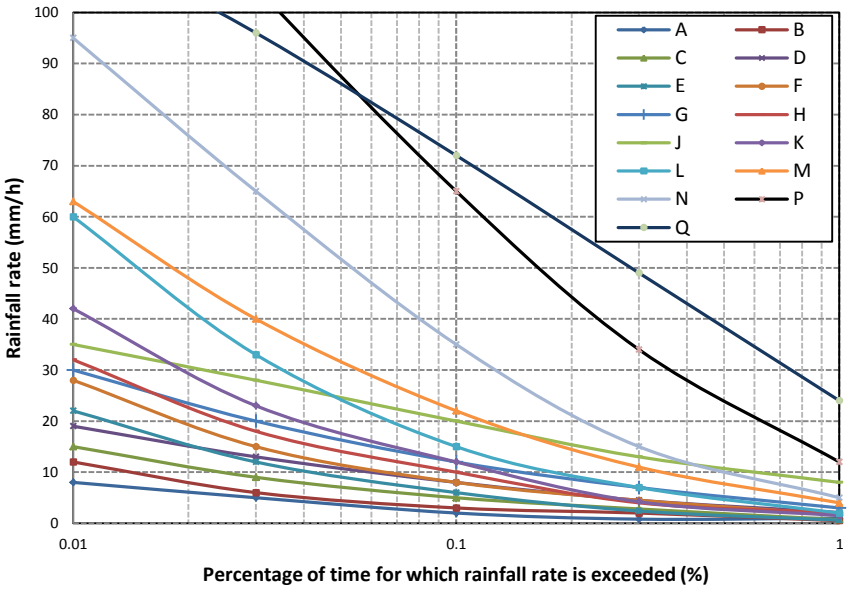

Figure 2-6: ITU-R rain-rate model for different parts of the world

2.7.1.2 The Global Crane Rain Rate Model

The global Crane rain rate model is used for the estimation of rain fade from different parts of the world [*Crane*, 1980; 2003]. Crane was able to establish these values by collecting rainfall data from different parts of the world and calculating their respective rain attenuation. In this model, rainfall patterns around the world are classified into 12 zones namely: A, B, B1, B2, C, D1, D2, D3, E, F, G and H. Thus, the global Crane model is similar to the ITU-R model except in the adoption of 12 rainfall region instead of ITU-R's 15 regions. Table 2-3 and Figure 2-7 gives the zonal rainfall exceedences for different parts of the world.

In calculating the other parameters for rain rate attenuation, the Crane model also uses equations similar to ITU-R recommendation [*ITU-R P.838-3*, 2005] which are derived from *Olsen et al.*

Table 2-3: The Global Crane Rain Rate Model [*Crane*, 1996]

Global Percent	A	B	B1	B2	C	D1	D2	D3	E	F	G	H
1	0.2	1.2	0.8	1.4	1.8	2.2	3	4.6	7	0.6	8.4	12.4
0.1	2.5	5.7	4.5	6.8	7.7	10.3	15.1	22.4	36.2	5.3	31.3	66.5
0.01	9.9	21.1	16.1	25.8	29.5	36.2	46.8	61.6	91.5	22.2	90.2	209.3
0.005	13.8	29.2	22.3	35.7	41.4	49.2	62.1	78.7	112	31.9	118	283.4
0.001	28.1	52.1	42.6	63.8	71.6	86.6	114.1	133.2	176	70.7	197	542.6

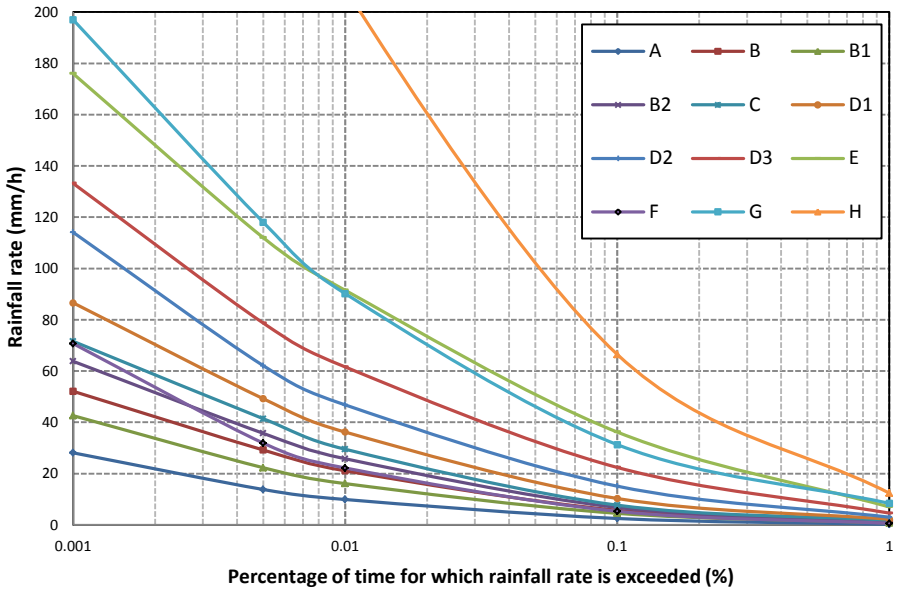

Figure 2-7: Global crane rain rate model for different parts of the world

[1978] to calculate the specific attenuation. A crane map showing the rainfall rate variation for the African and European region is provided in Appendix C-2.

2.7.1.3 Moupfouma I and Moupfouma II rain rate Models

Moupfouma [1984; 1987a] developed a rainfall rate model based on his radio experiments in Congo, a tropical site. The first rainfall rate model (or Moupfouma I) considers the semi-empirical rainfall rate function as:

$$P(R \geq r) = ar^{-b} \exp(-ur), r \geq 2 \text{ mm/h} \tag{2.24}$$

where r is the rainfall rate in mm/h. The parameters a and b both depend on $R_{0.01}$ and are both given as:

$$a = 10^{-4} {R_{0.01}}^{b} \exp(uR_{0.01}) \tag{2.24a}$$

and,

$$b = 8.22 {R_{0.01}}^{-0.584} \tag{2.24b}$$

The slope of the function, *u,* is given as 0.025 as suggested by Moupfouma for most parts of the world.

Based on the shortcomings of Moupfouma I [*Moupfouma*, 1984, 1987a; *Ajayi et al.*, 1996], the modified Moupfouma model (or Moupfouma II) was developed by *Moupfouma and Martin* [1993] as an updated version. The model is suitable for tropical climate because of its response to low rain rates and high rain rates [*Ojo et al.*, 2008]. It was shown in their work that rainfall CDFs can be used for prediction of rainfall rates when $R_{0.01}$ is a known value [*Ajayi, et al.*, 1996; *Salema*, 2003]. This is given as:

$$P(R \geq r) = \left(\frac{R_{0.01} + 1}{r + 1}\right)^{b_1} . e^{[u_1(R_{0.01} - r)] - \log_e(10^4)} \tag{2.25}$$

where *r* in mm/h represents the exceeded rain rate during time *P* and b_1 is governed by the shape of the rainfall rate and it is described as:

$$b_1 = \left(\frac{r - R_{0.01}}{R_{0.01}}\right) . \ln\left(\frac{1 + r}{R_{0.01}}\right) \tag{2.25a}$$

The values for u_1 being the slope of the rain CDF being dependent on the climatic region under consideration. Usually, different values of u_1 exist for tropical and temperate zones [*Ajayi et al.*, 1996] and are given as:

$$u_1 = \frac{\ln(10^4)}{R_{0.01}} \exp\left[-\lambda\left(\frac{r}{R_{0.01}}\right)^{\alpha}\right] \tag{2.25b}$$

where this function corresponds to geographical features of a tropical location with λ = 1.066 and α = 0.214. For temperate zones, the function is given as:

$$u_1 = \frac{\ln(10^4)}{R_{0.01}} \times \frac{1}{\left(1 + \eta\left(\frac{r}{R_{0.01}}\right)^{\beta}\right)} \tag{2.25c}$$

where η and β are 4.56 and 1.03 respectively.

2.7.1.4 Gamma Rainfall Rate Distribution Model

The gamma probability function for rainfall rate has been identified by *Moupfouma* [1982; 1984a] as a good function for prediction of high rainfall rates. The gamma probability function as given in *Weber and Arfken* [2003] and *Soong* [2004] has been applied in the recent rainfall studies of *Owolawi* [2010; 2011] is given by:

$$f(r) = \frac{r^{\alpha-1}\, exp\left(-r/\beta\right)}{\beta^{\alpha}\, \Gamma(\alpha)} \quad \text{for} \quad 0 \le r \le +\infty, \alpha > 0, \beta > 0 \qquad (2.26)$$

where α and β are the input parameters of 2.26 to be determined by point estimation technique [*Kreyszig*, 2006].

The gamma function has a rapidly decaying feature at high rainfall rates, which is similar to the behaviour of probability functions for rainfall rate. Therefore, it is works well at regions with high rainfall rates.

2.7.1.5 Lognormal Rainfall Rate Distribution Model

The lognormal probability function is a distribution utilised for the estimation of low precipitation rates as discussed in *Moupfouma* [1982; 1984a]. The lognormal function as applied in the recent studies of *Owolawi* [2010, 2011a] is given by:

$$f(r) = \frac{1}{r\sigma\sqrt{2\pi}} exp\left[\frac{-[ln(r) - \mu]^2}{2\sigma^2}\right] \quad 0 \le r < +\infty, \qquad 2.27$$

where μ and σ are the standard mean and standard deviation of the total population of the rainfall samples.

The lognormal function has very good estimates at low rainfall rates, similar to that of a typical probability function for rainfall rate. Therefore, it work wells at regions with low rainfall rates.

2.8 Rainfall Drop-Size Distribution (DSD)

The quest to develop location-specific rain drop-size distribution (DSD) models has led to the

development of several statistical models [*Atlas and Ulbrich*, 1974; *Sekine and Lind*, 1982; *Ulbrich*, 1983; *Ajayi and Olsen*, 1985; *Jiang et al.*, 1997]. With this, different rainfall DSD models at different locations around the world have been used to predict path attenuations of microwave links. The prominent models in use are: Laws and Parsons model, negative exponential model, Weibull model, lognormal model and the modified gamma model. The last four models have been used extensively in rainfall research and hence, are more popular.

The general mathematical expression for rainfall drop-size distribution [*Marzuki et al.*, 2010; *Owolawi*, 2011b; *Afullo*, 2011] is given as:

$$N(D) = N_C \times f^*(D) \tag{2.28}$$

where the factor N_C is defined as the total concentration per unit volume of rainfall drops and $f^*(D)$ is the probability density function (PDF) of the rain drop-size. N_C and $f^*(D)$ both have a unit of m^{-3} and mm^{-1} respectively.

2.8.1 Rainfall Drop-Size Distribution Models

Raindrop size distribution (DSD) is defined as the number of raindrops at a given diameter per unit volume. Raindrop size is an essential rainfall microstructural property essential in the modelling and prediction of rain attenuation. There exist several models used in many previous works [*Laws and Parsons*, 1943; *Marshall and Palmer*, 1948; *Ajayi et al.*, 1996]:

(a.) Laws and Parsons Rain DSD Model

(b.) Marshall and Palmer Exponential Rainfall DSD Model

(c.) Lognormal Rainfall DSD Model

(d.) Weibull Rainfall DSD Model

(e.) Modified Gamma Rainfall DSD Model

2.8.1.1 Laws and Parsons Rainfall DSD Model

The Laws and Parsons model is adopted as the ITU-R model [*Ajayi et al.*, 1996] and is therefore used extensively in studies related to rain attenuation prediction. *Laws and Parsons* [1943] were able to establish a relationship between rainfall DSD and its input parameters (volume fraction percentage and rain-drop terminal velocity) given by:

$$N(D) = \frac{10^3 R\,\beta(m)da}{4.8\,\pi a^3\,v(a)} \quad m^{-3} \text{ for } \left(a - \frac{da}{2}\right) \le a \le \left(a + \frac{da}{2}\right) \qquad (2.29)$$

where a is the radius of the raindrop for the interval $\left(a - \frac{da}{2}\right) \le a \le \left(a + \frac{da}{2}\right)$, $\beta(m)da$ represents the volume fraction percentage, $v(a)$ is the terminal velocity of individual rain drops, da is the size interval and R stands for the rain rate in mm/h.

The Laws and Parsons model has been shown to be more suitable for temperate regions and not a good model for rainfall DSD estimation for regions outside Europe and North America [*Yeo et al.*, 1993]. The Law and Parsons model for different rainfall rates and drop sizes have been summarised as shown in Table 2-4.

Table 2-4: The Law-Parsons rainfall DSD model for different rainfall rates [*Sadiku*, 2000]

Drop Diameter (mm)	**Terminal Velocity (m/s)**	**Rainfall Rate (mm/h)**								
		0.25	1.25	2.5	5	12.5	25	50	100	150
		Percentage of water volume								
0.5	2.1	28.0	10.9	7.3	4.7	2.6	1.7	1.2	1	1.0
1	3.9	50.1	37.1	27.8	20.3	11.5	7.6	5.4	4.6	4.1
1.5	5.3	18.2	31.3	32.8	31	24.5	18.4	12.5	8.8	7.6
2	6.4	3.0	13.5	19.0	22.2	25.4	23.9	19.9	13.9	11.7
2.5	7.3	0.7	4.9	7.3	11.8	17.3	19.9	20.9	17.1	13.9
3	7.9		1.5	3.3	5.7	10.1	12.8	15.6	18.4	17.7
3.5	8.35		0.6	1.1	2.5	4.3	8.2	10.9	15	16.1
4	8.7		0.2	0.6	1	2.3	3.5	6.7	9	11.9
4.5	9.0			0.2	0.5	1.2	2.1	3.3	5.8	7.7
5	9.2				0.3	0.6	1.1	1.8	3	3.6
5.5	9.35					0.23	0.5	1.1	1.7	2.2
6	9.5						0.3	0.5	1	1.2
6.5	9.6							0.2	0.7	1
7										0.3

2.8.1.2 Modified Gamma Rainfall DSD Model

The modified gamma model has three input parameters: N_m, μ and Λ. The modification here lies in the factor D_i^{μ} which effects the gamma behaviour on the function. *Atlas and Ulbrich* [1974] gives the gamma model as:

$$N(D_i) = N_m D_i{}^{\mu} \exp(-\Lambda D_i) \quad [m^{-3}mm^{-1}] \tag{2.30}$$

The input, D_i, is the mean diameter of the rainfall drops. The relationship between the input parameters and rainfall rate are given as:

$$N_m = aR^b \tag{2.30a}$$

$$\Lambda = a_\Lambda R^{b_\Lambda} \tag{2.30b}$$

The parameter, μ, can assume the value of a constant (2 or 3 in most cases) or a regression fit to rainfall as the case may require. The modified gamma model provides good response to rainfall DSDs at both low and high rainfall rates [*Ulbrich*, 1983]. This is mainly due to the function truncation at the lower diameter spectrum. It has been applied in tropical regions such as Singapore and Taiwan [*Tseng* et al., 2005; *Kumar et al.*, 2010].

2.8.1.3 Lognormal Rainfall DSD model

The two-parameter lognormal model is a statistical model with two input parameter mainly the mean shape parameter , μ and standard deviation scale parameter , σ. In rainfall studies, an additional parameter N_T (concentration of rainfall drops) is required to fit the measurement. *Ajayi et al.* [1985] gave the lognormal rainfall DSD model:

$$N(D_i) = \frac{N_T}{\sigma D_i \sqrt{2\pi}} \exp\left\{-\frac{1}{2}\left[\frac{\text{In}\,(D_i) - \mu}{\sigma}\right]^2\right\} \quad [m^{-3}mm^{-1}] \tag{2.31}$$

The independent input, D_i, is the mean diameter of the rainfall drops which can be obtained directly from measurement. The input parameters N_T, μ and σ are obtained by regression fitting procedures with the corresponding rainfall rate, R, to yield:

$$N_T = a_o R^{b_o} \tag{2.31a}$$

$$\mu = A_\mu + B_\mu \,\text{In}\,(R) \tag{2.31b}$$

$$\sigma^2 = A_\sigma + B_\sigma \,\text{In}\,(R) \tag{2.31c}$$

where a_o, b_o, A_μ, B_μ, A_σ and B_σ all represent the regression coefficients of input parameters corresponding to the lognormal model. The lognormal distribution has been widely accepted as a

Table 2-5: Lognormal DSD parameters for different rainfall types [*Ajayi and Adimula*, 1996]

Rain type	N_T		μ		σ^2	
	a_o	b_o	A_μ	B_μ	A_σ	B_σ
Drizzle (R < 5 mm/h)	718	0.399	-0.505	0.128	0.038	0.013
Widespread 5 mm/h ≤ R ≤ 10 mm/h	264	0.232	-0.473	0.174	0.161	0.018
Shower 10 mm/h ≤ R ≤ 40 mm/h	137	0.370	-0.414	0.234	0.223	-0.034
Thunderstorm (R > 40 mm/h)	63	0.491	-0.718	0.195	0.209	-0.030

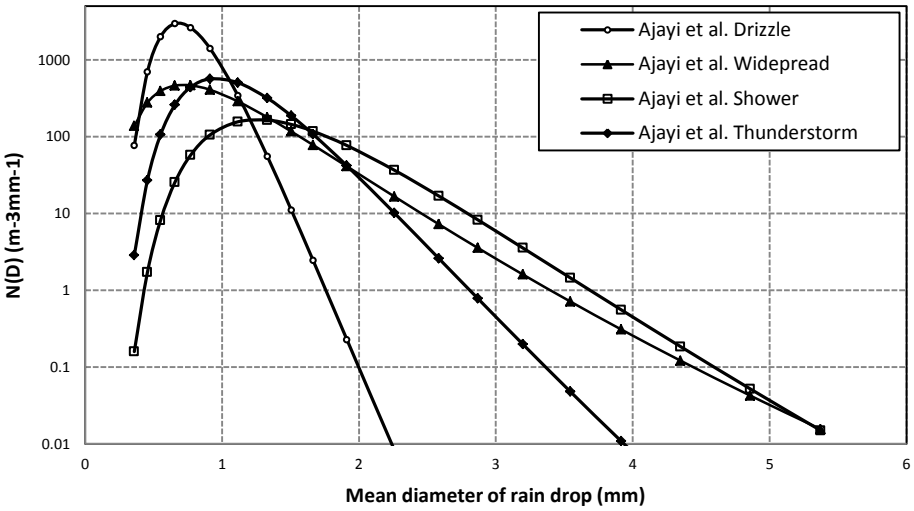

Figure 2-8: Lognormal distribution for different rainfall types using rainfall regime parameters [*Adimula and Ajayi*, 1996]

good distribution for locations with high rainfall rates [*Ajayi et al.*, 1996; *Das et al.*, 2010]. However, at low rainfall rates, it has a poor estimation of rainfall DSD. Table 2-5 and Figure 2-8 show results from the research of *Ajayi and Adimula* [1996] from tropical sites in Nigeria.

2.8.1.4. Weibull Rainfall DSD model

The Weibull DSD model was developed by *Sekine et al.* [1982; 1985] and has not been too extensively used by rainfall researchers. The two-parameter Weibull model to be applied has a modified parameter, N_w. The input parameters are β (shape parameter) and η (scale parameter). The function is given as:

$$N(D_i) = N_w \left(\frac{\beta}{\eta}\right)\left(\frac{D_i}{\eta}\right)^{\beta-1} \exp\left[-\left(\frac{D_i}{\eta}\right)^{\beta}\right] [m^{-3}mm^{-1}] \qquad (2.32)$$

In (2.32) above, the data series D_i is the input variable of a known random process *i.e.* rain drop-size. β is the shape parameter, while η is the scale parameter. Statistically, equation (2.32) increases monotically when $\beta \leq 1$ and becomes unimodal when $\beta > 1$; therefore, β is largely the determinant of the shape of the Weibull function [*Murthy et al.*, 2004]. Weibull is a type III minimum–value asymptotic distribution which has been extensively used for analysis of strength of materials and reliability studies [*Weibull*, 1951; *Murthy et al.*, 2004].

The power-law regression coefficients corresponding to (2.32) are given by:

$$N_w = aR^b \tag{2.32a}$$

$$\beta = a_\beta R^{b\beta} \tag{2.32b}$$

$$\eta = a_\eta R^{b\eta} \tag{2.32c}$$

where a, b, a_β, b_β, a_η and b_η all represent the regression coefficients of input parameters corresponding to the Weibull DSD model and R represents rainfall rate in mm/h for each rainfall sample. *Jiang et al*. [1997] observed that the Weibull model gives a good estimation for weak and strong rainfall rates, with closer performance to the modified gamma model.

2.8.1.5 Marshall-Palmer (MP) Negative Exponential Rainfall DSD Model

The negative exponential model is a special case of the modified gamma function when the shape parameter, $\mu = 0$. The popular Marshall-Palmer rain drop-size model uses this function for drop-size distribution estimation. The input parameters are the similar to those in (2.30). *Marshal and Palmer* [1948] as gives this model:

$$N(D_i) = N_o \exp(-\Lambda D_i) \quad [m^{-3}mm^{-1}] \tag{2.33}$$

The input, D_i, has the same definition as in (2.30) while the power-law relationships in (2.30*a*) – (2.30*b*) are also true for (2.33).

The MP model has been identified as inadequate for areas with high rainfall intensities like tropical regions [*Ajayi and Olsen*, 1985; *Massambani*, 1990; *Green*, 2004]. *Jiang et al.* [1997] also showed that it is most suitable for areas with low rainfall rates and temperate climates. The different variants of the MP model proposed by *Marshall-Palmer* [1948] and *Joss* [1968] are presented in Table 2-6.

Table 2-6: Negative exponential parameters for different rainfall types [*Marshall and Palmer*, 1948; *Joss*, 1968]

Models	N_o	Λ	
		a	b
General (M-P)	8000	4.1	-0.21
Joss-Drizzle	30000	5.7	-0.21
Joss-Widespread	7000	4.1	-0.21
Joss-Thunderstorm	1400	3	-0.21

2.9 Rainfall Attenuation Estimation and Prediction

2.9.1 Specific Attenuation Prediction

It follows that the total attenuation, A_T, suffered by a forward travelling electromagnetic wave interacting in a rainy medium is a function of an exponential factor with increasing distance, *d*. This expression of the attenuated wave component is given by [*Van de Hulst*, 1957; *Sadiku*, 2000]:

$$A_T = e^{-\gamma d} \tag{2.34}$$

where γ is the propagation constant with a unit equal to the inverse of unit of distance, *d*.

To find a suitable amplitudinal level for the wave component, the decibel factor is applied so that (2.34) becomes:

$$Log_{10}(A_T) = 10\, Log_{10}\, \frac{1}{e^{-\gamma d}} \tag{2.35}$$

This expression is reduced to:

$$A_T = \gamma d \times 10\, Log_{10}\, e\, [dB] \tag{2.36}$$

where *e* is a constant of the *Napierian* type logarithm equal to 2.718281828.
From (2.36), the derived attenuation also known as the path attenuation is given by:

$$A_P = 4.343\, \gamma d\ [dB] \tag{2.37}$$

which can otherwise be written in dB/km as:

$$A_s = 4.343 \times 10^3 \gamma \ [dB/km] \tag{2.38}$$

By definition, $\gamma = N(D)Q_{ext}(D)$, in [*Sadiku*, 2000] specifies the propagation constant over an averaged path in a rainy medium and $Q_{ext}(D)$ is the extinction cross section of the rainfall droplets at the plane of arrival. For an infinite number of rain droplets of diameter D, γ is defined as:

$$\gamma = \int_0^\infty N(D)Q_{ext}(D)\, dD \tag{2.39}$$

By substituting the function of γ in (2.38), another expression is derived and this is given by:

$$A_s = 4.343 \times 10^3 \int_0^\infty N(D)Q_{ext}(D)\, dD \quad [dB/km] \tag{2.40}$$

Equation (2.40) is the expression representing the specific attenuation due to rainfall droplets and $N(D)$ is the rain drop-size distribution.

2.9.2 Path Reduction Factor and Rain Cell Effects

Based on the earlier discussion on rainfall cells in section 2.5.2, it was noted that signals travelling through rainfall experiences varying degree of rainfall intensity. The rainfall intensity will depend on the structure of the rain cells. Based on this, the path reduction factor is used the estimate the actual length of the transmission path, d_o, affected by rainfall [*Crane*, 1996; *Khamis et al.*, 2005; *Sharma et al.*, 2011], this is depicted in Figure 2-9. Authors have proposed that rainfall convective cells in tropics may experience larger cell diameter and as thus, may not require path reduction; this has led to different models for path length reduction [*Khamis et al.*, 2005; *Sharma et al.*, 2011]

Some of these proposed path reduction factor models are:

- *Garcia-Lopez and Peiro* [1983] path reduction model
- *Moupfouma* [1984] path reduction model
- The CETUC model proposed by *Perez-Garcia and da Silva Mello* [2004]
- The *ITU-R P.530-13* [2009] path reduction model

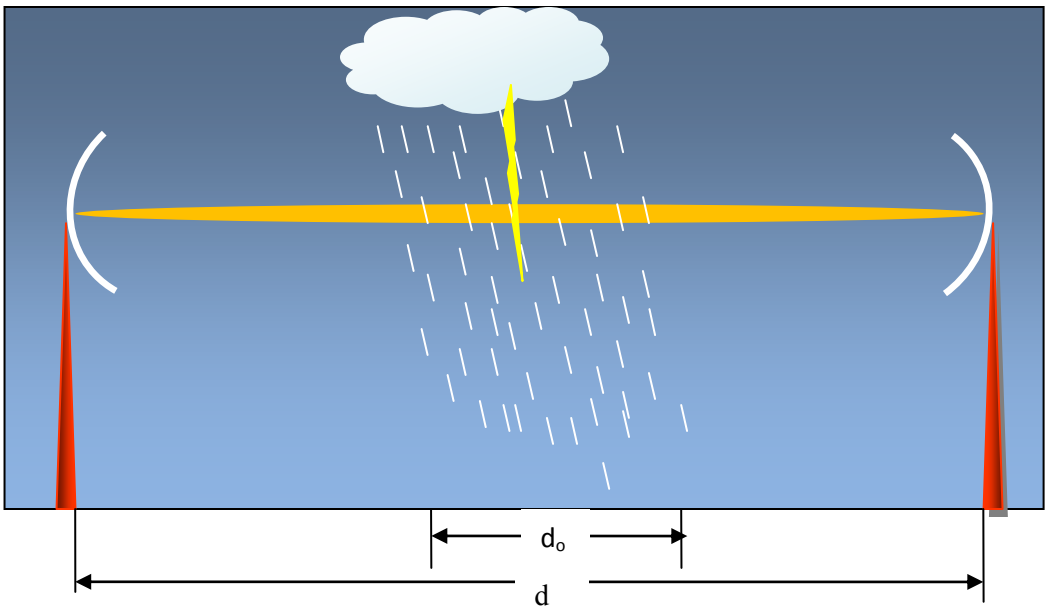

Figure 2-9: Actual link distance and actual rainfall distance

These models basically apply the rain cell theory, as well as, rainfall growth principle to determine the variation in transmission path length.

2.9.3 Path Attenuation Prediction

Rain attenuation is a very important parameter in signal propagation. It varies from region to region since it is clearly dependent on the local rainfall characteristics. Researchers have since come up with two rain parameters, which are useful in the measurement of attenuation. The rainfall path attenuation is defined as:

$$A_p\,[dB] = f(rain\ rate, rain\ DSD, frequency, temperature, distance) \qquad (2.41)$$

(2.41) is a heterogeneous quantity which depend on parameters such as specific attenuation, radio link path length, volume density of rainfall drops and the horizontal-vertical cross-section of the rainfall under consideration as seen above.

Modelling of rain attenuation can be done in three: physically, analytically and empirically ways [*Crane*, 2003; *Ojo et al.*, 2008; *Emiliani et al.*, 2009]. A simple modelling procedure is approached by defining its relationship in terms of the specific attenuation, propagation or link path length and reduction factor.

Mathematically, rainfall path attenuation in relation to rainfall specific attenuation can be obtained from ITU-R recommendation [*ITU-R P.530-13*, 2009] as:

$$A_P\ (dB) = A_s \times r \times d \qquad [\text{dB}] \tag{2.42}$$

where A_s is the specific attenuation in dB/km, r is the reduction factor and d is the link path length in km.

Olsen et al. [1978] also suggested that the rain-rate is also related by a power-law relationship to the specific attenuation (A_s) as:

$$A_s = kR_{0.01}^{\alpha} \qquad [\text{dB/km}] \tag{2.43}$$

where k and α depend on the wave frequency and polarization for a given model of the rain microstructure. They are obtained from the equations given below:

$$k = [K_H + K_V + [K_H - K_V]\, cos^2\, \theta \cos 2\tau]/2 \tag{2.44}$$

K_H and K_V are the respective polarization values in the horizontal and vertical polarization available in ITU-R P.838 [*ITU-R P.838-3*, 2005]. Also, τ and θ are the tilt angle and the elevation angle of the link respectively and are also related to α as given in 2.45 :

$$\alpha = \frac{1}{2k}\{K_H\alpha_H + K_V\alpha_V + [K_H\alpha_H - K_V\alpha_H]cos^2\, \theta \cos 2\tau\} \tag{2.45}$$

where θ is the path elevation angle and τ is the polarization tilt angle relative to horizontal. Usually, 45^o is assumed for circular polarization. The different values of k and α in (2.43) at different frequencies and polarization schemes are presented in Appendix A-2.

2.10 Effects of Rainfall in South African Areas

South Africa is located at the southernmost tip of the African continent at latitude (22^{o}S to 34^{o}S) and longitude (16^{o}E to 32^{o}E) [*Encyclopaedia Britannica*, 2009]. It is bordered by five countries: Namibia, Botswana, Zimbabwe, Swaziland and Mozambique. Based on the nomenclature of the ITU-R recommendation [*ITU-R P.837-5*, 2008], the country is classified into five rainfall zones namely: E, F, K, L and M. Figure 2-10 shows the map of South Africa with the some local cities.

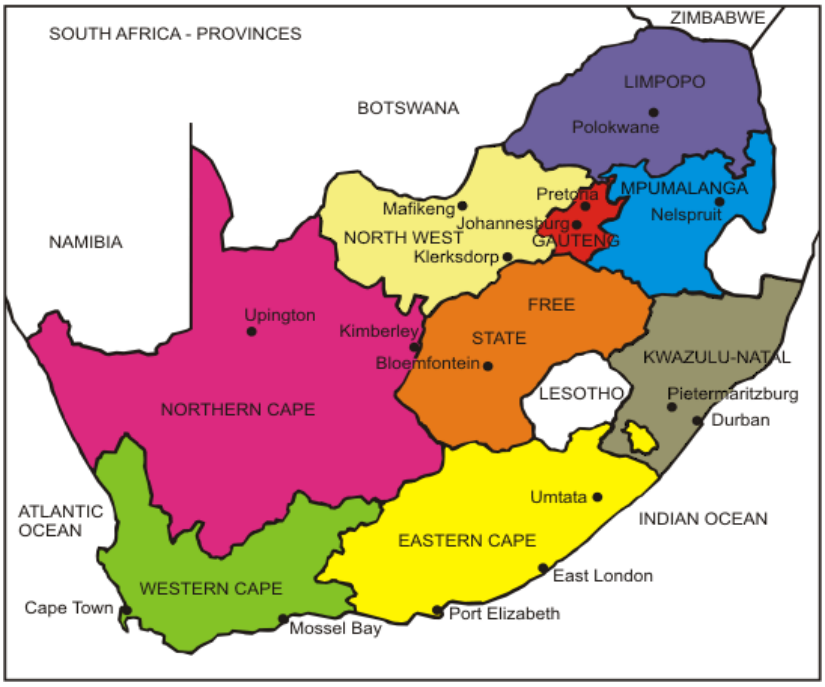

Figure 2-10: Map showing South Africa region and the surrounding countries

[http:\\www.proseo.co.za]

South Africa has a mix of several climatic variations, for example, the coastal locations are under the influence of the Indian and Atlantic oceans are predominantly wet. On the other hand, the areas in the hinterland remain mainly dry and sometimes experience snowfalls during winter. Also, the climatic conditions in South Africa are specifically dependent on the seasonal cycles. According to [*Fashuyi et al.*, 2006], there are four seasons in South Africa namely:

(i) Summer which occurs between mid-October and mid-February

(ii) Autumn which occurs between mid-February and April

(iii) Winter which occurs between May and July

(iv) Spring which occurs between August and mid-October

These four seasons largely determine the variation in rainfall and other hydrometeors throughout the year. However, the highest rainfall occurrence in South Africa usually is centred around summer period [*Fashuyi et al.*, 2006; *Odedina and Afullo*, 2008]. Figures 2-11a to 2-11c show the variation in averaged rainfall rate pattern for 1-minute converted[1] samples, at three South African cities for five years. Interestingly, the annual variations in rainfall rate for Durban and East London

[1]Converted using Fashuyi's rainfall rate conversion factors, where $R_{1\text{-min}} = 9.228 R_{60\text{-min}}^{0.8437}$

show *bimodal* peaks with a dip in rainfall rate around winter. On the contrary, the annual rainfall rate variation in Cape Town can be said to be *unimodal* with its peak coinciding to winter period in other cities. This anomaly has been explained in the studies of *Fashuyi et al.* [2006] and *Owolawi et al.* [2008].

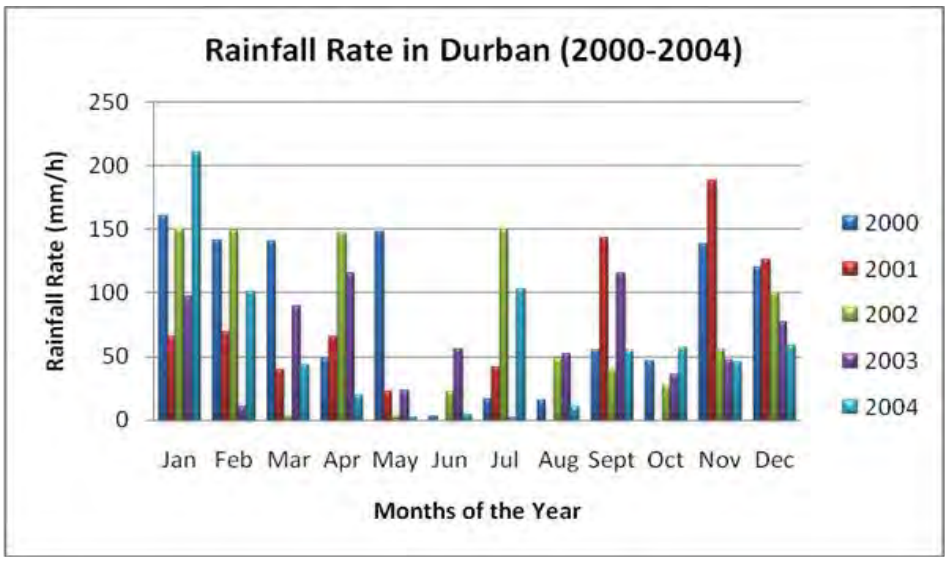

Fig 2-11a: Annual rainfall rate variation in Durban for a 5-year period

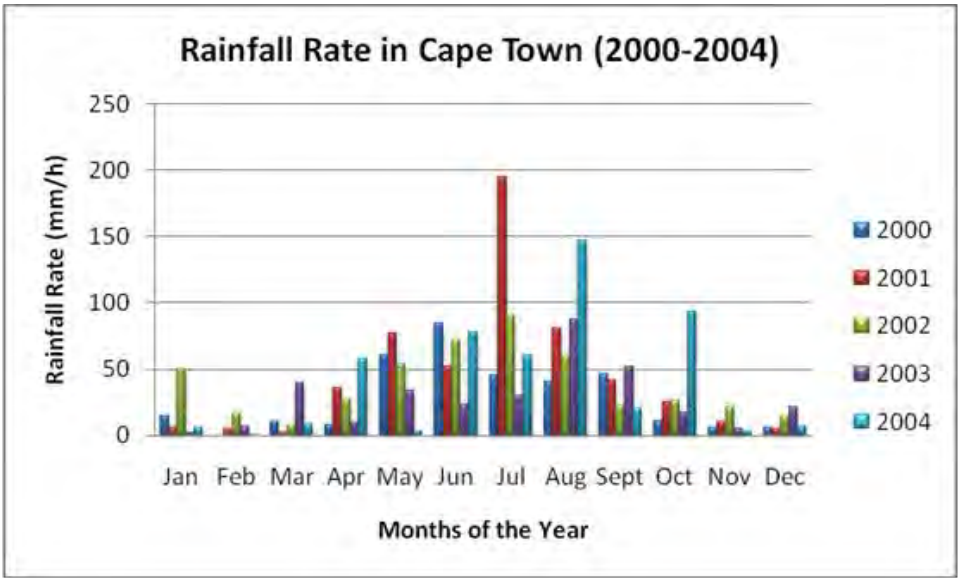

Fig 2-11b: Annual rainfall rate variation in Cape Town for a 5-year period

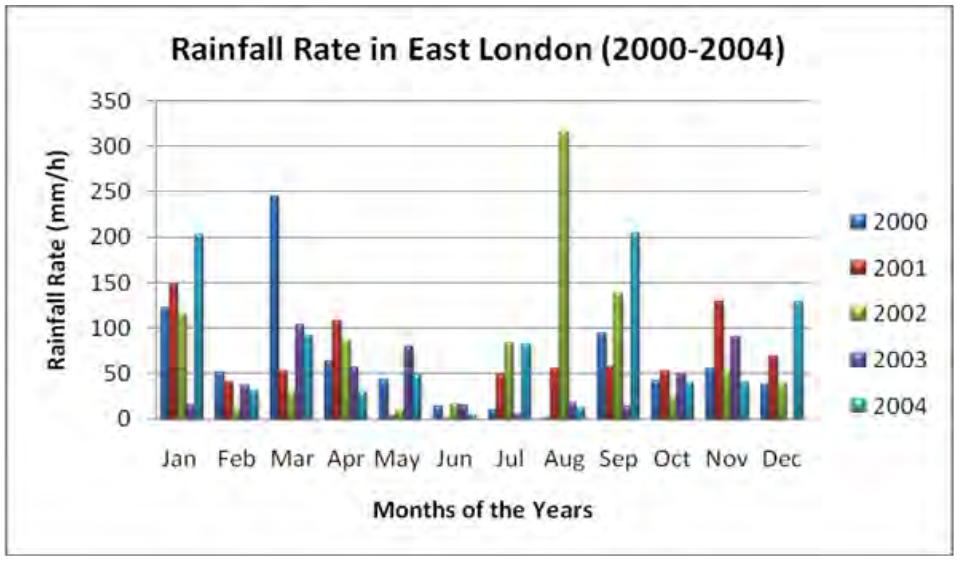

Fig 2-11c: Annual rainfall rate variation at East London for a 5-year period

2.10.1 Progress in Microwave Studies in South Africa

Over the years, studies carried out have shown the relationships between rainfall parameters and the validity of ITU-R model in South Africa. Interestingly, most of the studies were executed at the University of KwaZulu-Natal, Durban. The research mainly focused on rainfall rate modelling and attenuation prediction for different locations in South Africa. *Fashuyi et al.* [2006] used one-minute integration time to obtain the rainfall rate CDFs for 12 locations in South Africa using five year data span. The results showed that Richard's Bay had the highest rain rate intensity at 182.66 mm/h, while Brandvlei had the lowest with 67.02 mm/h. New climatic zones (N, M, P and Q) were also proposed for South Africa.

Owolawi et al. [2008] further considered the rainfall characteristics for four locations (Durban, Richard's Bay, Cape Town and Pretoria in South Africa. In that research, it was determined that all the locations except Cape Town had summer season as the peak of their rainfall and worst month radio performance. A relationship was established between the average worst month and average year percentage of exceedences using one-minute integration time. *Odedina et al.* [2008] later obtained the seasonal CDFs of rainfall rate and seasonal attenuation for five locations (Durban, Pretoria, Cape Town, Bloemfontein and Brandvlei) using ITU-R model. In addition, the research used a 19.5 GHz LoS link at 6.73km link distance to obtain attenuation values for Durban.

Odedina and Afullo [2009b] developed a multipath propagation model using LoS links at 19.5 GHz at 6.73 link path between Howard Campus and Westville Campus of the University of KwaZulu-

Natal in Durban to obtain data for clear-air propagation and compared it with ITU-R propagation model. *Mulangu and Afullo* [2009], while investigating the effects of rain on propagation coefficients in Botswana, were able to establish a similarity in the behaviour of rainfall DSD with some locations in Botswana and Durban. It was finally established that the Tropical Thunderstorm (TT) model was most suitable for Botswana when the rain rate greater than 21 mm/h. *Owolawi et al.* [2007] supported the results of seasonal variability of rainfall in *Fashuyi et al.* [2006] and observed the differences in the rainfall pattern along the western and eastern Cape of South Africa. It was also verified that the modified Moupfouma model appears to be suitable in the estimation of rain distribution in South Africa.

More recently, attempts have been made to compare existing rainfall DSD models for the city of Durban [*Odedina and Afullo*, 2009a; *Odedina and Afullo*, 2010; *Odedina*, 2010a, 2010b]. From these results, the lognormal rainfall DSD and modified gamma DSD models proved effective for Durban. In a related work, the latest reports by *Afullo* [2011] and *Owolawi* [2011] attempted different modelling techniques for the derivation of the two mentioned rainfall DSD models for Durban.

However, the progress so far in rain attenuation studies in South Africa has suggested the need to improve the modelling techniques. Since the application of rain studies is useful in terrestrial and satellite communication systems, it is imperative that localized models for both rainfall rate and rainfall DSD be developed from the existing models. The benefit of this model will be a milestone in solving and validating similar models, which are largely been unsuitable for the observed rainfall pattern in South Africa.

2.11 Chapter Summary

This chapter is mainly concerned with the background studies involving the propagation of microwave and millimetric waves for terrestrial communication. Rainfall has been identified as the paramount agent in all types of hydrometeor-induced attenuation in microwave and millimetric communication systems. Therefore, the discussions in this chapter have focused mainly on the microstructure and the physics of rainfall phenomena in wave propagation. A review of rainfall studies, using various analytical, statistical and empirical functions to describe rainfall rate and rainfall drop-size distribution, was examined. It is shown that rainfall attenuation can be predicted

using any of the models discussed, albeit using values specific to regional climatic conditions. Finally, the climatic region of South Africa and its unique rainfall features was briefly examined.

The next chapter describes rainfall rate, a microstructural parameter and the general importance of its mechanism to the understanding of rainfall attenuation. The modelling procedure and results from rainfall measurement undertaken in Durban is examined.

CHAPTER THREE

Rainfall Rate Modeling and Analysis

3.1 Introduction

Rainfall rate is one of the microstructural parameters required to determine the threshold of rainfall attenuation in a locality. As seen in the documentations of *Crane* [1996] and *ITU-R recommendation P. 530-13* [2009], it is an integral tool linked to the measurement of rainfall attenuation at different levels of signal propagation. Point rainfall rate measurements provide a good description of the spatial and temporal variation of rainfall within a rain cell. More importantly, the concept of point rainfall rates can be better explored when approached from an empirical perspective *i.e*. from rainfall database. Therefore, empirical evidence from rainfall can provide a suitable avenue to explore the development of local rainfall empirical models. Previous studies [*Fashuyi et al.*, 2006; *Owolawi and Afullo*, 2007; *Odedina and Afullo*, 2008; *Owolawi*, 2010] on different locations have provided information on the rainfall rate variability around South Africa. However, these research have mainly been undertaken using a "generalized" concept for the rainfall rate conversion from hourly rainfall rates. The closest study to 1-minute rainfall sampling was undertaken by *Owolawi* [2010; 2011a], although, 5-minute rainfall sampling was considered in his research.

In this chapter, one-minute rainfall samples are analyzed under different rainfall classifications: monthly, seasonal, event/regime based and annual while their respective rainfall rate exceedences are computed. Based on the temporal classification of rainfall samples, estimators for different statistical models are proposed using the method of maximum likelihood (ML). The suitability of each proposed model for the temporal rainfall classification undertaken is examined using error statistic tests and the appropriate model(s) are determined.

3.2 Rainfall Rate Measurement

Rainfall rate is generally defined as being proportional to the third moment of the rainfall drop-size distribution as observed in expression in (2.14). The measurement of rainfall rate is dependent on the measuring instrument being deployed for such purpose. *Ajayi et al.* [1996] already identified various equipment used in rainfall measurement. In this study, a rainfall rate measurement campaign spanning two-years is undertaken at the control site and consequent analysis is

undertaken to understand the data. The disdrometer has been chosen for this study because it has an advantage of providing point rainfall measurement related the dynamic heterogeneous changes in the spatial distribution of rainfall droplets, and hence, rainfall rate [*Chen et al*., 2011].

3.3 Data Acquisition

In the rainfall campaign undertaken in this chapter and succeeding chapters, all rainfall measurements are obtained from two independent sources. The main measurements for this research work were undertaken at the Howard campus control site of the University of KwaZulu-Natal, Durban using a Joss-Waldvogel RD-80 impact disdrometer. The period of rainfall measurement spanned two years, precisely from January 2009 to December 2010 although few instances of outages were experienced. The information from the database - are one-minute sampled - rainfall rate data and rainfall drop-size density data for the city of Durban, South Africa. The second measurements were obtained from the South African Weather Service (SAWS) network of rain gauges undertaken between January 2000 and December 2004. The database used here contains five-year hourly (or 60-minute) rainfall rate samples for eight different locations in South Africa.

3.3.1 Joss-Waldvogel RD-80 Impact Disdrometer

The Joss-Waldvogel RD-80 impact disdrometer is a rainfall data acquisition system specifically designed to measure in real-time rainfall microstructural parameters - among which include - rain rate, rainfall drop-size, rain accumulation and rain reflectivity. It is a product of Disdromet Ltd, Switzerland [http://www.distromet.com/83/Product_Description/Data_Aquisition.html].

The RD-80 disdrometer (or distrometer) is an improvement of the earlier version RD-69 that adopts the *Gunn and Kinzer* [1949] concept of rainfall diameter interval and drop terminal (or fall) velocity. The data acquisition system consists of two independent units connected to the microcomputer via an RS-232 Ethernet link: the outdoor unit and the indoor unit. Figure 3-1a shows the system architecture for the disdrometer set-up and Figure 3-1b shows the circuit block diagram of the disdrometer. The outdoor unit is an electromechanical assembly that amplifies generated signals from the pressure transducer due to the impact of rain drops on the topmost cone; of sampling area with a volumetric sweep of 0.005 m^2 at a sampling time of 60 seconds. On the other hand, the indoor unit is an embedded system with signal processing capacity; it also acts as a processing interface to the computer archive. The generated signal from the outdoor unit is sent via

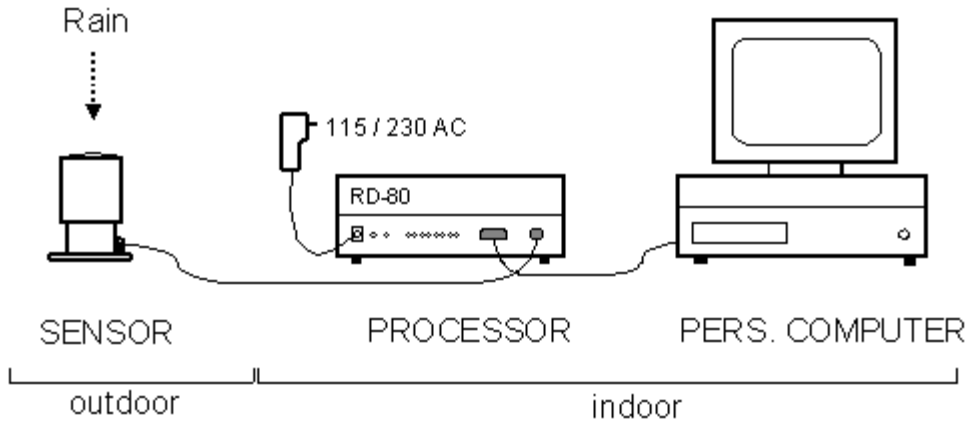

Figure 3-1a: Joss-Waldvogel RD-80 impact disdrometer system architecture showing the outdoor and indoor units with the personal computer (archive) (RD-80 product information: http://www.distromet.com/1_index_e.htm)

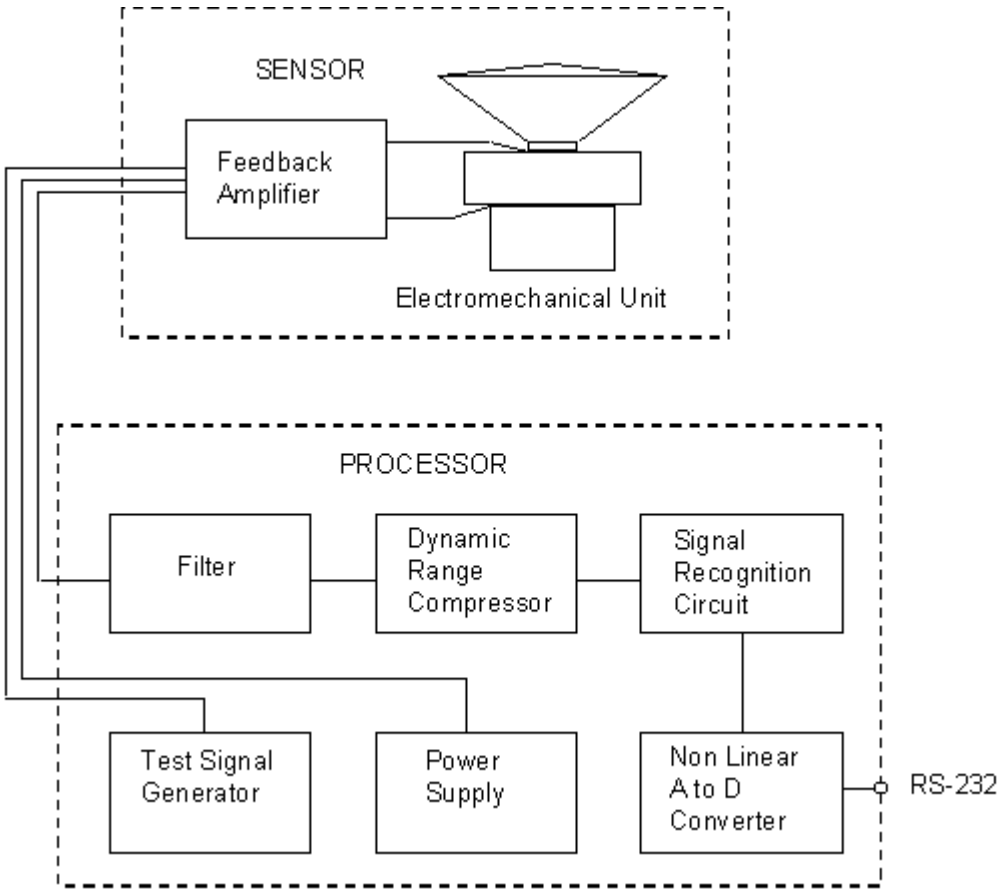

Figure 3-1b: Circuit block diagram for the connection of several units of RD-80 disdrometer (RD-80 product information: http://www.distromet.com/1_index_e.htm)

the Ethernet link to the indoor unit where it undergoes signal processing algorithms to compute the required real-time rainfall parameters. The processed data generated from the indoor unit is archived to the microcomputer via a proprietary software in a file readable format from which it can be accessed later.

The disdrometer has an inbuilt instrumentation capable of detecting rainfall drops of 20 diameter classes (from 0.359 mm to 5.373 mm) with 20 dedicated bins at 5 % measurement accuracy. The diameter range for each class is equivalent to $\left(D \pm \frac{\Delta D}{2}\right)$ mm, so that the minimum bound for any class is $\left(D - \frac{\Delta D}{2}\right)$ mm, while the maximum bound is $\left(D + \frac{\Delta D}{2}\right)$ mm. Appendix D-1 show the details of the disdrometer reference table for each diameter classes, lower diameter thresholds and their corresponding fall velocities and diameter intervals.

3.3.2 Data Processing and Rainfall Categorisation

The J-W RD-80 disdrometer is installed at the School of Electrical, Electronics and Computer Engineering, University of KwaZulu-Natal, Durban at spatial coordinates of longitude 29°52'S and latitude 30°58'E at a vertical height of 139.7 m. The measurements were taken over a period of two years between January 2009 and December 2010, although a few instances of equipment outages were experienced.

It should be noted that the highest rainfall rate recorded was 117.15 mm/h, while the lowest rainfall rate was 0.003 mm/h. As explained earlier on, rainfall events can undergo event transition from lower rainfall types to higher rainfall types. One of such notable event occurred on April 25, 2009 between 1621 hours and 1722 hrs where a maximum rainfall rate of 117.15 mm/h was recorded. In this particular event, it is observed that all the various rainfall types were present. The rainfall started as a drizzle rain type, and later transited into widespread and shower types. On attaining its peak as thunderstorm rainfall type at 1639 hrs, it gradually decayed. This rainfall event progression can be seen in Figure 3-2.

Generally, the disdrometer computes rainfall rate based on 20 independent bins with computations similar to (2.15). The computation for rainfall rate is the same derived from (2.11) to (2.15) but with a maximum bound equal to 20 [*Bartholomew*, 2009], so that:

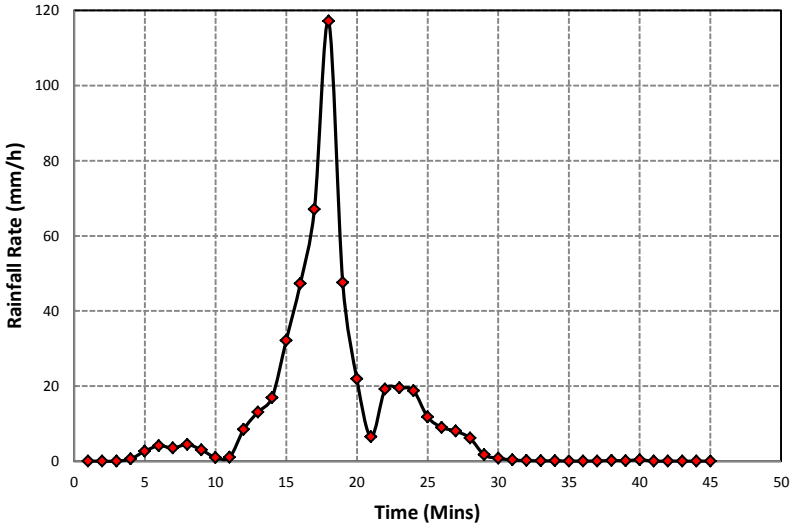

Figure 3-2: Time series of thunderstorm event in Durban on April 25, 2009 between 1621 hours and 1722 hours.

$$R = \frac{6\pi \times 10^{-4}}{A \times T} \sum_{i=1}^{20} C_i D_i{}^3 = \sum_{i=1}^{20} R_i \quad [mm/h] \tag{3.1}$$

and, the rainfall DSD, is given as:

$$N(D_i) = \frac{C_i}{A \times T \times v(D_i) \times \Delta D_i} \quad [m^{-3}mm^{-1}] \tag{3.2}$$

where in (3.1) and (3.2), A is the sampling area given as 0.005 m^2, T is the disdrometer sampling time given as 60 seconds, C_i is the number of rain drops available at the ith diameter bin and D_i is the average diameter of the ith bin. The fall velocity is $v_t(D_i$ and ΔD_i is the diameter interval of the rain drops.

The rainfall accumulation or rainfall amount [*Bartholomew*, 2009], on the other hand, is computed by the disdrometer per diameter bin as:

$$R_A = R \times \frac{T}{3600} = \frac{\pi \times 10^{-6}}{A} \sum_{i=1}^{20} C_i D_i{}^3 \quad [mm] \tag{3.3}$$

where R_A is the rainfall accumulation or rainfall amount in mm for a period of 60 seconds.

Based on recommendations from the related work on filtering and processing of disdrometer data [*Das et al.*, 2010], some factors were taken into consideration as follows:

1. Rain rate samples with total sum of drops less than 10 were discarded.
2. A minimum duration of five minutes was assumed as the interval between two independent rain events. A rain event is described as the period encompassing the complete duration of rainfall.

The one-minute samples obtained from the RD-80 disdrometer after this procedure were regrouped based on the following criteria:

- Monthly variation of rainfall rate
- Seasonal variation of rainfall rate
- Event or regime variation of rainfall rate

The seasonal classification for rainfall is based on the seasonal cycle of rainfall rate pattern in Durban earlier explained in section 2.10. The event or regime variation, the maximum rain rate recorded in a single rain event was considered. A total of 1301 rainfall events were recorded in Durban after data processing with 1141 drizzle events, 75 widespread events, 69 shower events and 16 thunderstorm events. The rainfall samples are then separated into four different rainfall types

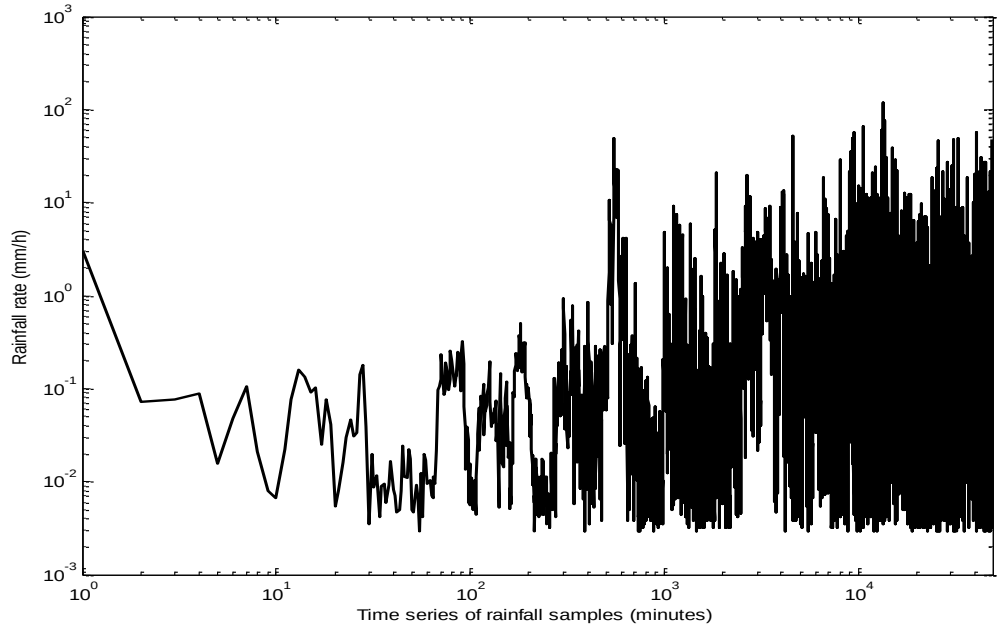

Figure 3-3: Time series of the annual rainfall rate in Durban for the two year disdrometer measurement (48, 195 rainfall samples)

based on the highest occurring rainfall rate in an event namely: drizzle (0 mm/h < R < 5 mm/h), widespread 5 mm/h ≤ R < 10 mm/h , shower 10 mm/h ≤ R < 40 mm/h and thunderstorm R ≥ 40 mm/h). Figure 3-3 shows the time series resolution of all the filtered samples for the period of measurement. Table 3-1 provides statistical information on the collected data from the two-year disdrometer measurement in Durban.

Table 3-1: Statistical Information obtained from RD-80 disdrometer for Durban for the period of measurement

CATEGORY	Number of Samples	Maximum Rainfall Rate (mm/h)	Total rainfall time (minutes)	Percentage of Group Data (%)
Annual	48, 195	117.15	803.25	100
MONTHLY				
January	10225	48.93	170.42	13.07
February	9559	52.19	159.32	12.22
March	6845	66.25	114.08	8.75
April	5261	117.15	87.68	6.73
May	5369	76.43	89.48	6.86
June	4597	38.61	7.65	5.88
July	3978	22.36	66.3	5.09
August	3795	12.60	63.25	4.85
September	5977	12.45	99.62	7.64
October	6853	20.37	114.22	8.76
November	6836	57.67	113.93	8.74
December	8937	47.83	148.95	11.42
SEASONAL				
Summer	22770	57.67	379.5	47.25
Autumn	8995	117.15	149.92	18.67
Winter	3878	76.43	64.63	8.05
Spring	12552	20.37	209.2	26.03
EVENT				
Drizzle	36461	4.99	607.68	65.93
Widespread	8710	9.97	145.17	15.75
Shower	9134	38.61	152.23	16.52
Thunderstorm	998	117.15	16.63	2.8

3.4 Analysis of Rainfall Rate Data for Durban

The statistical information obtained for Durban is based on the cumulative distribution function (CDF) for the period of measurement. The CDFs obtained are for the monthly, seasonal, event and annual rainfall rates in Durban using the two-year rainfall measurements from disdrometer.

3.4.1 Monthly distribution of Rainfall rate

For the monthly distribution in Durban, a double maxima or bimodal pattern is observed throughout the years of 2009 and 2010 at their respective $R_{0.01}$; this was earlier mentioned by *Owolawi* [2006]. Durban, as with most other South African cities, has this monthly cycle pattern except locations around coastal Western Cape Province.

Figures 3-4 presents the monthly distributions for each of the months for the period of measurement. The respective rainfall rate percentage exceedences at 1%, 0.1%, 0.01% and 0.001% are also presented in Table 3-2. The rainfall rate for the months of April is observed to the highest with $R_{0.01}$ = 90.83 mm/h; April is the threshold month prior to the commencement of winter in Durban. Generally, the values of monthly $R_{0.01}$ are observed to rise from the January to April signifying the climax of the summer season in Durban. The summer season is characterised by intense rainfall at higher rainfall rates. From the months of May to August, there is a gradual decrease in the values of $R_{0.01}$ due to influence of winter. The rainfall pattern in August and September are also observed to be similar, being the lowest among the months with $R_{0.01}$ = 12.16 mm/h and 12.32 mm/h respectively. This may be due to the after-effects of severe "dry spell" winter with lower rainfall rates in Durban. From the months of September, the $R_{0.01}$ for the succeeding months are observed to increase due to the onset of spring season, although it appears there is an overlapping of winter and spring seasons. There is also a sharp rise in the rainfall rate

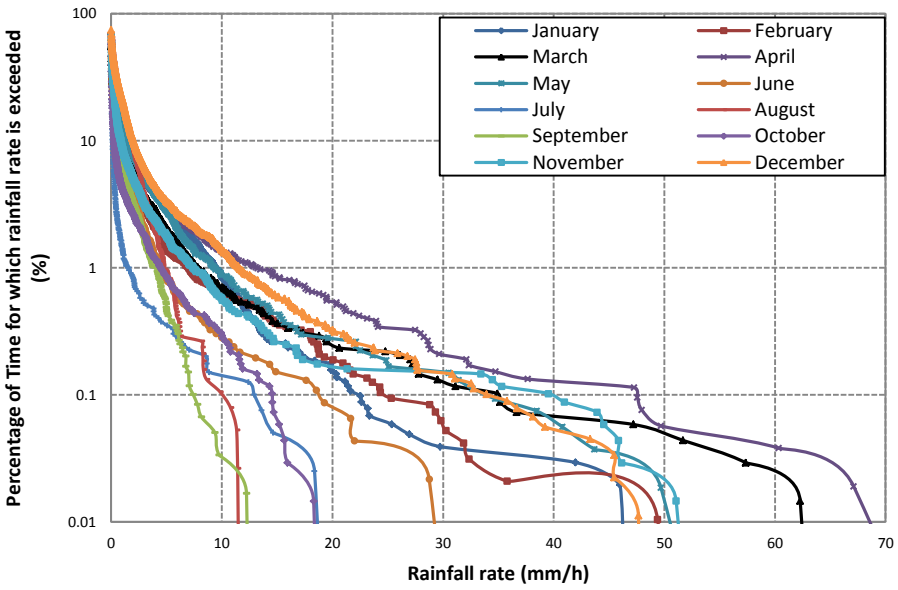

Figure 3-4: Monthly cumulative distribution of rainfall rate in Durban for the period of measurement

Table 3-2: Monthly statistics on rainfall rate exceeded in Durban for the period of measurement

Time for which rainfall rate is exceeded (%)		1	0.1	0.01	0.001
JANUARY	(mm/h)	9.445	22.33	46.22	48.65
FEBRUARY		7.024	24.75	49.51	51.92
MARCH		7.85	34.96	63.54	65.99
APRIL		13.14	47.49	90.83	114.52
MAY		9.34	33.94	62.08	75
JUNE		4.47	18.82	34.07	38.16
JULY		1.60	12.94	20.78	18.28
AUGUST		4.76	10.04	12.16	12.56
SEPTEMBER		4	7.42	12.32	12.44
OCTOBER		4.47	14.55	18.95	20.23
NOVEMBER		7.39	39.76	53.15	57.22
DECEMBER		11.57	34.04	47.68	47.82

in November at $R_{0.01}$ = 53.15 mm/h and a slight drop in December at $R_{0.01}$ = 47.68 mm/h.

From the above analysis, it is obvious that the first five months and last three months of the year are the wettest periods of intense microwave attenuation due to rainfall. This has been confirmed in the studies of *Odedina and Afullo* [2008] and *Odedina* [2010b].

3.4.2 Seasonal Variation of Rainfall rate

The influence of seasonal variation on the coastal city of Durban has been explained in section 2.10. The four seasons in Durban are, therefore, a function of the monthly variations in rainfall as discussed in the immediate section 3.4.1.

From the result provided in Figure 3.5, it is observed that the rainfall rate exceedences for autumn season at $R_{0.01}$ = 72.15 mm/h is the highest. It is suspected that this might be as a result of the overlapping seasonal transition between the summer and autumn season in the month of April. The seasons of summer and winter are also observed to have closer values of $R_{0.01}$ at 50.48 mm/h and 53.37 mm/h respectively. The season of spring has the lowest $R_{0.01}$ at 18.51 mm/h. Even though the winter season has a high $R_{0.01}$ value, it does appear that rainfall is not generally high during winter; this can be seen in Table 3-1. There are fewer rainfall samples at high rainfall rates suggesting the preponderance of low rainfall rate samples. In comparison with winter season, summer has more rainfall samples with high rainfall rates, and therefore, will suffer more intense rainfall attenuation.

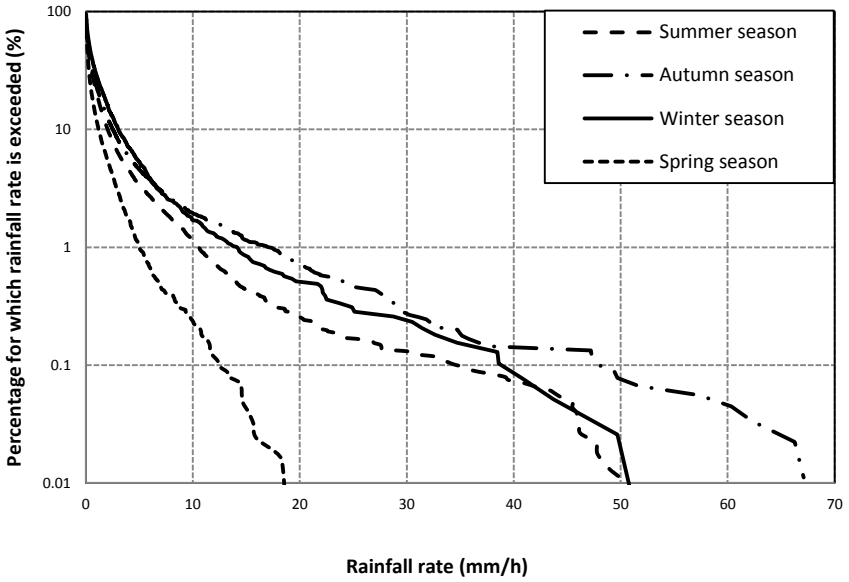

Figure 3-5: Cumulative distribution of rainfall rate in Durban for different seasons between 2009 and 2010

Table 3-3: Seasonal statistics on rainfall rate exceeded in Durban for the period of measurement

Time for which rainfall rate is exceeded (%)		1	0.1	0.01	0.001
SUMMER	(mm/h)	10.52	34.64	50.48	56.42
AUTUMN		17.18	47.98	72.15	112.65
WINTER		14.15	38.88	53.37	75.40
SPRING		5.025	12.52	18.51	20.14

The seasonal distribution of rainfall in Durban seem to suggest rainfall attenuation usually peaks at months closer to the onset of winter, this has earlier been verified in the study of *Odedina* [2008].

3.4.3 Event distribution of Rainfall Rate

In this section, event classification of rainfall rate in Durban is done for four rainfall types: drizzle, widespread, shower and thunderstorm. It is clearly observed from Table 3-1 that Durban experiences a large percentage of drizzle rainfall, followed by widespread rainfall and then shower rainfall. Thunderstorm events are fewer, for example, only 2.8% of the total rainfall events for the period of measurement are of thunderstorm types.

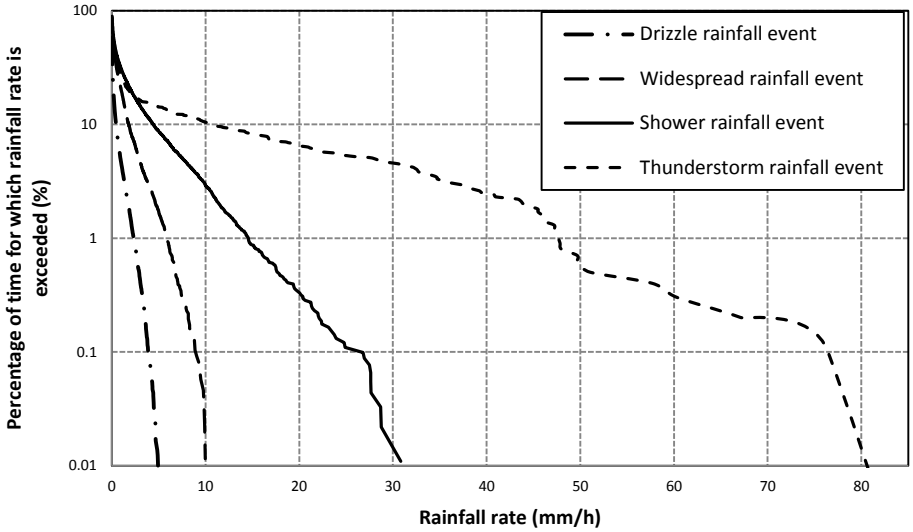

Figure 3-6: Event distribution of rainfall rate in Durban for different rainfall types between 2009 and 2010

Table 3-4: Rainfall events statistics on rainfall rate exceeded in Durban for the period of measurement

Time for which rainfall rate is exceeded (%)		1	0.1	0.01	0.001
Drizzle	(mm/h)	2.32	3.87	4.92	4.99
Widespread		5.86	8.94	9.96	9.97
Shower		14.56	26.54	31.52	37.90
Thunderstorm		47.66	76.52	82.5	116.74

The results from the rainfall measurements for events are presented in Figure 3-6 and Table 3-4. It is found that drizzle events have $R_{0.01}$ = 4.92 mm/h; widespread events with $R_{0.01}$ = 9.96 mm/h; shower events at $R_{0.01}$ = 31.52 mm/h and thunderstorm events at $R_{0.01}$ = 82.5 mm/h. It is worthy to note that the first two types of rainfall events both have their 0.01% rainfall exceedances closer to their maximum values suggesting that many rainfall samples exists closer to their $R_{0.01}$.

Most importantly, since microwave and millimeter wave communication links are severely affected by rainfall droplets at higher rainfall rate, it will be necessary to take cognizance of the thunderstorm events in rainfall design.

3.4.4 Annual Distribution of Rainfall Rate

The annual distribution of rainfall rates for the 1-minute data from Durban for the period of measurement is shown in the graph in Figure 3-7. Based on the graph, it can be seen that the rainfall rate exceeded at 1% of time is 10.6 mm/h; at 0.1 % of time is 34.66 mm/h; 0.01% of time is 60.69 mm/h and at 0.001% is 97.53 mm/h. The highest rainfall rate recorded for the measurement period is 117.15 mm/h.

Interestingly, the measured value of the rainfall exceeded at $R_{0.01}$ is closer to the recommended value from ITU-R P.837 at 60 mm/h for region L (discussed in 2.7.1.1) and the global Crane model at 61.6 mm/h for region D3 (discussed in 2.7.1.2). Therefore, it does buttresses the recent study of *Owolawi* (2011a) where the classification of Durban corresponds with suggestions of ITU-R and Crane rainfall zones for South Africa.

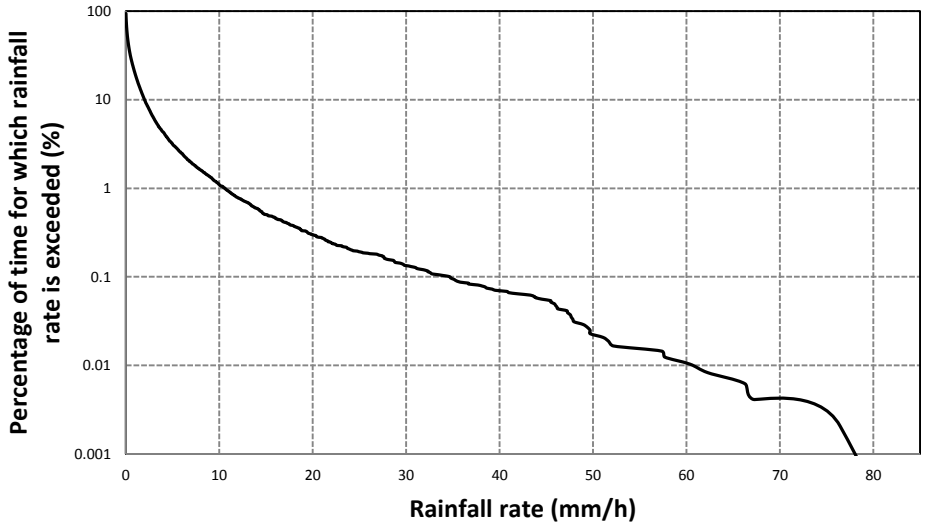

Figure 3-7: Annual distribution of rainfall rate in Durban between 2009 and 2010

3.5 Method of Maximum Likelihood Estimation Technique

The method of maximum likelihood (or ML) is a useful statistical tool often used in the point estimation of parameters related to a probability density function (PDF) of a random or deterministic quantity. The method employs the dynamic sampling of a quantity and maximizes the unknown parameters of the PDF by applying differential calculus to the log likelihood of the function.

In order to compute the maximum likelihood estimator of a density or mass function, an assumption of a continuous or discrete variability of the independent variable(s) is considered. *Cohen et al.* [1980] and *Kreyszig* [2006] describes the procedure for the maximum likelihood estimation with assumptions from the PDF of a function. Assuming the probability density function of a quantity with a continuous random variable, x, exists such that it has nth number of unknown parameters β_1, $\beta_2, \beta_3, \ldots . \beta_n$ is given by:

$$\text{pdf} = f(x; \beta_1, \beta_2, \beta_3, \ldots, \beta_n) \tag{3.4}$$

If the variable, x, is a product of a series of experimental procedure such that k independent events or observations are undertaken so that we have a row matrix for samples of x given by $x_1, x_2, x_3, \ldots, x_k$. Then, the likelihood function for all the events is given as:

$$L = f(x_1; \beta_1 \ldots \beta_n) \times f(x_2; \beta_1 \ldots \beta_n) \times \ldots \times f(x_k; \beta_1 \ldots \beta_n) = \prod_{i=1}^{k} f(x_i; \beta_1, \beta_2, \ldots \beta_n) \tag{3.5}$$

where,

$$L = L(x_1, x_2, x_3, \ldots, x_k | \beta_1, \beta_2, \beta_3, \ldots, \beta_n) \tag{3.6}$$

By finding the logarithm of the expression in (3.5), we develop the log likelihood of the PDF expression. This can be written as:

$$M = \ln(L) = \ln\left(\prod_{i=1}^{k} f(x_i; \beta_1, \beta_2, \ldots \beta_n) \right) \tag{3.7}$$

which according to the laws of logarithm can be written as:

$$M = \sum_{i=1}^{k} \ln\left(f(x_i; \beta_1, \beta_2, \ldots \beta_n) \right) \tag{3.8}$$

The maximization of (3.8) can be achieved by solving simultaneously, the partial derivatives of β_1, $\beta_2, \beta_3, \ldots . \beta_n$ set to zero, for nth system of equations so that:

$$\frac{\partial M}{\partial \beta_1} = 0$$
$$\frac{\partial M}{\partial \beta_2} = 0$$
$$\vdots$$
$$\frac{\partial M}{\partial \beta_n} = 0 \tag{3.9}$$

The solution of (3.9) these partial derivatives represent the maximum likelihood estimators of the PDF in (3.4). This method can provide a sufficient description of the input estimators applicable to a statistical function.

3.5.1 Gamma Rainfall Rate Parameter Estimation

The shape and scale parameters of the gamma model in 2.7.1.4. can be found by employing the ML method. *Thom* (1958) describes these estimators, $\hat{\alpha}$ and $\hat{\beta}$, using the ML method as:

$$\hat{\alpha} = \frac{1 + \left(1 + \frac{4\omega}{3}\right)^{\frac{1}{2}}}{4\omega} \tag{3.10}$$

and,

$$\hat{\beta} = (N_s \hat{\alpha}) \Big/ \sum_{J=1}^{N} x_j \tag{3.11}$$

N_s is taken as the number of samples of rainfall rate and x_j is the rainfall rate value at j=1 to N_s. The related parameter, ω, is defined as:

$$\omega = \ln\left(\frac{1}{N_s}\sum_{j=1}^{N_s} x_j\right) - \frac{1}{N_s}\left(\ln \sum_{j=1}^{N_s} x_j\right) \tag{3.12}$$

3.5.2 Lognormal Rainfall Rate Parameter Estimation

The two-parameter lognormal model is governed by two physical quantities specified by the mean μ and standard deviation σ. The ML estimators, $\hat{\mu}$ and $\hat{\sigma}$, are defined in *Eckhard et al.* [2001] and *Suhaila and Jemain* [2007] as:

$$\hat{\mu} = exp\left[\frac{1}{N}\sum_{i=1}^{N} Ln(x_i)\right] \tag{3.13}$$

$$\hat{\sigma} = exp\left[\left(\frac{1}{N-1}\sum_{i=1}^{N}\left[ln\left(\frac{x_i}{\hat{\mu}}\right)\right]^2\right)^{\frac{1}{2}}\right] \tag{3.14}$$

where N represents the number of rain samples in an event and x is the value of the rainfall rate at i = 1 to N.

3.5.2 Weibull Rainfall Rate Parameter Estimation

The Weibull rainfall rate model follows the two-parameter model proposed in (2.32) without N_o. In this case, the shape and the scale parameter of the rainfall rate model are, γ and η. The ML estimators for the Weibull function is defined in *Wong* [1977] and *Owolawi* [2011a] are governed by:

$$\hat{\gamma}(x) = \gamma(x-1) + h(x) \tag{3.16}$$

$$\hat{\eta}(x) = \eta(x-1) + k(x) \tag{3.17}$$

where the terms of h and k are corrections with an iteration terminated close to 0.002 using Newton-Raphson method at the xth iteration. These correction factors are given as:

$$\begin{bmatrix} h \\ k \end{bmatrix} = \begin{bmatrix} \frac{\partial^2 ln\,(L)}{\partial\gamma^2} & \frac{\partial^2 ln\,(L)}{\partial\gamma\partial\eta} \\ \frac{\partial^2 ln\,(L)}{\partial\gamma\partial\eta} & \frac{\partial^2 ln\,(L)}{\partial\eta^2} \end{bmatrix}^{-1} \begin{bmatrix} -\frac{\partial ln\,(L)}{\partial\gamma} \\ -\frac{\partial ln\,(L)}{\partial\eta} \end{bmatrix} \tag{3.18}$$

3.6 Comparison of Rainfall Rate Models

The rainfall models are compared using rainfall events classifications and the overall annual measurements from the disdrometer. The results are presented in the following sections.

3.6.1 Rainfall Rate Modelling for Rainfall Events Types

Under the rainfall events types, the gamma, lognormal, Weibull and Moupfouma I models are compared with the 1-minute rainfall measurements from Durban. The rainfall types considered in this section are of drizzle, widespread, shower and thunderstorm types. The parameters in Table 3-5 for the different rainfall types are derived from the simulations obtained from the ML method. The Moupfouma I model has been described in section 2.7.1.3 of chapter two.

As seen from the results presented in the graphs in Figures 3-8 to 3-11, there is varying degree of model performances as the rainfall type progress to a higher rainfall rate. In figure 3-8, the Weibull model appears to give the best estimation to the measurement for drizzle rainfall types, the gamma model and lognormal model follow respectively in providing good fits. The Moupfouma model is seen to have poor fits, widely under-estimating the measurements at most points of the plot.

Table 3-5: Estimators for different rainfall types in Durban

EVENT	Gamma model		Lognormal model		Weibull model		Moupfouma I model		
	α	β	μ	σ	γ	η	*a*	*b*	*u*
Drizzle	0.3136	0.5352	0.0189	9.7897	0.4359	0.0598	0.0198	3.2416	0.025
Widespread	0.4122	1.5618	0.1314	8.9935	0.5445	0.3718	0.01785	2.1473	0.025
Shower	0.3662	4.0931	0.2411	10.7637	0.5012	0.7437	0.0096	1.0957	0.025
Thunderstorm	0.2405	15.6382	0.1924	17.0055	0.3748	0.7867	0.01972	0.5196	0.025

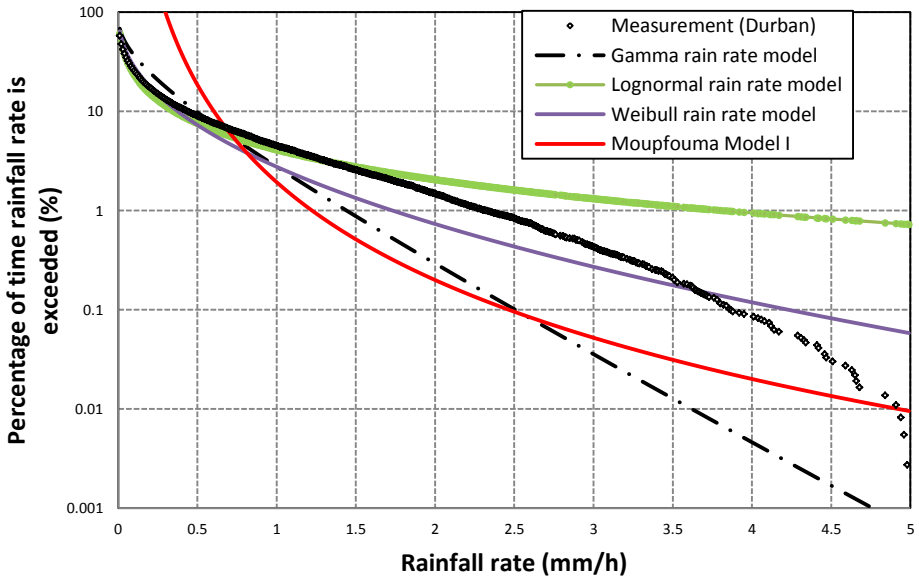

Figure 3-8: Comparison of the different model distributions for drizzle rain type

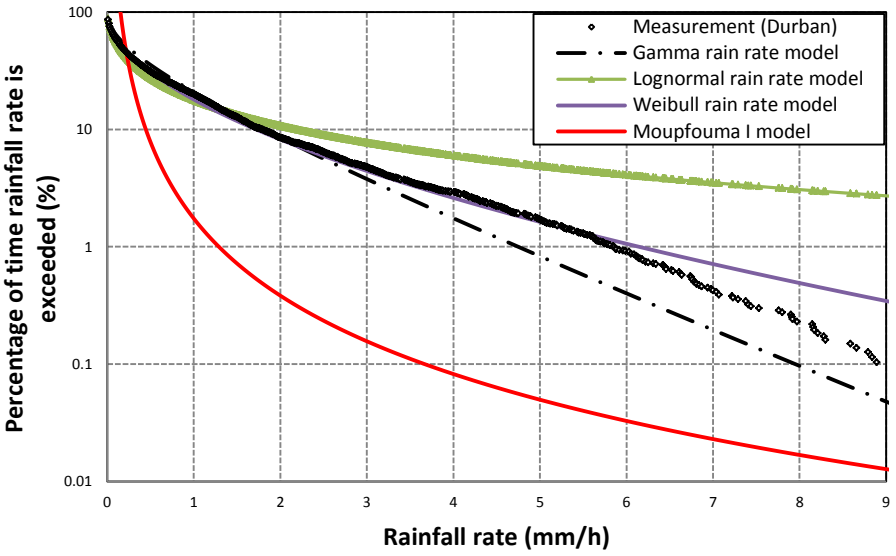

Figure 3-9: Comparison of the different model distributions for widepread rain type

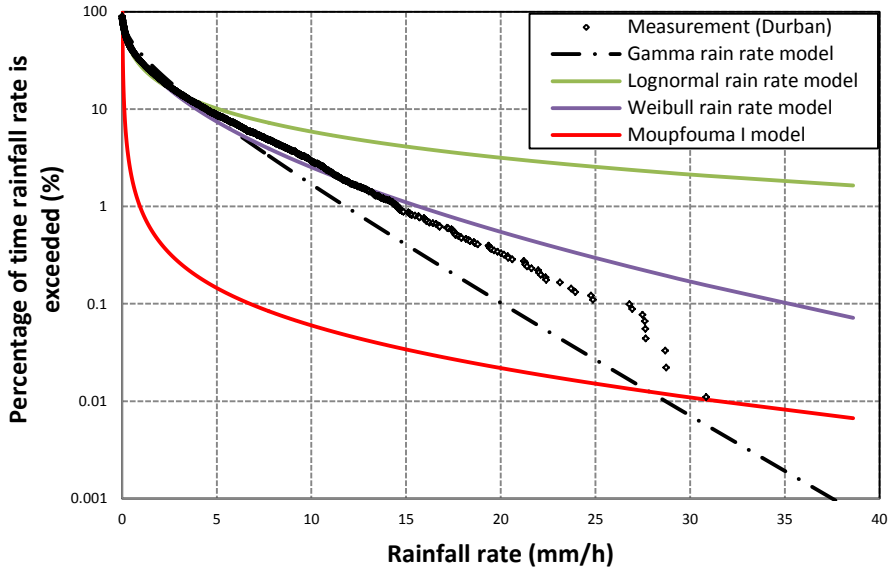

Figure 3-10: Comparison of the different model distributions for shower rain types

Interestingly, the lognormal model is observed to have higher estimates, while the gamma model has near-zero values towards the maximum rainfall rate for drizzle types.

Under the widespread category, the Weibull model again gives the best fit to the measured data,

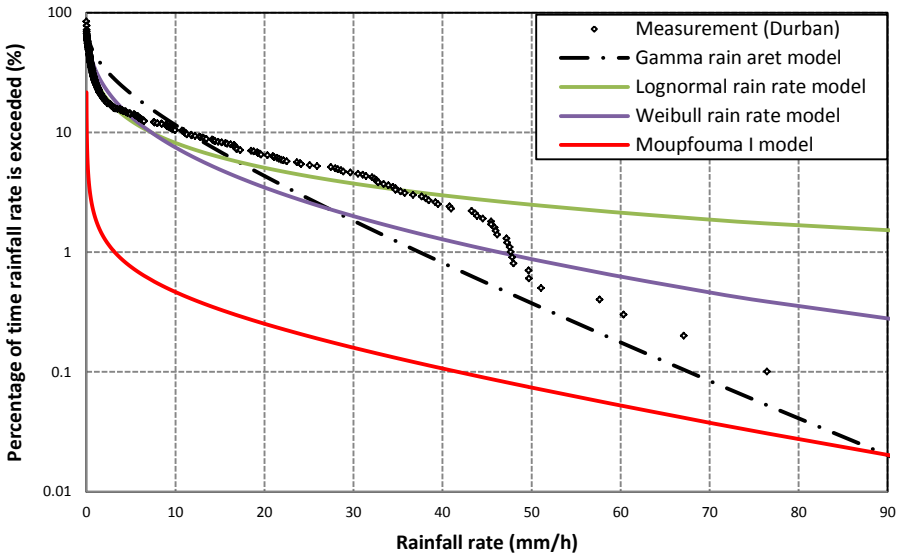

Figure 3-10: Comparison of the different model distributions for thunderstorm rain types

closely followed by the gamma model and lognormal model. The Moupfouma I and lognormal models both under-estimate and over-estimate the actual measurements. The Weibull model fits the actual measurement until a deviation is observed at 6mm/h; the gamma model also deviates at 2 mm/h and rainfall rates beyond.

For the shower rainfall category, the Weibull model again gives a better fit to the measurement for rainfall rates up to 15 mm/h. The gamma model also provided good estimates up to 6 mm/h. Again, the lognormal and Moupfouma I model both exhibit the same problem of over-estimation and under-estimation as the rainfall rate increases.

For the thunderstorm rainfall types, the closest model fits are the Weibull and gamma rainfall models. The gamma model to have closer fits especially for the rainfall rates above 50 mm/h. Again, the Moupfouma I model and lognormal model are not good fits to the measurement in Durban.

Overall, the lognormal model is found to generally over-estimate the measurements in Durban as the rainfall rate increases towards the maximum for any classification. The lognormal model, infact, fails to terminate the exceedence values beyond 1% confirming the observation of *Moupfouma* [1984a; 1987]. Therefore, it has been confirmed that lognormal models is most suitable for low rainfall rates and gamma model for high rainfall rates. For Durban, the Weibull model provides the

best fit for any rainfall type. This might be as a result of the breakdown in the failure pattern of rain droplets in rain events, which is typical of Weibull models. The gamma model also appears as a good estimate to the measurements as earlier in the recent studies of *Alonge and Afullo* [2011].

3.6.2 Comparison of Annual rainfall distribution models in Durban

The models considered for this comparison are the gamma model, lognormal model, Weibull model, Crane model, Moupfouma I model and ITU-R P.837-2 model. The ML estimators for the first three models are given in Table 3-6 and the Moupfouma model is also included.

As seen from the graph in Figure 3-10, the statistical models of Weibull, lognormal and gamma all appear to give large deviations at high rainfall rates. The gamma model appears to give a closer agreement to the measurements at high rainfall rates. Meanwhile, the rain zone models of Crane and ITU-R both seem to have closer estimates since the rainfall zone closer to $R_{0.01}$ in Durban has been selected for this comparison. The Moupfouma I model also appear to minimally fit the data reasonably well at high rainfall rates. The results of the error estimation in section 3.6.3 confirm their performances.

Table 3-6: Annual estimators and input parameters for the different models.

Year	Gamma model		Lognormal model		Weibull model		Moupfouma I model		
	α	β	μ	σ	γ	η	*a*	*b*	*u*
2009/2010	0.2567	8.226	0.1793	6.337	0.5571	0.4522	0.0098	0.7474	0.025

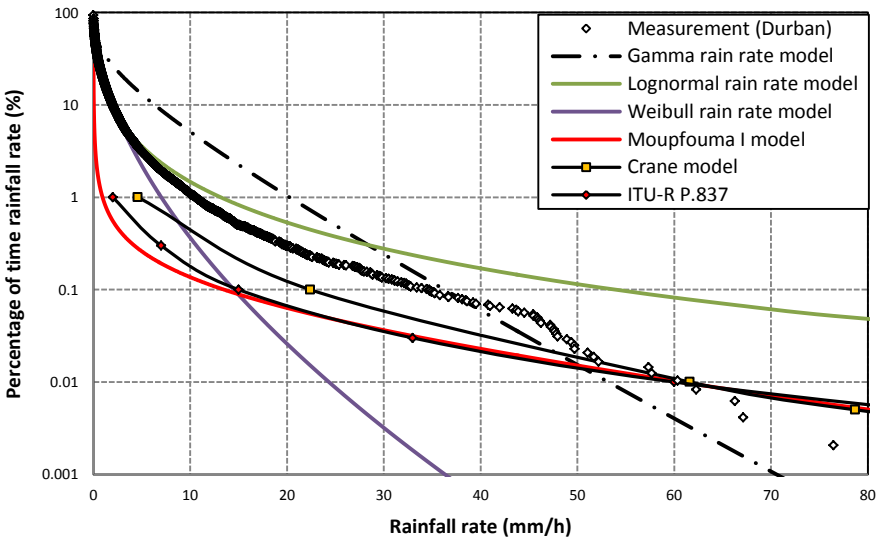

Figure 3-10: Comparison of the annual distributions for different rainfall rate models

3.6.3 Error Estimation for the Proposed Statistical Models

The error test employed in computing the deviation of the proposed models in this study is the root-mean-square (RMS) error test. By definition, the RMS error equation is given by:

$$RMSE = \left[\frac{1}{N}\sum_{i=1}^{N}[f^*(x_i) - f(x_i)]^2\right]^{\frac{1}{2}} \quad (3.19)$$

The variables $f^*(x_i)$ and $f(x_i)$ represent the data samples of the model and actual measurements of the data for Durban respectively. N represents the number of samples of $f^*(x_i)$ and f (x_i) in the population.

In addition to the RMS error applied in (3.19), the chi-square statistic test is proposed as another error tool. The chi-square (χ^2) is defined as:

$$\chi^2 = \sum_{i=1}^{N}\frac{[\,f(x_i) - f^*(x_i)\,]^2}{f^*(x_i)} \quad 3.20$$

The variables $f^*(x_i)$ and $f(x_i)$ in (3.20) represent the data samples of the model and semi-empirical measurements of the data for Durban. While N represents the number of samples of $f^*(x_i)$ and $f(x_i)$ in the population. χ^2 is used to examine the closeness of the theoretical model with the measurement.

Table 3-7: Error estimation from different rainfall rate models for Durban

CATEGORY	TESTS	GM	LGN	WBL	MOUP I	CRN	ITU-R
DRIZZLE	**RMS**	0.58	0.83	0.32	0.60		
	CHI	208.21	65.48	2.10	76.10		
WIDESPREAD	**RMS**	0.80	2.98	0.28	3.86		
	CHI	35.29	230.05	7.90	1174.18		
SHOWER	**RMS**	1.24	2.21	0.92	8.68		
	CHI	43.12	224.19	6.71	939.71		
THUNDERSTORM	**RMS**	0.3503	1.58	2.62	10.11		
	CHI	38.14	41.67	170.47	9393.58		
ANNUAL	**RMS**	0.54	0.18	0.20	0.18	1.46	4.55
	CHI	48.17	15.09	867.24	92.48	6.51	90.90

The significance level used in this work is 1%. The chi-square table is available in Appendix E for threshold values related to this result.

The results of the error estimation for different models are shown in Table 3-7. The degree of freedom is 89, which correspond to a χ^2 threshold of 122.94 at 1% significance level. The Weibull model best fits the measurement with: RMS and χ^2 of 0.32 and 2.10 for drizzle events, RMS and χ^2 of 0.28 and 7.90 for widespread events; RMS and χ^2 of 0.92 and 6.71 for shower events. The gamma model best fits at thunderstorm with RMS and χ^2 of 0.35 and 38.14. For the annual comparison, lognormal model best fits with RMS and χ^2 of 0.18 and 15.09. In addition, the Crane rain rate model shows better agreement with the measurement than the ITU-R rain rate model.

3.7 Chapter Summary

In this chapter - the subject of rainfall rate - a microstructural parameter, was investigated with respect to the data obtained from the disdrometer in Durban. The monthly, seasonal, events and annual distributions of rainfall rate for the measurement were also obtained. The results from the investigations show that summer and autumn months particularly March, April and May have higher rainfall rates than other months. Winter season, on the other hand, experience the lowest monthly rainfall rates in Durban with June, July, August and a spill-over to September being the months adversely affected. The spring season has the lowest rainfall rates due to the 'dragging' effects of the winter season. Based on rainfall event consideration, higher $R_{0.01}$ thresholds are observed for all shower and thunderstorm events, which can provide useful information for microwave planning. Also, the annual distribution has a $R_{0.01}$ = 60.69 mm/h, which is close to the ITU-R and Crane recommendation for the rainfall zone of Durban.

Finally, the Weibull rainfall rate model is seen an appropriate model for rainfall events involving drizzle, widespread and shower types of rainfall. However, the gamma model shows better estimates for thunderstorm events in Durban, making it preferable for thunderstorm rainfall types. For the annual distribution, the measurements in Durban seem to agree more with the Crane rain rate model than the ITU-R rain rate model with RMS and χ^2 of 1.46 and 6.51 respectively. Among the statistical models, the lognormal model has the best fit to the measurements with RMS and χ^2 of 0.18 and 15.09 respectively.

The next chapter focuses on rainfall DSD measurements, modelling and estimation using different

statistical models in Durban. The threshold of rainfall DSD is dependent on the variation of rainfall rate in a locality, therefore, the studies of rainfall rate vis-à-vis rainfall rate are discussed in chapter four.

CHAPTER FOUR

Rainfall Drop-Size Distribution Modelling

4.1 Introduction

In chapter three, the knowledge of rainfall rate distribution was explored to understand the design parameter of $R_{0.01}$ according to various rainfall classifications in Durban. With this knowledge, the rainfall rate probabilities from the control site could be employed to extend the definition of rainfall attenuation. Generally, the effects of rainfall attenuation in microwave and satellite communication become increasingly disturbing at frequencies above 10 GHz [*Ajayi et al.*, 1996; *Crane*, 1996]. At these higher frequencies (smaller wavelengths), the perturbations from the rain droplets in rainy medium often lead to signal absorption and scattering, and therefore, signal outage and deterioration [*Crane*, 1980]. Signal outages reduce bandwidth efficiency and spectrum utilization, which comes at great cost to providers of network services [*Li et al.*, 1995; *Li et al*., 2000; *Mulangu and Afullo*, 2009]. Usually, the aim of service providers is to ensure availability of services by compensating for these inadequacies through several corrective schemes such as complex base station power control algorithm. This process can be made possible by short term (or preferably long term) studies of rainfall microstructure, which of course, depend on the availability of rainfall data.

In this chapter, an investigation of rainfall microstructural parameter, rainfall drop-size distribution (DSD), which directly contribute to the determination of rainfall attenuation is highlighted. It is observed that the availability of rainfall DSD measurements provide a much more qualitative insight for radio engineers by taking into reckoning the mechanics of rainfall microstructure [*Crane*, 1996; *Crane*, 2003]. Therefore, the rainfall estimators for the lognormal, modified gamma and negative exponential DSD model are computed using the method of moment technique (MoM or MM) to develop empirical representations of rainfall DSD in Durban. Also, a new method of estimating the input parameters of the Weibull probability model is presented using the method of moments technique. The third, fourth and sixth moments of the RD-80 disdrometer measurements are used to derive our parameters for Durban, South Africa.

4.2 Brief discussion on Rainfall Droplets

Rainfall is made up of tiny droplets of spherical or oblate-shaped particles whose number density contribute to attenuation in a microwave or satellite link [*Odedina and Afullo*, 2010]. The number density of the rainfall droplets in a spatial coverage area often determines the attenuation level

during a rainfall event. Usually, the density determines the mean inter-droplet distance, which is an important parameter governing the process of scattering and absorption of EM waves.

Generally, the contribution of rain droplets to attenuation depends on other parameters such as rainfall rate, drop diameter, drop temperature, number of raindrops, fall velocity (or terminal velocity) of drops and drop diameter interval [*Ajayi et al.*, 1996]. While the drop diameter and drop temperature influence the scattering coefficients, other parameters help in the determination of the rainfall DSD and the resulting attenuation. The presence of these microphysical rainfall parameters can be used in the estimation of rainfall specific attenuation, and thus path attenuation, due to rain drops.

4.3 Experimental Procedure and Data Processing

The Joss-Waldogel RD-80 disdrometer is also used in this section as the measuring equipment since it is capable of measuring the number of rainfall drops in an single event. The experimental procedure undertaken for this section is the same as applied in section 3.2 for rainfall rate. The total number of precipitation samples collected for the same period is 87, 506 samples (9.74 % of the entire data).

However, the only divergence here is in the classification of rainfall regimes; the annual, and seasonal classifications are the same as given in the information in Table 3-1. The concept of rainfall regime classification replaces the event classification used in section 3.2. The regime classification is utilized because a closer study of rainfall mechanics needs to be consider and not the events that induce the mechanics. For example, several rainfall regime samples exist in a single rainfall event and therefore, the mechanics of rainfall is dynamic within the same rainfall duration. The regime classification is similar to earlier research on rainfall DSD by *Ajayi and Adimula* [1996] *Timothy et al.* [2002] and *Mandeep et al.* [2007]. The samples were categorized according to the following rainfall regimes in: drizzle ($R < 5$ mm/h , widespread $5 \leq R < 10$ mm/h , shower $10 \leq R < 40$ mm/h) and thunderstorm ($R \geq 40$ mm/h). After the data processing, the composition of the various rainfall regimes was in this order: drizzle rainfall (96.67 % of the data), widespread rainfall (2.07 % of the data), shower rainfall (1.03 % of the data) and thunderstorm rainfall (0.26 % of the data). The eventual total number of samples for the processed data are 48, 160 samples which is about 7.76 % of the collected data for the 2 years

Figure 4-1 shows the time resolution of the total sum of rain drops for 48, 195 rainfall samples used

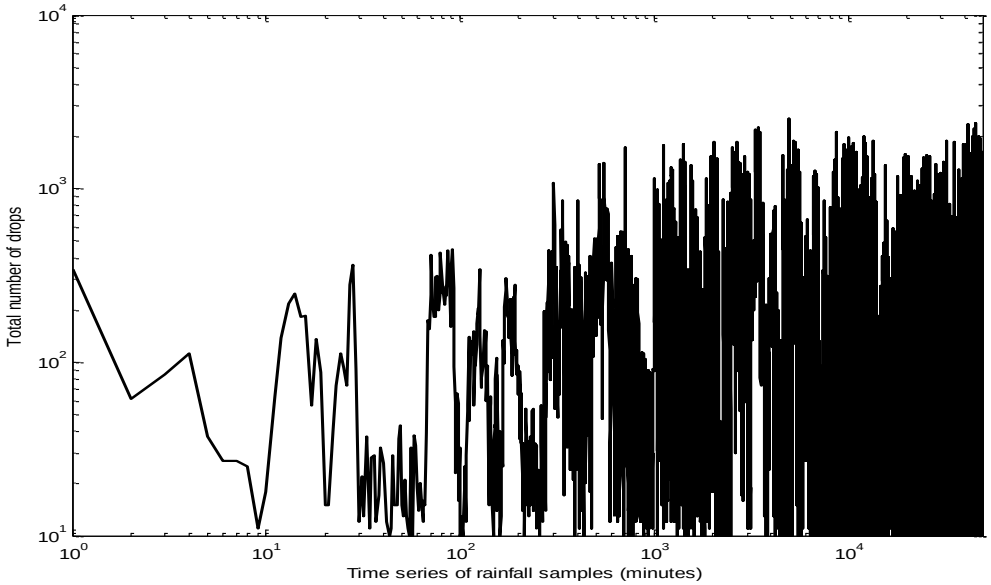

Figure 4-1: Time resolution of the total number of drops per rainfall sample for the period of measurement

Table 4-1: Rainfall regime analysis statistics for the two years of measurement in Durban

RAINFALL REGIME	NUMBER OF SAMPLES	MEAN RAINFALL RATE (mm/h)	TOTAL RAIN AMOUNT (mm)	MAXIMUM NUMBER OF DROPS	PERCENTAGE OF DATA (%)
Drizzle	46, 650	0.53	412.32	2534	96.67
Widespread	982	6.94	113.51	2256	2.07
Shower	494	16.49	135.80	2351	1.03
Thunderstorm	34	52.26	29.62	1819	0.26

in this section. The highest recorded sum of drops for the two years is 2534 drops and the highest recorded rainfall rate is 117.15 mm/h. In addition, for a statistical summary of the data processed for the regime analysis is presented in Table 4-1. It is observed that the drizzle rainfall regime has the highest rainfall amount (or accumulation) of 412.32 mm for the entire period of measurement. The least rainfall amount was found to be the thunderstorm rainfall regime with 29.62 mm at 34 rain minutes (or 34 rainfall samples).

The averaged probability density functions for these four rainfall regimes for the 20 disdrometer bins are shown in Figures 4-2(a) to 4-2(d). The observation is described as thus:

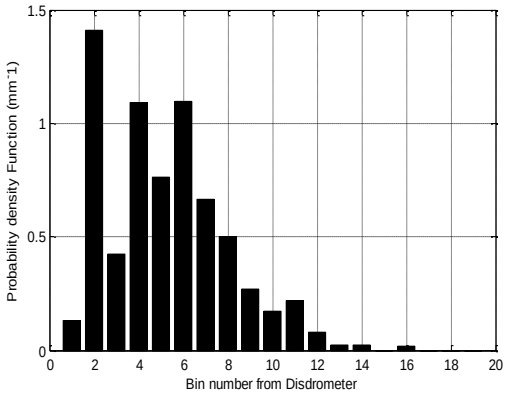

(a) Drizzle at 2.06 mm/h

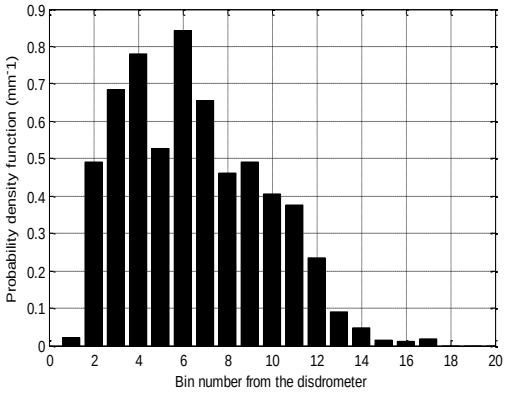

(c) Shower at 20.33 mm/h

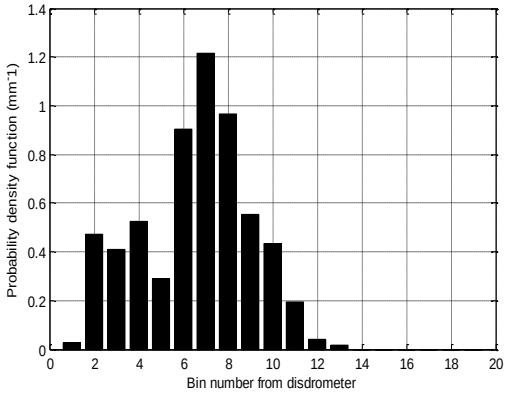

(b) Widespread at 7.05 mm.h

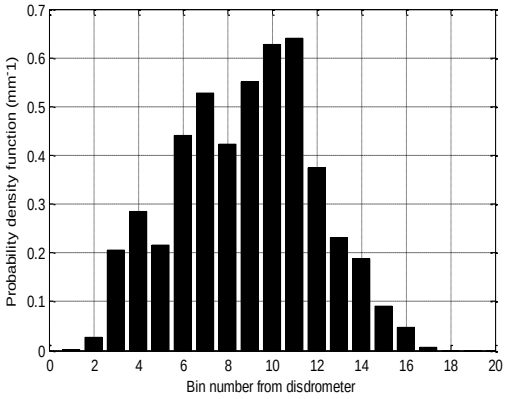

(e) Thunderstorm at 60.35 mm/h

Figure 4-2: Probability density function histograms for various rainfall regimes in Durban

- Drizzle rainfall in Durban at 2.06 mm/h have the highest drop probabilities between the bin 2 and bin 8 (0.455 mm and 1.331 mm diameter bound).
- Widespread rainfall in Durban at 7.05 mm/h have the highest drop probabilities between the bin 6 and bin 10 (0.913 mm and 1.665 mm diameter bound).
- Shower rainfall in Durban at 20.33 mm/h have the highest drop probabilities between the bin 2 and bin 11 (0.551 mm and 1.912 mm diameter bound).
- Thunderstorm rainfall in Durban at 60.35 mm/h have the highest drop probabilities between the bin 6 and bin 12 (0.913 mm and 2.259 mm diameter bound).

4.4 Modelling of Rain Drop-size Data

The need to develop a statistical representation for rain drop-size from measurements is essential in microwave engineering. The advantage of such statistical representation enables prediction of expected attenuation due to rainfall in order to reduce network downtime.

To establish a statistical correlation between the measurement and the proposed statistical models, an estimation method may be employed. Typical estimation methods are method of maximum likelihood (ML), method of moment (MM), Bayesian estimation and Kernel estimation [*Afullo*, 2011; *Timothy et al.*, 2002; *Owolawi*, 2011b]. In this study, the method of moment is utilised because of its use in similar scholarly articles and its inherent relationship to radio and radar parameters [*Ajayi and Olsen*, 1985; *Kozu et al.*, 1991; *Adimula and Ajayi*, 1996; *Timothy et al.*, 2002; *Das et al.,* 2010,]

4.5 Method of Moment Point Estimation Technique

The method of moment estimation technique (also known as MM or MoM) is a statistical method of evaluating the point estimators of mathematical functions, using their probability density functions. The method involves the location of the origin of a function by weighing the independent random variable of the function with the moments of its PDF.

The method of moment defined, according to *Soong* [2004] and *Kreyszig* [2006], describes the existence of an independent random variable X such that it has a real-valued function $c(X)$. The *mathematical expectation* of a continuous real-valued function $c(X)$ is equivalent to $E\{c(X)\}$ and is given by [*Soong*, 2004; *Kreyszig*, 2006] as:

$$E\{c(X)\} = \int_{-\infty}^{\infty} c(x) f_x(x)\ dx \tag{4.1}$$

where $f_x(x)$ contains a qualitative and complete description of a continuous random variable, X, whose interval is such that, $-\infty \leq x \leq \infty$, exists within infinite extreme bounds. This description can be taken as the probability density function of the continuous random variable, X.

By making a further assumption that $c(X)$ is such that it is equal to the nth power of the random variable, X, where n is an integer such that $n = 1, 2, 3, ...$Therefore, this assumption leads to an extension such that:

$$c(X) = X^n \text{ and } c(x) = x^n \tag{4.2}$$

thus,

$$E\{X^n\} = \int_{-\infty}^{\infty} x^n f_x(x)\ dx \tag{4.3}$$

The mathematical expectation, $E\{X^n\}$, can be set so that, $M_n = E\{X^n\}$ to give a convenient understanding of the function.
Hence,

$$M_n = \int_{-\infty}^{\infty} x^n f_x(x)\ dx \tag{4.4}$$

For a continuous random variable of x, M_n is called the nth moment function of the independent random continuous variable, X.

If x assumes a set of discretised values, then the possible values between the extreme infinite limits of x is equivalent to a set of discrete integers, x_i. Thus, the set of discrete random samples are $x_i = x_1, x_2, \ldots, x_n$ such that the moment function of the independent discrete random variable is given by:

$$M_n = \sum_{i=1}^{N} {x_i}^n\, p_x(x_i)\, \Delta x_i \tag{4.5}$$

Using the discrete samples, the parameters to be easily estimated can be obtained directly from the the computed moments of the discrete probability function, $p_x(x_i)$.

For rain drop-size distribution, the moment function for a discrete value of the random variable, as given by *Ajayi and Olsen* [1985] is:

$$M_n = \sum_{i=1}^{N} {D_i}^n N(D_i)\, \Delta D_i \tag{4.6}$$

where D_i is the diameter of the raindrops for N discrete samples, $N(D_i)$ is the rain drop-size distribution for N discrete number of rainfall samples and ΔD_i is the diameter interval of between successive rainfall drop sizes.

Equation (4.6) represents the *n*th moment obtained directly from the disdrometer measurements. A first and notable attempt at applying the method of moment in rain drop-size estimation was undertaken by *Waldvogel* [1974] and later by *Ajayi and Olsen* [1985] in their paper on rain drop-size distribution for tropical sites in Nigeria. Interestingly, several authors [*Kozu et al.*, 1991; *Timothy et al.*, 2002; *Das et al.,* 2010; *Afullo,* 2011] have applied this method in their studies on rainfall DSD. One of the notable features of the MM method is the stability in the estimation procedure of the unknown parameters. This technique is the only method that considers the raindrop concentration "growth" alongside the estimation of other known parameters. Apart from this unique feature, the method of moment has been reported to be related to other rainfall parameters and indices such as liquid water content, rainfall attenuation, rainfall rate *e.t.c.* [*Kozu and Nakamura*, 1991; *Adimula and Ajayi*, 1996; *Timothy et al.*, 2002; *Das et al.*, 2010].

Furthermore, the findings of *Kozu et al.* [1991], *Timothy et al.* [2002] and *Das et al.* [2010] also indicated that the typical values of *n* useful for radio and microwave engineering studies are the values of 3, 4 and 6. This is because they correspond to the liquid water content (LWC), specific attenuation and radar reflectivity of the measured data. Table 4-2 shows the moments of rainfall DSD and their related parameters in microwave engineering. The sub-section that follow show the equivalent moment functions of various statistical models and the solution of their various estimators. A unique application of the moment technique is also applied to the Weibull DSD model and its corresponding DSD estimators required for DSD trending.

Table 4-2: Moments of rainfall DSD and their related parameters of rainfall indices in microwave engineering [*Marzuki et al.*, 2010; *Das et al.*, 2010]

ORDER OF MOMENT	DISCRETIZED MOMENT FUNCTIONS	RELATED RAINFALL PARAMETER
Zeroth moment	$\sum_{i=1}^{N} N(D_i)\,\Delta D_i$	Rainfall drop concentration
Third moment	$\sum_{i=1}^{N} {D_i}^3 N(D_i)\,\Delta D_i$	Rainfall rate and Liquid water content (LWC)
Fourth moment	$\sum_{i=1}^{N} {D_i}^4 N(D_i)\,\Delta D_i$	Rainfall specific attenuation
Sixth moment	$\sum_{i=1}^{N} {D_i}^6 N(D_i)\,\Delta D_i$	Radar Reflectivity

4.5.1 Negative Exponential Rainfall DSD Moment Estimation

The negative exponential model for rainfall drop-size has its moment function given by:

$$M_n = N_o \frac{\Gamma(n+1)}{\Lambda^{n+1}} \tag{4.7}$$

The third, fourth and sixth moments are applied for the negative exponential model. The solution to the theoretical moments is obtained from the modified gamma moment solutions in *Kozu and Nakamura* [1991] by setting $\mu = 0$. Thus, the moment function becomes:

$$\Lambda = (4M_3)/M_4 \tag{4.7a}$$

$$N_O = \Lambda^4 M_3/\Gamma(4) \tag{4.7b}$$

The resulting moment functions are fitted with the rainfall samples using regression techniques.

4.5.2 Lognormal Rainfall DSD Moment Estimation

The moment function generator for a lognormal DSD is given as:

$$M_n = N_T \exp\left[n\mu + \frac{1}{2}(n\sigma)^2\right] \tag{4.8}$$

The third, fourth and sixth moments are considered sufficient to derive the input parameters N_T, μ and σ for the lognormal moment as suggested by *Kozu and Nakamura* [1991], *Timothy et al.* [2002] and *Das et al.* [2010]. The solutions to these three selected moments in (4.8) are:

$$N_T = \exp[(24L_3 - 27L_4 + 6L_6)/3] \tag{4.8a}$$

$$\mu = (-10L_3 + 13.5L_4 - 3.5L_6)/3 \tag{4.8b}$$

$$\sigma^2 = (2L_3 - 3L_4 + L_6)/3 \tag{4.8c}$$

In the above equations, the values of L_3, L_4 and L_6 represent the natural logarithms of the measured moments M_3, M_4 and M_6.

4.5.3 Modified Gamma Rainfall DSD Moment Estimation

The modified gamma model has its moment function given by:

$$M_n = N_m \frac{\Gamma(\mu + n + 1)}{\Lambda^{\mu+n+1}} \tag{4.9}$$

The moments considered here are also the third, fourth and sixth moments. The solution to the theoretical moments for the modified gamma is given in [*Kozu and Nakamura*, 1991] as:

$$\mu = \frac{11F - 8 + \sqrt{F(F+8)}}{2(1-F)} \tag{4.9a}$$

with,

$$F = \frac{{M_4}^3}{{M_3}^2 M_6} \tag{4.9b}$$

$$\Lambda = (\mu + 4)M_3/M_4 \tag{4.9c}$$

$$N_m = \Lambda^{\mu+4} M_3/\Gamma(\mu + 4) \tag{4.9d}$$

It has been shown that the two moments, M_3 and M_4, are sufficient to estimate the parameters of Λ and thus, N_m (concentration) provided that μ assumes a fixed constant.

4.5.4 Weibull Rainfall DSD

The derivation of parameters for Weibull rainfall probability distribution has been examined by *Sekine et al.*[1982;1985] and Jiang *et al.* [1997] using graphical method. However, there exists no literature that has discussed the derivation of Weibull rainfall DSD using the method of moment technique. Therefore, an approach is being proposed in this section to derive the estimators of the Weibull model using the MM technique.

In this technique, we assume that our corresponding data sample D_i exists such that its moment, m_i at its point of origin is already given in (4.6) as:

$$m_n = \sum_{i=1}^{N} {D_i}^n \, N(D) \Delta D_i \qquad [m^{-3} m m^n]$$

Then, the equivalent Weibull probability distribution raw moments, M_n, of the data sample at its point of origin is given in [*Murthy et al.*, 2004] as:

$$M_n = \left(\frac{1}{\eta^{\beta}}\right)^{-\frac{n}{\beta}} \Gamma\left(1 + \frac{n}{\beta}\right) \tag{4.10}$$

This can be reduced to:

$$M_n = \eta^n \, \Gamma\left(1 + \frac{n}{\beta}\right) \tag{4.11}$$

By modifying (4.11) to suit the new scaling parameter N_w, the nth raw moment becomes:

$$M_n = N_w \eta^n \, \Gamma\left(1 + \frac{n}{\beta}\right) \tag{4.12}$$

By adopting these values, we have three sets of equation representing the third, fourth and sixth moment of the Weibull distribution as below:

$$M_3 = N_w \eta^3 \, \Gamma\left(1 + \frac{3}{\beta}\right) \tag{4.13}$$

$$M_4 = N_w \eta^4 \, \Gamma\left(1 + \frac{4}{\beta}\right) \tag{4.14}$$

$$M_6 = N_w \eta^6 \, \Gamma\left(1 + \frac{6}{\beta}\right) \tag{4.15}$$

By basic definition of gamma functions, it follows that $\Gamma(x) = (x - 1)!$ and thus, $\Gamma(x + 1) = x!$. In this definition, x is assumed as a positive integer. By making a further assumption that $x_k \triangleq \frac{k}{\beta}$, we find a suitable expression for our gamma functions in (4.13) – (4.15) so that:

$$\Gamma(1 + x_3) = x_3! \tag{4.16}$$

$$\Gamma(1 + x_4) = x_4! \tag{4.17}$$

$$\Gamma(1 + x_6) = x_6! \tag{4.18}$$

By restricting the results of $\left(\frac{k}{\beta}\right)!$ to an integer, it follows that our representation might be difficult to express as a recurrent factorial order. Thus, in order to find an adequate representation for this problem, we employ the Stirling's asymptotic approximation [*Taylor and Mann*, 1983; *Weber and Arfken*, 2003]. This is defined as:

$$\text{n!} \approx \sqrt{2\pi n}\left(\frac{n}{e}\right)^n \tag{4.19}$$

where the constant, e = 2.718281828, is the Napierian index. By simplification, the gamma function in (4.16) – (4.18) can be represented as below:

$$\Gamma\left(1 + \frac{k}{\beta}\right) \approx \sqrt{2\pi k}\,.\,\left(\frac{k}{e}\right)^{\frac{k}{\beta}}.\,\beta^{-\left(\frac{\beta+2k}{2\beta}\right)} \tag{4.20}$$

where k in this case corresponds to 3, 4 and 6. In this study, the maximum error bound, ξ, attributed to Stirling's approximation is 8 % for the range $1 \leq \frac{k}{\beta} \leq 10$ [*Weber and Arfken*, 2003]. It should be noted that the error approaches zero as $\frac{k}{\beta}$ becomes very large.

Combining (4.13) – (4.20), we have our expressions for the 3rd, 4th and 6th moments of the Weibull probability distribution as:

$$M_3 = 4.3416\, N_w \eta^3\, \beta^{-\left(\frac{\beta+6}{2\beta}\right)}(1.1036)^{\frac{3}{\beta}} \tag{4.21}$$

$$M_4 = 5.0133\, N_w \eta^4\, \beta^{-\left(\frac{\beta+8}{2\beta}\right)}(1.4715)^{\frac{4}{\beta}} \tag{4.22}$$

$$M_6 = 6.1400\, N_w \eta^6\, \beta^{-\left(\frac{\beta+12}{2\beta}\right)}(2.2072)^{\frac{6}{\beta}} \tag{4.23}$$

The solution of (4.21), (4.22) and (4.23) can be obtained by taking the natural logarithms of these expressions and solving simultaneously for the three unknown parameters N_w, η and β.

The solutions for the three unknown parameters are given below:

For β, we have:

$$\beta = -\frac{0.7067}{ln\,(\varphi)} \tag{4.24}$$

where,

$$\varphi = \frac{0.9186\,{M_4}^3}{{M_3}^2.M_6} \tag{4.25}$$

for η, we have:

$$\eta = \frac{0.8660\,M_4}{M_3} \times (0.2867\beta)^{\frac{1}{\beta}} \tag{4.26}$$

and for N_w, we have:

$$N_w = \frac{0.2303\,M_3\,\beta^{\left(\frac{\beta+6}{2\beta}\right)}}{\eta^3(1.3443)^{\frac{1}{\beta}}} \tag{4.27}$$

4.5.4.1 Estimation of Weibull Parameters for Durban, South Africa

On obtaining the respective third, fourth and sixth moments of measurements, the least square regression fitting technique is then employed in relation to their respective rainfall rates to derive our parameters for N_w, η and β. From the results of the fitting, it is established that the accuracy of our fitting decreases as the rainfall rate increases. This is because we have lesser rainfall samples to correlate in Durban particularly from 40 m/h and above. This is also in consonance with previous studies which places it as a subtropical zone [*Owolawi et al.,* 2007; *Odedina et al.*, 2008].

Figure 4-3a, 4-3b and 4-3c show the scattergrams obtained for the three estimated parameters of the Weibull probability function in Durban for two years of measurement. The proposed results for the regression fitting technique for the scattergrams shown in Figures 4-3 for annual rainfall rates are presented in section 4.6. Also, other rainfall classifications are applied and compared with other models in the following sections.

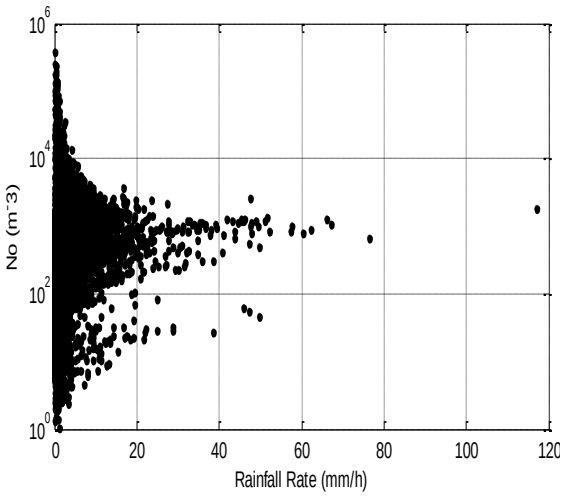

(a) Variation of N_w against the overall rainfall rate in Durban

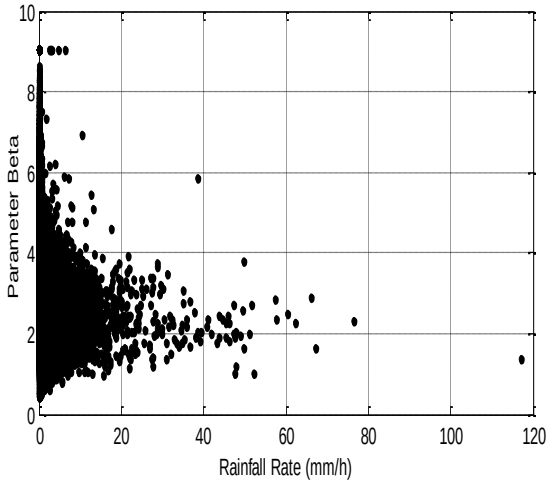

(b) Variation of β against the overall rainfall rate in Durban

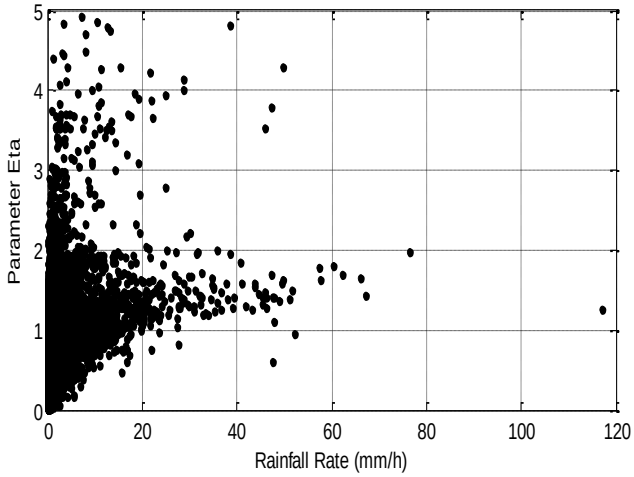

(c) Variation of η against the overall rainfall rate in Durban

Figure 4-3: Variation of Weibull estimators with rainfall rate in Durban

4.6 Results and Comparison of DSD Models for Durban

The method of moment (MM) technique as earlier explained is used for the estimation of the various input parameters for the proposed statistical models applied in this work. The input parameters obtained from the application of the moment equations for each models are parameterised as a function of rainfall rate via regression techniques. The results from the modelling are presented in the next subsections.

4.6.1 Monthly Variation of Rainfall DSD

Using the method of moments technique, the estimators for different proposed models for Durban were developed. The results for the different monthly DSDs are presented in Tables 4-3 to 4-6. The parameters for each of the proposed model as presented in these Tables have earlier been discussed in section 2.8 and the sub-sections that follow.

From the results, it is observed that the months of September, November and December have higher rainfall drops concentration for the different proposed models. The early start of the summer season indicates that the rainfall volume is higher for these months. However, the months of May, June, July and August experience lower concentration of rainfall drops due to 'dry winter spell'. The weaker values of the coefficients of determination (R^2) for other parameters of the distribution indicate the effects of lack of sufficient rainfall data for these winter months. Generally, it appears the rainfall drop concentration (N_T, N_o, N_m and N_w) play differing roles in the proposed models. For example, the lognormal DSD and Weibull DSD models have 'stronger' coefficients of determination compared to other models for all seasons.

The plotted graphs for these proposed seasonal models, at their respectively values of $R_{0.01}$, are presented in Figures 4-4 to 4-7. At $R_{0.01}$, it is observed that the month of November with $R_{0.01}$ at 57.22 mm/h has the highest $N(D)$ peak. This is followed by December with $R_{0.01}$at 47.82 mm/h, October with $R_{0.01}$ at 20.23 mm/h, March with $R_{0.01}$ at 63.54 mm/h and January with $R_{0.01}$ at 62.08 mm/h. Surprisingly, the month of April which has the highest recorded $R_{0.01}$ at 90.83 mm/h from the measurements, has a $N(D)$ peak slightly higher than that of February with $R_{0.01}$ at 49.51 mm/h. This suggests that high values of $R_{0.01}$ may not be used as the only determinant of $N(D)$ but the rainfall concentration plays a larger role.

In terms of drop diameter ranges, the months of May and June show appreciable rainfall DSD at diameter bounds above 4 mm compared to other months at $R_{0.01}$. For a greater part of the months, $N(D)$ has values above 1000 $m^{-3}mm^{-1}$ below the 1 mm diameter bound. However, the months of August, July, June and May have DSD estimates below 100 $m^{-3}mm^{-1}$ for diameter bound below 1 mm.

Table 4-3: Monthly estimates for input parameters of the lognormal rainfall DSD model in Durban

MONTH	N_T			μ			σ^2		
	a	b	R^2	A_μ	B_μ	R^2	A_σ	B_σ	R^2
January	327.02	0.4211	0.4086	-0.3708	0.1257	0.4868	0.0765	0.0112	0.2793
February	233.34	0.3641	0.2242	-0.2747	0.1432	0.4207	0.0735	0.0104	0.2283
March	288.13	0.4123	0.3174	-0.3111	0.1362	0.435	0.0635	0.0073	0.1494
April	224.34	0.4074	0.2895	-0.2504	0.1392	0.4139	0.067	0.0074	0.1489
May	28.3	0.1723	0.0941	0.3154	0.2139	0.672	0.0587	0.0029	0.0268
June	41.851	0.2289	0.0845	0.2083	0.1963	0.4499	0.0584	0.0041	0.042
July	56.937	0.2715	0.1036	0.0844	0.1782	0.3995	0.0797	0.0074	0.0821
August	83.102	0.2635	0.1875	-0.051	0.1701	0.5624	0.0979	0.0118	0.2097
September	453.88	0.4936	0.5074	-0.4508	0.1809	0.4465	0.0731	0.0099	0.2664
October	231.08	0.6203	0.3973	-0.2939	0.0848	0.1697	0.0832	0.0067	0.0622
November	562.71	0.5265	0.472	-0.5506	0.0937	0.2864	0.0874	0.0137	0.2047
December	416.54	0.4509	0.3564	-0.4487	0.1139	0.3267	0.0957	0.0137	0.1851

Table 4-4: Monthly estimates for input parameters of the Weibull rainfall DSD model in Durban

MONTH	N_w			η			β		
	a	b	R^2	a_η	b_η	R^2	a_β	b_β	R^2
January	484.61	0.4321	0.417	2.5792	-0.148	0.4123	0.6581	0.1159	0.3737
February	342.69	0.3737	0.2365	2.6484	-0.136	0.3441	0.7294	0.1348	0.3656
March	412.92	0.4145	0.3199	2.9334	-0.106	0.2513	0.7163	0.1334	0.3874
April	325.23	0.4136	0.2981	2.8465	-0.099	0.239	0.7546	0.1335	0.3695
May	40.191	0.1673	0.0865	3.0957	-0.054	0.0779	1.3504	0.2165	0.6339
June	59.625	0.2329	0.0834	3.13	-0.054	0.064	1.2091	0.1925	0.3943
July	83.693	0.2807	0.1064	2.1474	-0.093	0.1293	1.0448	0.1714	0.329
August	130.59	0.2904	0.213	2.103	-0.123	0.2994	0.8691	0.1504	0.4
September	653.23	0.5004	0.5204	2.5587	-0.135	0.4094	0.6205	0.103	0.3772
October	345.82	0.6278	0.4105	2.3775	-0.085	0.1117	0.7055	0.0789	0.1311
November	874.09	0.5512	0.4773	2.4055	-0.156	0.3557	0.5376	0.0729	0.1041
December	646.62	0.4722	0.3563	2.4639	-0.162	0.3757	0.5852	0.0968	0.1353

Table 4-5: Monthly estimates for input parameters of the modified gamma rainfall DSD model in Durban

MONTH	μ	N_m			Λ		
		a	b	R^2	a_Λ	b_Λ	R^2
January	2	1.095×10^5	-0.14	0.0216	6.6514	-0.165	0.5916
February	2	6.15×10^4	-0.237	0.0331	6.1048	-0.179	0.4813
March	2	9.99×10^4	-0.118	0.0109	6.5582	-0.162	0.495
April	2	6.123×10^4	-0.133	0.0124	6.0969	-0.165	0.4719
May	2	1621.7	-0.517	0.2236	3.5639	-0.224	0.7108
June	2	3325.9	-0.428	0.0099	3.9719	-0.211	0.5499
July	2	4611.6	-0.386	0.0683	4.1717	-0.204	0.4883
August	2	7482.1	-0.441	0.1592	4.4816	-0.211	0.6671
September	2	2.04×10^5	0.0036	0.0002	7.2906	-0.144	0.5321
October	2	5.495×10^4	0.2557	0.0296	6.0157	-0.108	0.2049
November	2	2.539×10^5	0.0192	0.0003	7.5108	-0.142	0.4649
December	2	1.512×10^5	-0.116	0.0104	6.9612	-0.162	0.4898

Table 4-6: Monthly estimates for input parameters of the negative exponential rainfall DSD model in Durban

MONTH	N_0			Λ		
	a	b	R^2	a_Λ	b_Λ	R^2
January	9774.6	0.1893	0.0736	4.4343	-0.165	0.5916
February	6516	0.31224	0.0179	4.0699	-0.179	0.4813
March	9182.4	0.2063	0.0633	4.3721	-0.162	0.495
April	6508	0.1974	0.0524	4.0646	-0.165	0.4719
May	504	-0.069	0.0103	2.3759	-0.224	0.7108
June	832.89	-0.007	0.00006	2.6479	-0.211	0.5499
July	1046.9	0.0228	0.0005	2.7811	-0.204	0.4883
August	1471.7	-0.019	0.0007	2.9877	-0.211	0.6671
September	15175	0.2907	0.1642	4.8604	-0.144	0.5321
October	5999	0.4721	0.1713	4.0105	-0.108	0.2049
November	17787	0.3026	0.1418	5.0072	-0.142	0.4649
December	12327	0.2072	0.0625	4.6408	-0.162	0.4898

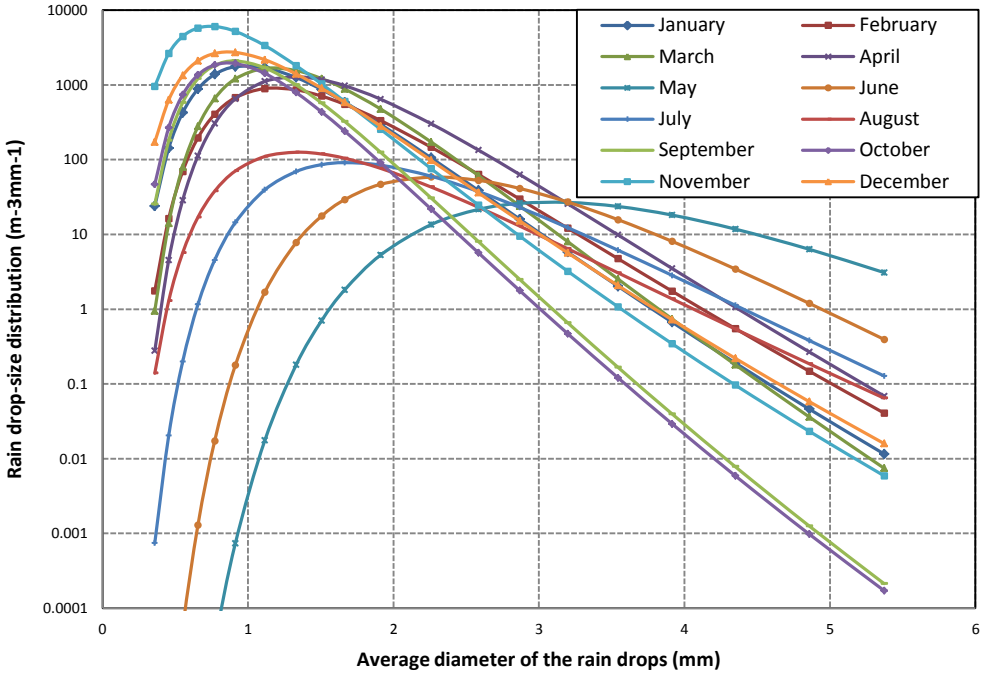

Figure 4-4: Rainfall DSD in Durban using lognormal DSD model at monthly values of their respective $R_{0.01}$

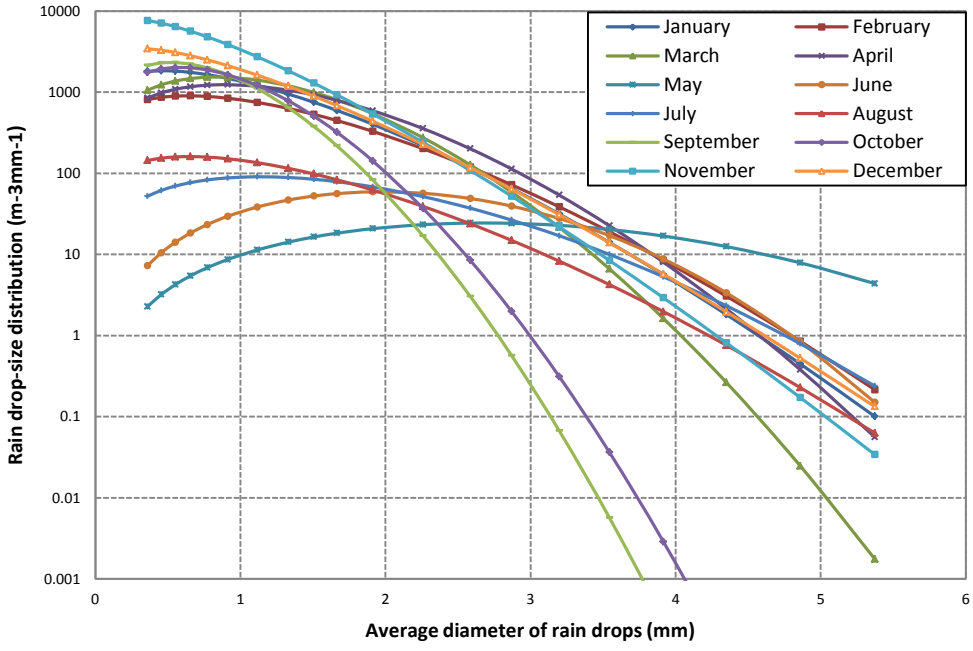

Figure 4-5: Rainfall DSD in Durban using Weibull DSD model at monthly values of their respective $R_{0.01}$

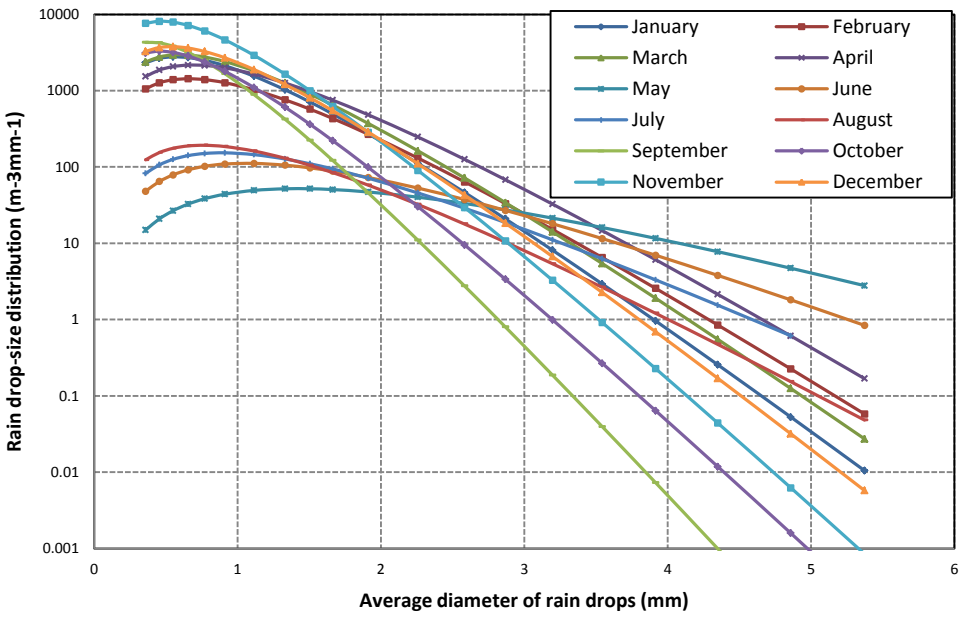

Fig 4-6: Rainfall DSD in Durban using modified gamma DSD model at monthly values of their respective $R_{0.01}$

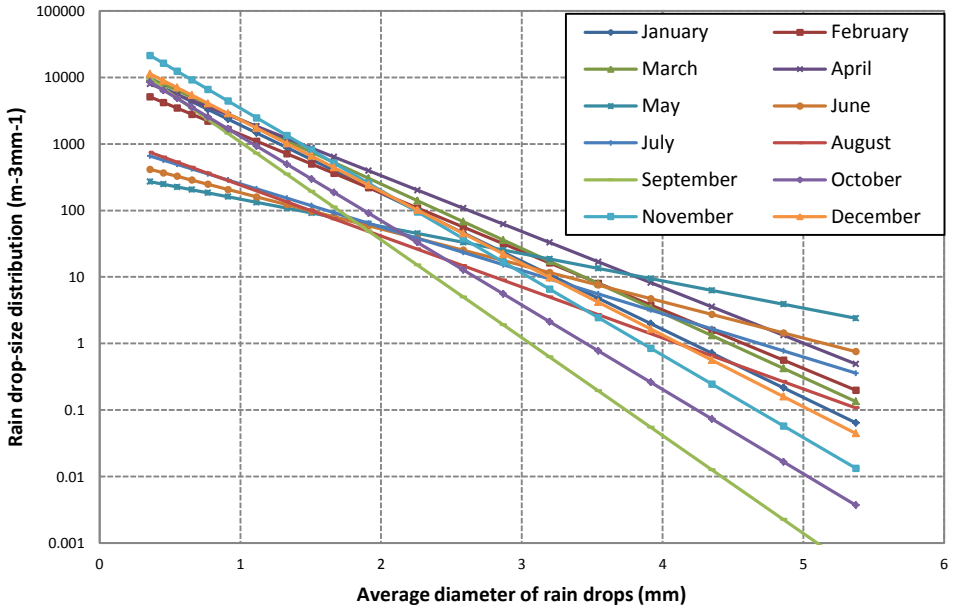

Fig 4-7: Rainfall DSD in Durban using negative exponential DSD model at monthly values of their respective $R_{0.01}$

4.6.2 Seasonal Variation of Rainfall DSD

The results obtained for the seasonal DSDs for the city of Durban using the method of moment estimation technique are presented in Table 4-7. The seasonal classification in South Africa earlier been discussed in section 2.10 is used to group the rainfall data for the city of Durban. The statistics for seasonal classification are available in Table 3-1.

In Table 4-6, the season of summer is observed to have the highest rain drop concentration with N_T and N_o for all the proposed models having high coefficients. The season of winter, on the other hand, has the lowest raindrop concentration indicating a low volume of rainfall for that period.
The plotted graphs from the results are shown in Figures 4-8 to 4-11 with the different DSD variation for different seasons in Durban.

The summer DSD plot at $R_{0.01}$ = 56.42 mm/h are shown in Figure 4-8 with the proposed models generally overestimating the DSD measurement for the first eight mean drop diameters. However, there seem to be some general agreement of the proposed models with the measurement at higher diameter region *i.e.* above 2 mm diameter bound. For autumn season with $R_{0.01}$ = 72.15 mm/h, the Weibull and lognormal models appear to provide better fits to the measurement as shown in Figure 4-9. The negative exponential and modified gamma models, on the other hand, are both seen to overestimate at lower diameter regions. A closer observation of summer and autumn seasons show that they both have similar DSD peaks, they do not however coincide at the same diameter bound for all proposed models. This may suggest that the rainfall pattern for both seasons are similar. For winter season at $R_{0.01}$ = 53.37 mm/h, the orientation of the plotted graphs as seen in Fig 4-10, for modified gamma and Weibull models, may suggest that the DSD is independent of the drop concentration; this may due to the effects of the 'winter dry spell'. The season is also seen to have lower DSD peaks when compared to summer and autumn seasons. This may be as a result of general climatic dryness and few occurrences of rainfall especially at the onset of the season. Finally, the season of spring at $R_{0.01}$ = 18.51 mm/h as seen in Figure 4-11 also has lower DSD peaks for all models confirming the spill-over effects of winter. The Weibull model in this season is seen as a good estimate of the measurement, thus, having the best fit. The lognormal model underestimates the measurement at the lower diameter region, while the negative exponential model overestimates the measurement. Generally, the proposed models are observed to have DSD estimates closer to zero at the maximum disdrometer diameter (5.373 mm). This may indicate the near-absence of rain drops at the diameter classes closer to the maximum diameter.

Table 4-7: Model parameters for different rainfall DSD statistical models for seasonal analysis in Durban, South Africa

Parameters	LOGNORMAL DSD MODEL					
	N_T		μ		σ^2	
	a_o	b_o	A_μ	B_μ	A_σ	B_σ
Summer	376.7	0.4505	-0.416	0.116	0.0816	0.0125
Autumn	239.13	0.3752	-0.2671	0.1454	0.0667	0.0081
Winter	35.78	0.163	0.2467	0.2163	0.0611	0.003
Spring	155.6	0.4077	-0.1922	0.1338	0.0849	0.0099

Parameters	WEIBULL DSD MODEL		
	β	η	N_w
Summer	$2.5048R^{-0.153}$	$0.616R^{0.1014}$	$571.78R^{0.4677}$
Autumn	$2.8453R^{-0.11}$	$0.7438R^{0.1404}$	$345.78R^{0.3806}$
Winter	$3.0063R^{-0.046}$	$1.2564R^{0.2162}$	$51.78R^{0.1622}$
Spring	$2.3298R^{-0.121}$	$0.7799R^{0.1234}$	$233.43R^{0.4211}$

Parameters	MODIFIED GAMMA DSD MODEL		
	μ	N_m	Λ
Summer	2	$1.32 \times 10^5 R^{-0.103}$	$6.8345R^{-0.16}$
Autumn	2	$6.8944 \times 10^4 R^{-0.194}$	$6.2056R^{-0.174}$
Winter	2	$2420.9R^{-0.535}$	$3.7854R^{-0.227}$
Spring	2	$2.6524 \times 10^4 R^{-0.156}$	$5.4019R^{-0.168}$

Parameters	NEGATIVE EXPONENTIAL MODEL	
	N_o	Λ
Summer	$11217R^{0.2161}$	$4.5563\ R^{-0.16}$
Autumn	$7027.9R^{0.1531}$	$4.137\ R^{-0.174}$
Winter	$667.44R^{-0.082}$	$2.5236\ R^{-0.227}$
Spring	$3591R^{0.1802}$	$3.6013\ R^{-0.168}$

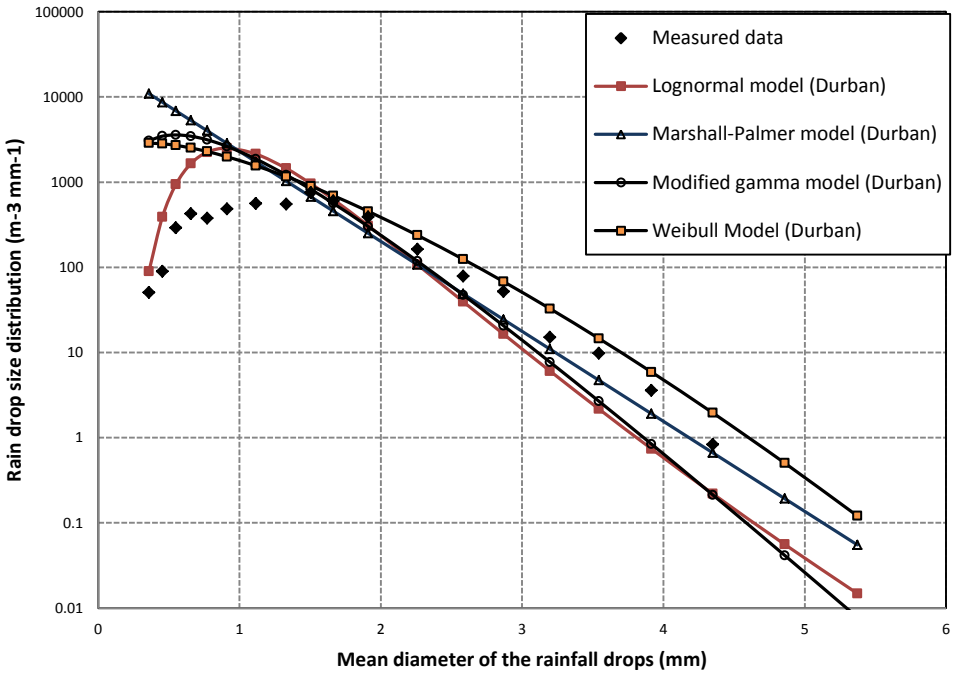

Figure 4-8: Rainfall DSD in Durban at summer season with $R_{0.01}$ = 56.42 mm/h

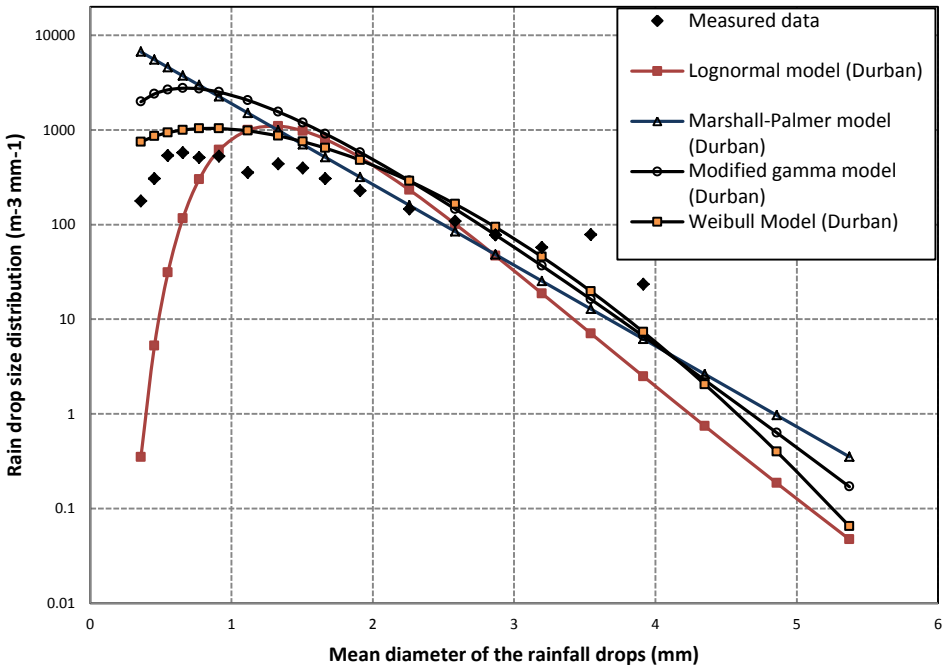

Figure 4-9: Rainfall DSD in Durban at autumn season with $R_{0.01}$ = 72.15 mm/h

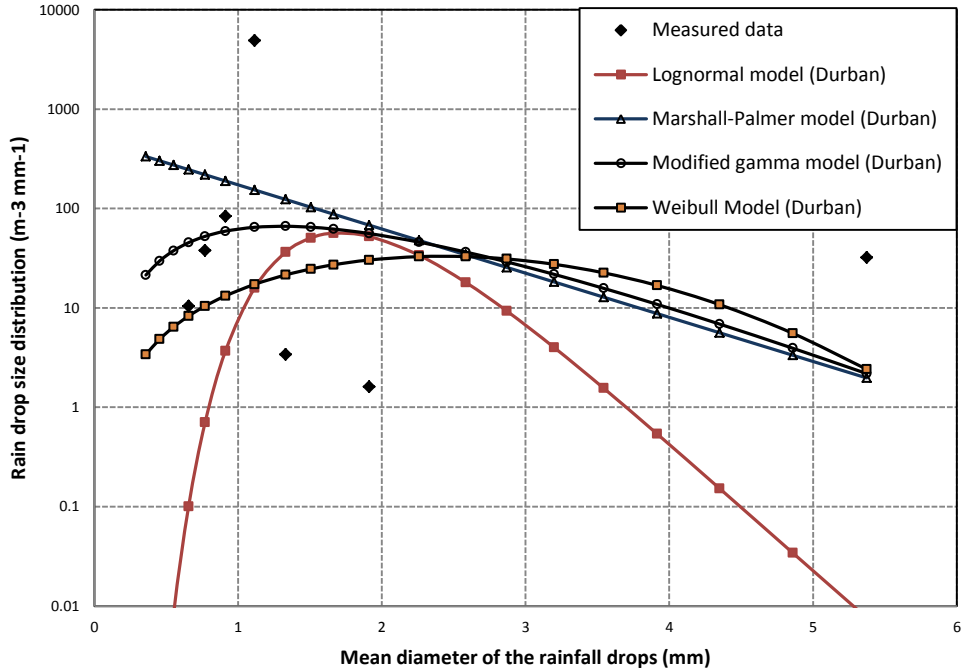

Figure 4-10: Rainfall DSD in Durban at winter season with $R_{0.01}$ = 53.37mm/h

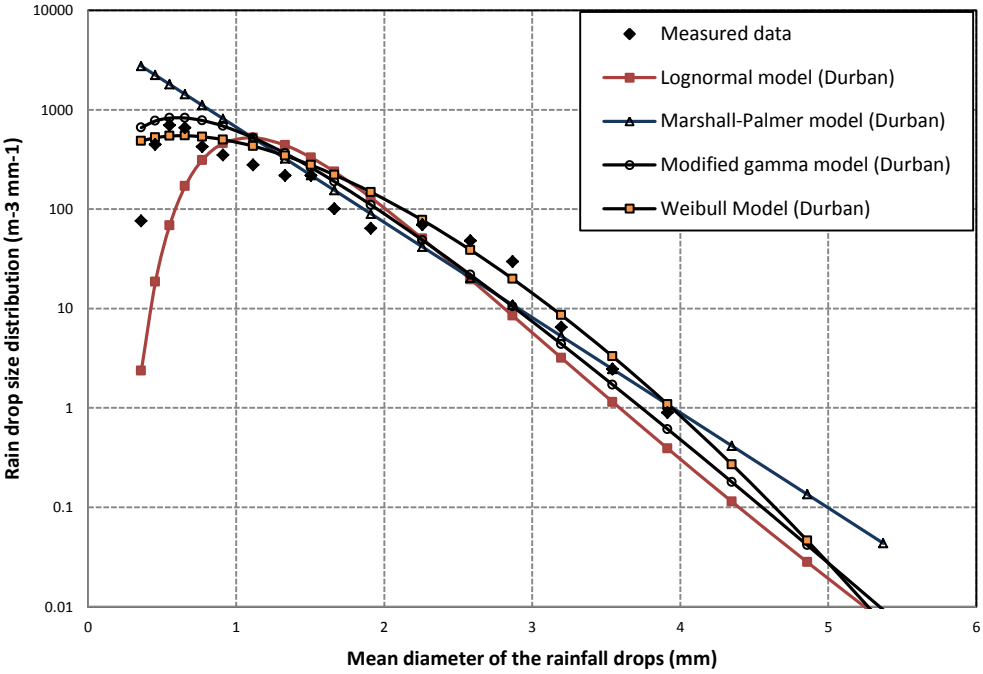

Figure 4-11: Rainfall DSD in Durban at spring season with $R_{0.01}$ = 18.51 mm/h

4.6.3 Regime Variation of Rainfall DSD

Table 4-8 gives the results of the applied regression fittings for the proposed statistical models according to their input parameters for all rainfall regimes. The classification used in this rainfall regime is explained in section 4.3 and is given as: drizzle (R < 5 mm/h), widespread (5 mm/h ≤ R < 10 mm/h), shower (10 mm/h ≤ R < 40 mm/h) and thunderstorm (R ≥ 40 mm/h . Drizzle rainfalls (and widespread rainfalls) are generally associated with stratiform types of rainfall. They generally have large rainfall cell diameters [*Mandeep and Allnut*, 2007; *Timothy et al.*, 2002], and therefore cover larger areas with longer event duration during a rain event. On the other hand, shower and thunderstorm rainfalls are mainly associated with convective types of rainfall with smaller rainfall cell diameters, with shorter event duration. Thus, with the majority of rainfall samples in Durban being of drizzle types, there are occasional instances of thunderstorms.

Figures 4-12 to 4-15 show the plotted graphs for the proposed rainfall drop-size distribution models developed for Durban. The graphs are plotted at four distinct rainfall rates: 4 mm/h, 9 mm/h, 25 mm/h and 75 mm/h. In Figure 4-12, it is shown that the measurements for drizzle rainfall regime at 4 mm/h is best fitted by the Weibull model. The negative exponential model shows the largest deviation with its maximum diameter bound over 4 mm, overestimating at larger diameter region. For the widespread rainfall regime at 9 mm/h in Figure 4-13, the modified gamma model, followed by the Weibull model, appear to provide better fits to the measurement. Also observed is the fact that the lognormal model grossly under-estimates the measurement at diameter bound less than 1 mm. In Figure 4-14, of all the models compared for shower rainfall regime, the Weibull model, followed by the modified gamma model appears to give the best fit. Lognormal DSD model again under-estimates the measurement for diameter bounds less than 1.5 mm. For thunderstorm rainfall regime in Figure 4-15, modified gamma DSD model and lognormal DSD model appear to provide better estimates to the measurement. However, Weibull model is seen to grossly under-estimate the measurement at diameter bound above 3 mm.

Overall, the statistical models employed in this study give good estimates to the measurement at the tested rainfall rates for each regime. The error estimates attributed to each of these proposed models are however discussed in Table 4-9.

Table 4-8: Model parameters for different rainfall DSD statistical models for regime analysis in Durban, South Africa.

Parameters	LOGNORMAL DSD MODEL					
	N_T		μ		σ^2	
	a_o	b_o	A_μ	B_μ	A_σ	B_σ
Drizzle	230.32	0.4089	-0.2837	0.1307	0.0793	0.0107
Widespread	322.41	0.102	-0.3923	0.2493	0.0832	-0.003
Shower	258.28	0.095	-0.3212	0.2418	0.0718	0.005
Thunderstorm	41.319	0.625	0.2989	0.063	0.0136	0.0223

Parameters	WEIBULL DSD MODEL		
	β	η	N_w
Drizzle	$2.5115R^{-0.135}$	$0.7125R^{0.1196}$	$343.95R^{0.422}$
Widespread	$2.5543R^{-0.007}$	$0.6182R^{0.2718}$	$499.98R^{0.0776}$
Shower	$2.7056\ R^{-0.052}$	$0.6962R^{0.2344}$	$378.33R^{0.107}$
Thunderstorm	$3.4671R^{-0.132}$	$1.665R^{-0.016}$	$44.298R^{0.7259}$

Parameters	MODIFIED GAMMA DSD MODEL		
	μ	N_m	Λ
Drizzle	2	$5.67 \times 10^4 R^{-0.16}$	$6.0373R^{-0.168}$
Widespread	2	$1.0306 \times 10^5 R^{-0.6}$	$6.6385R^{-0.24}$
Shower	2	$8.0544 \times 10^4\ R^{-0.714}$	$6.4351R^{-0.259}$
Thunderstorm	2	$5233R^{0.0681}$	$4.2425R^{-0.141}$

Parameters	NEGATIVE EXPONENTIAL MODEL	
	N_o	Λ
Drizzle	$6145.5R^{0.1764}$	$4.0249\ R^{-0.168}$
Widespread	$9238.8R^{-0.121}$	$4.4257\ R^{-0.24}$
Shower	$7684R^{-0.195}$	$4.2901\ R^{-0.259}$
Thunderstorm	$1148.6R^{0.3503}$	$2.8283\ R^{-0.141}$

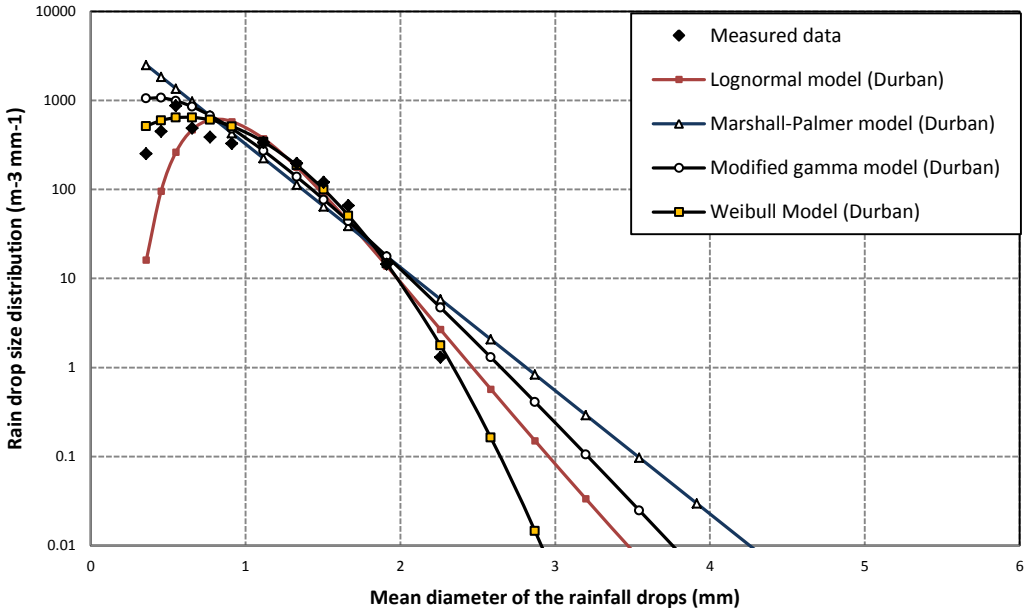

Figure 4-12: Rainfall DSD models in Durban for drizzle rainfall regime at 4 mm/h

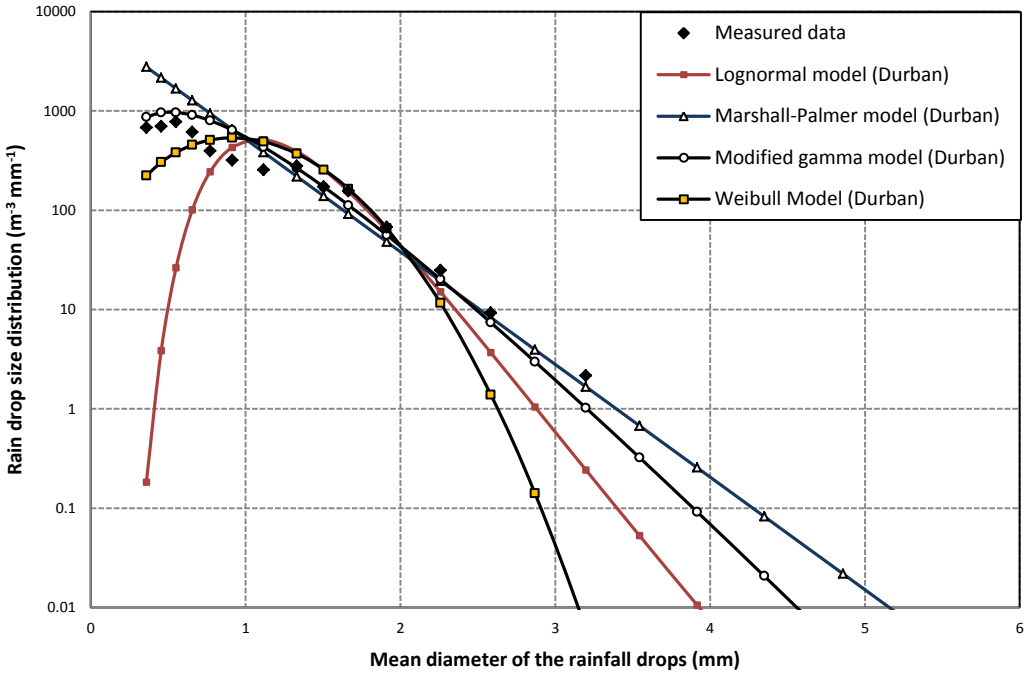

Fig 4-13: Rainfall DSD models in Durban for widespread rainfall regime at 9 mm/h

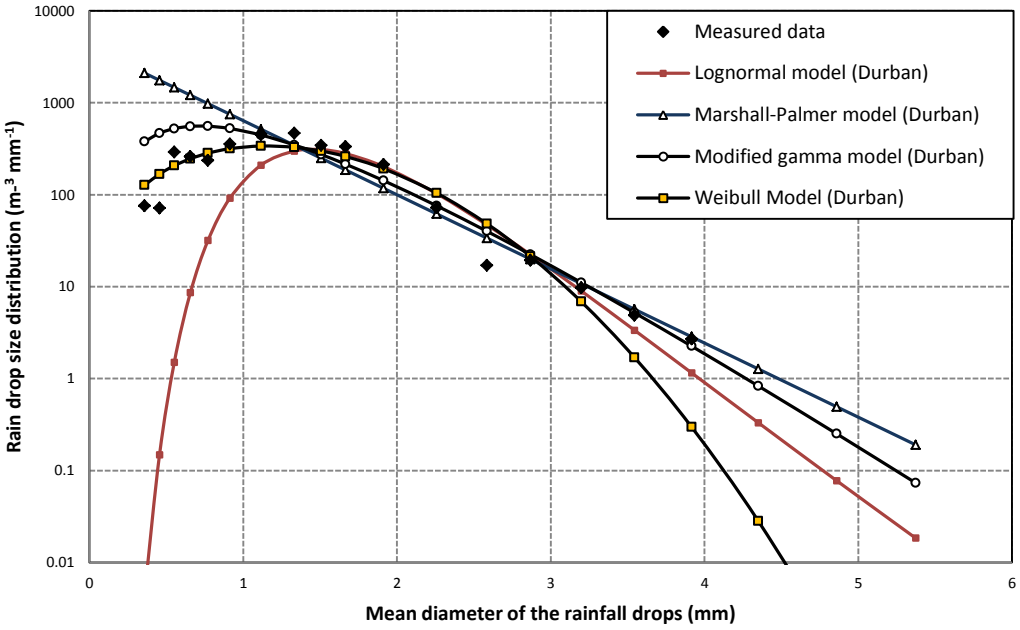

Figure 4-14: Rainfall DSD models in Durban for shower rainfall regime at 25 mm/h.

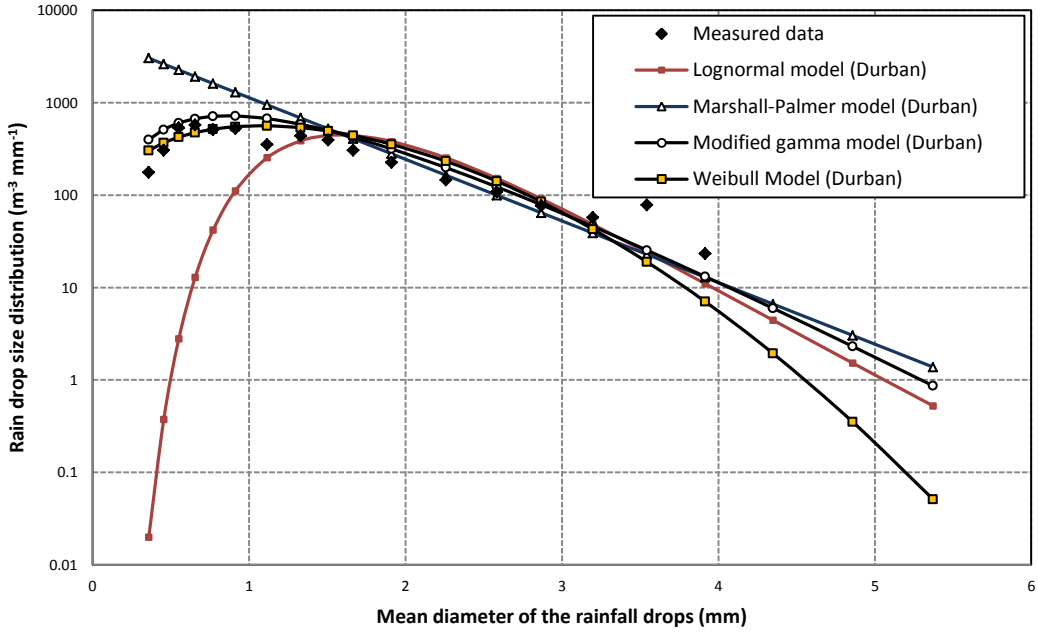

Figure 4-15: Rainfall DSD models in Durban for thunderstorm rainfall regime at 75 mm/h.

4.6.4 Annual Variation of Rainfall DSD

In this section, various proposed models for annual variation of rainfall DSD, are analyzed at rainfall rates between 0.003 mm/h and 117.15 mm/h. The method of moment technique as earlier explained is used to estimate the various estimators for four rainfall DSD models: lognormal DSD, Weibull DSD, modified gamma DSD and negative exponential DSD models.

Following the lognormal DSD model given in (2.31) and moment estimators given in (4.8*a*)-(4.8*c*), the parameters for the prediction of annual DSD in Durban for $R \leq 120$ mm/h are given by:

$$N_T = 220.85\, R^{0.3922} \tag{4.28}$$

$$\mu = -0.267 + 0.1373 \ln(R) \tag{4.29}$$

$$\sigma^2 = 0.0772 + 0.0099 \ln(R) \tag{4.30}$$

For the Weibull DSD model given in (2.32), the parameters obtained for $R \leq 120$ mm/h, using the moment estimators in (4.24) to (4.27) for annual rainfall DSD are given as:

$$N_w = 328.86\, R^{0.4042} \tag{4.31}$$

$$\eta = 0.7264\, R^{0.1272} \tag{4.32}$$

$$\beta = 2.5571 R^{-0.125} \tag{4.33}$$

For the modified gamma DSD model provided in (2.30) and moment estimators in (4.9*a*)-(4.9*d*), the parameters obtained for the annual DSD in Durban for $R \leq 120$ mm/h is given as:

$$N_m = 5.3522 \times 10^4 R^{-0.183} \tag{4.34}$$

$$\Lambda = 5.98 R^{-0.172} \tag{4.35}$$

$$\mu = 2 \tag{4.36}$$

Lastly, the negative exponential model (or Marshall-Palmer model) in (2.33) with moment estimators in (4.7*a*)-(4.7*d*) yields the DSD parameters given by:

$$N_O = 5910.8 R^{0.1607} \tag{4.37}$$

$$\Lambda = 3.9873 R^{-0.172} \tag{4.38}$$

The results from the proposed annual rainfall DSD models are presented in Figures 4-16 to 4-21 at rainfall rates of 3 mm/h, 9 mm/h, 25 mm/h and 75 mm/h respectively.

From the figures, a progressive change in the shape of the DSD measurements with rainfall rate increase in observed. In Figure 4-16, for a rainfall rate of 3 mm/h, the lognormal model is seen to underestimate the measurement at drop diameter regions less than 0.551 mm and closer to 2 mm. The other proposed models are observed to show better fits at this rainfall rate. At 9 mm/h, the Weibull model gives better estimates at lower diameter region when compared to other proposed models as seen in 4-17. The negative exponential and modified gamma models are seen to overestimate the measurement at lower diameter region, the contrary is however noticed for lognormal model. The modified gamma and negative exponential models are noted to have good fits at the higher rain drop diameter. Figure 4-18 shows the proposed DSD models at 25 mm/h, the measured is observed to have a skewed 'upside u' shape. At this rainfall rate, the lognormal model is seen as a good fit to the measurement as it takes the shape of the measurement. An overestimation is noted in the case of the other proposed models especially below 1.5 mm diameter bound for raindrops. There seem to be an agreement of all the models at higher drop diameter region. Finally at a rainfall rate of 75 mm/h in Figure 4-19, the lognormal model is again seen as a

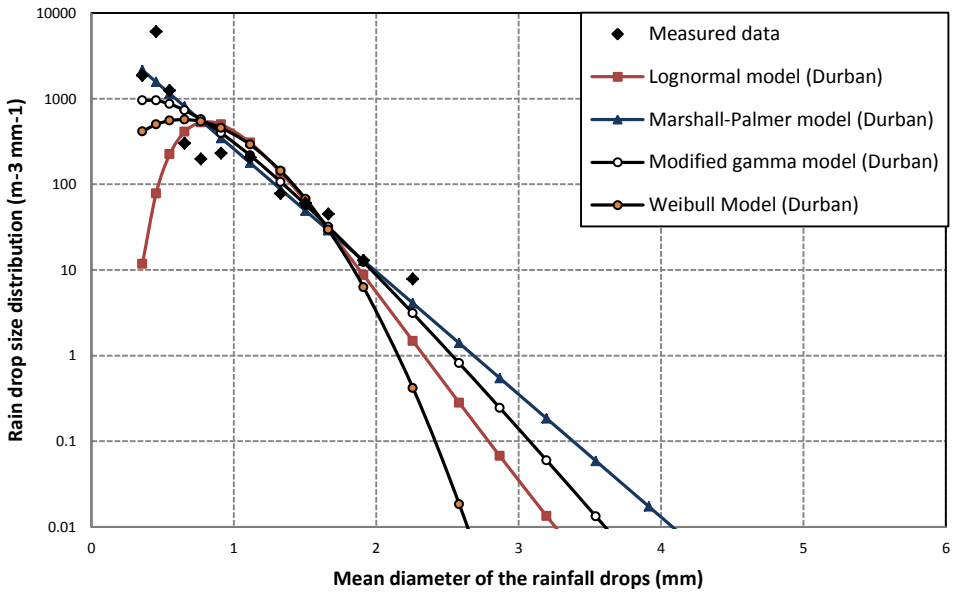

Figure 4-16: Comparison of proposed annual rainfall DSD models for Durban, South Africa at 3 mm/h

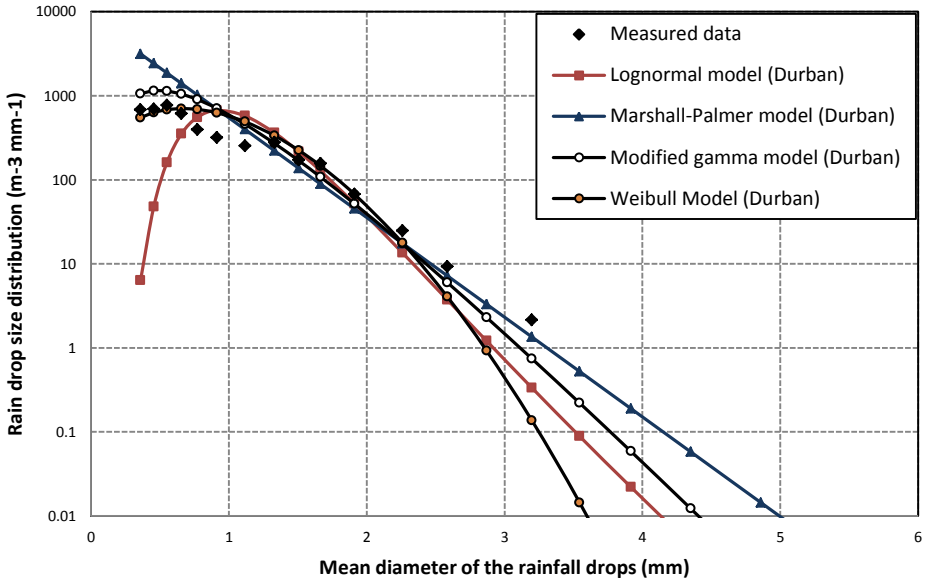

Figure 4.17: Comparison of proposed annual DSD models for Durban, South Africa at 9 mm/h

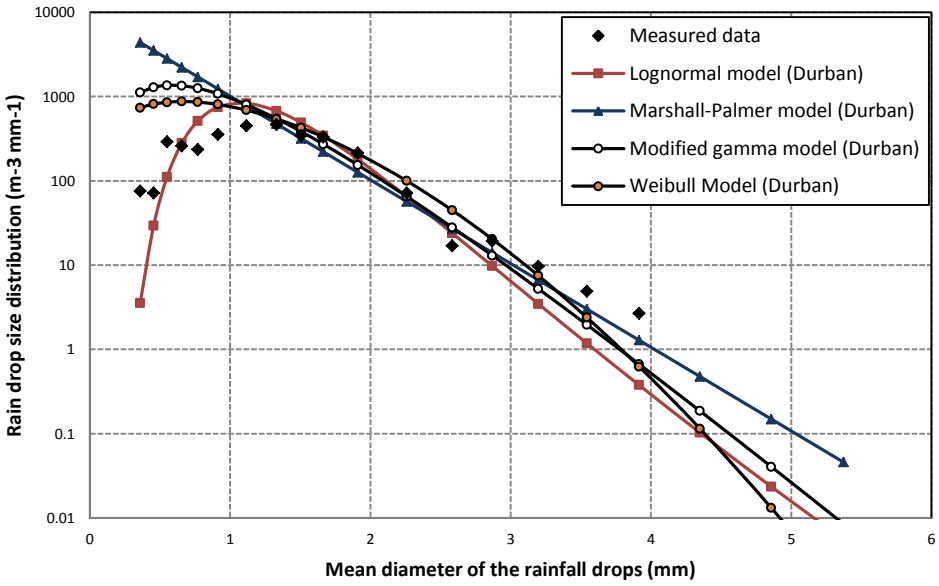

Figure 4-18: Comparison of proposed annual DSD models for Durban, South Africa at 25 mm/h

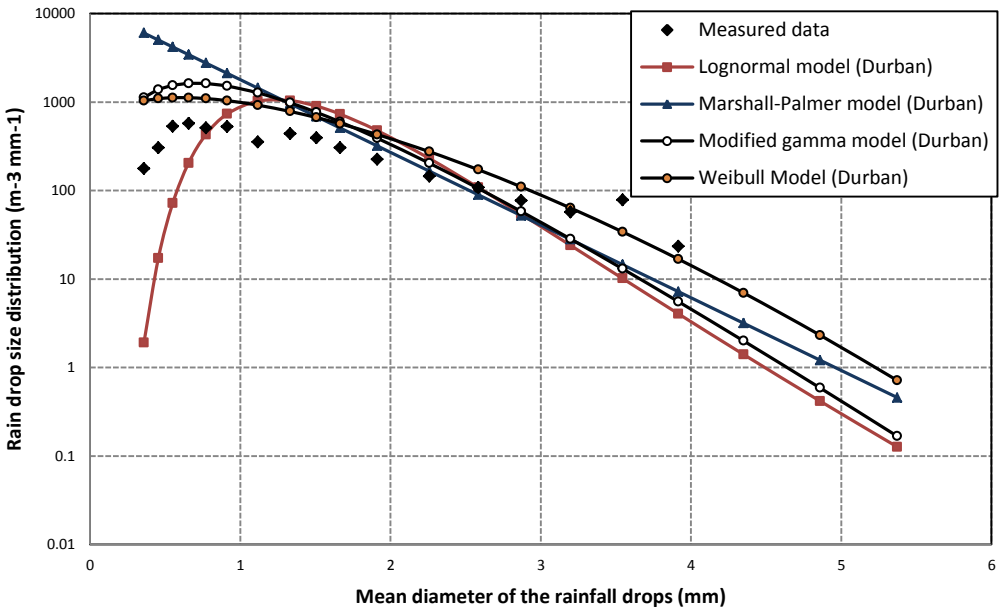

Figure 4-19: Comparison of proposed annual DSD models for Durban, South Africa at 75 mm/h

better fit to the measurement in comparison to the other proposed models for drop diameters less than 1 mm. Above 2.5 mm, there is lognormal model also has a better agreement with the DSDS measurement.

It can be seen that the proposed models have different performances as the rainfall rate is varied. Therefore, there is a need for proper error estimation at various rainfall rates to ascertain the best model(s) for different scenarios. This is the subject of the next section.

4.7 Error Estimation of Proposed Models

The PDFs of the proposed models are compared with the measured PDF, and the RMS errors are estimated. The error test are computed for the seasonal, regime and annual classification of rainfall rates and the results are shown in Tables 4-9 and 4-10. The models are tagged as thus: lognormal DSD model (LOG), Marshall-Palmer negative exponential (MPN), modified gamma model (MGM) and Weibull DSD model (WBL).

From the results in Table 4-9, the proposed Weibull model appears to be the best fit for rainfall rates below 40 mm/h in Durban under the DSD regime analysis. The Weibull DSD model has the

lowest fitting errors for drizzle, widespread and shower rainfall. However, beyond the 40 mm/h (thunderstorm), the proposed lognormal model had the lowest fitting errors followed by the Weibull model. The lognormal model has been observed as a good model at high rainfall rates [*Ajayi et al.*, 1996] and this is confirmed by the results of the error estimation.

Table 4-9: RMS errors from the proposed rainfall DSD models for different regimes in Durban

REGIME	RMS ERRORS			
	LOG	MPN	MGM	WBL
DRIZZLE	0.5158	0.6372	0.4336	0.3742
WIDESPREAD	0.3556	0.5308	0.4155	0.2836
SHOWER	0.3035	0.3294	0.1768	0.1138
THUNDERSTORM	0.1791	0.3900	0.2464	0.1932

Table 4-10: RMS errors from the proposed annual rainfall DSD models in Durban

Rainfall rate (mm/h)	RMS ERRORS			
	LOG	MPN	MGM	WBL
1	0.6839	0.7641	0.5436	0.4848
2	0.5828	0.7110	0.5023	0.4367
3.55	0.4717	0.5529	0.3503	0.2984
7	0.2381	0.4701	0.3314	0.2223
15	0.2104	0.3599	0.2861	0.1836
22	0.2075	0.3521	0.2829	0.1913
35	0.2481	0.3393	0.2529	0.1876
46	0.1539	0.3761	0.2922	0.2269
54	0.2177	0.4646	0.3946	0.3450
67	0.1501	0.4245	0.3656	0.3024
76.43	0.1803	0.3389	0.2477	0.1987
117.2	0.2446	0.4664	0.4192	0.3655
Average	**0.2991**	**0.4683**	**0.3557**	**0.2869**

From Table 4-10, the RMS errors for the annual DSD models are computed. For the error estimation, twelve rainfall DSD spectrals at different rainfall rates are compared with the proposed models as seen. The results show that the Weibull model provides a good fitting to the measurement for rainfall rates closer to 40 mm/h, for rainfall rates beyond this threshold, the proposed lognormal model performs better. Since microwave attenuation is mainly associated with contributions from high rainfall rates, it is therefore conclusive that the lognormal model is the best annual model for Durban.

4.8 Chapter Summary

In this chapter, the method of moment point estimation was applied to derive empirical rainfall DSD models for the city of Durban, South Africa. Different rainfall DSD models from the 1-minute samples were fitted and parameterised as function of rainfall rate. The classification of rainfall data into monthly, seasonal, regime and annual analysis has proven useful in the prediction of rainfall DSD conditions in Durban.

The monthly DSD results have shown that at their respective $R_{0.01}$, the four months of winter have the lowest DSD concentration in Durban. While at the same 0.01% rainfall exceedences, the months coinciding with summer and autumn, experience a high level of DSD concentration. Thus, seasonal characteristics play an important role in the variation of DSD at locations and therefore, influence attenuation statistics.

The proposed rainfall DSD models show a good agreement with measurements from the disdrometer. Of particular interest is the low fitting errors obtained for the proposed Weibull models for low rainfall rate below 40 mm/h and the proposed lognormal model for rainfall rates above 40 mm/h. This confirms the opinion of contemporary research that lognormal model is best suited for locations with frequent occurrence of high rainfall rates. With Durban being a subtropical region with largely pseudo-tropical rainfalls during summer, therefore, the proposed lognormal DSD model will prove important for microwave link designs at this location. However, there is still a need to encourage more rainfall DSD measurements as this increases the reliability and consistency in the prediction and modelling procedure.

The next chapter explores the estimation of rainfall attenuation from the proposed rainfall DSD models in Durban using the Mie scattering computational technique. The computed rainfall attenuation in this chapter is examined at varying transmission frequencies under different rainfall rate classifications.

CHAPTER FIVE

Estimation of Rainfall Attenuation in Durban

5.1 Introduction

In chapter four, the microstructural parameter, rainfall DSD was examined empirically from the drop-size measurements using the Joss-Waldvogel disdrometer. Standard statistical models were employed for different rainfall rate classification using the method of moment (MM) parameter estimation technique. The conclusion from this study has shown that there is a striking similarity in the rainfall DSD patterns in subtropical and tropical climates as indicated by the importance of lognormal model for DSD prediction at high rainfall rates [*Ajayi et al.*, 1996].

In the chapter, the prediction of rainfall attenuation in Durban is examined; Rainfall attenuation is basically attributed to the scattering and absorption of transmitted signal energy along the transmission path. Quantifying the amount of rainfall attenuation, or its threshold value, at a location depends not just on the knowledge of the drop-size distribution, but on the raindrop energy scatterers and absorbers. Raindrop energy scatterers have a larger diameter compared to the transmission wavelength, while raindrop energy absorbers have smaller diameters relative to the transmission wavelength. At microwave frequencies, raindrop scatterers play a major role and hence, account for bulk of the rainfall attenuation on deployed links. Therefore, it is of major interest to investigate the extent of raindrop scattering in rainfall attenuation. Major scattering analysis for small particles has been adopted for rainfall droplets; they are the Rayleigh scattering and Mie Scattering. The Rayleigh scattering, however, becomes inaccurate as the transmission frequency approaches 3 GHz, while the Mie scattering technique is much more accurate beyond the same frequency [*Mie*, 1908; *Bohren and Huffman*, 2004; *Naicker*, 2006; *Fu et al.*, 2008; *Hahn*, 2009]. Estimation of the widespread rain droplet scattering for a point rainfall measurement is the last step towards predicting rainfall attenuation vis-a-vis the availability of rain drop-size distribution.

Therefore, Mie scattering technique is adopted for the estimation of rainfall specific and path attenuation in this study. It is sensitive to rain drop-shapes and its performance varies with increasing raindrop shape even as rainfall rate increases. Rain drop-shape can be spherical, spheroidal, oblate-spheroidal or hamburger [*Li et al.*, 2000]. The spherical shape, is however, applied in this research and used for all assumptions in the scattering technique. The assumption of spherical rainfall droplets is needed for the purpose of simplicity and understanding of the rigorous

mathematics involved in the solution of the wave-boundary problem. The specific attenuation are estimated from the proposed rainfall DSD models for Durban and are investigated according to the monthly, seasonal, regime and annual variation in the radioclimatological pattern.

5.2 Modelling and Computational Procedure for Extinction Cross Section

The mechanisms of rainfall attenuation are of two kinds: reflection mechanism and absorption mechanism. The two mechanisms are dependent on the transmission frequency and polarization sequence of a microwave link. In theory, the reflection encountered during rainfall account for the scattering mechanisms of signals due to rainfall – this result in destructive coupling signals (noise) being added to the transmitted signal. The scattering coefficients can range from real to complex values, which are very helpful, in the calculations of propagation coefficients. *Mulangu and Afullo* [2009] and *Odedina and Afullo* [2010] in their recent studies on rainfall DSD determined the scattering parameters for locations in Botswana and South Africa respectively using the Mie scattering technique. The Mie scattering technique allows for the easy computation of the extinction cross section (ECS).

The ECS computed by *Odedina and Afullo* [2010a; 2010b] and *Mulangu and Afullo* [2009] assumed a spherical rainfall drop shape. Their work estimated the scattering parameters by using a combination of complex refractive index for water proposed by *Liebe et al*. [1991], droplet scattering theory suggested by *Mie* [1908] and MATLAB® program for Mie scattering coefficients by *Mätzler* [2002a; 2002b].

5.2.1 Computation of Complex Refractive Index of Water

The first step involves obtaining the equation for the complex refractive index of water. Mathematically, the complex refractive index is a function of the dielectric constant of water given from *Odedina* [2010b] as:

$$m(f,T) = \sqrt{\epsilon(f,T)} \tag{5.1}$$

where ϵ(f, T) is the dielectric constant of water which is both a function of the frequency and temperature.

According to *Liebe et al*. [1991], the dielectric constant of water is a complex function with real and imaginary parts given by:

$$\epsilon(f,T) = \epsilon' + i\epsilon'' \tag{5.2}$$

Furthermore, *Liebe et al.*[1991], obtained the expressions for the dielectric constant of water for temperature ranges between -20^{O}C and 60^{O}C. Their results were classified into three categories: single Debye model, double Debye model and the broadband model. The single Debye model is mainly designed for the estimation of dielectric constants for frequencies below 100 GHz and is given by:

$$\epsilon_D(f,T) = \frac{(\epsilon_o - \epsilon_\infty)}{1 - i(f/\gamma_D)} + \epsilon_\infty \tag{5.3}$$

where,

$$\theta = 1 - \frac{300}{[273.15 + T]} \tag{5.3a}$$

$$\epsilon_o(T) = 77.66 - 103.3\theta \tag{5.3b}$$

$$\epsilon_\infty = 0.066\epsilon_o \tag{5.3c}$$

$$\gamma_D(T) = 20.27 + 146.5\theta + 314\theta^2 \tag{5.3d}$$

where *i* is the notation of the complex number operator.

The double Debye model is used for the modelling of the complex refractive index of water for droplet frequency beyond 100 GHz. The property of this model is a slight deviation from the single Debye method in a way; the model equations are given by:

$$\epsilon_m(f,T) = \epsilon_o - f\left[\frac{(\epsilon_o - \epsilon_1)}{(f + i\gamma_1)} + \frac{(\epsilon_1 - \epsilon_2)}{(f + i\gamma_2)}\right] \tag{5.4}$$

where,

$$\epsilon_1 = 0.0671\epsilon_o \tag{5.4a}$$

$$\gamma_1 = 20.20 + 146.4\theta + 316\theta^2 \quad (5.4b)$$

$$\epsilon_2 = 3.52 + 7.52\theta \quad (5.4c)$$

$$\gamma_2 = 39.8\ \gamma_1 \quad (5.4d)$$

The last model is called the *broadband* model used for frequencies between 1 THz and 30 THz. This, however, will not be a subject of interest in this research. The expressions from (5.3) to (5.4d) all require two inputs, droplet frequency and ambient temperature. A Mie scattering MATLAB® program was developed for the computation of the complex refractive indices of water for frequencies between 2 GHz and 1 THz. The ambient temperature assumed for Durban is based on measurements from the initial microwave link set up in 2004 as proposed by *Odedina* [2010b]. The variation in the ambient temperature shows a gradual increase in the monthly temperature from February to April. Table 5-1 gives the summary of the average monthly temperature for Durban in 2004.

Table 5-1: Average temperature recorded in Durban from 19.5 GHz microwave link in 2004 [*Odedina*, 2010b]

MONTH	TEMPERATURE (^oC)
February	21.78
March	22.48
April	23.12
May	19.03
June	18.79
July	17.07
August	18.10
September	19.13
October	17.82
November	18.79
December	25.84
AVERAGE	**20.18**

5.2.2 Computation of the Extinction Cross Section

Electromagnetic (EM) wave propagation involves the transference of wave energy outwardly from either an isotropic or omni-directional source, to another. In microwave transmission, wave energy usually travels at incidence through different atmospheric media with varying refractive indices, based on dynamic parameters such as temperature and atmospheric pressure. In the presence of a rainy medium, EM waves at high frequencies interact with rain drop particles which are of different shapes, sizes, orientation, velocity and surrounding media parameters to yield different waves disturbances [*Li et al.,* 1995]. The degree to which the raindrop particles affect the travelling wave is primarily described in terms of scattering or absorption encountered within the rainy medium. The area of interaction, in which the effects of rain droplet scattering and absorption are prominent on wave energy particularly at microwave frequencies, is referred to as the *cross section of extinction* [*Cullen and Kumar*, 1970] . Thus, the extinction cross section (ECS) is an hypothetical abstraction used to describe the amount of wave energy interacting with rain droplets resulting in its scattering and absorption over an area [*Hahn*, 2009]. It is also the ratio of the total energy dispersed or scattered per unit time to the energy density of the incident electromagnetic wave [*Sadiku*, 2000].

Practically, the knowledge of the ECS for signal propagation in microwave networks for a rainy medium can be executed by assuming that raindrops are homogeneously spherical or homogeneously oblate-spheroids. The former is the simplest formulation applicable for the either the Mie or Rayleigh scattering theory and is insensitive to depolarization, while, the latter is the most complex, sensitive to depolarization and can be obtained using *Pruppacher and Pitter* (or P-P) model [1971; 1978], T-matrix method [*Li et al.*, 2002] *e.t.c.* In this work, the Mie scattering theory, proposed by Gustav Mie in 1908, is used alongside the results obtained from the computations of the complex refractive index of water, *m,* undertaken in section 5.1.1. In the Mie scattering theory, the real part of the forward scattering amplitude is used to determine the scattering parameters. By definition, the forward scattering amplitude is given by *Mie* [1908] as:

$$s(0) = \frac{1}{2}\sum_{n=0}(2n+1)[a_n(m,\alpha) + b_n(m,\alpha)] \tag{5.5}$$

where $a_n(m,\alpha)$ and $b_n(m,\alpha)$ correspond to the Mie scattering coefficients which are dependent on m the complex refractive index of water, and, α which depends on the ambient temperature and droplet frequency.

The *n*th truncation of the infinite series can be determined from the work of *Bohren and Huffman* [2004] and *Mulangu et al.* [2009], where:

$$n_{max} = \alpha + 4\alpha^{\frac{1}{3}} + 2 \tag{5.6}$$

for,

$$\alpha = k\bar{a} \tag{5.7}$$

where, $k = 2\pi/\lambda$, is the wave number; α is the particle size for all wavelengths of the rain drops; $\bar{a}$ is the radius for a spherical drop assumption.

The solution for *n*th truncated values of $a_n(m,\alpha)$ and $b_n(m,\alpha)$ of the forward scattering amplitude, $s(0)$, can be found using a combination of special spherical Bessel functions for spherical raindrops given by [*Sadiku*, 2000; *Mätzler*, 2002a, 2002b; *Fu and Sun*, 2006; *Hahn*, 2009; *Odedina*, 2010b]:

$$a_n(m,\alpha) = \frac{m^2 j_n(m\alpha)[\alpha j_n(\alpha)]' - j_n(\alpha)[m\alpha j_n(m\alpha)]'}{m^2 j_n(m\alpha)\left[\alpha h_n{}^{(1)}(\alpha)\right]' - h_n{}^{(1)}(\alpha)[m\alpha j_n(m\alpha)]'} \tag{5.8}$$

$$b_n(m,\alpha) = \frac{j_n(\alpha)[m\alpha j_n(m\alpha)]' - j_n(m\alpha)[\alpha j_n(\alpha)]'}{h_n{}^{(1)}(\alpha)[m\alpha j_n(m\alpha)]' - j_n(m\alpha)\left[\alpha\, h_n{}^{(1)}(\alpha)\right]'} \tag{5.9}$$

where m represents the complex refractive index of water at a specified ambient temperature; $j_n(m\alpha)$ and $j_n(\alpha)$ is the spherical Bessel of the first kind with $m\alpha$ and α as their arguments repectively; $h_n{}^{(1)}(\alpha)$ is the spherical Hankel function of the first kind.

Mathematically, *Arfken and Weber* [2003] describes the functionality of the spherical Bessel and Hankel functions used in (5.8) and (5.9) as:

$$j_n(a) = \sqrt{\frac{\pi}{2a}}\, J_{n+\frac{1}{2}}(a) \tag{5.10}$$

$$h_n{}^{(1)}(a) = \sqrt{\frac{\pi}{2a}}[j_n(a) + iy_n(a)] \tag{5.11}$$

where,

$$y_n(a) = (-1)^{n+1} \sqrt{\frac{\pi}{2a}} J_{-n-\frac{1}{2}}(a) \tag{5.12}$$

Using expressions (5.8) – (5.12), the arguments of the Bessel and Hankel functions can be substituted with α and *m*α as the case may require.

MATLAB® program developed by *Mätzler* [2002a; 2002b; 2003] were modified for the computation of *S*(*0*) from the Mie computations. The results obtained from the scattering coefficient computations can further be used to evaluate the corresponding extinction cross section. The ECS of a transmitted signal can thus be estimated by multiplying the real part of *s*(*0*) by a factor as given below [*Van der Hulst*, 1957]:

$$Q_{ext}(D) = \frac{4\pi}{k^2} Re\{s(0)\} \tag{5.13}$$

Odedina and Afullo [2009*a*; 2010*a*] concluded that the terms of $Q_{ext}(D)$ for Durban at an average temperature of 20°C can be reduced to a frequency-specific power law function in the form of :

$$Q_{ext}(D) = k_{ext} \bar{a}^{\varsigma_{ext}} \ [mm^2] \tag{5.14}$$

where k_{ext} and ζ_{ext} are the power-law coefficients corresponding to extinction cross section, Q_{ext}. These values are unique for each frequency and vary with the complex refractive index of water, where $\bar{a}$ is the radius of the drop-size such that $\bar{a} = D/2$, for all sizes of mean diameter, *D*.

Odedina and Afullo [2010*a*] had previously obtained the values of k_{ext} and ζ_{ext} for selected frequencies up to 35 GHz. However, the proposed power-law coefficients are only valid for rain drop-sizes of centimetre unit scale. Therefore, in this study, another regression technique was undertaken for rainfall drop-sizes of millimeter unit scale and for selected frequencies up to 1 THz. Some of the results from these computations are available in Appendix E. Table 5-2 shows the summary of the different results of the power law coefficient obtained from regression fitting technique undertaken for 37 selected frequencies. Figure 5-1a shows the results of the fitting

Table 5-2: Computed values for the extinction cross section power-law coefficients for Durban at 20°C for a frequency range of 2 GHz to 1000 GHz using Mie technique

FREQUENCY (GHz)	COMPLEX REFRACTIVE INDEX	k_{ext}	ς_{ext}
2	8.9014 + 0.4843*i*	0.0027	3.2737
4	8.7763 + 0.9442*i*	0.0191	3.7875
6	8.5830 + 1.3599*i*	0.0851	4.3988
8	8.3396 + 1.7196*i*	0.217	4.5805
10	8.0649 + 2.0188*i*	0.3857	4.5272
12	7.7755 + 2.2594*i*	0.5866	4.4443
15	7.3405 + 2.5234*i*	0.955	4.3453
16	7.1994 + 2.5892*i*	1.0939	4.3164
18	6.9272 + 2.6934*i*	1.3883	4.2576
19.5	6.7332 + 2.7509*i*	1.6169	4.2104
20	6.6705 + 2.7667*i*	1.6936	4.194
23	6.3171 + 2.8321*i*	2.1474	4.0885
25	6.1026 + 2.8532*i*	2.4567	4.0186
28	5.8107 + 2.8603*i*	2.8544	3.9035
30	5.6345 + 2.8530*i*	3.1204	3.8323
35	5.2500 + 2.8072*i*	3.7452	3.6639
40	4.9322 + 2.7383*i*	4.3106	3.5077
45	4.6668 + 2.6586*i*	4.8223	3.3646
50	4.4428 + 2.5752*i*	5.2855	3.2353
60	4.0869 + 2.4099*i*	6.0493	3.0094
70	3.8182 + 2.2560*i*	6.625	2.8209
90	3.4421 + 1.9907*i*	7.4097	2.5284
100	3.3061 + 1.8778*i*	7.6874	2.4156
[a]150	2.9154 + 1.5083*i*	8.3061	2.0691
200	2.7103 + 1.2655*i*	8.3464	1.9293
250	2.5871 + 1.1051*i*	8.2291	1.8785
300	2.5029 + 0.9932*i*	8.0777	1.8672
350	2.4395 + 0.9115*i*	7.935	1.87
400	2.3882 + 0.8493*i*	7.8144	1.875
500	2.3067 + 0.7597*i*	7.6315	1.8812
600	2.2418 + 0.6958*i*	7.488	1.8919
700	2.1880 + 0.6455*i*	7.3793	1.899
750	2.1644 + 0.6235*i*	7.3338	1.9021
800	2.1426 + 0.6032*i*	7.2899	1.9055
850	2.1226 + 0.5841*i*	7.2585	1.9088
900	2.1042 + 0.5662*i*	7.2183	1.9104
1000	2.0715 + 0.5332*i*	7.1602	1.915

[a]Estimation for frequencies above 100 GHz was done using the double debye method, the single Debye method was applied for frequencies below 100 GHz

procedure undertaken for Q_{ext} at four selected frequencies of 4 GHz, 10 GHz, 50 GHz and 150 GHz. Figure 5-1b show the variation of the power-law coefficients of k_{ext} and ζ_{ext} at different frequencies for 20°C ambient temperature.

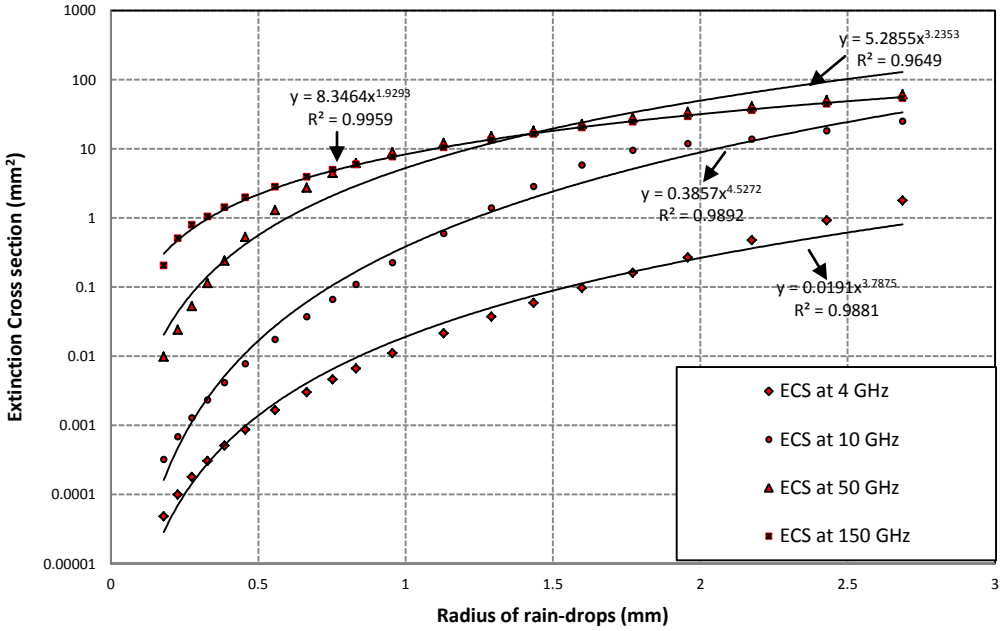

Figure 5-1a: Fitting procedure for extinction cross section for droplet frequency of 4 GHz, 10 GHz, 50 GHz and 150 GHz respectively at an ambient temperature of 20°C

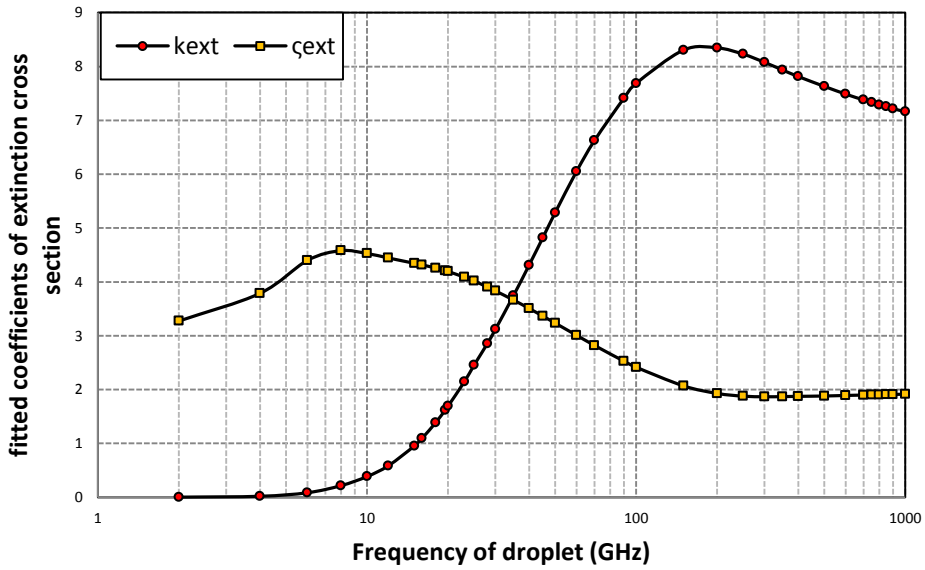

Figure 5-1b: Variations in the fitted parameters of k_{ext} and ζ_{ext} at an ambient temperature of 20°C

5.3 Computation of Specific Attenuation

Rain attenuation prediction from rainfall for signal transmission along a terrestrial path can be estimated from the expression in ITU-R recommendation [*ITU-R P.530-13*, 2009] as:

$$A_p = A_s \times d_{eff} \tag{5.15}$$

where A_s is given as the specific attenuation and d_{eff} is the effective transmission distance which is a product of the actual link distance and the path reduction factor.

By extension, the specific attenuation is given by [*Ajayi et al.*, 1996]:

$$A_s[dB/km] = 4.343 \times 10^{-3} \int_0 N(D)\, Q_{ext}(D)\, dD \tag{5.16}$$

where the extinction cross section (ECS) is $Q_{ext}(D)$ in mm^2 and dD is the change in diameter (or diameter interval) in mm; the rainfall drop-size distribution is represented by $N(D)$.

Thus, (5.16) can be reduced to an expression for specified 20 diametric sizes based on our disdrometer channels given by:

$$A_s[dB/km] = 4.343 \times 10^{-3} \sum_{i=1}^{20} N(D_i) \times k_{ext} \bar{a}_i^{\zeta ext} \times \Delta D_i \tag{5.17}$$

where k_{ext} and ζ_{ext} are the power law coefficients of the extinction cross section. ΔD_i is the diameter interval between two successive diameter classes with units in mm. The table in appendix E-1 shows the respective diameter interval corresponding to each diameter bin for the RD-80 disdrometer.

5.4 Comparison of proposed Specific Attenuation Models for Durban

In this section, the specific attenuation for the proposed models for Durban are computed using (5.17) and are based on the DSD models proposed in Chapter 4. The investigation undertaken is done using monthly, seasonal, regime and annual analysis of rainfall data in Durban. The results and computations for each of the investigation are available in section 5.4.1 to 5.4.4.

5.4.1 Monthly Variation of Specific Attenuation

This sub-section considers monthly analysis of attenuation based on the proposed monthly DSD models developed in section 4.7.3. The four proposed models were used to investigate the variation in the monthly specific attenuations in Durban. The specific attenuations were computed using equation (5.17) and other parameters used have earlier been discussed. Generally, the proposed Weibull DSD model is observed to have a higher specific attenuation estimates than all proposed models, for all the monthly values of $R_{0.01}$ for all the frequency ranges as seen in Figures 5-2 to 5-6. Below 100 GHz, the negative exponential DSD model is observed to have lower estimates. Interestingly, above 100 GHz, the negative exponential DSD model is observed to have higher estimates than the lognormal DSD model, but equally has closer estimates to that of modified gamma model. Figure 5-6 show some of individual plots for selected months of January, March, May, July, August, October, November and December.

As seen from the results, the month of April at $R_{0.01}$ = 90.83 mm/h is predicted to experience the highest specific attenuation below 90 GHz, when compared with the other eleven months, for all the proposed models. April has specific attenuation ranges between, 1.86 dB/km and 2.39 dB/km at 12 GHz; 7.21 dB/km and 12.21 dB/km at 25 GHz; 18.07 dB/km and 26.72 dB/km at 60 GHz; 26.62 dB/km and 33.75 dB/km at 100 GHz. At around 90 GHz, November has the highest specific attenuation at $R_{0.01}$ = 53.15 mm/h with specific attenuation varying between 27.42 dB/km and 38.70 dB/km for all models at 100 GHz. Below 12 GHz, the months of February, March, May and June all experience lower specific attenuations at their respective $R_{0.01}$ than the month of November. However at 30 GHz, only the months of March and May have specific attenuation estimates exceeding that of November.

From Figures 5-2 to 5-5, it is observed that the months with the lowest specific attenuation values due to the winter dry spell are May, June, July and August at $R_{0.01}$ of 62.08 mm/h, 34.07 mm/h, 20.78 mm/h and 12.16 mm/h respectively for all frequencies. The low specific attenuation figures in May can be attributed to the overlapping seasonal transition from autumn to winter. Above 90 GHz, the month of November experiences the largest specific attenuation followed by April, March and December. Again, the 'winter dry spell' months all experience lower estimates with the maximum figures at around 6.35 dB/km, 6.4 dB/km, 5.05 dB/km and 4.31 dB/km respectively.

Broadly speaking, the specific attenuation figures for all the months show a decreasing trend as the frequency approaches 1 THz (as seen in Figure 5-6) due to the unbiased depolarization effects of

Mie scattering due to the spherical assumption. Also, a back-to-back observation of the summer season from October to February indicates an initial rise in specific attenuation in October and a gradual dip from December to February. There is, however, a sharp increase in the specific attenuation estimates until the onset of winter in May. Consequently, it is observed that the

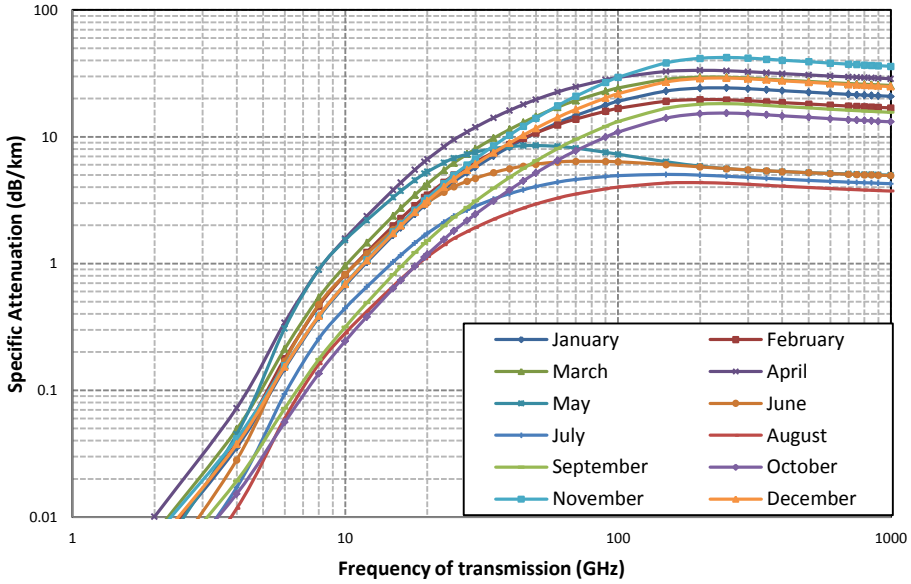

Figure 5-2: Monthly specific attenuation at their respective $R_{0.01}$ in Durban using lognormal DSD model

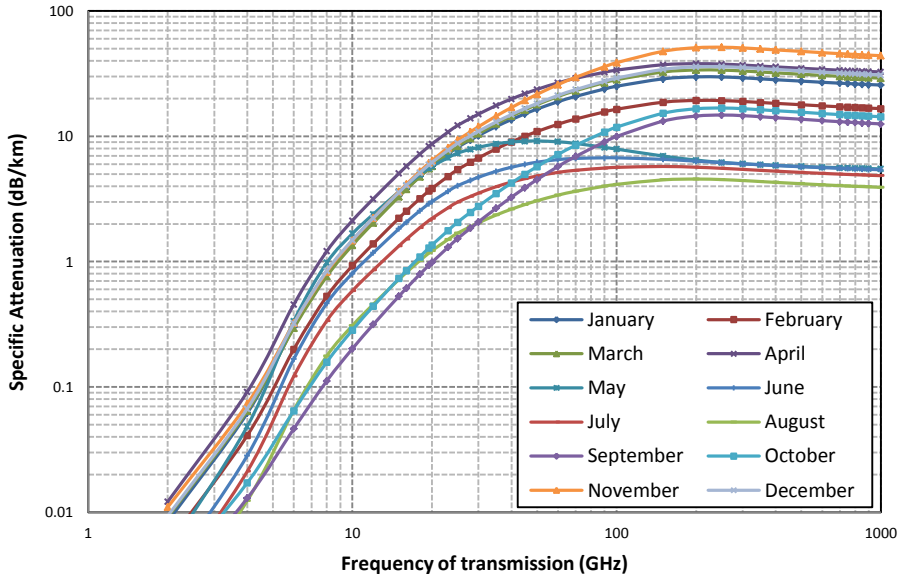

Figure 5-3: Monthly specific attenuation at their respective $R_{0.01}$ in Durban using Weibull DSD model

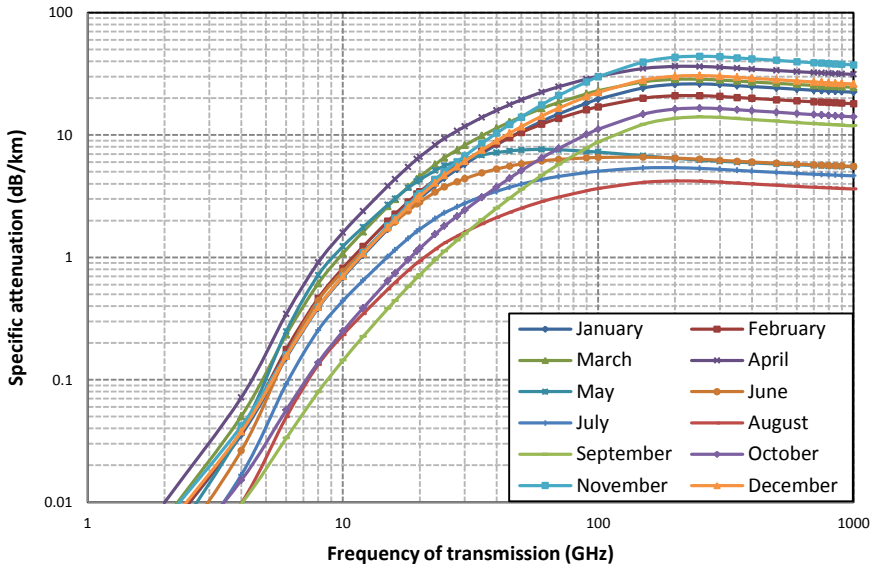

Figure 5-4: Monthly specific attenuation at their respective $R_{0.01}$ in Durban using modified gamma DSD model

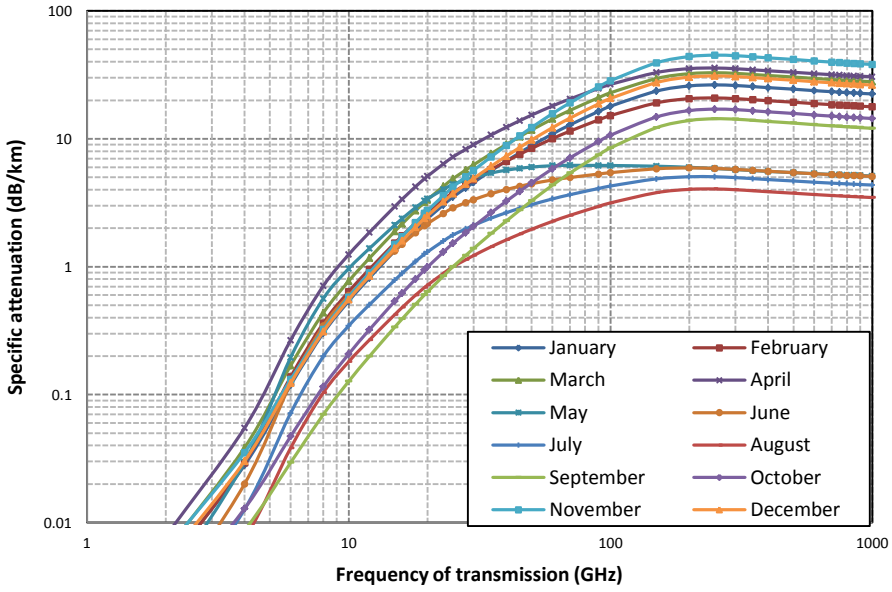

Figure 5-5: Monthly specific attenuation at their respective $R_{0.01}$ in Durban using negative exponential DSD model

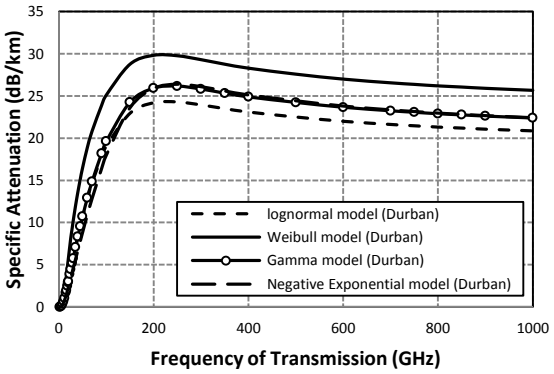

(a) January

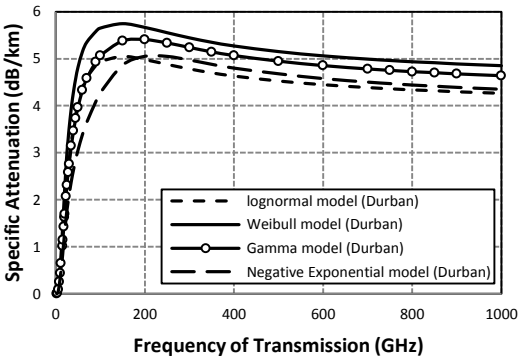

(d) July

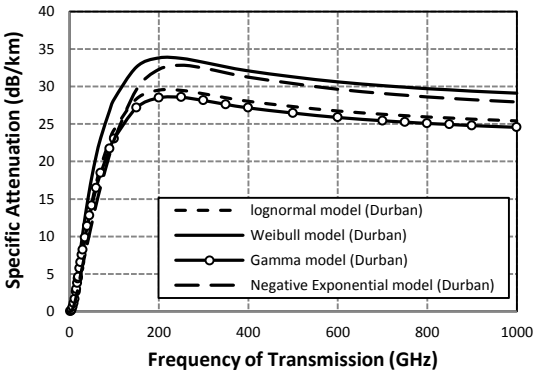

(b) March

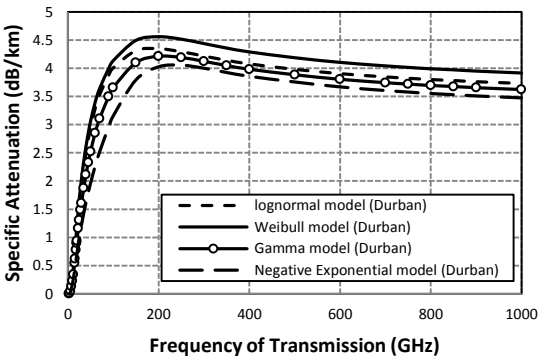

(e) August

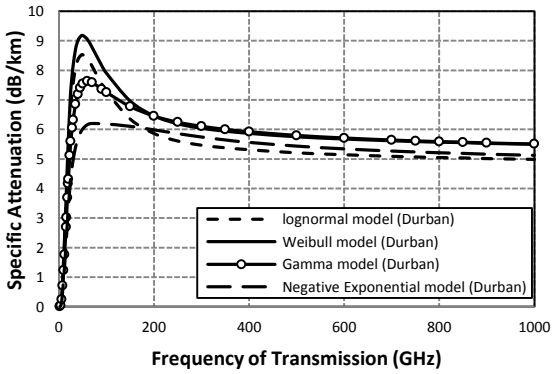

(c) May

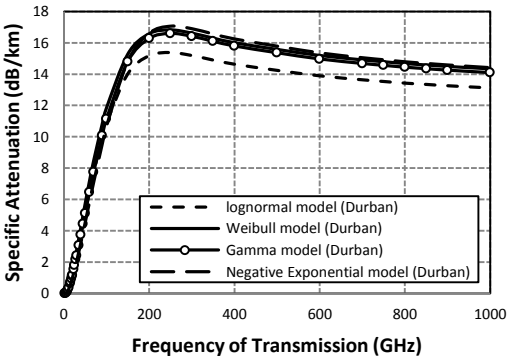

(f) October

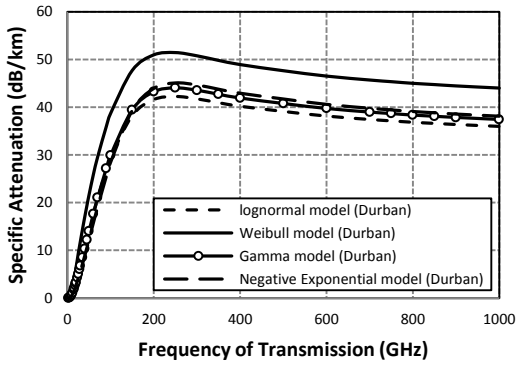

(g) November

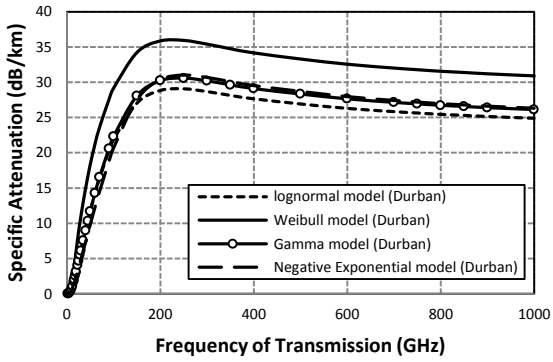

(h) December

Figure 5-6: Monthly specific attenuation performance for the proposed models for selected months at their respective $R_{0.01}$

composition of volume density of rain droplets and not only the high values of $R_{0.01}$ plays a huge role in influencing the variability of the specific attenuation. For example, the rainfall DSD plots in Figure 4-6 to 4-9, it is noticed that November and December experienced larger volume of smaller diameter raindrops than all other months. Although, $R_{0.01}$ in those two months is lower than those of the months of March and April, the specific attenuation figures of November are larger at higher frequencies.

5.4.2 Seasonal Variation of Specific Attenuation

The variation of seasonal specific attenuation is conspicuously evident in the graphs displayed from Figures 5-7 to 5-10. It is observed that the Weibull DSD model has a higher specific attenuation estimates for all the seasons in Durban. Below 100 GHz, the autumn season at $R_{0.01}$ = 72.15 mm/h is observed to have the highest estimates, with an average fluctuation of about 2 dB/km, when compared to summer season. The seasons of winter and spring are both predicted to witness the lowest figures of specific attenuation at 53.37 mm/h and 18.51 mm/h respectively. Also, the estimates for winter season are higher at 100 GHz when compared with that of the spring season. In addition, above 100 GHz , the summer season has the highest estimates when compared with other seasons. Although, it appears that summer and autumn have similar estimates with the negative exponential, lognormal and gamma DSD models especially at frequencies closer to 1 THz. On the contrary, the winter and spring seasons have the lowest estimates above 100 GHz. The spring season is, however, observed to have higher estimates than the winter season; this is possibly as a

result of high density of rainfall drops in spite of its lower value of $R_{0.01}$ of 18.51 mm/h in comparison with winter at 53.37 mm/h.

A comparative examination of the specific attenuation for all the proposed models at selected frequencies and respective $R_{0.01}$ is undertaken. At 12 GHz: summer season estimates ranges from 0.89 dB/km to 2.3 dB/km; autumn season from 1.44 dB/km to 2.65 dB/km; winter season from 1.272 dB/km to 2.10 dB/km; spring season from 0.35 dB/km to 0.65 dB/km. At 60 GHz: summer season estimates ranges from 12.54 dB/km to 21.53 dB/km; autumn season from 14.45 dB/km to 22.11 dB/km; winter season from 5.93 dB/km to 8.13 dB/km; spring season from 6.20 dB/km to 6.31 dB/km. At 400 GHz: summer season estimates ranges from 27.60 dB/km to 33.84 dB/km; autumn season from 25.60 dB/km to 29.53 dB/km; winter season from 5.51 dB/km to 6.17 dB/km; spring season from 8.38 dB/km to 9.69 dB/km.

In general, the negative exponential model gives lower estimates at frequencies below 100 GHz but has higher estimates above the 100 GHz frequency domain. Based on seasonal variability, investigation has shown that the two seasons of summer and autumn respectively account for the highest specific attenuation in Durban, with interchangeable roles, below 100 GHz and above 100 GHz. On the other hand, the seasons of winter and spring produces lower attenuation, with interchangeable roles, below 100 GHz and above 100 GHz.

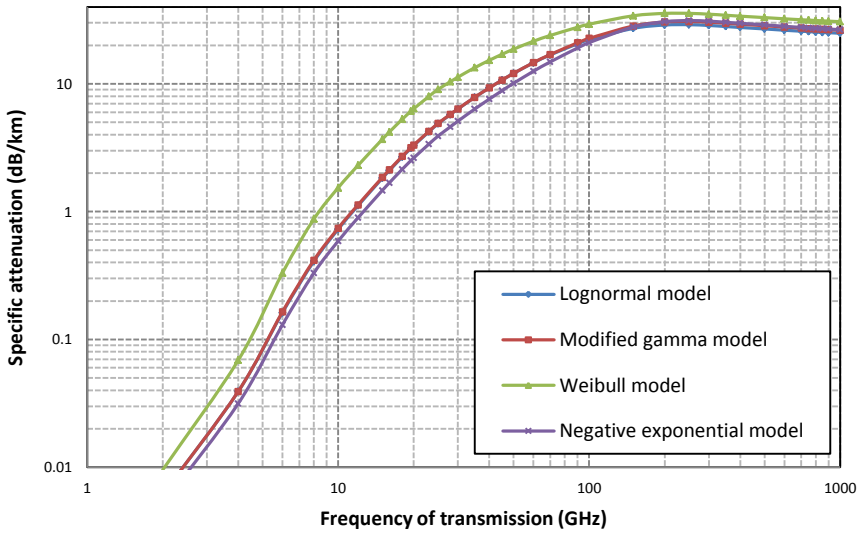

Figure 5-7: Proposed specific attenuation in summer season in Durban for $R_{0.01}$= 50.48 mm/h for all models

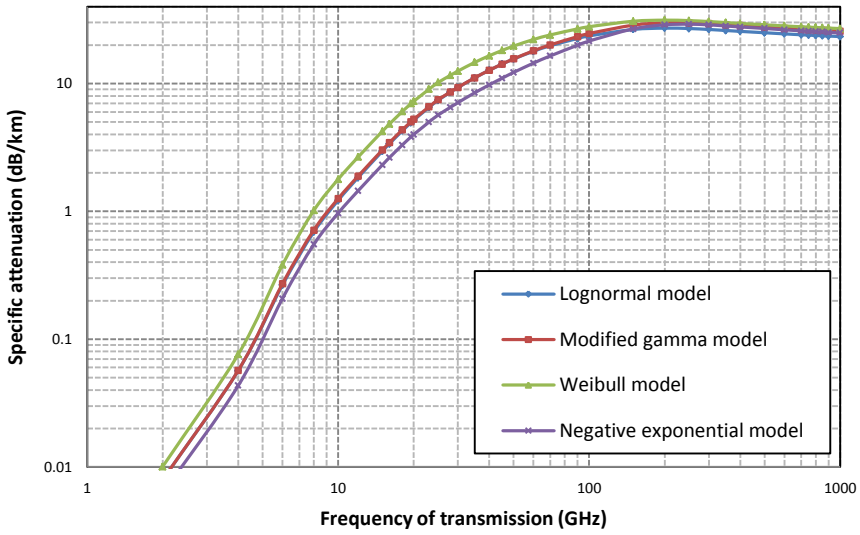

Figure 5-8: Rainfall drop-size distribution in Durban at autumn season with $R_{0.01}$ = 72.15mm/h

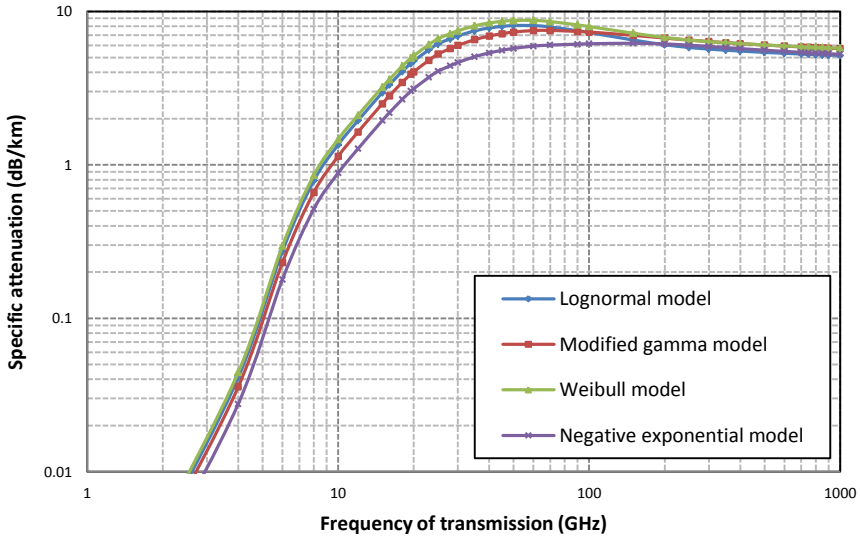

Figure 5-9: Proposed specific attenuation in winter season in Durban for $R_{0.01}$= 53.37mm/h for all models

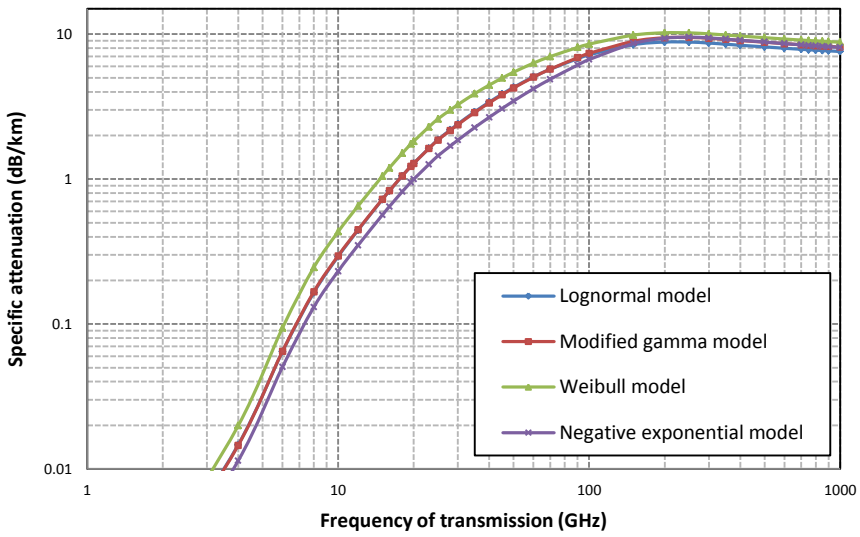

Figure 5-10: Proposed specific attenuation in spring season in Durban for $R_{0.01}$= 18.51mm/h for all models

5.4.3 Regime Variation of Specific Attenuation

By employing the equations in section 5.2, the specific attenuation for four averaged rainfall rates representing the different rainfall regime are computed. The rainfall rates considered are 4 mm/h, 9 mm/h, 25 mm/h and 75 mm/h with an ambient temperature of 20^{o}C taken for Durban. The frequency range for our results is from 2 GHz to 100 GHz. The ITU-R recommendation [*ITU-R P.838-3*, 2005] estimates for horizontal and vertical polarization are also included in these results for the purpose of comparison (concise methods for estimating rainfall specific attenuation in ITU-R P.838-3 are provided in the Appendix B). The measured specific attenuation used as the basis of comparison was taken as a semi-empirical value which is a product of the measured DSD from the disdrometer and theoretical scattering coefficients. It is, therefore, dependent on the accuracy of the scattering parameters.

The results obtained are shown in Figures 5-11 to 5-14 for each regime. In Figure 5-11, the lognormal model is at par with that of the modified gamma model for drizzle rainfall regime up to 75 GHz. The ITU-R models for both vertical and horizontal polarization are close, although the estimates of horizontal polarization are higher. It is also observed that the negative exponential model under-estimates all other models and the semi-empirical measurement. In this regime, the

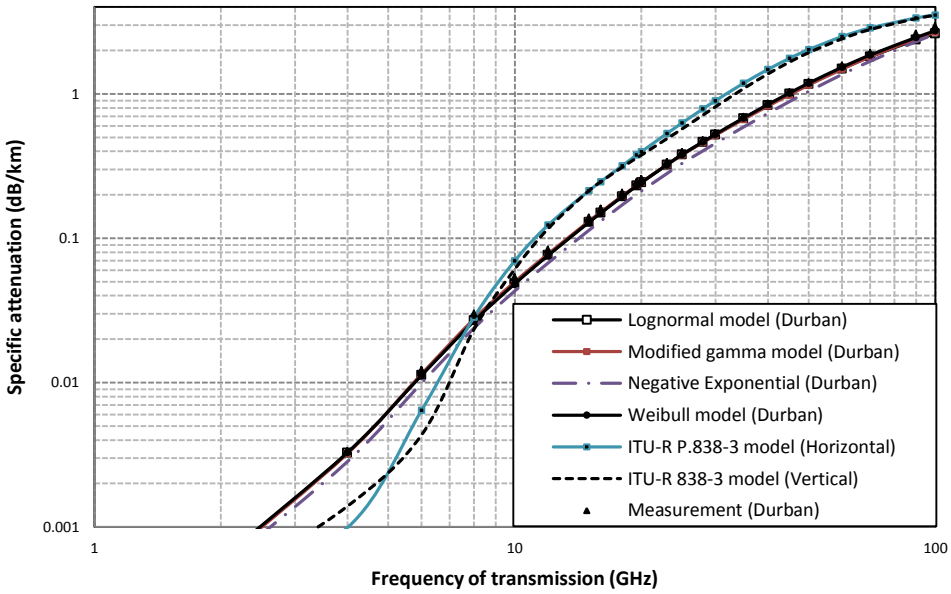

Figure 5-11: Comparison of estimated specific attenuation for Durban at 20°C for drizzle rainfall regime at 4 mm/h

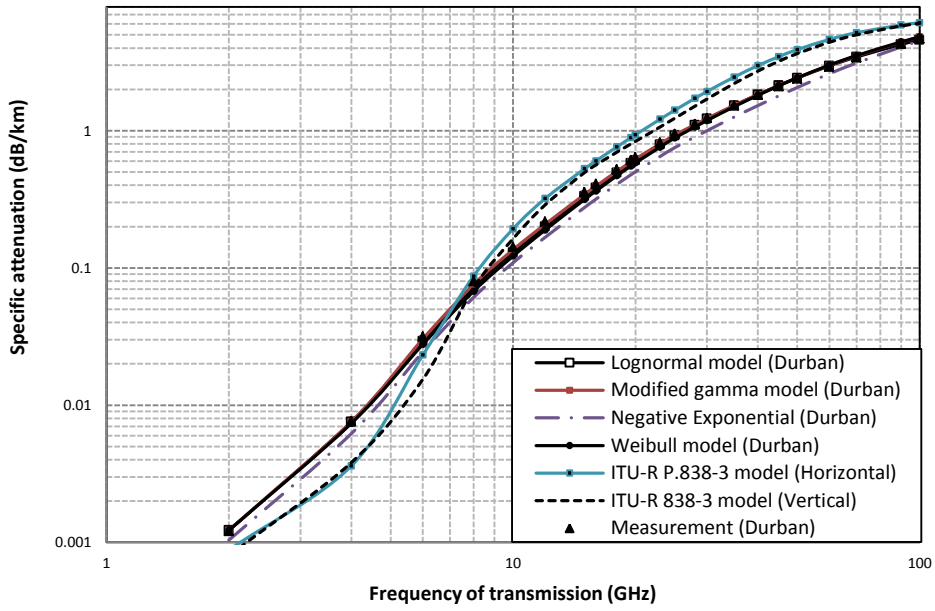

Figure 5-12: Comparison of estimated specific attenuation for Durban at 20°C for widespread rainfall regime at 9 mm/h

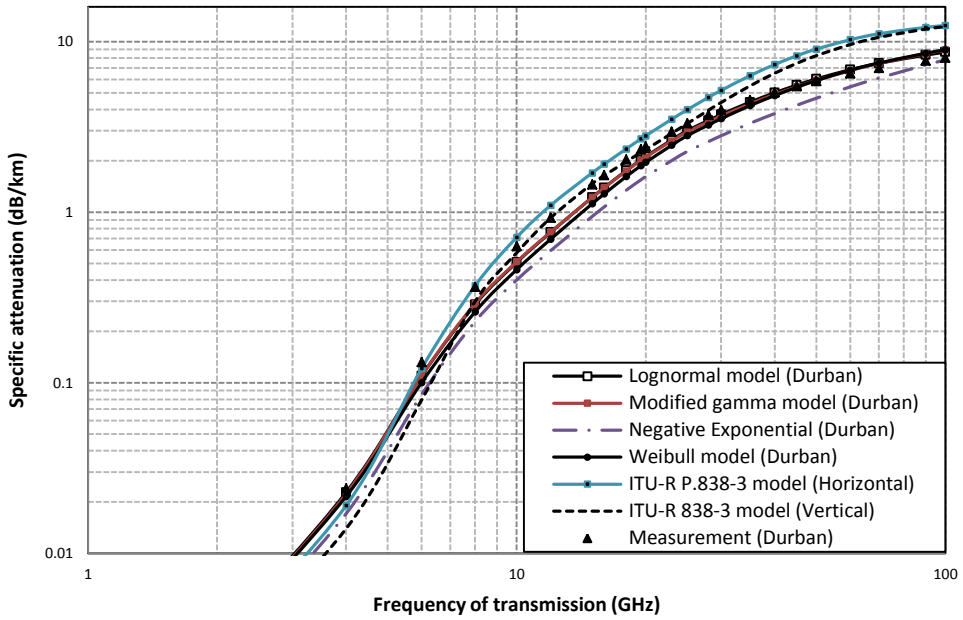

Figure 5-13: Comparison of estimated specific attenuation for Durban at 20°C for shower rainfall regime at 25 mm/h

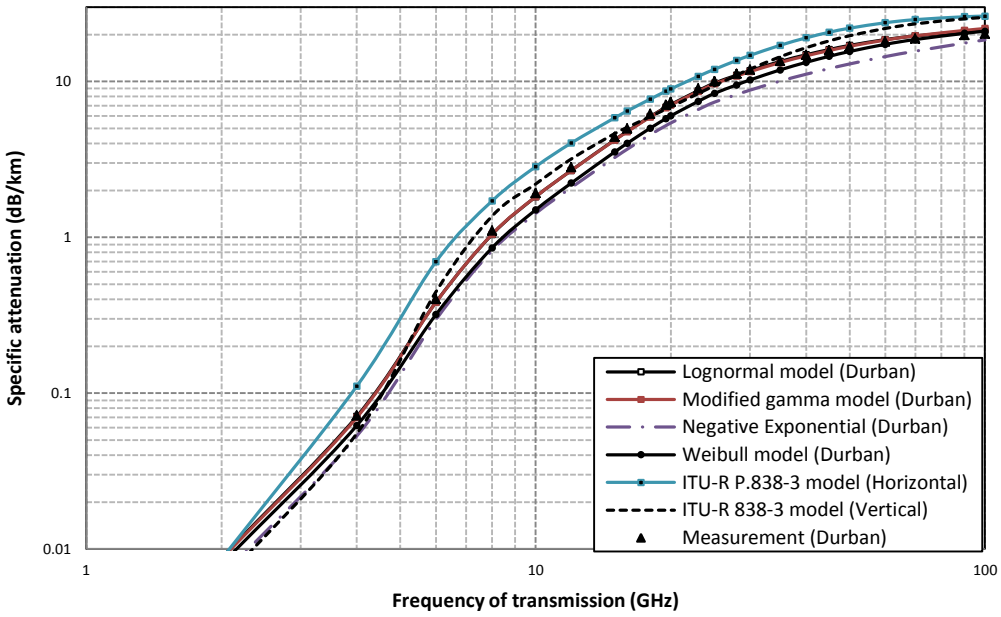

Figure 5-14: Comparison of estimated specific attenuation for Durban at 20°C for thunderstorm rainfall regime at 75 mm/h

lognormal, Weibull and modified gamma model appear to have a good fit to the averaged measurement.

For widespread rainfall regime at 9 mm/h shown in Figure 5-12, the ITU-R models are both observed to over-estimate the proposed models and empirical measurement. The negative exponential model again under-estimates all other compared models above 10 GHz. It is observed that Weibull model and modified gamma model are closer (though higher) to the measurements, while the lognormal model matches the measurement most especially above 60 GHz.

For shower rainfall regime averaged at 25 mm/h in Figure 5-13, the two ITU-R models are observed to over-estimate all proposed models and measurements. The proposed negative exponential model again under-estimates both the measurement and other models. The three other models appear to match the measurement at all frequencies, until the Weibull and modified gamma models over-estimate beyond 50 GHz. However, at 70 GHz the lognormal model deviates towards the measurement.

Finally, for thunderstorm rainfall regime at 75 mm/h shown in Figure 5-14, the ITU-R models again over-estimate all other models. However, there is a sharp increase in the horizontal polarization estimates over that of the vertical polarization estimates. The negative exponential model again under-estimates the measurement and other models. The Weibull model underestimates the measurement at frequencies less than 70 GHz; beyond 70 GHz, there is a good prediction. The modified gamma model and the lognormal model both match the measurement at frequencies less than 50 GHz. However, at 70 GHz, there is a deviation in the prediction of both models with the modified gamma model having higher estimates.

Generally, it is observed that the Weibull and modified gamma models show similar characteristics for rainfall attenuation prediction within the drizzle and widespread rainfall regimes. They also show good agreement with the empirical measurements between the frequency range of 2 GHz and 70 GHz. Therefore, the proposed modified gamma and Weibull models will provide good attenuation estimates for rainfall rates up to 10 mm/h. On the other hand, the lognormal model and modified gamma model show similar characteristics for rainfall attenuation prediction within the shower and thunderstorm rainfall regimes. Since rainfall rates greater than 10 mm/h are of major interest to radio planning and link budgeting engineers, it will be worthwhile to take note of these anomalies. It appears from our results that both models over-estimate the measurements above 50

GHz. Also, a deviation occurs at 70 GHz making the lognormal model more closer to the measurements.

5.5 Specific Attenuation Constants for Proposed Models

The power-law regression technique was applied for all the proposed annual models in Durban. According to *Olsen et al.* [1978], the specific attenuation due to rainfall at a location can be completely described as a function of rainfall rate, so that:

$$A_s = kR_{0.01}{}^{\alpha} \tag{5.18}$$

where k and α are the power-law coefficients from the regression technique.

Each of the proposed models are fitted for a rainfall range of $0 < R \leq 120$ mm/h and the results for k and α for each models are presented in Table 5-3. The graphs in Figures 5-15 and 5-16 show the comparative values of k and α for the proposed models and the ITU-R P.838-3 values (available in Appendix A-2).

Table 5-3: Values of k and α for the proposed models for Durban at 20°C for 2 GHz ≤ f ≤ 400 GHz

Frequency (GHz)	LOGNORMAL MODEL			MODIFIED GAMMA MODEL			WEIBULL MODEL			NEGATIVE EXPONENTIAL MODEL		
	k	α	R^2	k	α	R^2	k	α	R^2	k	α	R^2
2	0.0002	0.8938	1	0.0002	0.8968	1	0.0001	1.0055	0.9993	0.0002	0.8537	1
4	0.0008	0.9817	1	0.0008	0.9838	1	0.0007	1.1276	0.9992	0.0008	0.9403	1
6	0.0025	1.0893	1	0.0026	1.0875	1	0.0019	1.2781	0.999	0.0023	1.0491	0.9999
10	0.0106	1.1123	1	0.011	1.1092	1	0.008	1.3103	0.999	0.0099	1.0733	0.9999
12	0.017	1.0974	1	0.0174	1.0952	1	0.0129	1.2895	0.999	0.0158	1.0581	0.9999
15	0.0294	1.0797	1	0.03	1.0784	1	0.0226	1.2647	0.9991	0.0271	1.0399	0.9999
19.5	0.0542	1.0558	1	0.0547	1.0555	1	0.0423	1.2312	0.9991	0.0497	1.0154	0.9999
25	0.0931	1.022	1	0.093	1.023	1	0.0744	1.1839	0.9991	0.0849	0.981	0.9999
40	0.2297	0.9335	1	0.2262	0.9364	1	0.1949	1.0606	0.9992	0.2108	0.8925	1
60	0.4584	0.8495	1	0.4543	0.8521	1	0.412	0.9445	0.9994	0.4347	0.8115	1
70	0.5765	0.8183	1	0.5759	0.8204	1	0.5296	0.9018	0.9995	0.5574	0.7825	1
100	0.9091	0.7523	1	0.9344	0.7526	1	0.8758	0.8129	0.9996	0.9287	0.7233	0.9999
150	1.2896	0.6772	1	1.3753	0.6954	1	1.2953	0.7402	0.9997	1.4016	0.6762	0.9998
200	1.4501	0.6653	1	1.575	0.6726	1	1.4819	0.7119	0.9998	1.6221	0.6582	0.9997
250	1.4899	0.6674	1	1.6298	0.6643	1	1.5322	0.7077	0.9998	1.6851	0.6518	0.9997
300	1.4761	0.6657	1	1.6172	0.6625	1	1.5201	0.6995	0.9998	1.6736	0.6504	0.9997
350	1.4467	0.6661	1	1.5844	0.6629	1	1.4893	0.7	0.9998	1.6396	0.6508	0.9997
400	1.4189	0.6669	1	1.5528	0.6637	1	1.4598	0.701	0.9998	1.606	0.6514	0.9997

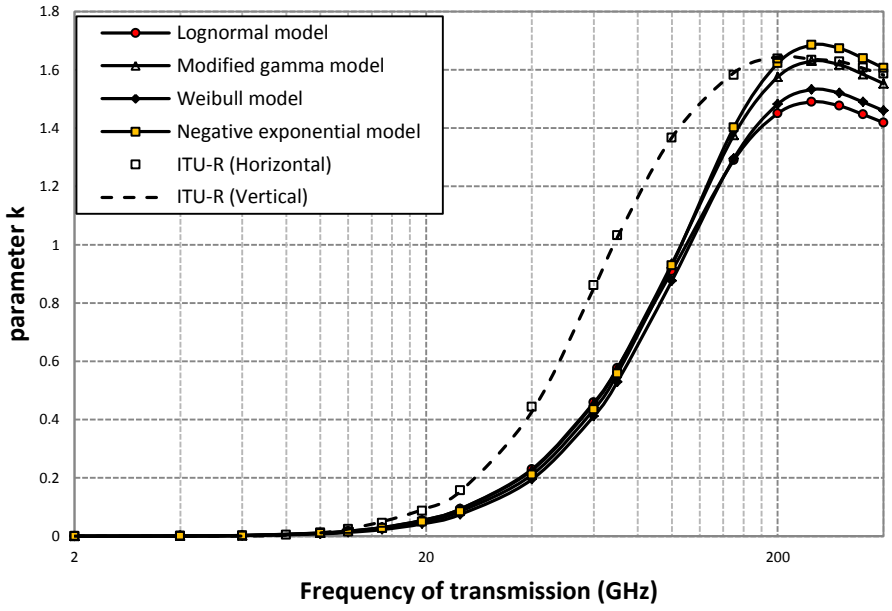

Figure 5-15: Plot of the various k-coefficients for the proposed models in Durban at 20^{o}C

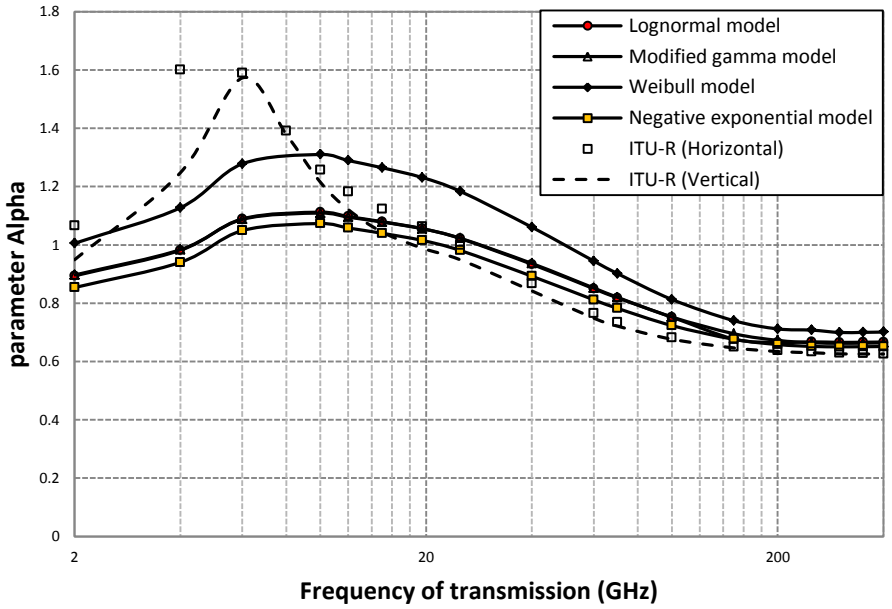

Figure 5-16: Plot of the various α-coefficients for the proposed models in Durban at 20^{o}C

5.6 Error Estimation from Proposed Models

The error estimation is applied in this work to determine the deviation of the proposed model from the measurements (actual or semi-empirical). The error statistic equation in 3.19 and χ^2 statistic test expression in (3.20) are utilised in this section for the purpose of computing model error. The error tests are considered for the specific attenuation estimates obtained from the regime analysis and are presented in Table 5-4. The semi-empirical attenuation computations used here are related to the disdrometer calculations.

From the results, it can be seen that the Weibull model and modified gamma model are both appropriate for Durban for drizzle rainfall regime. It is noticed that the RMS errors of both models are quite close, as are their χ^2 statistic values. Weibull model, however has the least RMS error and χ^2 test values of 0.0572 and 0.0722 respectively.

For widespread rainfall regime, the modified gamma model is the most appropriate for Durban with an RMS error and χ^2 value of 0.1282 and 0.1685 respectively. The Weibull model is also a good model, albeit with higher RMS error value and χ^2 test value than the modified gamma model. Also, the lognormal model has a higher χ^2 statistic than Weibull and modified gamma model, and therefore, has a lower efficiency.

For the shower rainfall regime, the modified gamma model and lognormal model have similar error indices. Modified gamma has the lowest RMS and χ^2 statistic values of 0.2164 and 0.2845 respectively, and therefore, it is the most appropriate for this regime. Finally, in the thunderstorm rainfall regime, the lognormal model has the lowest RMS and χ^2 statistic value of 0.5629 and 0.7571 respectively.

Hence, the results show that the modified gamma model has the best prediction characteristics to fit any type of rainfall regime in Durban. However, for the purpose of terrestrial radio planning at high frequencies below 100 GHz (and high rainfall rates), the lognormal DSD model would provide an excellent rainfall attenuation prediction

Table 5-4: Error analysis of the proposed models with predicted measurements for 2 GHz ≤ *f* ≤ 100 GHz

MODELS	RMS ERROR	[a]CHI-SQUARE	PREFERABLE MODEL(S)
DRIZZLE (R < 5 mm/h)			
Lognormal	0.0636	0.0696	[1]Weibull model [2]Modified gamma model
Negative Exponential	0.0859	0.1932	
Modified Gamma	0.0594	0.0603	
Weibull	[b]0.0572	[b]0.0696	
ITU-R P.838-3 (Horizontal)	0.3686	2.0389	
ITU-R P. 838-3 (Vertical)	0.3412	1.7531	
WIDESPREAD (5 mm/h ≤ R < 10 mm/h)			
Lognormal	0.1579	0.2297	[1]Modified gamma model [2]Weibull model
Negative Exponential	0.2708	0.7664	
Modified Gamma	[b]0.1282	[b]0.1645	
Weibull	0.1412	0.1923	
ITU-R P.838-3 (Horizontal)	0.7583	4.1220	
ITU-R P. 838-3 (Vertical)	0.6417	2.9403	
SHOWER (10 mm/h ≤ R < 40 mm/h)			
Lognormal	0.2365	0.292	[1]Modified gamma model [2]Lognormal model
Negative Exponential	0.8146	4.2268	
Modified Gamma	[b]0.2164	[b]0.2845	
Weibull	0.2503	0.4604	
ITU-R P.838-3 (Horizontal)	1.7975	8.6897	
ITU-R P. 838-3 (Vertical)	1.4405	5.2876	
THUNDERSTORM (R ≥ 40 mm/h)			
Lognormal	[b]0.5629	[b]0.7571	[1]Lognormal model [2]Modified gamma model
Negative Exponential	2.8320	17.3024	
Modified Gamma	0.6351	0.9001	
Weibull	1.4091	5.5417	
ITU-R P.838-3 (Horizontal)	3.2518	12.1901	
ITU-R P. 838-3 (Vertical)	2.0889	4.7993	

[a]The significance level chosen for this work is 1% with 19 degrees of freedom; Hence, the threshold value is given as 36.191 from the chi-square table.
[b]The lowest values of the theoretical model that best fits and agree with the semi-empirical measurements in Durban, South Africa.
[1,2] Signifies the order of preference of the preferred models in a descending manner

5.7 Comparison of Proposed Models with Link measurements at 19.5 GHz

In this section, the microwave link measurements undertaken in 2004 at 19.5 GHz, 6.73 km link distance for a horizontally polarized transmission, are utilized. The set-up stations are located at the Howard Campus College and the Westville Campus of the University of KwaZulu-Natal. The details of equipment deployment and specifics of the link are documented in the reports of *Naicker* [2004; 2006] and *Odedina* [2010].

5.7.1 Annual Variation of Specific Attenuation at 19.5 GHz

The specific attenuation from the link measurements was calculated using the ITU-R equation provided in (5.18) with $R_{0.01}$ = 60.69 mm/h (from section 3.4.4). The graph in Figure 5-17 shows the comparison of the proposed models and the link measurements at 19.5 GHz. It is observed that the link measurements had higher specific attenuation estimates than the proposed models, particularly for maximum and average attenuation. However, the results from the physical experiments are applied to validate the proposed rainfall DSD models for Durban by applying statistic tests. The statistic tests applied are: the RMS error and χ^2 with the results are presented in Table 5-5. The χ^2 estimates were obtained using (N-1) degree of freedoms, where N = 20 samples. Therefore, the degree of freedom used is 19, with an acceptable threshold at 1% given as 36.191 from the χ^2 table in Appendix D. The four proposed models considered are lognormal DSD model (LOG), Marshall-Palmer negative exponential DSD model (MPN), modified gamma DSD model (MGM) and Weibull (WBL) model.

From the results in Table 5-5, it can be seen that the proposed models have lower RMS errors and acceptable χ^2 for minimum specific attenuation from the link. However, the Weibull model appears to have a higher RMS error and χ^2 estimates at 1.7075 and 8.3026 respectively. For the average specific attenuation, the Weibull model has lowest estimates of RMS error and χ^2 being 1.3595 and 20.3614 respectively. All the models except the proposed Marshall-Palmer negative exponential estimates for Durban pass the 1% hypothesis for χ^2, thus this model is unsuitable for Durban.

Broadly speaking, it is interesting to note that the modified gamma and lognormal model all have similar estimates of RMS error and χ^2, suggesting the closeness of their specific estimates. On the other hand, the ITU-R specific estimates also agree more with the average and minimum

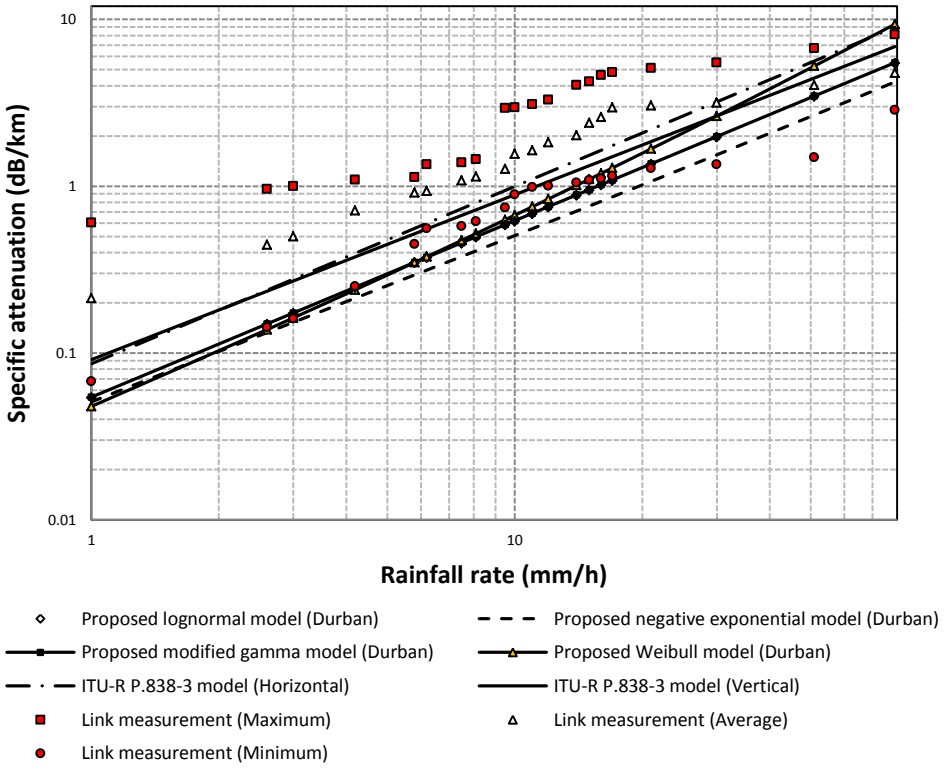

Figure 5-17: Comparison of the specific attenuation computed of the proposed models with link measurements in Durban at 19.5 GHz

Table 5-5: Error Statistics at 19.5 GHz from the Proposed Models in Durban using the Link Measurements in 2004

MODEL	MINIMUM SPECIFIC ATTENUATION		AVERAGE SPECIFIC ATTENUATION		MAXIMUM SPECIFIC ATTENUATION	
	RMS	[a]CHI	RMS	[a]CHI	RMS	[a]CHI
LGN	0.7552	3.2023	0.9995	23.7986	2.4649	130.7486
MPN	0.4708	3.0522	1.1715	37.6062	2.7326	181.6632
MGM	0.7644	3.216	0.9939	23.3122	2.4555	128.9109
WBL	1.7075	8.3026	1.3595	20.3614	2.1793	105.6419
ITU-R (H)	1.7137	9.6129	1.1453	7.4372	1.8451	52.6198
ITU-R (V)	1.1658	5.5128	0.8403	8.9675	2.0664	68.7807

[a]The significance level chosen for this work is 1% with 19 degrees of freedom; Hence, the threshold value is given as 36.191 from the chi-square table.

measurements from the link. In summary, it is concluded that the proposed models fairly agree with the link measurements, albeit, at minimum and average attenuations.

5.7.2 Comparison of Path Attenuation Models at 19.5 GHz

The path attenuation for the proposed models are computed using a link distance of 6.73 km and the ITU-R recommended path reduction factor. The comparisons of the computed path attenuations alongside the link measurement are shown in Figure 5-18. From the previous discussion, the proposed models were seen to agree with the minimum and average path attenuation measurements from link. In this case however, the proposed models are seen to agree more with the minimum path attenuation due to most especially with rainfall rates beyond 30 mm/h. As higher rainfall rates are approached, there is an agreement of all the proposed models, with the exception of the negative exponential model, with the link measurements.

Error statistics for this comparison is presented in Table 5-5, all the tested models, except the Weibull model and ITU-R (V) model, satisfy the 1% threshold for the χ^2 hypothesis at 36.191 (with19 degree-of – freedoms) for minimum link measurements. The proposed models all have low RMS errors for average and maximum link measurements but with unacceptable figures of χ^2. Therefore, the proposed models can be said to be within the bounds of link measurement, albeit, the minimum bounds

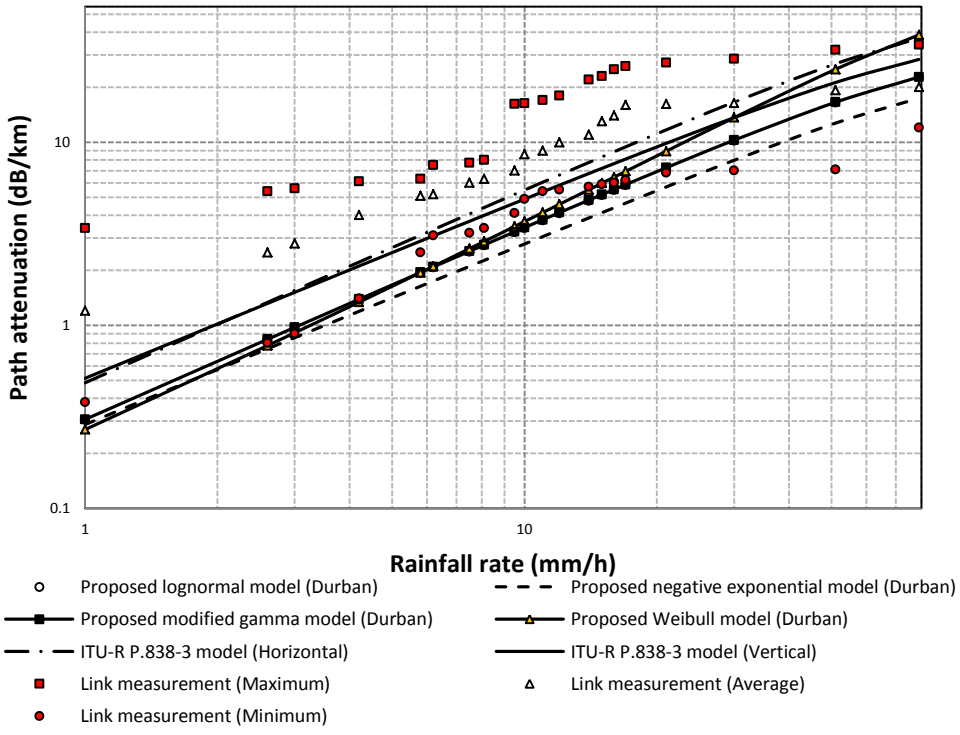

Figure 5-18: Comparison of the path attenuation computed of the proposed models with link measurements in Durban at 19.5 GHz

Table 5-5: Error Statistics at 19.5 GHz from the Proposed Models in Durban using the Link Measurements in 2004

MODEL	MINIMUM PATH ATTENUATION		AVERAGE PATH ATTENUATION		MAXIMUM PATH ATTENUATION	
	RMS	CHI	RMS	CHI	RMS	CHI
LGN	3.3274	14.8476	5.3534	129.2573	13.0261	708.3819
MPN	2.1988	15.6090	6.2619	203.8402	14.2631	979.6469
MGM	3.3658	14.8700	5.3204	126.6041	12.9802	698.4827
WBL	7.3703	37.0534	6.3515	107.8302	11.6965	576.2909
ITU-R (H)	7.6457	44.2610	5.1278	37.3561	9.9206	286.5026
ITU-R (V)	5.1578	25.2390	4.2017	47.6935	11.0466	373.2083

5.8 Semi-Empirical Comparison of Measurement with Link Measurements at 19.5 GHz

The concept of the semi-empirical comparison involves computing the specific attenuation directly from the disdrometer measurement via theoretical scattering coefficients. The procedure undertaken to achieve this comparison as are follows:

- The rainfall DSDs at different rainfall rates in this section are calculated using the recommended disdrometer computation already provided in (3.2).
- The specific attenuation is estimated using the discretized equation in (5.17) and applying the theoretical scattering coefficients derived at 20 GHz in Table 5-2, thus generating a *semi-empirical* estimation from the rainfall data.
- The resulting specific attenuation from these computations are then regrouped according to rainfall rates obtained from the link measurements in 2004. Similar rainfall rates corresponding to the link measurements are re-classified according to the minimum, average and maximum peaks of their respective specific attenuations.

This semi-empirical comparison is undertaken because of the following reasons:

- To verify the similarity in the rainfall specific attenuation patterns obtained from the disdrometer and link measurements
- To determine the level of specific attenuations experienced at the two distinct periods of measurements in Durban, South Africa.

The results obtained from the procedure above are presented in Figure 5-19 to 5-21; the ITU-R measurements are also included in the comparison. For the minimum attenuation in Figure 5-19, the

semi-empirical measurement compares well with the link measurements up to 21 mm/h. Beyond this rainfall rate, the link measurement dips further. The absolute mean deviation of the link measurement to the semi-empirical measurement is 0.5044. The sudden drop in the actual specific attenuation for the link measurement may indicate a decrease in the number of rainfall drops in the higher diameter category at that rainfall. This is also possible if the samples are collected closer to the boundary of a rainfall cell or at the edge of a rainfall duration.

In Figure 5-20, the semi-empirical measurement appears to agree with the ITU-R models especially that of the horizontal polarization for maximum attenuation. The link measurements are higher than both the semi-empirical values and the ITU-R estimates, but the values appear to converge around 79 mm/h. Again, the higher specific attenuation values can be linked to the prevailing rainfall conditions in the rain cells. The peak specific attenuation recorded by the link is 8.22 dB/km, while that of the semi-empirical measurement is 7.09 dB/km. The absolute mean deviation of the link measurement is 1.5486 when compared to that of the semi-empirical estimates.

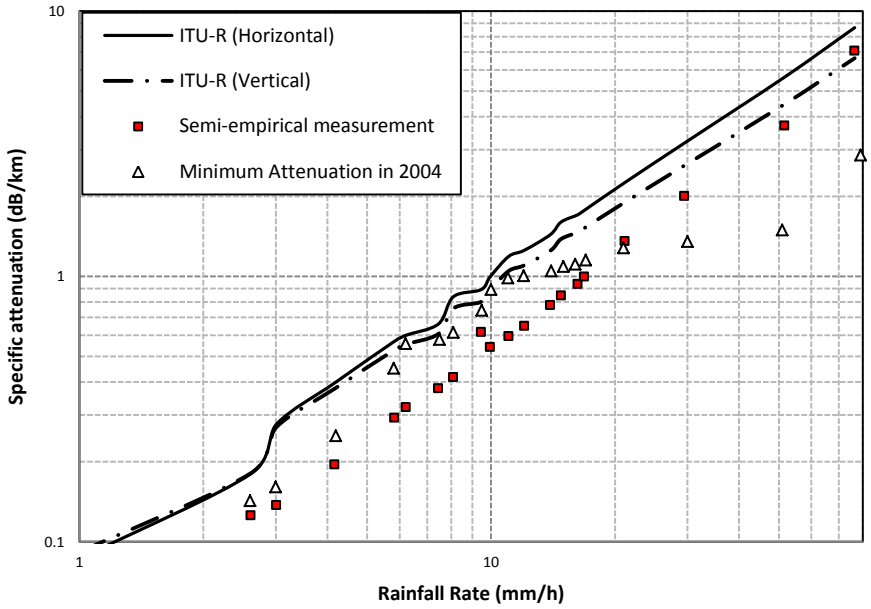

Figure 5-19: Minimum specific attenuation for both the link measurement in 2004 and semi-empirical computations at 19.5 GHz

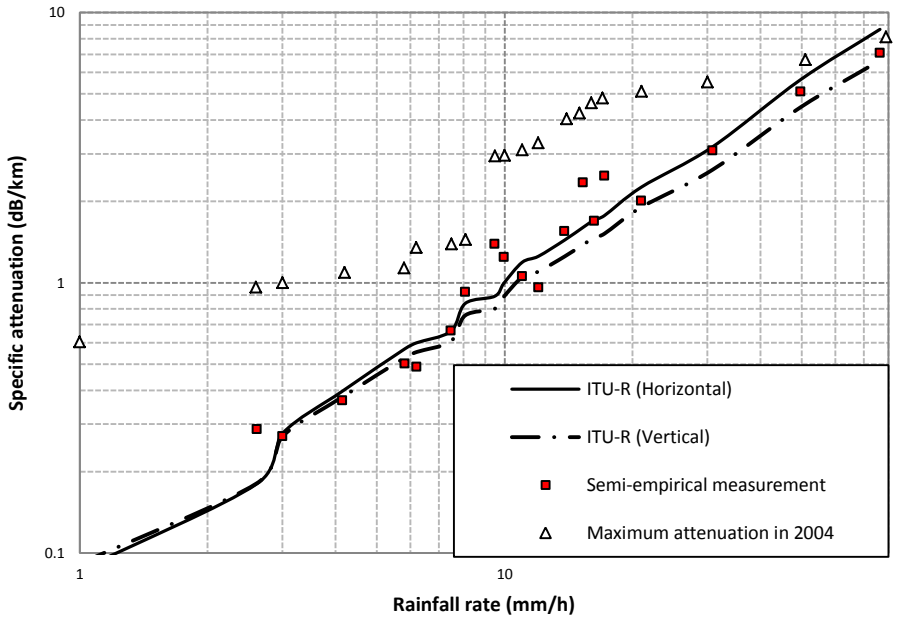

Figure 5-20: Maximum specific attenuation for both the link measurement in 2004 and semi-empirical computations at 19.5 GHz

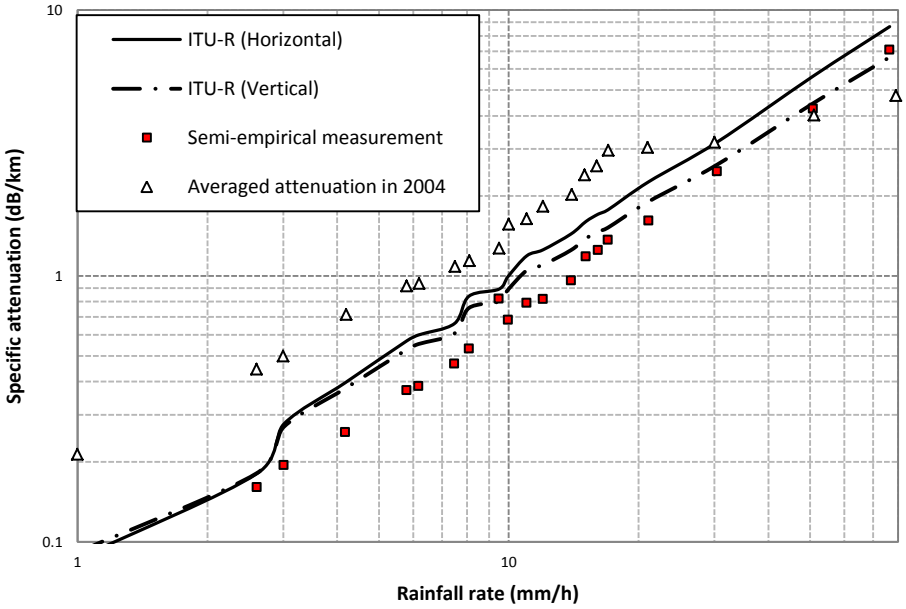

Figure 5-21: Averaged specific attenuation for both the link measurement in 2004 and semi-empirical computations at 19.5 GHz

For the averaged specific attenuation in Figure 5-21, the link measurements are also higher than the ITU-R and semi-empirical estimates. It also appears that the averaged semi-empirical measurement closely fit the ITU-R figures for vertical polarization. Here, the absolute mean deviation is given as 0.8272.

In general, the ITU-R models generally under-estimate the link measurements for both the averaged and maximum measurements. This, of course, indicates the shortcomings of the ITU-R model for Durban based on the link measurement. Also, it is observed that the level of specific attenuation in 2004 is higher than the predicted semi-empirical measurements from the disdrometer at the control site.

Table 5-7 shows the comparison of the power-law specific attenuation between the link measurements ads the computed semi-empirical values from the disdrometer. Firstly, it is shown that the scale factors for the link measurements are higher, while the scale factors for the semi-empirical measurements are higher.

Table 5-7: Actual and semi-empirical specific attenuation power-law estimates for Durban at 19.5 GHz

SPECIFIC ATTENUATION	[a]2004 LINK MEASUREMENT	R^2	SEMI-EMPIRICAL MEASUREMENT	R^2
MINIMUM	$0.0089R^{0.8649}$	0.9145	$0.0389R^{1.1593}$	0.9961
MAXMUM	$0.2404R^{0.7733}$	0.9565	$0.0529R^{1.1252}$	0.9662
AVERAGE	$0.4815R^{0.7137}$	0.8941	$0.0855R^{1.0743}$	0.9967

[a]The power-law measurements were derived from the initial measurements available in the studies of *Naicker* [2004a; 2004b] and *Odedina* [2010].

5.8.1 Discussions on Link Measurements

In the previous section, it was noted that the link measurements for specific attenuation in Durban have higher figures than the semi-empirical measurements. The higher estimates may be due to two reasons: lower link reduction factor and unaccounted depolarization effects in the scattering computation. A marginal factor, η, is proposed to ascertain the multiplier constant for the specific attenuation ratio of the link measurement to that of the semi-empirical measurement. Mathematically, the marginal factor is given as:

$$\eta = \frac{\text{due to link at 19.5 GHz}}{\text{due to the semi empirical results}} \qquad 5.19$$

where, A_s, refers to the specific attenuation.

Figure 5-22 shows the variation of marginal factors for the minimum, maximum and averaged attenuation for both measurements. It is observed that this factor ranges from $0.4 \leq \eta \leq 1.53$ for minimum attenuation, $0.65 \leq \eta \leq 4$ for averaged attenuation and $1.16 \leq \eta \leq 9$ for maximum attenuation. This shows that the semi-empirical measurement shows fairly good correlation for minimum attenuation and poor correlation for both average and maximum attenuation. Additionally, the semi-empirical measurement appears to have better fits at higher rainfall rates for the three categories of attenuation.

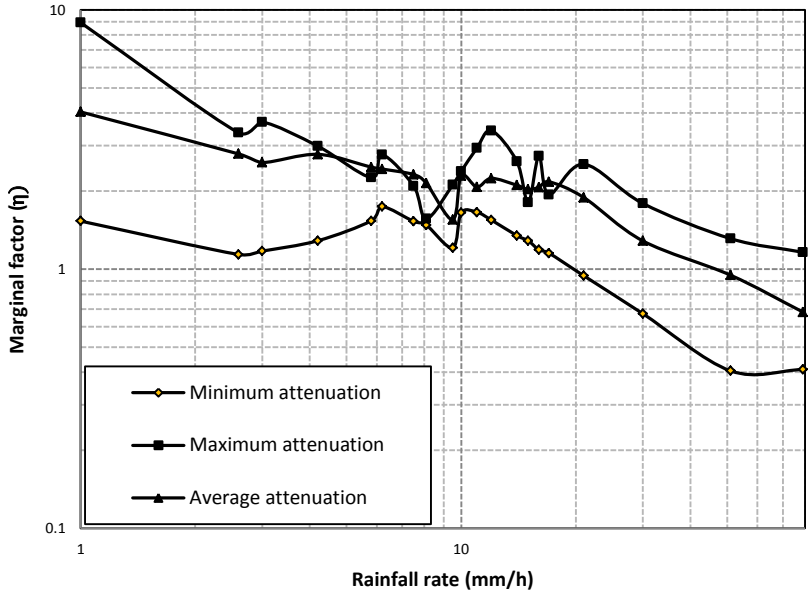

Figure 5-22: The ratio of the actual link measurements to the semi-empirical measurements

In microwave studies, the maximum attenuation and higher rainfall rates are two interrelated parameters as they are responsible for major network outages, which could last for several minutes. The maximum path attenuations from both the link measurements and the semi-empirical measurements are further analyzed since they provide the upper bound of link attenuations in Durban. This is achieved by utilizing both the maximum path attenuation from the link in 2004 and maximum specific attenuation from the semi-empirical measurements to derive the empirical reduction factor.

The marginal factor between the maximum path attenuation and the maximum path attenuation (semi-empirical using ITU-R reduction factor) as a power-law function is given as:

$$\eta_{max} = 5.56\, R^{-0.354} \quad (5.19)$$

where R is the rainfall rate in mm/h for values up to 80 mm/h
Thus, the new relationship between the two attenuation measurements is given as:

$$A_{PL\,(\max)} = 5.56\, A_{P(\max)} R^{-0.354} \quad (5.20)$$

where A_{PL} is the path attenuation of the link and A_P is the semi-empirical attenuation.

The reduction factor, so it appears, plays a huge role in the mechanics of rainfall in Durban at all rainfall rates. Some authors have provided explanation for this anomaly. *Sharma et al.* [2011] observed that rainfall rates above 30 mm/h have values greater than unity; this was attributed to the larger cell sizes of rainfall over the path length as rainfall rate increases. *Akuon and Afullo* [2011] in a recent study also suggested the mechanics of rainfall growth in different cells as important in the calculation of path reduction factor. Based on a combination of empirical and theoretical computations, they proposed that the rain cell diameter in subtropical areas - like Durban - is given by:

$$D_c = 51R^{-0.46} \quad (5.21)$$

where R is the rainfall rate in mm/h.

The consequence of (5.21) is such that rainfall rates values ranging from 1 mm/h ≤ R ≤ 120 mm/h, have corresponding rain cell diameters, D_c, from 51 km ≤ D_c ≤ 5.64 km. Thus, a minimum rainfall rate of 81.67 mm/h and beyond is required to achieve a rain cell diameter of 6.73 km and hence, effect the application of the ITU-R path reduction factor. Therefore, the path reduction factor for the microwave link measurements in this study will be equal to or greater than unity from observation since the path is fully encircled by the rainfall. This is one of the reasons for the under-estimation from the proposed models and then, the semi-empirical measurements using the ITU-R reduction factor. Another reason for the deviation may be as a result of depolarization effects from the Mie computation due to the raindrop spherical assumption especially at high rainfall rates. The spherical assumption may not be able to account for the droplet deformation that affect rain droplets at high rainfall rates as explained in section 2.5.2.

5.9 Chapter Summary

This chapter focused mainly on the studies of rainfall attenuation in Durban, South Africa. The concept of EM wave energy scattering by rainfall droplets was examined and the scattering parameters are proposed for frequencies up to 1 THz. The specific attenuations from the proposed rainfall DSD models for Durban are investigated at four different rainfall classifications. Firstly, it was established from the monthly estimates that at $R_{0.01}$, the winter months of May, June, July and August have the lowest specific attenuation. On the other hand, the summer months, particularly April, March and November experience intense specific attenuation at $R_{0.01}$, albeit, at varying frequencies. Therefore, the seasons of summer and autumn in Durban record the highest levels of specific attenuation.

From the regime and annual computations for the specific attenuation, it was observed that the proposed Weibull rainfall DSD model provided good estimates at low rainfall rates and the proposed lognormal rainfall DSD at high rainfall rates. The threshold for the performance of these two models in Durban is around 40 mm/h, which is theoretically, where the thunderstorm types of rainfall are assumed to commence.

The results from the 19.5 GHz, 6.73 km microwave link measurements in 2004 show that the proposed models have values closer to the minimum and averaged attenuations. A further investigation from the disdrometer semi-empirical measurements revealed that the link measurements, indeed, do have higher estimates than usual. This has been linked to the influence of 'stronger' rainfall cells during rainfall, leading to the notion that the reduction factor for the microwave link may be unity or greater than unity.

In the future, more work is needed to resolve the issue of discriminatory polarization effects using robust scattering techniques owing to the fact that at higher frequencies and higher rainfall rates, depolarization effects become prominent due to spherical assumption from Mie technique [Li *et al*, 1995; Li *et al*, 2000]. The consequence of the Mie spherical assumption results in severe under-estimation of scattering due to rainfall attenuation because the dynamic rain drop-shape is not considered [*Pruppacher and Pitter*, 1971; *Pruppacher and Klett*, 1978; *Sadiku*, 2000]. The dynamic rainfall drop-shape method could be applied to cater for scattering effects from differential depolarization especially above 10 GHz.

This study has provided useful information on the need to develop localized reduction factor functions based on link measurements. This is most useful for microwave engineers involved in network planning and link budget. The next chapter focuses on the resolution of rainfall correlation involving parameter correlation and extending its definition to other locations in South Africa.

CHAPTER SIX

Rainfall Correlation for South African Areas

6.1 Introduction

In the previous chapter, the rainfall attenuation in Durban was predicted using the proposed rainfall DSD models and the Mie scattering technique. The predictions, undertaken at microwave and millimeter wave frequencies, were examined at different rainfall parameters. The results from the rainfall attenuation prediction at Durban are consistent with results from tropical and subtropical region investigated by *Ajayi et al.* [1996] and *Adimula and Ajayi* [1996].

In this chapter, a case is made for the comparison of rainfall parameters in different regions using the property of rainfall correlation where resources required undertaking long-term rainfall microstructural measurements are capital-intensive. The equipments deployed may include a network of rainfall gauges, disdrometers and specialized long-range radar services. As a result, fewer control sites for rainfall measurements are available across the African continent and even in South Africa. The disadvantage of this, usually result in the utilization of ITU-R global parameters for network planning, which are often not suitable for the location of interest. The usage of global parameters pose a huge limitation to radio planning for microwave and millimetric wave systems, which result in the under-estimation or over–estimation of rainfall attenuation indices. A temporal approach to address the paucity of measuring equipment is to mathematically exploit the *priori* climatological characteristics (or dissimilarities) of a control site and extend such definition elsewhere using probability tools via statistical analysis.

In this chapter, the definition of rainfall measurements in Durban is extended to seven other selected locations. The approach used involves the estimation of 1-minute rainfall rate conversion from hourly rainfall data for seven locations using the conversion method originally proposed by *Akuon and Afullo* [2011]. Using the *priori* principle of comparative rainfall rate analysis, an empirical rain drop-size distribution model for Durban is developed, and then extended to seven other locations in South Africa.

6.2 Review of Rainfall Rate Conversion in South Africa

In Africa, one of the known works on rainfall was undertaken at Ile-Ife in Nigeria by *Ajayi and Ofoche* [1983]. In their work, it was suggested that the ITU-R one-minute integration time was the most suitable for microwave link designs. *Watson et al.*[1981] and later *Segal* [1986], also

suggested a two-parameter power-law function which has been exhaustively used in the conversion of higher rain rate to 1-minute integration time in several locations. The power-law function is given as:

$$R_1(P_\mathrm{T}) = a'[R_\tau(P_T)]^{b'} \quad [mm/h] \tag{6.1}$$

where *a'* and *b'* are the conversion parameters of the rain rates $R_1(P_\mathrm{T})$ and $R_\tau(P_\mathrm{T})$ at one-minute and τ-minute respectively exceeded at equal probability (P_T%).

Segal [1986], as defined the rainfall rate conversion factor as:

$$\rho_\tau(P) = \frac{R_1\,(P)}{R_\tau(P)} \tag{6.2}$$

where $R_1(P)$ and $R_\tau(P)$ are the rainfall rate exceeded, with equal probability, P, at different integration times, one-minute and τ-minute.

Later, *Moupfouma* [1984] developed an exponential relationship for the estimation of the cumulative distribution of rain rate in the tropics and equatorial regions. This was extended in *Moupfouma and Martin* [1993] to accommodate new parameters for temperate and tropical regions. ITU-R recommendation [*ITU-R P.837-5*, 2008] also presented approximate rain rate conversion equations for countries such as China, Brazil and Korea with minimal errors. However, the region of Africa has been left out mainly because of insufficient long-term experimental data and scarcity of deployed equipment. This led to the adoption of regional classification of rainfall as indicated in the ITU-R designations in [*ITU-R P.837-5*, 2008]. *Emiliani et al*. [2009] also examined the various methodologies required for the classification of rainfall rate conversion techniques.

Interestingly, ITU-R classifications have their limitations with regards to microwave link planning and budgeting. *Fashuyi et al*. [2006] and *Owolawi et al.* [2008] reported classification discrepancies in the ITU-R rainfall designations for South Africa. In addition, *Fashuyi et al*. [2006] used the approach in [*Watson et al.*, 1981; *Ajayi and Ofoche*, 1983; *Segal*, 1986] to obtain the rain rate conversion parameters for Durban for conversion of higher integration time and also reclassified ITU-R designations for South Africa. By comparing 5-year hourly rain rate distributions with measurements at a similar region using equiprobable rain rate exceedances, values of *a'* = 9.228

and b' = 0.8207 for Durban were obtained. These power-law parameters were then assumed for eleven other cities in South Africa in the estimation of rain attenuation. *Odedina et al.* [2008] used the $R_{0.01}$ values obtained from the work in [*Fashuyi et al.*, 2006] to determine the fade margins in five climatic locations in South Africa. More recently, *Owolawi et al.* [2007] and *Owolawi* [2011a] investigated the validity of the various statistical models for South Africa. In *Owolawi and Afullo* [2007], the Moupfouma tropical model was investigated for the South African subtropical region, with parameters *a*, *b* and *u* being obtained. In *Owolawi* [2011a], by employing a hybrid method for rain rate conversion, rainfall rate probability functions using Weibull, lognormal and gamma distribution models with five-minute rainfall data were examined. The method adopted a second-order polynomial function with three regression coefficients *a, b* and *c* for rain rate conversion from five-minutes to one-minute as given by:

$$R_1(\mathrm{P}) = a[R_5(\mathrm{P})]^2 + b[R_5(P)] + c \quad [mm/h] \tag{6.3}$$

where the values of a = 0.0014, b = 1.2021 and c = –0.3543 were obtained for Durban from his work under equiprobable rain rate exceedences.

In all the research related to rainfall rate in South Africa [*Fashuyi et al.*, 2006; *Owolawi et al.*, 2008; *Odedina and Afullo*, 2008; *Owolawi and Afullo*, 2007; *Owolawi*, 2011], the apparent lack of one-minute data to determine appropriate rainfall attenuation parameters is a challenge. More importantly, rainfall rate conversion factors as proposed by *Fashuyi et al.* [2006] are insufficient to be assumed for all locations in South Africa as they have distinct geographic characteristics. Therefore, different conversion factors have to be derived for different locations as will be shown shortly.

6.2.1 One-minute Rainfall Rate Conversion for Various Locations in South Africa

In a recent study, rainfall rate conversion for eight locations in South Africa was undertaken by applying a comparative analysis of rainfall exceedence for different locations [*Akuon and Afullo*, 2011]. In their paper, power law coefficients, α' and β', from regression fitting were used to establish a relationship between Durban and selected cities. An initial comparison was undertaken between 1-minute and 60-minute rainfall samples for Durban at the same exceedence probability. The derived relationship is given by:

$$R_{1\,min}(P,t) = \alpha'[R_{1\,hr}(P,t)]^{\beta'} \qquad \text{for } t \in [0,T] \tag{6.4}$$

where α' and β' both represent the power-law coefficients for the sampling time, *T*.
Similarly, another comparison was undertaken to establish the relationship between Durban and the other locations with *a* and *b* as the regression coefficients. The derived relationship was given as:

$$R_{1\,hr,\ x}(P,t) = \gamma_1\left[R_{1\,hr,\ Durban}(P,t)\right]^{\gamma_2} \tag{6.5}$$

$R_{1\ hr,\ x}(P,\ t)$ is the rainfall rate at the location being compared; γ_1 and γ_2 are the power-law coefficients relating one-hour rainfall samples of another location and Durban.

The combination of expressions (6.4) and (6.5) gives new the expected relationship between Durban and other cities. This is given by:

$$R_{1\,min}(P,t) = aR_{1\,hr}(P,t)^b \quad \text{for } t \in [0,T] \text{ and } 0.01\,\% \leq P \leq 1\,\% \tag{6.6}$$

where the coefficients *a* and *b* are functions given by:

$$a = \gamma_1(\alpha')^b \tag{6.6a}$$

and,

$$b = \gamma_2\beta' \tag{6.6b}$$

The conversion factors obtained for the selected locations in South Africa are 138ummarized in Table 6-1. From the table, Richards Bay is noted to have the highest power-law coefficients among the selected cities in South Africa. Also, the one-minute converted rainfall rate versus the 60-minute rainfall rates for different locations in South Africa are plotted in Figure 6-1 using the parameter in Table 6-1. The result show that locations like Pietermaritzburg and Brandvlei may have highest rain rates at one-minute, as are 60-minutes rainfall rates. Durban and East London are seen to have closer converted values of 1- minute rainfall rate, while, Richards Bay is seen to have similar rainfall rates with Durban beyond 70 mm/h. Vryheid is seen to have the lowest observed values for both one-minute and 60-minutes rainfall rates.

Table 6-1: Rainfall rate conversion factors for locations in South Africa [*Akuon and Afullo*, 2011]

LOCATION	COORDINATES	*a*	*b*	R^2
Durban	29°.97'S, 30°.95'E	6.3313	0.6837	0.9895
Pretoria	25°.73'S, 28°.18'E	5.0935	0.6743	0.983
Cape Town	33°.97'S, 18°.60'E	3.2445	0.6514	0.9958
Pietermaritzburg	29°.63'S, 30°.40'E	6.1143	0.8393	0.9847
East London	33°.03'S, 27°.83'E	5.4701	0.6928	0.9796
Richards Bay	28°.78'S, 32°.02'E	9.8863	0.6426	0.9847
Vryheid	27°.78'S, 30°.80'E	2.7552	0.9334	0.9965
Brandvlei	30°.47'S, 20°.48'E	0.8485	1.3147	0.9822

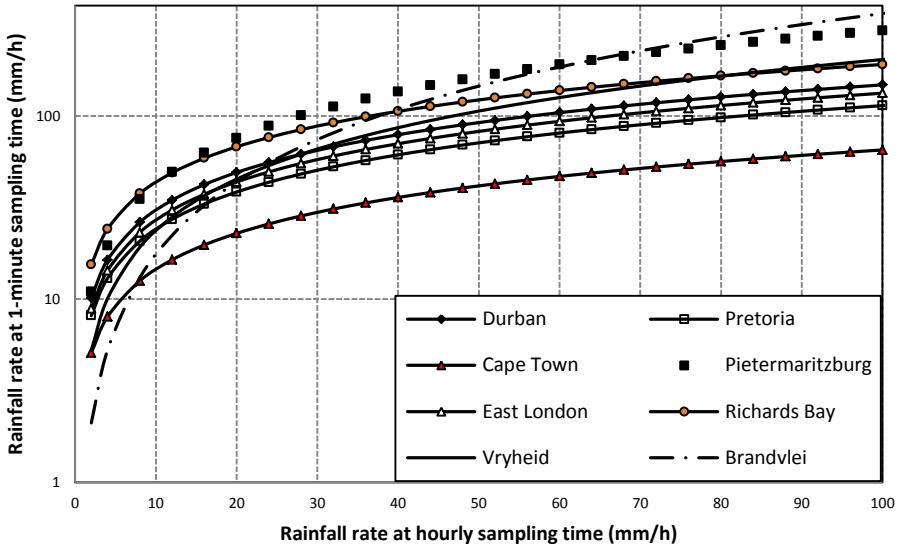

Figure 6-1: Converted one-minute rainfall rate versus one hour rainfall rate for selected locations in South Africa

6.3 Correlation of Rain drop-Size Distribution with Rainfall Rate

In this section, the Pearson correlation tool is utilized to compare rainfall parameters. Firstly, the rain drop-size distribution or $N(D)$ is computed from the standard disdrometer function which is given by:

$$N(D_i) = \frac{C_i}{A \times T \times v(D_i) \times \Delta D_i} \tag{6.7}$$

where the parameters in (6.7) have been earlier explained in chapter two.

Equation (6.7) is applied to enable the easy retrieval of raindrop number from the distribution as this procedure entails. The correlation procedure was mainly done for two independent rainfall functions using the Pearson correlation functions. Firstly, the rainfall DSD was compared with the total rainfall rate and then the individual rainfall rate attributed to specific diameters of the disdrometer. Figure 6-2 shows twenty scattergrams displaying the variation of the computed rainfall DSD with rainfall rate in Durban in relation to the disdrometer bins. The correlation results are presented in Table 6-2 for all the twenty bins present in the disdrometer processing. From the results, it is shown that all the bins except the 0.359 mm channel all have positive correlation with rainfall DSD.

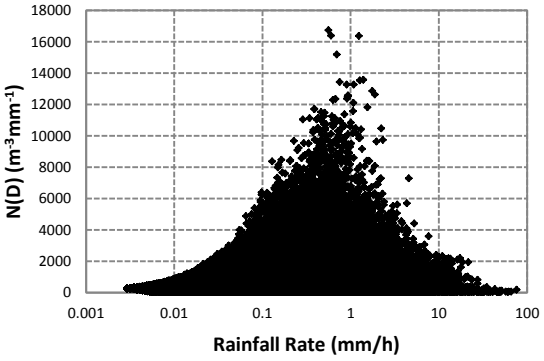

(a) 0.359 mm bin (41393 samples)

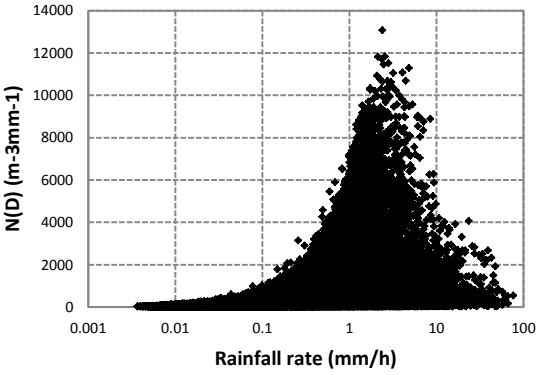

(c) 0.551 mm bin (42576 samples)

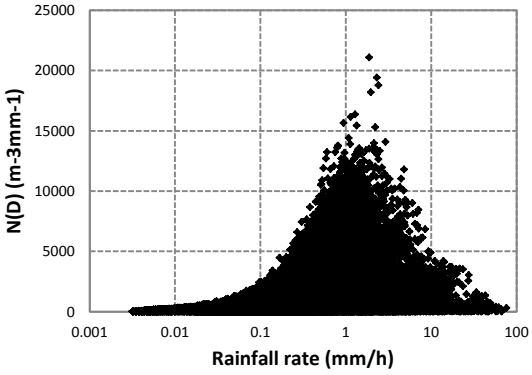

(b) 0.455 mm bin (45220 samples)

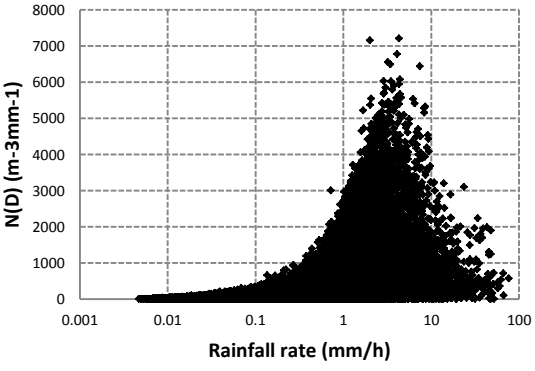

(d) 0.656 mm bin (38822 samples)

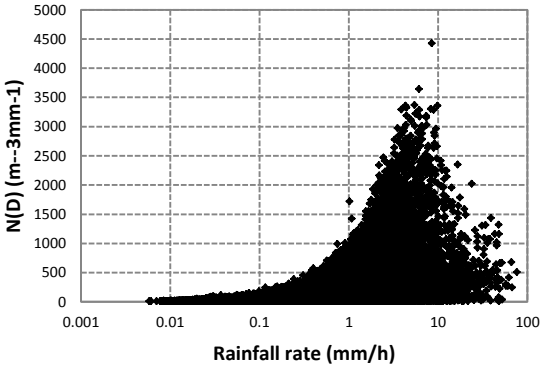

(e) 0.771 mm bin (32287 samples)

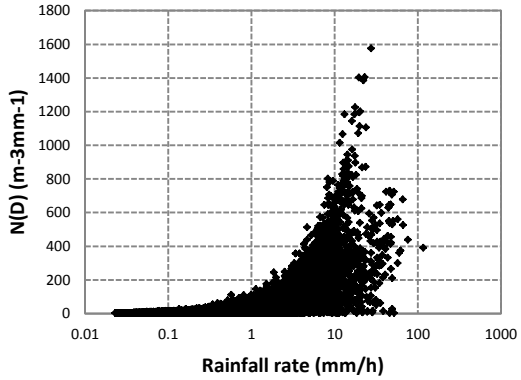

(h) 1.331mm bin (19277 samples)

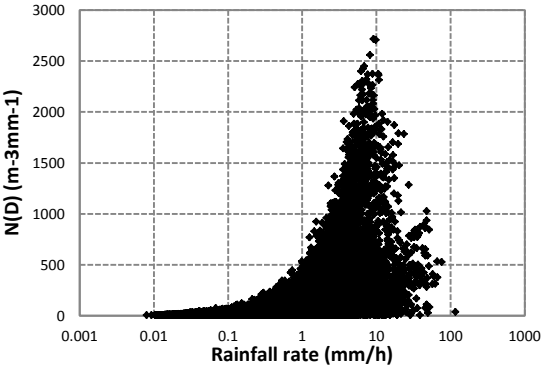

(f) 0.913 bin (30036 samples)

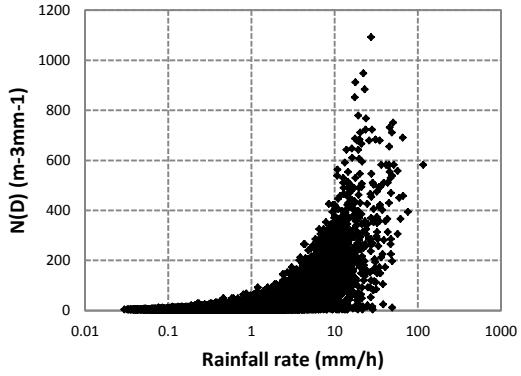

(i) 1.506 mm bin (14158 samples)

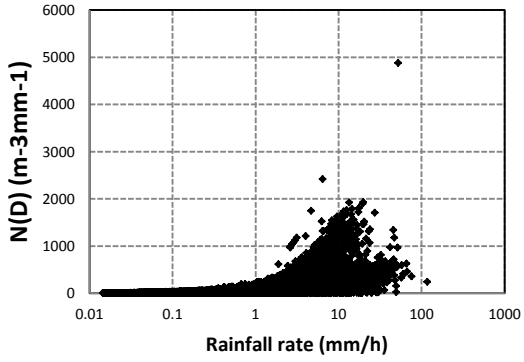

(g) 1.116 mm bin (25959 samples)

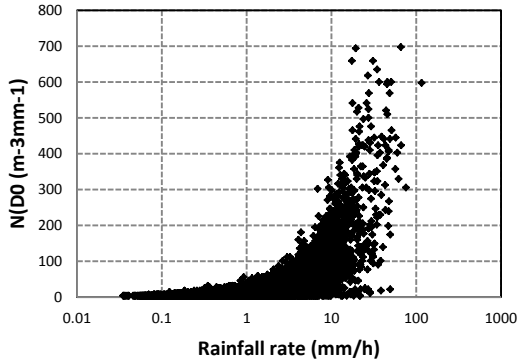

(j) 1.665 mm bin (11528 samples)

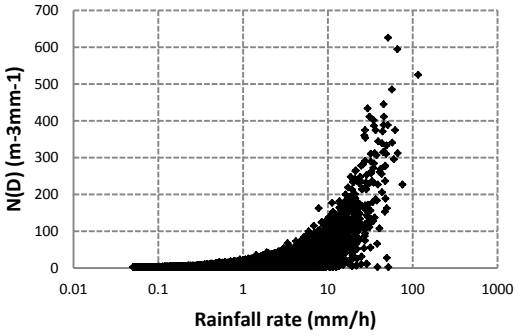

(k) 1.912 mm bin (10071 samples)

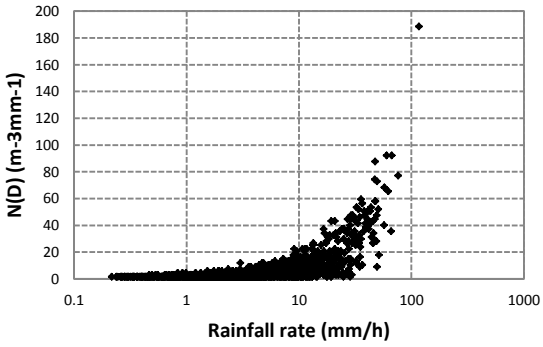

(n) 2.869 mm bin (1870 samples)

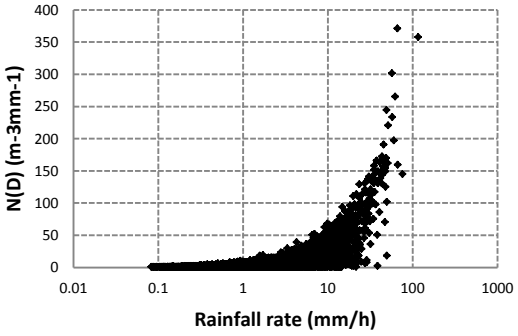

(l) 2.259 mm bin (6158 samples)

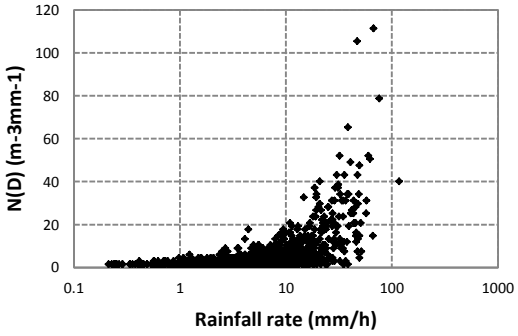

(o) 3.198 mm bin (1241 samples)

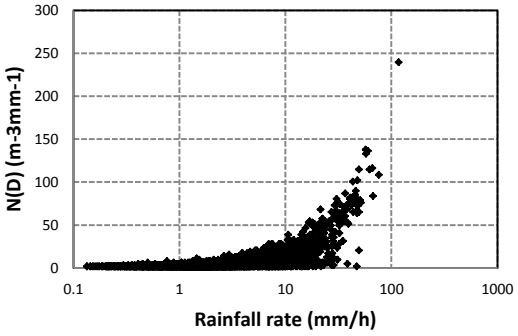

(m) 2.584 mm bin (3125 samples)

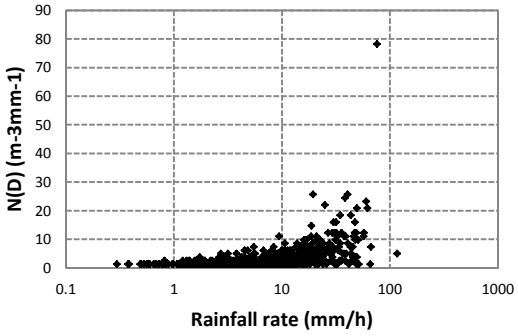

(p) 3.544 mm bin (659 samples)

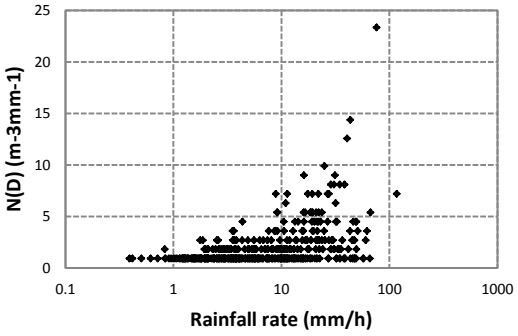

(q) 3.916 mm bin (447 samples)

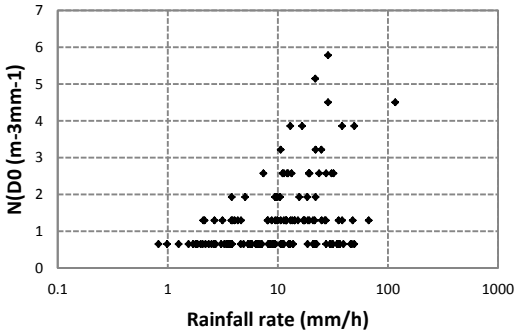

(s) 4.859 mm bin (149 samples)

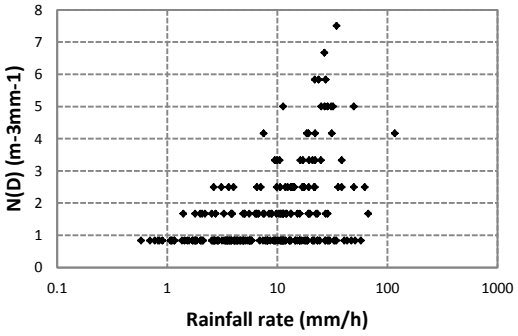

(r) 4.35 mm bin (230 samples)

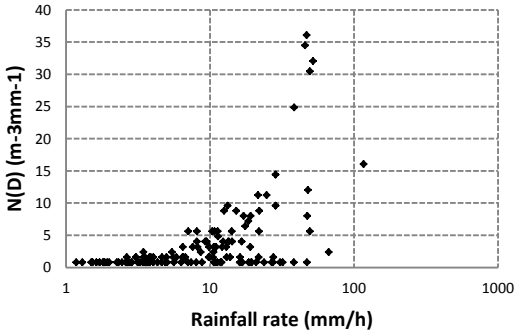

(t) 5.373 mm bin (136 samples)

Figure 6-2: Scattergrams showing the variation of rainfall DSD against rainfall rate for 20 diameter classes of the disdrometer measurement

From the correlation table in Table 6-2, it is also found out that the rainfall rate is much more correlated to the rain drop-size distribution $N(D_k, R(t))$. Except for the 0.359 mm class where a weak negative correlation exists, the other disdrometer classes have a positive correlation with better relationship with $N(D_k, R(t))$. This suggests that the rainfall rate and drop-size distribution have a mutual relationship. For the 20 diameter classes, the correlation is observed to approach unity for mid-classes of the disdrometer class range *i.e.* between 1.506 mm and 1.912 mm bin. Interestingly, the rainfall rate alone as a parameter lacks sufficient information for a location of geographic interest. As seen in the scattergram plots of $N(D_k, R(t))$ against rainfall rate in Figure 6-2, the properties of rainfall rate is obviously unstable for different classes. The $N(D_k, R(t))$ versus rainfall rate scattergram seem to suggest three phases of relationship may be present in Durban for the rainfall patterns obtained from the disdrometer measurements. The phases are as follows: a

Table 6-2: Correlation coefficients of rain drop-size distribution with rainfall rate in Durban from disdrometer

Diameter present in bins	CORRELATION COEFFICIENT		
	Corr ($N(D_k)$, R) (*with zero N(D) samples*)	Corr ($N(D_k)$, R) (*no zero N(D) samples*)	Corr ($N(D_k)$, R_k)
0.359	-0.03	-0.03	1
0.455	0.07	0.07	1
0.551	0.16	0.17	1
0.656	0.26	0.25	1
0.771	0.37	0.34	1
0.913	0.47	0.43	1
1.116	0.59	0.56	1
1.331	0.69	0.75	1
1.506	0.77	0.80	1
1.665	0.80	0.84	1
1.912	0.84	0.84	1
2.259	0.82	0.86	1
2.584	0.79	0.87	1
2.869	0.74	0.85	1
3.198	0.65	0.73	1
3.544	0.55	0.57	1
3.916	0.48	0.47	1
4.35	0.36	0.39	1
4.859	0.32	0.39	1
5.373	0.31	0.60	1

normal distribution relationship may exist between 0.359 mm and 0.913 mm diameter classes; a left-sided normal distribution or power-law relationship may exist between 1.116 mm and 1.665 mm classes; a linear relationship may exist from 1.912 mm diameter class and above. This varying relationship explains the randomness of rainfall rate as a single parameter for modelling drop-size distribution. However, the correlation undertaken for rainfall rate samples from each diameter bin does unity correlation for all diameters. Therefore, an empirical derivation of rainfall DSD for Durban is possible with this unity relationship as will be seen in the next section.

6.4 Empirical Derivation of Rainfall DSD for Durban

Initial results from Table 6-2 have shown that the rainfall rate samples from the specific diameters have a better correlation indices for all the available disdrometer bins. Therefore, the specific rainfall rates computed for each bin will serve as the basis to undertake an empirical derivation of rainfall DSD. This is possible because R_k has a perfect relationship with $N(D_k, R(t))$.

From (2.20) in chapter 2, the equation representing the rainfall DSD for the disdrometer is computed. This equation can be reduced to:

$$N(D_k) = U_k R(D_k, t) \tag{6.8}$$

where,

$$U_k = \frac{10^4}{6\pi v_t(D_k) {D_k}^3} \tag{6.9}$$

A plot of U_k against the mean diameter of the drops is shown in Figure 6-3. In that graph, a negative relationship is shown to exist between the two parameters. The parameter, $R(D_k, t)$ can be computed from (2.15) and (2.18) in chapter two and it corresponds to the rainfall rate contribution at diameter D_k within the sampling time interval, $t \in [0, T]$. The parameter U_k will have a unit of $m^{-3}mm^{-2}h$ and $N(D_k)$ has a linear relationship with this parameter.

Since,

$$R(t) = \sum_{k=1}^{20} R(D_k, t) \tag{6.10}$$

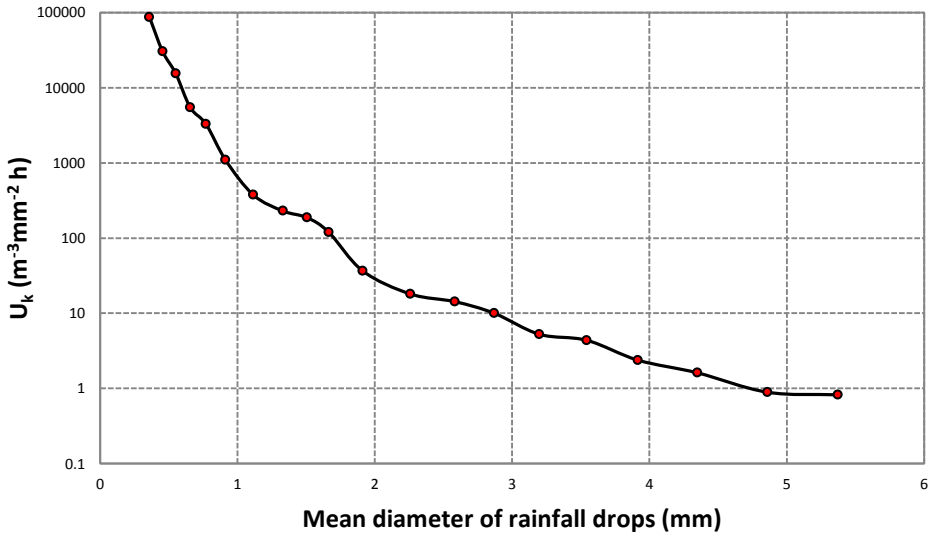

Figure 6-3: Variation of parameter U_k with different rainfall droplet diameter

where $R(D_k, t)$ represents the rainfall rate attributed to the particular drop-size diameter within the sampling time domain, for $t \in [0, T]$. It is observed that the variation in $R(D_k, t)$ is mainly due to the randomness in the number of rainfall drops collected at each bin corresponding to a diameter class. Thus, based on the dynamic space-time properties of the arriving droplets, the relationship between $R(t)$ and $R(D_k, t)$ will be random.

A power-law model and linear model is observed to provide good fits for the mean diameters of droplets within various diameter ranges. Therefore, the proposed models can be written as:

$$R(D_k, t) = a[R(t)]^b \tag{6.11}$$

and,

$$R(D_k, t) = a[R(t)] + b \tag{6.12}$$

So that from (6.8), the functions representing $R_i(D_k, t)$ can be substituted in (6.11) and (6.12) yielding:

$$N(D_k) = U_k[a[R(t)]^b] \tag{6.13}$$

and,

$$N(D_k) = U_k[a[R(t)] + b] \tag{6.14}$$

From (6.13) and (6.14 , the expressions can be described completely by two variables, ξ_1 and ξ_2, such that $N(D_k)$ in (6.15) and (6.16) are given respectively as:

$$N(D_k) = \xi_1[R(t)]^{\xi_2} \tag{6.15}$$

and,

$$N(D_k) = \xi_1 R(t) + \xi_2 \tag{6.16}$$

By considering the best regression fits that represents the rainfall at different diameter ranges, the proposed empirical model for Durban is given as:

$$N(D_k, R(t)) = \begin{cases} \xi_1[R(t)]^{\xi_2} & \text{for } 0.359\,mm \leq D_k \leq 1.506\,mm \\ \xi_1 R(t) + \xi_2 & \text{for } 1.665\,mm \leq D_k \leq 3.544\,mm \\ \xi_1[R(t)]^{\xi_2} & \text{for } 3.916\,mm \leq D_k \leq 5.373\,mm \end{cases}$$

$$\text{for } t \in [0, T] \quad (6.17)$$

where the computed values corresponding to ξ_1 and ξ_2 for the city of Durban are regression coefficients with respect to $R(t)$ for different diameter classes.

Table 6-3 gives the fitted values of the power-law coefficients from the regression technique undertaken for each disdrometer bins for measurements in Durban. It should be noted that the values of ξ_1 decreases as the diameter class increases. Figures 6-4 and 6-5 show the fitting procedure undertaken for the parameters ξ_1 and ξ_2 according to the bin diameters of the disdrometer.

Table 6-3: Parameters showing the fitted values for each disdrometer bin for the function in Durban

Diameter (mm)	$\xi(t) = \xi_1 R(t)^{\xi_2}$		
	ξ_1	ξ_2	R^2
0.359	1155	0.1107	0.7765
0.455	613.9329	0.3416	0.8214
0.551	521.0769	0.5456	0.8705
0.656	269.1731	0.6519	0.8879
0.771	154.3184	0.6843	0.8985
0.913	86.2348	0.7338	0.8988
1.116	46.9094	0.7844	0.9097
1.331	24.4833	0.7848	0.9228
1.506	16.3587	0.7161	0.9245
1.665	9.1545	4.4458	0.9203
1.912	5.8480	-0.1790	0.9082
2.259	2.9002	-1.2751	0.9064
2.584	1.4787	-0.5428	0.9175
2.869	0.9468	-0.6245	0.9235
3.198	0.4290	0.3508	0.9113
3.544	0.1995	0.9418	0.8906
3.916	0.8166	0.303	0.8417
4.35	0.7942	0.2429	0.8268
4.859	0.5863	0.2681	0.7838
5.373	0.4991	0.6355	0.7678

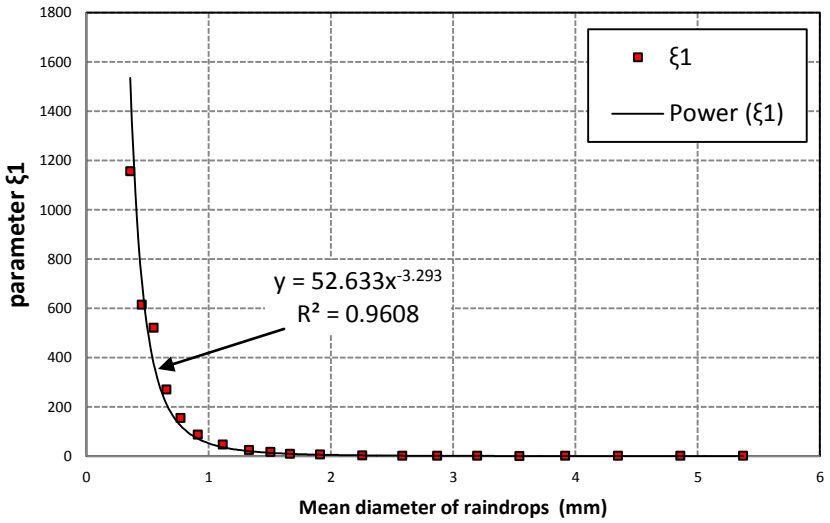

Figure 6-4: Fitting procedure for ξ_1 against the diameter of the disdrometer bin for $0.359 \text{ mm} \leq D_i \leq 5.373 \text{ mm}$

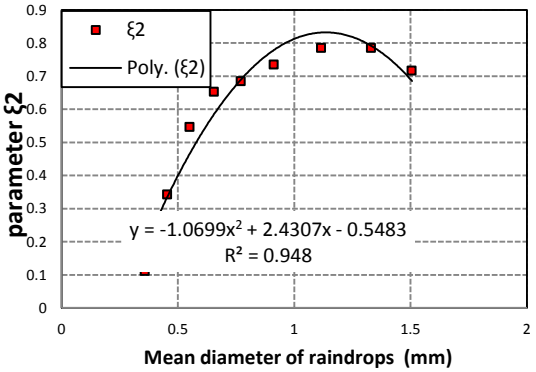

(a) $0.359 \text{ mm} \leq D_i \leq 1.506 \text{ mm}$

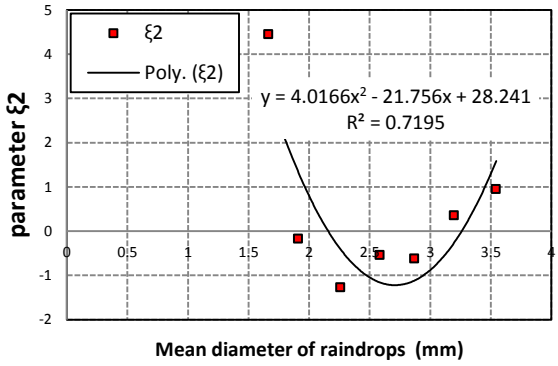

(b) $1.665 \text{ mm} \leq D_i \leq 3.544 \text{ mm}$

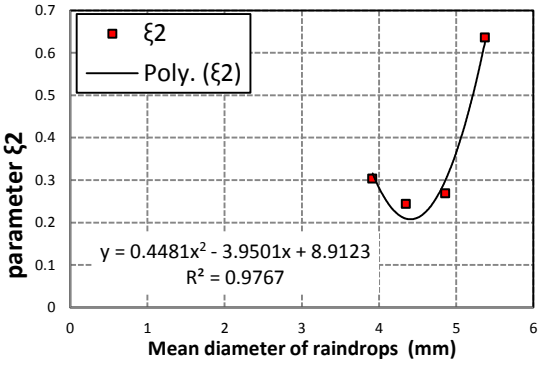

(c) $3.916 \text{ mm} \leq D_i \leq 5.373 \text{ mm}$

Figure 6-5: Polynomial fitting procedure for ξ_2 against the diameter of the disdrometer bins in Durban

Functional polynomial fits for ξ_1 and ξ_2, which rely on the bin diameters provided in Table 6-3, have been proposed so that:

$$\xi_1 = 52.633 {D_i}^{-3.293} \quad \text{for } 0.359\, mm \leq D_i \leq 5.373\, mm \quad (6.18)$$

For the second parameter, ξ_2, a three-tier equation dependent on D_i is proposed to cater for the variations in the values of ξ_2. Thus, this parameter is given as:

$$\xi_2 = \alpha {D_i}^2 + \beta D_i + \gamma \quad (6.19)$$

Figure 6-4 provides the details for the values of α, β and γ obtained from regression fitting technique for the empirical model in Durban.

Table 6-4: The three-level functional fits of ξ_2 with their various diameter bounds for Durban

α	β	γ	Valid diameter range (mm)	R^2
-1.0699	2.4307	-0.5483	$0.359 \leq D_i \leq 1.506$	0.948
4.0166	-21.756	28.241	$1.665 \leq D_i \leq 3.544$	0.7195
0.4481	-3.9501	8.9123	$3.916 \leq D_i \leq 5.373$	0.9767

6.5 Derivation of Parameters for Empirical rainfall DSD models in South Africa

The application of the cumulative distribution provides essential information on the behaviour of a random process, as in the case of rainfall. The rainfall exceedence function is utilized at equal probability to extrapolate the behaviour of rainfall drop-size distribution at selected locations in South Africa.

6.5.1 Derivation of Rainfall Rate Relationships from Distribution Function

Assuming the percentage of time, $P(R \geq R(t))$, for which a 1-minute rainfall rate is exceeded can be represented for a location x such that:

$$P_x(R \geq R_x(t)) = \varphi_x R_x(t)^{\Psi_x} \quad (6.20)$$

where x is the distinct location for the proposed power-law CDF, which in this case is Durban, because we have our reference data at that control site.

By general assumption, if two locations, x and y are separated by spatial distance within the same climatic region so that the power-law PDF of location y is given by:

$$P_y(R \geq R_y(t)) = \varphi_y R_y(t)^{\Psi_y} \tag{6.21}$$

Therefore, their respective equiprobable distribution functions can be obtained by mathematically equating their time exceedence functions in (6.20) and (6.21) such that:

$$P_x(R \geq R_x) = P_y(R \geq R_y) \tag{6.22}$$

$$\varphi_x R_x(t)^{\Psi_x} = \varphi_y R_y(t)^{\Psi_y} \tag{6.23}$$

Mathematically, a new function can be derived with $R_x(t)$ being the subject of the function given by:

$$R_x(t) = \left(\frac{\varphi_y}{\varphi_x}\right)^{\frac{1}{\Psi_x}} R_y(t)^{\frac{\Psi_y}{\Psi_x}} \tag{6.24}$$

so that,

$$R_x(t) = \varphi {R_y}^{\Psi}(t) \tag{6.25}$$

where,

$$\varphi = \left(\frac{\varphi_y}{\varphi_x}\right)^{\frac{1}{\Psi_x}} \text{ and } \Psi = \frac{\Psi_y}{\Psi_x} \tag{6.26}$$

Consequently, if $R_x = R_y = R$, as the case will always require since they have the same unit. This simply means that the rainfall rate at location x will have a power-law equivalent at location y given by the expressions in (6.17) and (6.18) or simply a *scaled* equivalent. This method is similar to the concept of power-law rainfall conversion technique, except that only 1-minute rainfall samples are compared in this case.

However, because of the systematic errors that may arise from applying a power-law fit to model the rainfall rate exceeded, a procedural approach was employed in the implementation of the process in (6.20) - (6.26). The procedures are hereby given:

- The hourly rainfall rate samples obtained from SAWS for 5 years are converted to 1-minute rainfall samples using the conversion factors in Table 6-1. The resulting 1-minute samples were then compared at equal probabilities using Durban (5-year SAWS data also) as the control site and fitted using a power-law regression fitting technique. Thus at 1-minute integration time, for any location y, we have:

$$R_{Durban}(t) = \beta_1 R_Y(t)^{\beta_2} \tag{6.27}$$

  where β_1 and β_2 are the power-law coefficients derived from the regression fitting technique.

- For Durban, the converted 1-minute rainfall rate samples from SAWS are compared with the measured 1-minute rainfall rate samples obtained from the RD-80 disdrometer at equal probability. This comparison is undertaken to reduce the errors that may arise from different equipment configurations and disparities arising from the use of rainfall data from different years. For the power-law fit obtained here, it is found that:

$$R_D(t) = \varphi' R_{Durban}(t)^{\Psi'} \tag{6.28}$$

  where φ' and Ψ' represent the power-law coefficients correlating $R_D(t)$ to $R_{Durban}(t)$. $R_D(t)$ is the rainfall rate measurement obtained from the disdrometer in Durban.
  The relationship obtained from the regression fitting is given as:

$$R_D(t) = 0.0157[R_{Durban}(t)]^{1.7638} \quad R^2 = 0.9963 \tag{6.28a}$$

- The rainfall rate power-law in (6.27) and (6.28) were then combined so that a single function relating the rainfall rate measurements from the RD-80 disdrometer in Durban with other cities is developed. This is given by;

$$R_D(t) = \varphi' \left[\beta_1 R_y(t)^{\beta_2}\right]^{\Psi'} \tag{6.29}$$

which can otherwise be written as:

$$R_D(t) = \varphi R_Y(t)^{\Psi} \tag{6.30}$$

where $\varphi = 0.0517^{1.7638}\beta_1$ and $\Psi = 1.7638\beta_2$ in (6.30) above using the values from (6.28*a*).

The results of φ and ψ were computed for seven locations in South Africa using this approach and the results are presented in Table 6-5. Also included in the table are the values of β_1 and β_2 obtained from the regression fitting of the other locations with respect to the city of Durban.

Table 6-5: Parameters for the power-law relationships between Durban and other cities in South Africa

LOCATION	RAINFALL RATE EQUIVALENT				
	[a]Converted 5-year data			1-min disdrometer data	
	β_1	β_2	R^2	φ	Ψ
CAPE TOWN	1.7372	1.2762	0.9956	0.0416	2.2510
PIETERMARITZBURG	1.963	0.7313	0.9911	0.0516	1.2899
EAST LONDON	1.2467	1.0144	0.9973	0.0232	1.7892
RICHARDS BAY	0.4746	1.0727	0.9982	0.0042	1.8920
PRETORIA	1.1882	1.0038	0.9977	0.0213	1.7705
[b]VRYHEID	4.412	0.6754	0.9802	0.2512	1.1909
[b]BRANDVLEI	8.4064	0.5177	0.9713	0.6710	0.9131

[a]The 5 year rainfall measurements from SAWS were converted using the proposed coversion factors from *Akuon and Afullo* [2011].
[b]The few number of rainfall samples may account for the higher values of β_1 in this case

6.5.2 Development of Empirical Rainfall DSD Models for selected Locations

In this section, the expressions derived in (6.15), (6.16) and (6.30) are applied to derive empirical rainfall DSD expressions for seven selected locations in South Africa.

From (6.15) and (6.16), it is obvious that $R(t)$ is the same as $R_D(t)$ in (6.30). By replacing, $R_D(t)$ with $R(t)$, the definition of the rainfall DSD becomes:

$$N(D_k, R(t)) = \xi_1' a^{\xi_2'} R^{b\xi_2'} \tag{6.31}$$

and,

$$N\big(D_k, R(t)\big) = \xi_1{}' a R^b + \xi_2{}' \tag{6.32}$$

where ξ_1' and ξ_2' are the coefficients earlier proposed for Durban in Table 6-3. Using the approach in (6.15) and (6.16), the rainfall DSD equations derived for other locations becomes:

$$N\big(D_k, R(t)\big) = \xi_1 R^{\xi_2} \tag{6.33}$$

and,

$$N\big(D_k, R(t)\big) = \xi_1 a R^b + \xi_2 \tag{6.34}$$

Thus, the rainfall equation DSD for other locations aside Durban can therefore be defined as:

$$N(D_k, R(t)) = \begin{cases} \xi_1[R(t)]^{\xi_2} & \text{for } 0.359\,mm \le D_k \le 1.506\,mm \\ \xi_1[R(t)]^b + \xi_2 & \text{for } 1.665\,mm \le D_k \le 3.544\,mm \\ \xi_1[R(t)]^{\xi_2} & \text{for } 3.916\,mm \le D_k \le 5.373\,mm \end{cases}$$

$$\text{for } t \in [0, T] \tag{6.35}$$

The table showing the results simulated for each of the seven selected locations in South Africa is shown in Appendix G-1. However, the regression fits for ξ_1 and ξ_2 of these locations are also proposed. For ξ_1, the power-law fits are derived for the bin diameter range such that, 0.359 mm $\geq D_i \geq$ 5.373 mm; the results are presented in Table 6-6.

Table 6-6: The functional fits of ξ_1 for different locations in South Africa for diameter bound 0.359 mm $\geq D_i \geq$ 0.455 mm

LOCATION	ξ_1	R^2
CPT	$6.67\,D_i^{-3.55}$	0.8329
PMB	$7.6817 D_i^{-3.531}$	0.8437
PTA	$4.518 D_i^{-3.62}$	0.7996
ELN	$4.5714 D_i^{-3.597}$	0.8206
RBY	$1.508 D_i^{-3.737}$	0.7138
BRV	$40.248 D_i^{-3.349}$	0.9468
VRY	$19.413 D_i^{-3.417}$	0.9113

For the coefficients of ξ_2, the values are presented in Table 6-7. In the two tables, abbreviations used are as thus: Cape Town (CPT), Pietermaritzburg (PMB), Pretoria (PTA), East London (ELN), Richards Bay (RBY), Brandvlei (BRV) and Vryheid (VRY). From Table 6-6, it is noted that the high scale factor, ξ_1, for Brandvlei is closer to that of Durban, although this does not suggest the closeness of their rainfall DSD.

Table 6-7: The proposed three-level functional fits of ξ_2 with their various diameter bounds for different locations in South Africa

LOCATION	*b*	ξ_2			Valid diameter range (mm)	R^2
		α	β	γ		
CPT	2.2510	-2.408	5.4717	-1.2342	$0.359 \le D_i \le 1.506$	0.948
		4.0166	-21.756	28.241	$1.665 \le D_i \le 3.544$	0.7195
		1.0087	-8.8918	20.062	$3.916 \le D_i \le 5.373$	0.9767
PMB	1.2899	-1.381	3.1308	-0.6995	$0.359 \le D_i \le 1.506$	0.939
		4.0166	-21.756	28.241	$1.665 \le D_i \le 3.544$	0.7195
		-0.578	-5.0949	11.495	$3.916 \le D_i \le 5.373$	0.9767
PTA	1.7705	-1.8942	4.3035	-0.9707	$0.359 \le D_i \le 1.506$	0.948
		4.0166	-21.756	28.241	$1.665 \le D_i \le 3.544$	0.7195
		0.7934	-6/9938	15.78	$3.916 \le D_i \le 5.373$	0.9767
ELN	1.7892	-1.9141	4.3488	-0.9809	$0.359 \le D_i \le 1.506$	0.948
		4.0166	-21.756	28.241	$1.665 \le D_i \le 3.544$	0.7195
		0.8017	-7.0667	15.944	$3.916 \le D_i \le 5.373$	0.9767
RBY	1.8920	-2.0241	4.5988	-1.0373	$0.359 \le D_i \le 1.506$	0.948
		4.0166	-21.756	28.241	$1.665 \le D_i \le 3.544$	0.7195
		0.8479	-7.4744	16.864	$3.916 \le D_i \le 5.373$	0.9767
BRV	0.9131	-0.9767	2.2191	-0.5005	$0.359 \le D_i \le 1.506$	0.948
		4.0166	-21.756	28.241	$1.665 \le D_i \le 3.544$	0.7195
		0.4092	-3.6074	8.1391	$3.916 \le D_i \le 5.373$	0.9767
VRY	1.1909	-1.247	2.8947	-0.6529	$0.359 \le D_i \le 1.506$	0.948
		4.0166	-21.756	28.241	$1.665 \le D_i \le 3.544$	0.7195
		0.5367	-4.7305	10.67	$3.916 \le D_i \le 5.373$	0.9767

6.6 Variation of Specific Attenuation at Different Locations

The specific attenuation for each of the selected locations are computed using the expressions in section 5.2 and applying the proposed scattering coefficients at 20^{o}C ambient temperature. The computations are undertaken at four rainfall rates notably at 4 mm/h, 9 mm/h, 25 mm/h and 75

mm/h. From the graphs provided in Figures 6-6 to 6-9 and the comparison with ITU-R values in Table 6-8, the variations in the specific attenuation at various rainfall rates are shown for a frequencies between 2 GHz and 100 GHz. The computed specific attenuations undertaken for each location is presented in a table in Appendix H.

At 4 mm/h, Durban is predicted to have the highest specific attenuation. For other locations, the predicted average margin for their respective specific attenuations in descending order are as thus: Brandvlei (1.39), Vryheid (2.12), Cape Town (2.32), Pietermaritzburg (3.95), East London (4.15), Pretoria (4.27) and Richards Bay (7.48). The close average margins for the locations of Pietermaritzburg, East London and Richards Bay suggest similarity in the rainfall DSD mechanics at this rainfall rate.

At 9 mm/h, Durban is again predicted to have the highest specific attenuation. In descending order, the ranking of the average margin of the specific attenuation figures with respect to Durban for other locations are as thus: Cape Town (1.35), Brandvlei (1.52), Vryheid (2.1), East London (3.58), Pretoria (3.72), Pietermaritzburg (4.17) and Richards Bay (7.33).

At 25 mm/h, Cape Town is predicted to suffer greater specific attenuation than other locations. This might be due to the limit imposed by the converted 1-minute data for Cape Town where highest rainfall sample is 20.71 mm/h. For other locations, their average margins with respect to Cape Town are as thus: Durban (1.98), Brandvlei (3.63), Vryheid (3.96), East London (4.91). Pretoria (5.25), Pietermaritzburg (8.38) and Richards Bay (11.91).

Finally, at 75 mm/h, Durban is predicted to have the highest specific attenuation. For this comparison, Cape Town is excluded because the computed figures become unstable and hence, unreliable. The rainfall bound as explained in the discussion for 25 mm/h is responsible for this. For other locations, their respective average margins with respect to Durban are presented in descending order as thus: East London (1.36), Pretoria (1.49), Vryheid (1.80), Brandvlei (1.92), Richards Bay (3.66) and Pietermaritzburg (3.9).

In general, the control site in Durban is generally predicted to experience higher specific attenuations than all other sites for the investigated rainfall rates, except with Cape Town at around 25 mm/h. Even at $R_{0.01}$, the prediction from our models is seen to have values ranging between the ITU-R horizontal and vertical specific attenuations. Broadly speaking, comparing the overall results

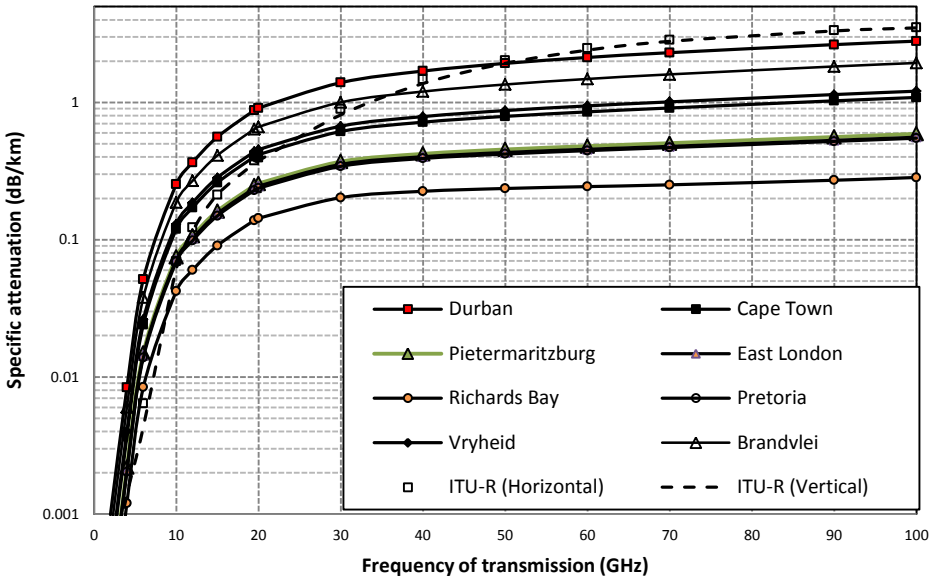

Figure 6-6: Computed specific attenuation for eight locations in South Africa at 20°C ambient temperature for rainfall rate of 4 mm/h

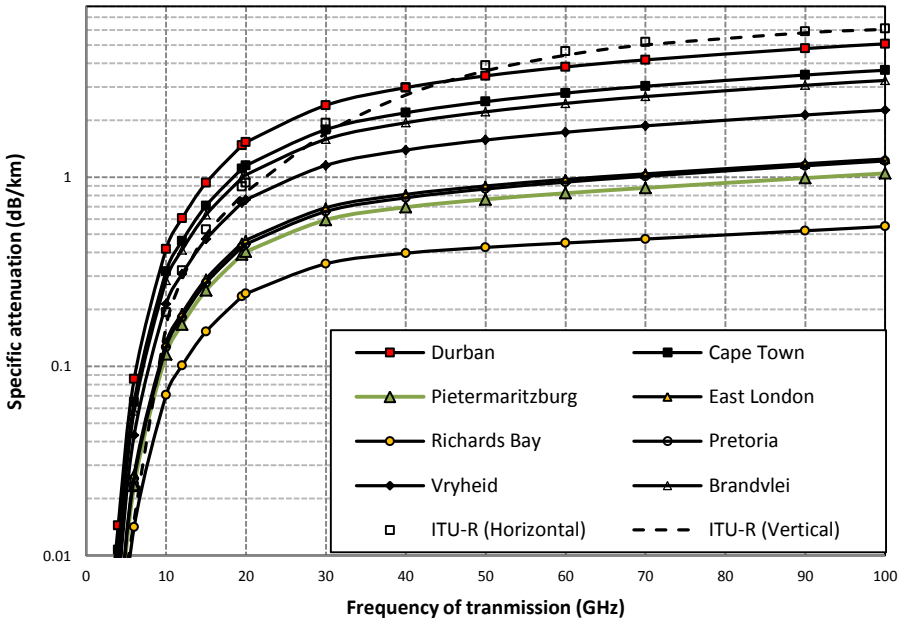

Figure 6-7: Computed specific attenuation for eight locations in South Africa at 20°C ambient temperature for rainfall rate of 9 mm/h

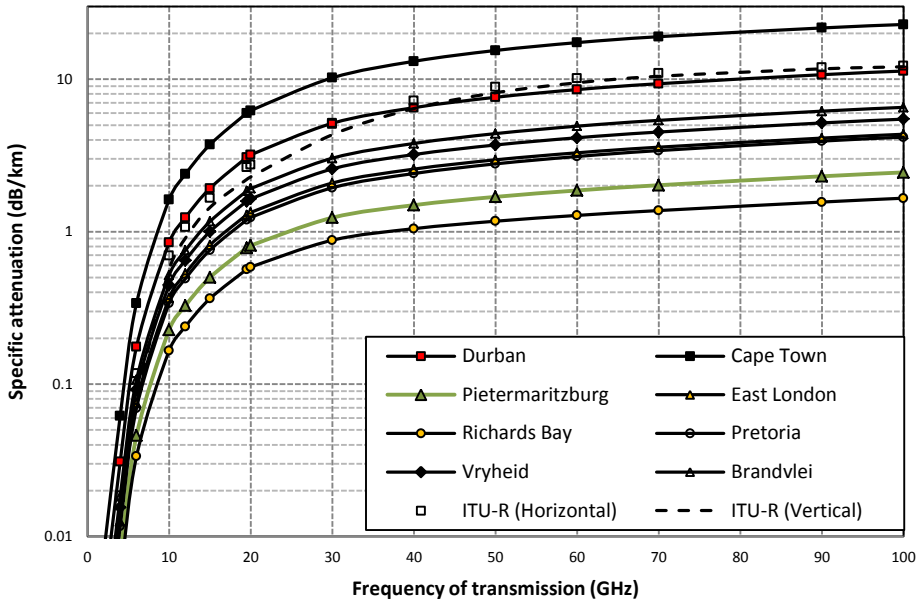

Figure 6-8: Computed specific attenuation for eight locations in South Africa at 20°C ambient temperature for rainfall rate of 25 mm/h

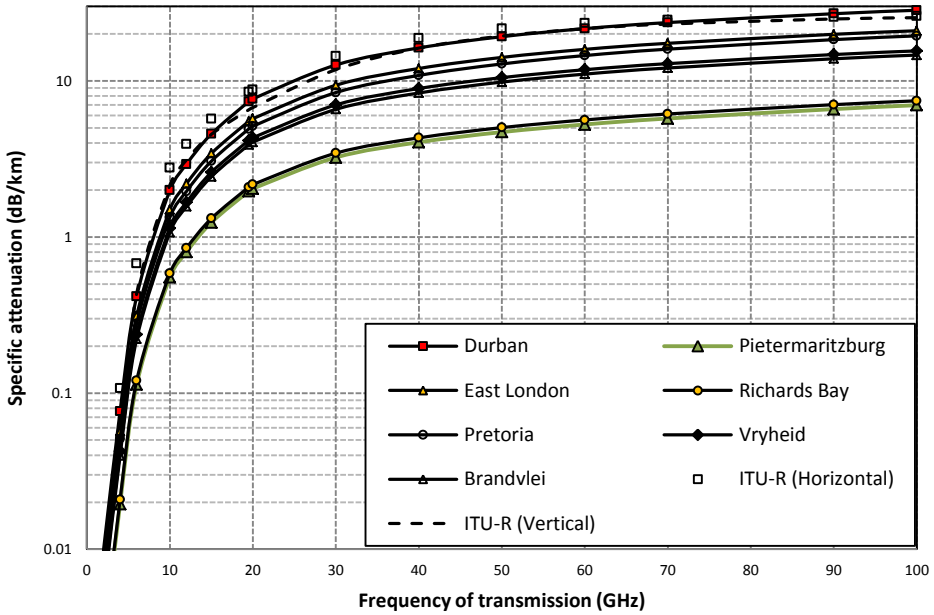

Figure 6-9: Computed specific attenuation for eight locations in South Africa at 20°C ambient temperature for rainfall rate of 75 mm/h

Table 6-8: Comparison of the proposed specific attenuation with ITU-R predictions

LOCATION	FREQUENCY (GHz)	PREDICTED MODEL RESULTS		ITU-R DESIGNATION		
		$R_{0.01}$ (mm/h)	Specific Attenuation (dB/km)	$R_{0.01}$ (mm/h)	Specific Attenuation (H) (dB/km)	Specific Attenuation (V) (dB/km)
DBN	4	60.69	0.0639	60	0.0752	0.0407
	15		3.8467		4.4542	3.5979
	25		8.7939		9.3913	7.4677
	60		17.99		19.77	16.24
CPT	4	20.41	0.04241	22	0.0151	0.0116
	15		2.5937		1.4432	1.2623
	25		5.8698		3.4466	2.8816
	60		11.81		9.174	7.373
PMB	4	165	0.0429	60	0.0752	0.0407
	15		2.6292		4.4542	3.5979
	25		5.9497		9.3913	7.4677
	60		11.9806		19.77	16.24
PTA	4	66.49	0.0428	60	0.0752	0.0407
	15		2.5885		4.4542	3.5979
	25		5.8928		9.3913	7.4677
	60		12.1479		19.77	16.24
ELN	4	63.46	0.0443	60	0.0752	0.0407
	15		2.7043		4.4542	3.5979
	25		6.1270		9.3913	7.4677
	60		12.35		19.77	16.24
RBY	4	126.41	0.0449	60	0.0752	0.0407
	15		2.7440		4.4542	3.5979
	25		6.2210		9.3913	7.4677
	60		12.5616		19.77	16.24
BRV	4	49.20	0.02923	42	0.0425	0.0231
	15		1.8188		2.9838	2.4793
	25		4.0722		6.5760	5.3232
	60		8.0469		15.0509	12.2659
VRY	4	60.09	0.0342	60	0.0752	0.0407
	15		2.0858		4.4542	3.5979
	25		4.7639		9.3913	7.4677
	60		9.4684		19.77	16.24

with the recommended ITU-R values shows that $R_{0.01}$ may not necessarily be the only parameter for the determination of rainfall attenuation in a locality. The prevailing climatological factors at a locality play a much more visible role in the intensity and volume of rainfall drops, as well as, their distribution in homogeneous rainfall types. Another observed trend is that the computed average margins of other locations with respect to Durban seem to decrease as rainfall rate increases suggest that rainfall DSD in these locations may be similar at higher rainfall rates. This can be true provided that the maximum yearly rainfall rates for those locations are above the 75 mm/h bound.

6.7 Chapter Summary

In this chapter, an approach was developed to derive empirical rainfall DSD model directly from the recommended disdrometer computation. With a *priori* knowledge of the raindrop microstructural mechanics in each disdrometer bin, an empirical rainfall DSD is developed, and then applied, in the estimation of rainfall attenuation in Durban.

Firstly, it was established that a positive correlation may exist between the rainfall DSD samples and overall rainfall rates samples at the same time interval, except at the 0.359 mm diameter class. This suggests that rainfall DSD increases with rainfall rates for all bins, except the 0.359 mm bin. However, there is a stronger positive correlation between the two rainfall parameters between the 1.331 mm and 3.198 mm diameter classes, where the least coefficient is 0.73. A left-sided normal distribution, and later, a linear relationship is obtained at this bound. This behaviour may be linked to the stability in the rain growth pattern of rainfall of rainfall droplets at mid-diameter bounds. However, a unity correlation was obtained for the specific rainfall rates and rainfall DSD corresponding to each diameter classes, with a linear relationship.

The concept of rainfall rate cumulative distribution at equal exceedence probability was applied to derive power-law relationships for other locations with Durban as the reference location. With this, a unique equivalent rainfall rate relationship is established between Durban and other locations. This relationship is used to estimate the rainfall DSD at these locations to enable the estimation of their respective rainfall specific attenuation. From the specific attenuation results, it is shown that signal outages during rainfall may not be as universal as suggested by ITU-R. Different specific attenuation levels are observed to exist at different locations at the same rainfall rates and frequency of transmission. From the predictions, the coastal city of Durban may experience more intense signal degradation than the coastal cities of East London and Richards Bay, except the city of Cape Town at 20 mm/h and beyond. Interestingly, the ITU-R proposes the similar $R_{0.01}$ exceedence levels for some of these selected locations at the same specific attenuations.

The methodological approach used for this work is not subjective and requires more improvements and data validation using attenuation results from the selected control sites. Also, long-term studies and analysis of rainfall attenuation data for these locations will provide a more stable and robust approach for the mathematical transference of local disdrometer measurements to other locations from a control location.

CHAPTER SEVEN

Conclusion and Recommendations

7.1 Introduction

Link budget for microwave and millimeter networks require adequate compensation for signal losses arising from rainfall attenuation. Insufficient data at different parts of the world has limited many network architects and engineers to the use of ITU-R, which is not always very reliable.

In this research, it is established that rainfall water volume is not uniform around the world as suggested by ITU-R related rainfall models. Apart from this, the ITU-R concept also assumes a singular attenuation figure for single rainfall rate, which is at least a generalization, subject to climatic and seasonal variation of a locality. Therefore, the rainfall rate linked to water volume, varies around the world and as seen in Durban, produces varying degrees of rainfall attenuation. Invariably, rainfall attenuation mechanics are more related to the natural variables affecting a locality than the global variables affecting a region.

In this research, the combination of the knowledge of rainfall rate distribution and rainfall DSD has been applied to predict the effects of rainfall attenuation in Durban, South Africa. The summary from this research are presented in the following sections.

7.2 Conclusion

The conclusions garnered from this research work are presented based on their chapters and are as follows:

7.2.1 Chapter 3 – Rainfall Rate Modelling and Analysis

The rainfall statistics obtained from the Durban measurements were investigated on the basis of monthly, seasonal, events and annual distributions. It was observed that Durban has $R_{0.01}$ as high as 50.48 mm/h in summer, 72.15 mm/h in autumn, 53.37 mm/h in winter and 18.51 mm/h in spring. The monthly figures indicate that the winter months have the lowest $R_{0.01}$ values, while, the summer and autumn months have the highest $R_{0.01}$ values. The immediate implication of this to microwave link designers is that adequate budget be made for rain fade in summer and autumn. Durban is seen to experience more rainfall hours of drizzle types and widespread types with wider coverage of rainfall cells. Thunderstorm and shower rain types have fewer rainfall hours, and therefore, have

much smaller rainfall cells. Additionally, the rain events distribution suggested that thunderstorm rainfall in Durban could have $R_{0.01}$ as high as 82.5 mm/h. The network outage experienced during a thunderstorm event exceeds that of annual distribution where $R_{0.01}$ is found to be 60.69 mm/h. Also, the $R_{0.01}$ for the annual distribution is observed to be closer to global estimates.

Finally, an attempt to find a suitable model for the prediction of rainfall rate in Durban was undertaken using the maximum likelihood (ML) estimation technique. The Weibull model was found to fit the measurements at rainfall rates below 40 mm/h and at higher rainfall rates, the gamma model seem a better choice. The lognormal model is also found to provide better fit for the entire period of measurement, with the Crane rain rate model closer to the measurements.

7.2.2 Chapter 4 – Rain drop-size Distribution Modelling

The method of moment (MM) point estimation technique was employed in the development of rainfall DSDs for different rainfall classifications using lognormal, modified gamma, Weibull and negative exponential models. From the result, it was observed that monthly rainfall DSDs in Durban are influenced annually by seasonal characteristics. The winter months in Durban are predicted to suffer less from the effects of rainfall attenuation due to the low rainfall water volume and low values of $R_{0.01}$, resulting in low rainfall DSDs. On the contrary, the summer and autumn months will suffer from intense effects of rainfall attenuation with high rainfall water volume and high values of $R_{0.01}$.

Based on the error statistics on rainfall regimes analysis, the proposed Weibull rainfall DSD model was found desirable for Durban at rainfall rates lower than 40 mm/h. Conversely, the proposed lognormal rainfall DSD model performed best at rainfall rates beyond 40 mm/h. A similar result is also confirmed in the error estimation for annual rainfall DSD undertaken for the proposed models. Therefore, the lognormal model is the most preferable rainfall DSD model for Durban at high rainfall rates.

7.2.3 Chapter 5 – Estimation of Rainfall Attenuation in Durban

Based on the computations of the extinction cross section using Mie scattering technique at 20^{O}C, an estimation of rainfall attenuation in Durban was embarked upon. From the monthly rainfall DSD statistics, the computed specific attenuation was found to be higher, for the months coinciding with the summer and autumn seasons indicating severe signal impairment between 2 GHz and 1 THz

frequencies. The winter months have lower specific attenuation indices for the same period indicating less signal outages by rainfall durations.

The specific attenuation of the proposed models, compared on the basis of rainfall regime classification, shows that the Weibull DSD model fits well below 10 mm/h; modified gamma DSD model at 10 mm/h and beyond, and also, lognormal DSD model at 40 mm/h and beyond. Therefore, the lognormal model provides the best estimation of specific attenuation at high rainfall rates in Durban.

The link measurements undertaken in 2004 at 19.5 GHz and 6.73 km link distance were compared with the proposed models. It was found that the models all passed the χ^2 threshold test at 36.191 for the minimum and average bounds of link measurements for specific attenuation. The path attenuation, however, fitted only the minimum bounds and passed the χ^2 threshold test. The link measurements for 2004 were found to be higher than the recent measurements and this was confirmed by the comparisons with the actual samples of the disdrometer at different attenuation bounds. The suspect, with respect to the discrepancy lies in the application of the ITU-R reduction factor, which assumes the link as being a fractal part of a rain cell. It was established that the link path was shorter than the average rainfall cell for subtropical zones, and therefore concluded, that a reduction factor equal to or greater than unity is required for valid model comparison with the link. In addition, the spherical droplet assumption for the scattering may contribute to the anomalies noted in the modelling. As rightly stated by *Das et al.* [2010], *"the higher rain rates consist of bigger rain drops which are not strictly spherical"*, thus, some errors may be present in the spherical assumption.

7.2.4 Chapter 6 – Rainfall Correlation for South African Areas

This chapter applied converted 1-minute rainfall samples from the five-year SAWS data for the estimation of rainfall DSD from the previous results of *Akuon and Afullo* [2011].

Firstly, an averagely positive correlation was found to exist for the relationship between computed rainfall DSDs and rainfall rates in Durban for rain droplets greater than 0.359 mm. The unity relationship between specific bin rainfall rates and total rainfall rates was used to derive an empirical rainfall DSD for Durban. The resulting empirical DSD was refitted based on their bin characteristics and a functional model was found for Durban. The results show that a stronger correlation is present between 1.331 mm and 3.198 mm diameter classes of the measurements, than

other classes. This may suggest that the randomness in the rainfall pattern is minimal for rainfall droplets in this bound for Durban.

By employing comparison of 1-minute rainfall rates at different locations, the corresponding rainfall DSDs for other locations were predicted, and hence, their specific attenuations. The specific attenuations were computed based on the scattering results obtained for Durban at 20^{O}C. The results show that Durban may experience a higher attenuation level than other selected locations, with the exception of Cape Town. Also, deviations from the ITU-R values were noticed for these locations based on the applied procedure in this work.

7.3 Suggestions for Future Work

- The use of long-term rainfall data from rainfall measurements need to be considered for locations around South Africa. The accuracy of rainfall attenuation models is totally dependent on the number of sampled years of rainfall experiments. In addition, other varieties of exotic rainfall measuring instruments like the Micro Rain Radar (MRR) can be utilised for rainfall measurement, as suggested by *Owolawi* [2010].

- The use of a robust, and perhaps, more efficient method that considers the raindrop shape effects for Mie scattering technique needs to be applied to the proposed DSD models. An example of such is the application of the scattering techniques for spheroidal and oblate-spheroidal raindrops suggested by *Li et al.* [2000]. This will help differentiate between the effects of horizontal and vertical polarization on microwave networks.

- Development of rainfall DSD models should be approached by using the maximum number of drops recorded per rainfall sample. The modelling procedure for rainfall DSDs applied in this work appears to favour average link measurements while neglecting maximum attenuation bounds. This is also applicable to the ITU-R models, as it has been noticed that the model works fairly well at average link measurements in Durban.

- Improvements in the correlated attenuation prediction developed in the study should be supported with at least the installation of another disdrometer system at any of the selected control sites. This will enable the validation of the mathematical idea being proposed in correlating rainfall parameters in Chapter 6.

REFERENCES

Adimula, I.A and G.O. Ajayi 1996 : 'Variation in raindrop size distribution and specific attenuation due to rain in Nigeria,' *Ann. Telecom*, vol.51, No. 1-2, pp. 87–93.

Afullo, T.J., (2011): 'Raindrop size distribution modeling for radio link design along the Eastern coast of South Africa' *Progress in Electromagnetic Research B*, Vol. 34, pp.345-366.

Ajayi, G.O. and E.B.C. Ofoche (1983), "Some Tropical Rainfall Rate Characteristics at Ile-Ife for Microwave and Millimeter Wave Application,*' J. of Climate and Applied Meteor.*,Vol. 23, pp. 562-567.

Ajayi, G.O. and R.L. Olsen 1985 : 'Modeling of a tropical raindrop size distribution for microwave and millimeter wave applications', *Radio Science*, Vol. 20, number 2, pp. 193–202, Apr.

Ajayi, G.O., S. Feng, S.M. Radicella, B.M. Reddy (1996): Handbook on Radiopropagation Related to Satellite Communications in Tropical and Subtropical Countries, ICTP, Trieste, pp. 7–14, 1996.

Akuon, P.O and T.J. Afullo 2011 : 'Path reduction factor modeling for Terrestrial links based on rain cell growth,' *IEEE AFRICON 2011* conference, Zambia, ISBN: 978-1-61284-991-1.

Alonge, A.A. and T.J. Afullo (2011): 'Rainfall rate modeling for various rainfall types in South Africa', *IEEE AFRICON 2011* conference, Zambia, ISBN: 978-1-61284-991-1.

Amarjit and R.P.S. Gangwar (2009): 'The simple mathematical model for prediction of rain attenuation in microwave and millimeter wave frequencies,' *J. Instn Engr.-pt ET*, vol. 90, pp. 41-6, July.

Atlas, D. and C.W. Ulbrich 1974 : 'The physical basis for attenuation-rainfall relationships and the measurement of rainfall parameters by combined attenuation and radar methods,' *J. Rech. Atmos.*, 8, pp. 275–298.

Aydin, K. and S.E.A. Daisley 2002 : 'Relationships between rainfall rate and 35-GHz attenuation and differential attenuation: modeling the effects of raindrop size distribution, canting and oscillation,' *IEEE Trans. Geosci. Remote Sens.*, vol. 40(11), pp. 2343-2352, Nov.

Baldotra, A.K. and I.S. Hudiara 2004 : 'Rain Attenuation Statistics Over Terrestrial Microwave Link at 19.4 GHz at Amritsar,' *IEEE Trans. Antennas Propag.*, vol. AP-52, N. 6, pp 1505-1508.

Banjo, O.P. and E, Vilar 1986 : 'Measurement and Modelling of Amplitude Scintillation on Low-Elevation Earth-Space paths and Impact on Communication Systems,' *IEEE Trans, Commun.*, Vol. COM-34, pp 774-780.

Bartholomew, M.J. 2009 : 'Disdrometer and tipping bucket raingauge handbook,' DOE/SC-ARM/TR-079, ARM Climate Research Facility, Dec.

Bohren, C.F. and D.R. Huffman (2004): Absorption and scattering of light particles, Wienheim: John Wiley.

Capsoni, C., F. Fedi, C. Magstroni, A. Paraboni and A. Pawlina 1987 : 'Data and theory for a new model of the horizontal structure of rain cells for propagation applications,' *Radio Sci.*, 22(3), pp. 395-404.

Chen, K.S., C.Y. Chu and Y.C. Tseng 2011 : 'A semi-empirical model of rain attenuation at Ka-band in Northern Taiwan,' *Progress in Electromagnetic Research M*, Vol. 16, pp. 213–223.

Cohen, C.A. and B.J. Whitten (1980): 'Estimation in the three-parameter lognormal distribution,' *J. of American Stat. Assoc.*, 75(370), pp. 399-404.

Crane, R.K., (2003): Propagation Handbook for Wireless Communication System Design, CRC Press LLC, Florida. pp. 1-3, 66-67.

Crane, R.K., 1980 : 'Prediction of Attenuation by Rain,*" IEEE Trans. On Comm.*, Vol. 28(9), pp 1717-1733.

Crane, R.K., (1996): Electromagnetic Wave Propagation Through Rain, John Wiley and Sons Inc., New York. pp 1-4, 39-40.

Cullen, A.L. and A. Kumar 1970 : 'The absolute determination of extinction cross sections by the use of an open resonator,' *Proc. Roy. Sec. Lond*., 315, pp. 217-230.

Das, S., A. Maitra and A.K. Shukla 2010 : 'Rain attenuation modeling in the 10-100 GHz frequency using drop size distributions for different climatic zones in tropical India,' *Progress in Electromagnetics Research,* vol. 25, pp. 211–224, 2010.

Eckhard, L., A.S. Werner and A. Markus 2001 : 'Lognormal distributions across the sciences: Key and clues,' *BioScience*, vol. 51, No. 5, pp. 341-352, May.

Emiliani, L.D., L. Luini and C. Capsoni 2009 : 'Analysis and parameterization of methodologies for the conversion of rain-rate cumulative distributions from various integration times to one minute,' *IEEE Antennas Propagat. Mag.*, vol. 51, No. 3, pp. 70–84, June.

Encyclopaedia Britannica (2009): *Map of South Africa*, Student and Home Edition: software.

Fashuyi, M.O., P.A. Owolawi and T.O. Afullo 2006 : 'Rainfall rate modelling for LoS radio systems in South Africa,' *Trans. of South African Inst. of Elect. Engineers (SAIEE)*, vol. 97, pp 74–81.

Fu, Q. and W.W. Sun (2006): 'Light scattering and absorption of spherical particles in an absorbing medium,' 10th ARM proc., San Antonio, Texas, March.

Garcia-Lopez, J.A. and J. Peiro (1983): 'Simple rain-attenuation prediction technique for terrestrial radio links, *Electronic Letters*, 19(21), pp. 444-448.

Green, H.E., (2004): 'Propagation Impairment on Ka-Band SATCOM links in tropical and equitorial regions,' *IEEE Antennas Propag. Magazine*, Vol. 46, no. 2, pp. 31-44.

Gunn, R. and K.D. Kinzer (1949): 'The terminal velocity of fall for water droplets in stagnant air,' *J. Meteor.*, 6(4), pp. 243-248.

Hahn, D.W. (2009): 'Light scattering theory,' Department of Mechanical and Aerospace Engineering, University of Florida, July.

Hall, M.P.H., L.W. Barclay and M.T. Hewitt (1996): Propagation of Radiowaves, IEEE press, London.

Hassan, M., Ali, A., and M., Alhadier (1985): 'Rain Measurements for MM-wave Propagation: A review', *J. Eng. Sci.*, 1985, pp. 179–200.

ITU-R Recommendation P.530-13 (2009): 'Propagation data and prediction methods for the design of terrestrial line-of-sight systems,' Radiocommunication sector, Geneva.

ITU-R Recommendation P.618-10 2009 : 'Propagation Data and Prediction Models Required for Design of Earth-Space Telecommunication System,' International Telecommunication Union, radiocommunication sector, Geneva.

ITU-R Recommendation P.837-1,2,3,4,5 (2008):'Characteristics of Precipitation for Propagation Modelling,' International Telecommunication Union, Radiocommunication Sector, Geneva.

ITU-R Recommendation P.838-3 (2005): 'Specific Attenuation Model for Rain for use in Prediction Methods,' International Telecommunication Union, Radiocommunication Sector, Geneva.

Jiang, H., M. Sano and M. Sekine 1997 : 'Weibull raindrop-size distribution and its application to rain attenuation', *IEE Proc Microw. Antennas propag.*, 144(3), June.

Joss, J., J.C. Thams and A. Waldvogel 1968 : 'The variation of raindrop-size distribution at Locarno,' *Proc. of Inter. Conf. on Cloud Physics*, pp. 369-373, 1968.

Khamis, N.H.H., J. Din and T.A. Rahman (2005): 'Derivation of path reduction factor from the Malaysian meterological radar data,' *IEEE Antennas Propag.*, pp. 207-2010.

Kozu, T. and K. Nakamura 1991 : 'Rainfall parameter estimation from dual-radar measurements combining reflectivity profile and path-integrated attenuation,' *J. of Atmos. and Oceanic tech.*," pp. 259–270.

Kreyszig, E, (2006): Advanced Engineering Mathematics, John Wiley and Sons, 9th edition, 2006, pp. 1046-1047.

Kumar, L.S., Y.H. Lee and J.T. Ong (2010): 'Shape slope parameter distribution modelling of electromagnetic scattering by rain drops,' *Progress in Electromagnetic Research B*, Vol. 25, pp. 191-209.

Lakshmi, S., Y.H. Lee and J.T. Ong (2007): 'The role of particular rain drop size on rain attenuation at 11 GHz', Proc. ICICS, doi: 10.1109/ICICS.2007.4449738.

Laws, J.O. and D.A. Parsons 1943 : 'The Relation of raindrop-size to intensity,' *Trans. Amer. Geophys. Union,* 24, pp 452-460.

Li, L.-W., Z.-C. Li, T.-S. Leo and M-.S. Leong 2002 : 'Extinction cross sections of realistic raindrops: Data-bank established using T-matrix method and nonlinear fitting technique' *J. of Electromagn. and Appl.*, Vol. 16, No. 7, pp. 1021-1039.

Li, L., P. Kooi, M. Leong and T. Yeo 1995 : 'Microwave attenuation by realistically distorted raindrops: part I–theory," *IEEE Trans. Antennas*, Vol. 43, no. 8, pp. 811–822, Aug.

Li, L., T. Yeo, P. Kooi and M. Leong 2000 : 'An efficient calculation approach to evaluation of microwave specific attenuation,' *IEEE Trans. Antennas*, 48(8), pp. 1220–1229,

Liebe, H.J., G.A. Hufford and T. Manabe (1991): 'A model for the complex permittivity of water at frequencies below 1 THz,' *Inter. J. of Infrared and Millimeter Waves*, 12 (7), pp. 659–678.

Maitra, A., 2004 : 'Rain Attenuation Modelling From Measurements of Rain Drop Size Distribution in the Indian Region,' *IEEE Antennas Wireless Propag. Lett*, Vol. 3, pp 180-181.

Mandeep, J.S., and J.E. Allnut (2007): 'Rain attenuation predictions at Ku-band in South East Asia countries,' *Progress in Electromagnetic Research*, 2007, pp. 65–74.

Mandeep, J.S., and Tanaka, K. (2007): 'Effect of atmospheric parameters on satellite link', Int. J. of Infrared Milli. Waves, pp. 789–795.

Marshall, J. S. and W. Palmer 1948 : 'The distributions of raindrop with size,' *Journal of Meteorology*, 5**,** pp. 165–166.

Marzuki, M., W.L. Randeau, M. Schönhuber, V.N. Bringi, T. Kozu and T. Shimomai (2010): 'Raindrop size distribution parameters of distrometer data with different bin sizes' *IEEE Trans Geosci. Remote Sens.*, vol. 48, pp. 3075-3080.

Massambani, O. and C.A.M. Rodriguez (1990): 'Specific attenuation as inferred from drop size distribution measurements in the tropics,' *Proc. URSI Comm. F. Sym. on Regional Factors in predicting Radiowave Attenuation*, Rio de Janeiro, Brazil, pp. 25-28.

Mätzler, C. (2003): 'Advanced model of extinction by rain and measurements at 38 GHz and 94 GHz and in the visible range,' *IAP Res. Rep. 2003-18*, Univ. of Bern, Bern, Feb.

Mätzler, C. (2002a): 'Drop-size distributions and Mie computation,' *IAP Res. Rep. 2002-16*, Univ. of Bern, Bern, Nov.

Mätzler, C. (2002b): 'MATLAB functions for Mie scattering and absorption,' *IAP Res. Rep. 2002-08*, Univ. of Bern, Bern, Jun.

Mie, G. (1908): 'Beiträge zur optik trüber medien, speziell kolldaler metallösungen,' *Ann. Phys*., 25, pp. 377–445, doi:10np.19083300302.

Mondal, N.C., Bhattacharya, A.B., and Sarkar, S.K. (1999): 'Attenuation of centimeter, millimeter and sub-millimeter waves due to rain over tropical Indian stations,' *Int. J. Infrared and millimeter waves*, 20(4), pp. 699–724.

Moupfouma F. (1987b : 'Rain Induced Attenuation Prediction Model for Terrestrial and Satellite-Earth Microwave Links,' *Annales des Telecommunications*, Vol. 42, pp 539-550.

Moupfouma, F. and L. Martin 1993 : 'Point Rainfall Rate Cumulative Distribution Function valid at various Locations,' *Electron. Letters*, Vol. 29, pp. 1503-1505.

Moupfouma, F. (1982): 'Empirical model for rainfall rate distribution,' *Electron. Lett.*, Vol. 18, pp. 460–461.

Moupfouma, F. 1984 : 'Improvement of a Rain Attenuation Prediction Method for Terrestrial Microwave Links,' *IEEE Trans. Antennas Propag.*, Vol. AP-32, pp 1368-1372.

Moupfouma, F. (1987a): 'More about rainfall rates and their prediction for radio systems engineering,' *IEE Proc*., 134(6), pp. 527-537, Dec.

Mulangu, C.T. and T.J. Afullo 2009 : 'Variability of the propagation coefficients for microwave links in Southern Africa,' *Radio Sci.*, Vol. 44.

Murthy, D.N., M. Xie and R. Jiang (2004): Weibull models, John Wiley and Sons Inc., New York, pp. 50–58, 68–74.

Nader, J., (1998): 'Modelling and Performance of Microwave Radio Links in Rain,' M.Sc Thesis, McGill Uni., Montreal, Canada. August.

Naicker, K. and S.H. Mneney (2004): 'Propagation measurements and modeling for terrestrial line-of-sight links at 19.5 GHz,' *Proc. of IEEE conf.*, vol. 01, pp. 95─100.

Naicker, K., 2006 : 'Rain attenuation modelling for line-of-sight terrestrial links, M.Sc thesis, School of Electrical, Electronics and Computer Engineering, Uni. of KwaZulu-Natal, Durban, South Africa. Sept.

Odedina, M.O. and T.J. Afullo (2009a): 'Analytical modeling of rain attenuation and its application to terrestrial LOS links,' *Proc. of SATNAC*.

Odedina, M.O. and T.J. Afullo 2008 : 'Characteristics of seasonal attenuation and fading for line-of-sight links in South Africa,' *Proc. of SATNAC*, pp. 203–208.

Odedina, M.O. and T.J. Afullo 2010a : 'Determination of rain attenuation from electromagnetic scattering by spherical raindrops: Theory and experiment,' *Radio Sci.*, vol. 45.

Odedina, M.O. (2010b): 'A Semi-Empirical Formulation for Determination of Rain Attenuation on Terrestrial Radio Links, Ph.D Thesis, Uni. of KwaZulu-Natal, Durban, South Africa, November.

Odedina, P.K. and Afullo, T.J. (2009b): 'Multipath Propagation Modeling and Measurement in a Clear-Air Environment for LOS Link Design Application,' *Proc. of SATNAC*, September.

Oguchi, T., (1973): 'Attenuation of electromagnetic wave due to rain with distorted raindrops (Part II),' *J. Radio Research Lab.*, 20(102), pp. 79-118, Sep.

Oguchi, T. (1977): 'Scattering from hydrometeors: A survey,' *Radio Sci.*, 16(5), pp. 691-730, Sep.

Ojo, J.S., M.O. Ajewole and S.K. Sarkar 2008 : 'Rain Rate and Rain Attenuation Prediction for Satellite Communication in Ku and Ka Bands over Nigeria,' *Prog. in Electromagnetics Research (PIER)*, Vol 5, pp 207-233.

Olsen, R.L., D.V. Rogers, D.B. Hodge 1978 : 'The aR^b Relation in the calculation of rain attenuation,' *IEEE Trans. Antennas Propag.*, 26(2), 1978, pp. 547-556, 1978.

Owolawi, P.A. and T.J. Afullo 2007 , 'Rainfall rate modelling and worst month statistics for millimetric line-of–sight radio links in South Africa,' *Radio Sci.*, Vol. 42.

Owolawi, P.A. 2011a : 'Rain rate probability density evaluation and mapping for the estimation of rain attenuation in South Africa and surrounding Islands,' *Progress in Electromagnetic Research*, vol. 112, pp. 155–181.

Owolawi, P.A. (2010): 'Characteristics of Rain at Microwave and Millimetric Bands for Terrestrial and Satellite Links Attenuation in South Africa and Surrounding Islands,' Ph.D thesis, Uni. of KwaZulu-Natal, Durban, July

Owolawi, P.A. (2011b): 'Raindrop size distribution model for the prediction of rain attenuation in Durban,' *Progress in Electromagnetics Research*, Vol. 7, No. 6, pp. 516-523, 2011.

Owolawi, P.A. (2006): 'Rainfall rate and rain drop size distribution models for line-of-sight millimetric systems in South Africa,' M.Sc dissertation, Uni. of KwaZulu-Natal, Durban, South Africa, February.

Owolawi, P.A., T.J. Afullo and S.B. Malinga 2008 : 'Rainfall rate characteristics for the design of terrestrial link in South Africa,' *Proc. of SATNAC*, pp. 71–76, Sept.

Pastoriza, V., A. Núñec, P. Mariño, F.P. Fontán and U.-C. Fiebig 2010 : 'Raincell identification and Modeling for propagation studies from weather radar images,' *IEEE Antennas Propag.*, 52(5), Oct.

Perez-Garcia, N.A. and L.A.R. da Silva Mello (2004): 'Improved method for prediction of rain attenuation in terrestrial links,' *Electronic Letters*, 40(11), pp. 683-684.

Pozar, D.M. (1998): Microwave Engineering, Second Edition, John Wiley and Sons, Inc., New York. Pp. 6.

Pruppacher, H.R. and J.D. Klett (1978): Microphysics of clouds and precipitation. Dordrecht: Riedel.

Pruppacher, H.R. and R.L. Pitter (1971): 'A semi-empirical determination of the shape of cloud and raindrops,' *J. Atmos. Sci*., 28, pp. 86–94.

Ramachandran, V. And V. Kumar (2007): 'Modified rain attenuation model for tropical regions for KU band signals,' *Int. J. Satell. Commun. Network*, Vol. 25, pp. 53-67.

Rogers, D.V., L.J. Ippolito and F. Davarian 1997 : 'System Requirement for Ka-Band Earth-Satellite Propagation Data*, Proc. of the IEEE*, 85(6), pp 810-820.

Sadiku, M.N.O. (2000): Numerical Techniques in Electromagnetics, 2nd edition, CRC press, pp. 96–103.

Saikia, M., M. Devi, A.K. Barbara and H.K. Sarmah (2009): 'Raindrop size distribution profile by laser distrometer and rain attenuation of centimeter radio waves,' *Indian J. of radio and space phy.*, vol. 38, pp. 80-85, April.

Salema, C. (2003): Microwave Radio Links, John Wiley and Sons, New York. pp 66-67.

Savvaris A., C.N. Kassanides and I.E. Otung 2004 : 'Observed effects of Cloud Wind on the Intensity and Spectrum of Scintillation," *IEEE Trans. Antenna Propag.,* 52(6), pp. 1492-1498.

Segal, B. 1986 : 'The influence of rain gauge integration time on measured rainfall-intensity distribution functions,' *J. of Atmospheric and Oceanic Tech*. vol. 3, pp. 662–671.

Sekine, M. and G. Lind 1982 : 'Rain attenuation of centimeter, millimeter and submillimeter radio waves,' *Proc. of 12th European Microwave Conference*, pp. 584–589.

Sekine, M. and C. Chen and T. Musha 1985 : 'Rain attenuation from log-normal and Weibull raindrop-size distribution', *IEEE Trans. Antennas propagat*., 35(3), Mar.

Seybold, J.S. (2005): Introduction to RF Propagation, John Wiley and Sons, New York, pp 218-245.

Sharma, P., S.I. Hudiara and M.L. Singh 2011 : 'Estimation of path length reduction factor by using one year attenuation statistics over a line of sight link operating at 28.75 GHz in Amristar INDIA ,' *J. Infrared Milli. Terahz. Waves*, Vol. 32, pp. 137−142.

Soong, T.T. (2004): 'Fundamentals of Probability and Statistics for Engineers,' John Wiley, Chichester, pp. 209-19, 235.

Srivastava, S.K. and B.R. Vishwakarma 2003 : 'Cross-polarization and Attenuation of Microwave/Millimetre wave Propagation in Storm Layer containing Sand, Silt and Clay as Dust Constituents,' *The Inst.of Engineers (India),*ET, Vol. 84.

Suhaila, J. and A. A. Jemain 2007 : 'Fitting daily rainfall amount in Malaysia using the normal transformer distribution,' *J. of Appl. Sci.*, 7(14).

Taylor, A.E. and W.R. Mann (1983): Advanced Calculus, John Wiley and Sons Inc., pp. 699–703.

Thom, H. C. (1958): 'A note on the gamma distribution,' *Monthly Weather Review*, vol. 86, pp. 117–122.

Timothy, K.I., J.T. Ong and E.B.L. Choo 2002 : 'Raindrop size distribution using method of moments for terrestrial and satellite communication applications in Singapore,' *IEEE Antennas Propag.*, Vol. 50, pp. 1420–1424, Oct.

Tseng, C.H., K.S. Chen and C.H. Chu (2005): 'Prediction of KA-band terrestrial rain attenuation using 2-year raindrop size distribution measurements in Northern Taiwan,' *J. of Electromagn. Waves and Appl.*, vol. 19, No. 13, pp. 1833-1841.

Ulbrich, C.W. (1983): 'Natural variation in the analytical form of the raindrop size distribution,' *J. of Climate and Applied Meteor.*, vol. 23, pp. 1764–1775.

Van der Hulst, H.C. (1957): Light scattering by small particles, John Wiley and Sons Inc., New York.

Waldvogel, A. (1974): 'The N_o jump of raindrop spectra,' *J. Atmos Sci.*, pp. 1067-1078

Watson, A., Sasthiaseelan and B. Potter (1981): 'Development of a climatic map of rainfall attenuation for Europe,' Post Graduate School of Electrical and Electronic Engineering, Uni. of Bradford, UK, Rep. No. 300, pp. 134-136.

Weber, H.J. and G.B. Arfken (2003): Essential Mathematical Methods for Physicists, Academic Press, San Diego, pp. 523–544.

Weibull, W. (1951): 'A statistical distribution function of wide applicability,' *J. of App. Mechanics*, pp. 293–297, Sept.

Wong, R.K.W. (1997): 'Weibull distribution, iterative likelihood techniques, and hydrometeorological data' *J. Appl. Metor.*, vol. 16, pp. 1360-1364.

Yeo, T.S., P.S. Kooi and M.S. Leong (1993): 'A two-year measurement of rainfall attenuation of CW microwaves in Singapore,' *IEEE Ant. Propagat.*, 41(6), pp. 709-712, June.

Zhang, G., Q. Cao, M. Xue, P. Chilson, M. Morris and R. Palmer 2008 : 'A field experiment to study rain microphysics using video disdrometers, profiler, and polarimetric S- and X-band radars', *Symp. on Recent Developments in Atmos. Application of Radar and Lidar*, New Orleans, Jan.

Internet References

http://old.weathersa.co.za/Climat/Climstats/DurbanStats.jsp accessed August, 2011.

http://www.distromet.com accessed November, 2011

http://www. proseo.co.za accessed November, 2011.

http://www.itl.nist.gov/div898/handbook/eda/section3/eda3674.htm accessed November, 2011.

Appendices

Appendix A:

Appendix A-1: Frequency Band description [Hall, 1996]

The International Telecommunication Union (ITU) specifies frequency bands for terrestrial, satellite and personal area networks some of which are under broader spectrum designation. The available frequency bands and their respective designations are hereby presented below:

UNIT	FREQUENCY RANGE	WAVELENGTH	AVAILABLE DESIGNATION	
KHz	< 3	Above 100 km		ELF
	3 - 30	10 – 100 km	Myriametric waves	VLF
	30 - 300	1-10 km	Kilometric waves	LF
	300 - 3000	100 – 1000 m	Hectometric waves	MF
MHz	3 - 30	10 – 100 m	Decametric waves	HF
	30 - 300	1 – 10 m	Metric waves	VHF
	300 - 3000	10 -100 cm	Decimetric waves	UHF
GHz	3 - 30	1 – 10 cm	Centimetric waves	SHF
	30 - 300	1 -10 mm	Millimetric waves	EHF
	300 - 3000	0.1 – 1 mm	Sub-Millimetric waves	
THz	3 - 30	10 -100 μm	Far-Infrared waves	
	30 - 430	0.7 – 10 μm	Near Infrared waves	
	430 - 860	0.35 – 0.7 μm	Optical	

Appendix A-2: ITU-R Parameters for the Estimation of Specific Attenuation [ITU-R P.838-3, 2005]

According to ITU-R recommendation P. 838-3, the specific attenuation at different frequencies can be prediction by getting the values of k and α, as well as the R0.01 of a locality. The specific attenuation is thus given as:

$$A_s = kR_{0.01}{}^{\alpha} \qquad (A.1)$$

The recommended values of k and α for horizontal and vertical polarization modes are presented below:

Frequency (GHz)	k_H	α_H	k_V	α_V
1	0.0000259	0.9691	0.0000308	0.8592
1.5	0.0000443	1.0185	0.0000574	0.8957
2	0.0000847	1.0664	0.0000998	0.9490
2.5	0.0001321	1.1209	0.0001464	1.0085
3	0.0001390	1.2322	0.0001942	1.0688
3.5	0.0001155	1.4189	0.0002346	1.1387
4	0.0001071	1.6009	0.0002461	1.2476
4.5	0.0001340	1.6948	0.0002347	1.3987
5	0.0002162	1.6969	0.0002428	1.5317
5.5	0.0003909	1.6499	0.0003115	1.5882
6	0.0007056	1.5900	0.0004878	1.5728
7	0.001915	1.4810	0.001425	1.4745
8	0.004115	1.3905	0.003450	1.3797
9	0.007535	1.3155	0.006691	1.2895
10	0.01217	1.2571	0.01129	1.2156
11	0.01772	1.2140	0.01731	1.1617
12	0.02386	1.1825	0.02455	1.1216
13	0.03041	1.1586	0.03266	1.0901
14	0.03738	1.1396	0.04126	1.0646
15	0.04481	1.1233	0.05008	1.0440
16	0.05282	1.1086	0.05899	1.0273
17	0.06146	1.0949	0.06797	1.0137

Frequency (GHz)	k_H	α_H	k_V	α_V
18	0.07078	1.0818	0.07708	1.0025
19	0.08084	1.0691	0.08642	0.9930
20	0.09164	1.0568	0.09611	0.9847
21	0.1032	1.0447	0.1063	0.9771
22	0.1155	1.0329	0.1170	0.9700
23	0.1286	1.0214	0.1284	0.9630
24	0.1425	1.0101	0.1404	0.9561
25	0.1571	0.9991	0.1533	0.9491
26	0.1724	0.9884	0.1669	0.9421
27	0.1884	0.9780	0.1813	0.9349
28	0.2051	0.9679	0.1964	0.9277
29	0.2224	0.9580	0.2124	0.9203
30	0.2403	0.9485	0.2291	0.9129
31	0.2588	0.9392	0.2465	0.9055
32	0.2778	0.9302	0.2646	0.8981
33	0.2972	0.9214	0.2833	0.8907
34	0.3171	0.9129	0.3026	0.8834
35	0.3374	0.9047	0.3224	0.8761
36	0.3580	0.8967	0.3427	0.8690
37	0.3789	0.8890	0.3633	0.8621
38	0.4001	0.8816	0.3844	0.8552
39	0.4215	0.8743	0.4058	0.8486
40	0.4431	0.8673	0.4274	0.8421
41	0.4647	0.8605	0.4492	0.8357
42	0.4865	0.8539	0.4712	0.8296
43	0.5084	0.8476	0.4932	0.8236
44	0.5302	0.8414	0.5153	0.8179
45	0.5521	0.8355	0.5375	0.8123
46	0.5738	0.8297	0.5596	0.8069
47	0.5956	0.8241	0.5817	0.8017
48	0.6172	0.8187	0.6037	0.7967
49	0.6386	0.8134	0.6255	0.7918
50	0.6600	0.8084	0.6472	0.7871
51	0.6811	0.8034	0.6687	0.7826
52	0.7020	0.7987	0.6901	0.7783

Frequency (GHz)	k_H	α_H	k_V	α_V
53	0.7228	0.7941	0.7112	0.7741
54	0.7433	0.7896	0.7321	0.7700
55	0.7635	0.7853	0.7527	0.7661
56	0.7835	0.7811	0.7730	0.7623
57	0.8032	0.7771	0.7931	0.7587
58	0.8226	0.7731	0.8129	0.7552
59	0.8418	0.7693	0.8324	0.7518
60	0.8606	0.7656	0.8515	0.7486
61	0.8791	0.7621	0.8704	0.7454
62	0.8974	0.7586	0.8889	0.7424
63	0.9153	0.7552	0.9071	0.7395
64	0.9328	0.7520	0.9250	0.7366
65	0.9501	0.7488	0.9425	0.7339
66	0.9670	0.7458	0.9598	0.7313
67	0.9836	0.7428	0.9767	0.7287
68	0.9999	0.7400	0.9932	0.7262
69	1.0159	0.7372	1.0094	0.7238
70	1.0315	0.7345	1.0253	0.7215
71	1.0468	0.7318	1.0409	0.7193
72	1.0618	0.7293	1.0561	0.7171
73	1.0764	0.7268	1.0711	0.7150
74	1.0908	0.7244	1.0857	0.7130
75	1.1048	0.7221	1.1000	0.7110
76	1.1185	0.7199	1.1139	0.7091
77	1.1320	0.7177	1.1276	0.7073
78	1.1451	0.7156	1.1410	0.7055
79	1.1579	0.7135	1.1541	0.7038
80	1.1704	0.7115	1.1668	0.7021
81	1.1827	0.7096	1.1793	0.7004
82	1.1946	0.7077	1.1915	0.6988
83	1.2063	0.7058	1.2034	0.6973
84	1.2177	0.7040	1.2151	0.6958
85	1.2289	0.7023	1.2265	0.6943
86	1.2398	0.7006	1.2376	0.6929
87	1.2504	0.6990	1.2484	0.6915

Frequency (GHz)	k_H	α_H	k_V	α_V
88	1.2607	0.6974	1.2590	0.6902
89	1.2708	0.6959	1.2694	0.6889
90	1.2807	0.6944	1.2795	0.6876
91	1.2903	0.6929	1.2893	0.6864
92	1.2997	0.6915	1.2989	0.6852
93	1.3089	0.6901	1.3083	0.6840
94	1.3179	0.6888	1.3175	0.6828
95	1.3266	0.6875	1.3265	0.6817
96	1.3351	0.6862	1.3352	0.6806
97	1.3434	0.6850	1.3437	0.6796
98	1.3515	0.6838	1.3520	0.6785
99	1.3594	0.6826	1.3601	0.6775
100	1.3671	0.6815	1.3680	0.6765
120	1.4866	0.6640	1.4911	0.6609
150	1.5823	0.6494	1.5896	0.6466
200	1.6378	0.6382	1.6443	0.6343
300	1.6286	0.6296	1.6286	0.6262
400	1.5860	0.6262	1.5820	0.6256
500	1.5418	0.6253	1.5366	0.6272
600	1.5013	0.6262	1.4967	0.6293
700	1.4654	0.6284	1.4622	0.6315
800	1.4335	0.6315	1.4321	0.6334
900	1.4050	0.6353	1.4056	0.6351
1 000	1.3795	0.6396	1.3822	0.6365

Appendix B

Appendix B-1 discusses the rain attenuation models for both ITU-R for terrestrial communication. The models are used for the estimation of rainfall attenuation given the knowledge of $R_{0.01}$ of a location.

Appendix B-1: ITU-R Rainfall Attenuation Model [ITU-R P.530-13, 2009]

The following technique is used to estimate the specific attenuation at $R_{0.01}$ exceeded for 0.01% (with an integration time of 1-min) of the time:

- Compute the specific attenuation, γ_R (dB/km) for the frequency, polarization and rain rate of interest using the recommendation ITU-R P.838.

- Compute the effective path length , d_{eff}, of the link by multiplying the actual path length by a distance factor *r*. An estimate of this factor is given by:

$$r = \frac{1}{1 + d/d_o} \qquad (A.1)$$

where, for $R_{0.01} \leq 100$ mm/h:

$$d_o = 35e^{-0.015R_{0.01}} \qquad (A.2)$$

For R > 100 mm/h, the value of $R_{0.01}$ is used

- An estimate of the path attenuation exceeded for 0.01% of the time is given by:

$$A_{0.01} = \gamma_R d_{eff} = \gamma_R dr \quad \text{[dB]} \qquad (A.3)$$

Appendix C

Appendix C-1: ITU-R Worldwide Map for Rainfall Rate Exceeded at 0.01% [*ITU-R P.837-5*, 2005]

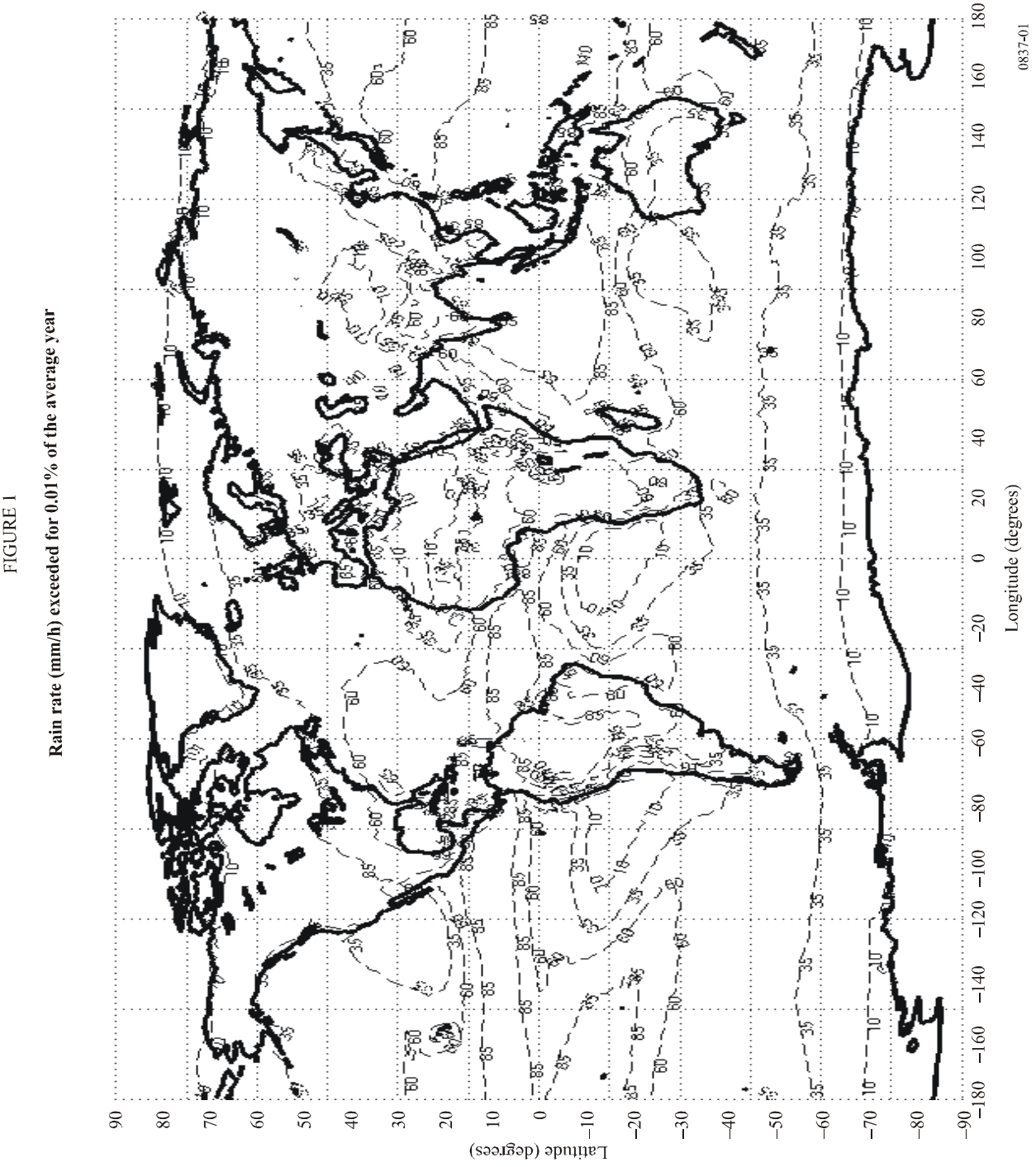

Appendix C-2: Crane Contour Map for the Variation of $R_{0.01}$ in Africa and Europe [*Crane*, 1996]

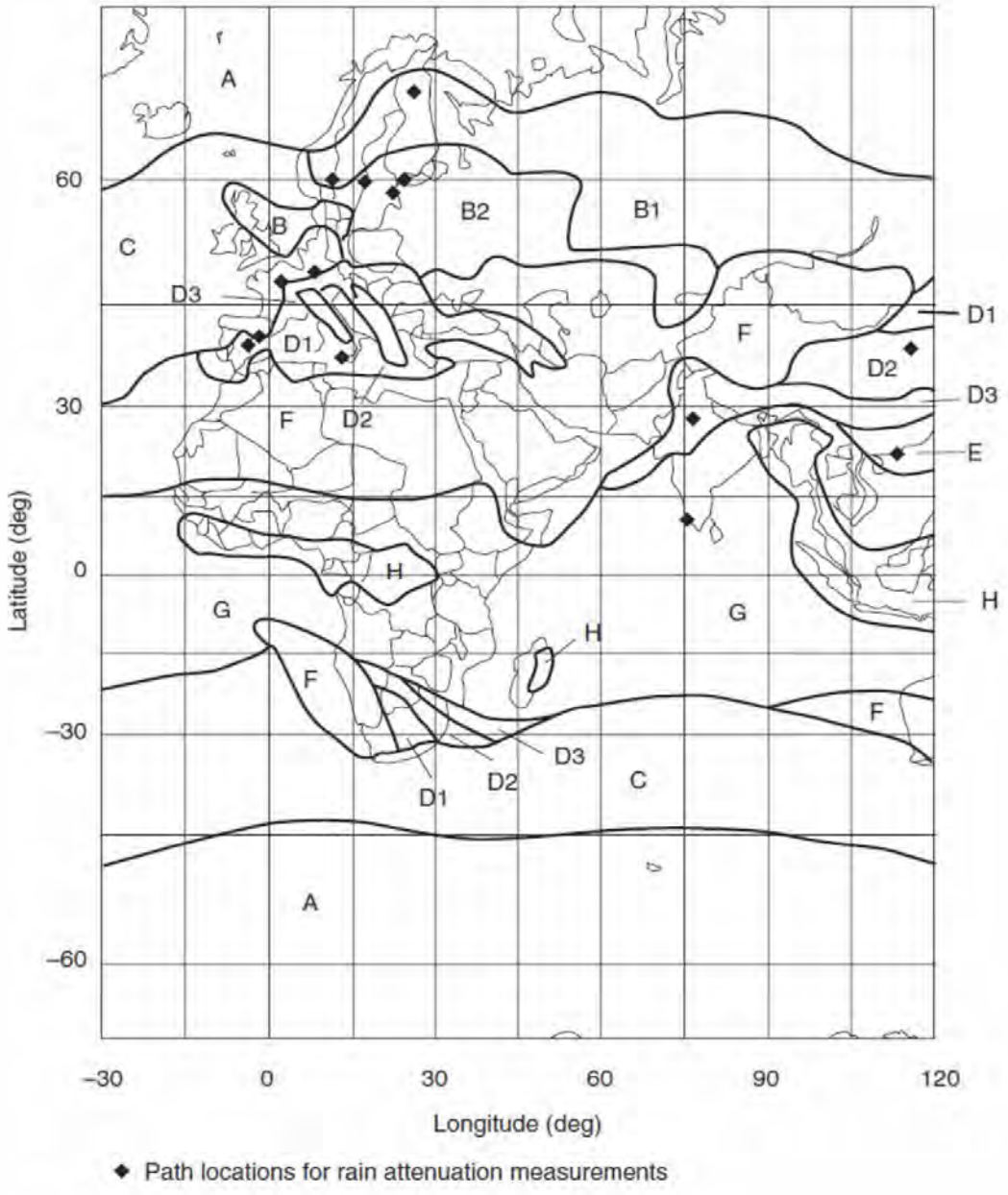

Appendix D

Appendix D-1: RD-80 Disdrometer Bin Catalogue

The Joss-Waldvogel RD-80 impact disdrometer is completely described by 20 independent diameter bins with different diameter classes, drop fall velocity and diameter interval. The Table below shows the corresponding values related to each bin and classes according to [*Bartholomew*, 2005; www.disdromet.com].

Dropsize class in DISDRODATA program	Lower threshold of drop diameter (mm)	Average diameter of drops in class *i* D_i (mm)	Fall velocity of a drop with diameter $v(D_i)$ (m/s)	Diameter interval of drop size class i ΔD_i (mm)
1	0.313	0.359	1.435	0.092
2	0.405	0.455	1.862	0.1
3	0.505	0.551	2.267	0.091
4	0.596	0.656	2.692	0.119
5	0.715	0.771	3.154	0.112
6	0.827	0.913	3.717	0.172
7	0.999	1.116	4.382	0.233
8	1.232	1.331	4.986	0.197
9	1.429	1.506	5.423	0.153
10	1.582	1.665	5.793	0.166
11	1.748	1.912	6.315	0.329
12	2.077	2.259	7.009	0.364
13	2.442	2.584	7.546	0.286
14	2.727	2.869	7.903	0.284
15	3.011	3.198	8.258	0.374
16	3.385	3.544	8.556	0.319
17	3.704	3.916	8.784	0.423
18	4.127	4.35	8.965	0.446
19	4.573	4.859	9.076	0.572
20	5.145	5.373	9.137	0.455

Appendix E

Mie Scattering Parameters at Selected Frequencies

Based on the Mie computations applied in this research [*Mie*, 1908], results for some simulation undertaken at selected frequencies are presented at 10 GHz, 25 GHz, 70 GHz, 100 GHz and 400 GHz. The ambient temperature for Durban at 20^{O}C was assumed for the spherical rain droplets. The computations are achieved using Liebe's complex refractive index [*Liebe et al.*, 1991] and Mätzler's functional MATLAB codes [*Mätzler*, 2002a; 2002b].

Table E-1: Computation at 10 GHz with m = 8.0649 + 2.0188*i*

RADIUS (mm)	SIZE	SCATTERING AMPLITUDE		Q_{ext} (mm^2)
		REAL	IMAGINARY	
0.1795	0.037594	1.11972E-06	-5.13371E-05	0.000321
0.2275	0.047647	2.3907E-06	-0.000104759	0.000685
0.2755	0.057701	4.49674E-06	-0.000186583	0.001288
0.328	0.068696	8.16455E-06	-0.000316081	0.002339
0.3855	0.080739	1.45196E-05	-0.000515734	0.00416
0.4565	0.095609	2.73512E-05	-0.000862718	0.007836
0.558	0.116867	6.11056E-05	-0.001595932	0.017505
0.6655	0.139382	0.000131065	-0.002752791	0.037547
0.753	0.157708	0.000232685	-0.004051534	0.066659
0.8325	0.174358	0.000381362	-0.005565035	0.109252
0.956	0.200224	0.000790146	-0.008672441	0.22636
1.1295	0.236562	0.002077579	-0.014965855	0.595183
1.292	0.270596	0.004915829	-0.023311933	1.408281
1.4345	0.300441	0.010009151	-0.032384097	2.867411
1.599	0.334894	0.020313749	-0.0426023	5.81946
1.772	0.371127	0.033231596	-0.048776691	9.520151
1.958	0.410083	0.041752076	-0.053771274	11.96109
2.175	0.455531	0.048476316	-0.068358117	13.88744
2.4295	0.508833	0.063814741	-0.09575442	18.28158
2.6865	0.562659	0.087980428	-0.127796804	25.20454

Table E-2: Computation at 25 GHz with m = 6.1026 + 2.8532*i*

RADIUS (mm)	SIZE	SCATTERING AMPLITUDE		Q_{ext} (mm^2)
		REAL	IMAGINARY	
0.1795	0.093986	4.96414E-05	-0.000805965	0.002275
0.2275	0.119119	0.000114479	-0.001654508	0.005247
0.2755	0.144251	0.000234912	-0.002967615	0.010768
0.328	0.17174	0.000472465	-0.005070726	0.021656
0.3855	0.201847	0.000943274	-0.008355899	0.043237
0.4565	0.239023	0.00204584	-0.014136088	0.093774
0.558	0.292168	0.005472611	-0.026354018	0.250846
0.753	0.39427	0.024228639	-0.062825769	1.110559
0.8325	0.435896	0.037496516	-0.081049001	1.718714
0.8325	0.435896	0.037496516	-0.081049001	1.718714
0.956	0.50056	0.063340445	-0.113571681	2.903312
1.1295	0.591405	0.116302441	-0.173012494	5.330911
1.292	0.67649	0.195629735	-0.23764299	8.967007
1.4345	0.751102	0.29178798	-0.290971965	13.37458
1.599	0.837234	0.430361028	-0.337136977	19.7263
1.772	0.927817	0.595531344	-0.356761554	27.29715
1.958	1.025206	0.772162591	-0.345228937	35.39333
2.175	1.138827	0.95685352	-0.313626673	43.85893
2.4295	1.272083	1.15225306	-0.291083	52.81539
2.6865	1.406648	1.358002598	-0.302833674	62.24625

Table E-3: Computation at 70 GHz with m = 3.8182 + 2.2560*i*

RADIUS (mm)	SIZE	SCATTERING AMPLITUDE		Q_{ext} (mm^2)
		REAL	IMAGINARY	
0.1795	0.263161	0.003416442	-0.017693405	0.019974
0.2275	0.333532	0.008828902	-0.036898139	0.051618
0.2755	0.403904	0.020276261	-0.066778132	0.118545
0.328	0.480873	0.045129721	-0.113233646	0.263851
0.3855	0.565173	0.095834095	-0.178896876	0.560295
0.4565	0.669264	0.205524895	-0.269481184	1.201603
0.558	0.818071	0.459561901	-0.361295013	2.686832
0.6655	0.975674	0.765551859	-0.348040077	4.475805
0.753	1.103956	0.975585118	-0.303339509	5.703766
0.8325	1.220509	1.148547478	-0.281023093	6.714992
0.956	1.401569	1.441869534	-0.299715725	8.429902
1.1295	1.655933	1.999863502	-0.363736612	11.69222
1.292	1.894171	2.633387142	-0.342996563	15.39612
1.4345	2.103087	3.187242591	-0.292442167	18.63424
1.599	2.344256	3.864160063	-0.28289586	22.59184
1.772	2.597888	4.701820511	-0.286003025	27.48923
1.958	2.870578	5.69105614	-0.225556212	33.27281
2.175	3.188717	6.892737442	-0.159666204	40.29845
2.4295	3.561833	8.492005015	-0.109646585	49.64858
2.6865	3.938615	10.25427534	0.003792504	59.9517

Table E-4: Computation at 100 GHz with m = 3.3061 + 1.8778*i*

RADIUS (mm)	SIZE	SCATTERING AMPLITUDE		Q_{ext} (mm^2)
		REAL	IMAGINARY	
0.1795	0.375944	0.01502127	-0.051128529	0.043033
0.2275	0.476475	0.041790007	-0.106325795	0.11972
0.2755	0.577006	0.100933899	-0.186253351	0.289154
0.328	0.686962	0.224951807	-0.286852864	0.644439
0.3855	0.807389	0.439413732	-0.367476573	1.258828
0.4565	0.956091	0.748165945	-0.363703478	2.143338
0.558	1.168672	1.099901485	-0.276783711	3.150986
0.6655	1.39382	1.456400639	-0.282527713	4.17228
0.753	1.57708	1.847466582	-0.327244327	5.292602
0.8325	1.743584	2.275194537	-0.332586103	6.517952
0.956	2.002242	2.96785922	-0.268757079	8.50229
1.1295	2.365619	3.997064492	-0.228041088	11.45075
1.292	2.705958	5.172070558	-0.185402703	14.81689
1.4345	3.00441	6.275759531	-0.092783508	17.97873
1.599	3.348938	7.663463005	-0.02694762	21.9542
1.772	3.711268	9.307028131	0.081098655	26.66267
1.958	4.100826	11.19378798	0.21430088	32.06784
2.175	4.555309	13.64305292	0.369642915	39.08447
2.4295	5.088333	16.77627788	0.591457949	48.0605
2.6865	5.626592	20.2796083	0.836283694	58.0968

Table E-5: Computation at 400 GHz with m = 2.3882 + 0.8493*i*

RADIUS (mm)	SIZE	SCATTERING AMPLITUDE		Q_{ext}(mm^2)
		REAL	IMAGINARY	
0.1795	1.503776	1.775956664	-0.346586051	0.317984
0.2275	1.9059	2.834277199	-0.214346205	0.507475
0.2755	2.308023	3.890676524	-0.075164433	0.696623
0.328	2.747846	5.383867213	0.050085104	0.963978
0.3855	3.229557	7.240205849	0.227607621	1.296354
0.4565	3.824365	9.922797364	0.526631902	1.77667
0.558	4.67469	14.40481327	1.019527718	2.579172
0.6655	5.57528	20.01331475	1.62737068	3.58337
0.753	6.308318	25.22700115	2.183945875	4.516877
0.8325	6.974336	30.4634517	2.736136311	5.45446
0.956	8.008967	39.5435788	3.672645092	7.080251
1.1295	9.462477	54.22342007	5.139060331	9.708666
1.292	10.82383	70.0008833	6.656950325	12.53361
1.4345	12.01764	85.44320982	8.096378774	15.29855

1.599	13.3958	105.1291	9.8747	18.8233
1.772	14.8451	127.9756	11.8721	22.914
1.958	16.4033	154.9823	14.1566	27.7495
2.175	18.2212	189.6812	16.9906	33.9623
2.4295	20.3533	234.743	20.5319	42.0306
2.6865	22.5064	285.0187	24.3318	51.0324

Appendix F

Appendix E-1: Chi-Square Statistics Table [NIST/SEMATECH, 2010]

	Probability of exceeding the critical value				
ν	0.10	0.05	0.025	0.01	0.001
1	2.706	3.841	5.024	6.635	10.828
2	4.605	5.991	7.378	9.210	13.816
3	6.251	7.815	9.348	11.345	16.266
4	7.779	9.488	11.143	13.277	18.467
5	9.236	11.070	12.833	15.086	20.515
6	10.645	12.592	14.449	16.812	22.458
7	12.017	14.067	16.013	18.475	24.322
8	13.362	15.507	17.535	20.090	26.125
9	14.684	16.919	19.023	21.666	27.877
10	15.987	18.307	20.483	23.209	29.588
11	17.275	19.675	21.920	24.725	31.264
12	18.549	21.026	23.337	26.217	32.910
13	19.812	22.362	24.736	27.688	34.528
14	21.064	23.685	26.119	29.141	36.123
15	22.307	24.996	27.488	30.578	37.697
16	23.542	26.296	28.845	32.000	39.252
17	24.769	27.587	30.191	33.409	40.790
18	25.989	28.869	31.526	34.805	42.312
19	27.204	30.144	32.852	36.191	43.820
20	28.412	31.410	34.170	37.566	45.315
21	29.615	32.671	35.479	38.932	46.797
22	30.813	33.924	36.781	40.289	48.268
23	32.007	35.172	38.076	41.638	49.728
24	33.196	36.415	39.364	42.980	51.179
25	34.382	37.652	40.646	44.314	52.620
26	35.563	38.885	41.923	45.642	54.052
27	36.741	40.113	43.195	46.963	55.476
28	37.916	41.337	44.461	48.278	56.892
29	39.087	42.557	45.722	49.588	58.301
30	40.256	43.773	46.979	50.892	59.703
31	41.422	44.985	48.232	52.191	61.098

32	42.585	46.194	49.480	53.486	62.487
33	43.745	47.400	50.725	54.776	63.870
34	44.903	48.602	51.966	56.061	65.247
35	46.059	49.802	53.203	57.342	66.619
36	47.212	50.998	54.437	58.619	67.985
37	48.363	52.192	55.668	59.893	69.347
38	49.513	53.384	56.896	61.162	70.703
39	50.660	54.572	58.120	62.428	72.055
40	51.805	55.758	59.342	63.691	73.402
41	52.949	56.942	60.561	64.950	74.745
42	54.090	58.124	61.777	66.206	76.084
43	55.230	59.304	62.990	67.459	77.419
44	56.369	60.481	64.201	68.710	78.750
45	57.505	61.656	65.410	69.957	80.077
46	58.641	62.830	66.617	71.201	81.400
47	59.774	64.001	67.821	72.443	82.720
48	60.907	65.171	69.023	73.683	84.037
49	62.038	66.339	70.222	74.919	85.351
50	63.167	67.505	71.420	76.154	86.661
51	64.295	68.669	72.616	77.386	87.968
52	65.422	69.832	73.810	78.616	89.272
53	66.548	70.993	75.002	79.843	90.573
54	67.673	72.153	76.192	81.069	91.872
55	68.796	73.311	77.380	82.292	93.168
56	69.919	74.468	78.567	83.513	94.461
57	71.040	75.624	79.752	84.733	95.751
58	72.160	76.778	80.936	85.950	97.039
59	73.279	77.931	82.117	87.166	98.324
60	74.397	79.082	83.298	88.379	99.607
61	75.514	80.232	84.476	89.591	100.888
62	76.630	81.381	85.654	90.802	102.166
63	77.745	82.529	86.830	92.010	103.442
64	78.860	83.675	88.004	93.217	104.716
65	79.973	84.821	89.177	94.422	105.988
66	81.085	85.965	90.349	95.626	107.258
67	82.197	87.108	91.519	96.828	108.526
68	83.308	88.250	92.689	98.028	109.791
69	84.418	89.391	93.856	99.228	111.055
70	85.527	90.531	95.023	100.425	112.317
71	86.635	91.670	96.189	101.621	113.577
72	87.743	92.808	97.353	102.816	114.835
73	88.850	93.945	98.516	104.010	116.092
74	89.956	95.081	99.678	105.202	117.346
75	91.061	96.217	100.839	106.393	118.599
76	92.166	97.351	101.999	107.583	119.850
77	93.270	98.484	103.158	108.771	121.100
78	94.374	99.617	104.316	109.958	122.348
79	95.476	100.749	105.473	111.144	123.594
80	96.578	101.879	106.629	112.329	124.839
81	97.680	103.010	107.783	113.512	126.083
82	98.780	104.139	108.937	114.695	127.324
83	99.880	105.267	110.090	115.876	128.565
84	100.980	106.395	111.242	117.057	129.804
85	102.079	107.522	112.393	118.236	131.041

86	103.177	108.648	113.544	119.414	132.277
87	104.275	109.773	114.693	120.591	133.512
88	105.372	110.898	115.841	121.767	134.746
89	106.469	112.022	116.989	122.942	135.978
90	107.565	113.145	118.136	124.116	137.208
91	108.661	114.268	119.282	125.289	138.438
92	109.756	115.390	120.427	126.462	139.666
93	110.850	116.511	121.571	127.633	140.893
94	111.944	117.632	122.715	128.803	142.119
95	113.038	118.752	123.858	129.973	143.344
96	114.131	119.871	125.000	131.141	144.567
97	115.223	120.990	126.141	132.309	145.789
98	116.315	122.108	127.282	133.476	147.010
99	117.407	123.225	128.422	134.642	148.230
100	118.498	124.342	129.561	135.807	149.449
100	118.498	124.342	129.561	135.807	149.449

Appendix G

Equivalent Rainfall DSD Parameters at Different Locations in South Africa

The relationships relating the empirical rainfall DSD and rainfall rate proposed in Chapter 6 are being extended to seven other locations. The functions for each disdrometer bin for different location are given from (6.35) as:

$$N(D_k, R(t)) = \begin{cases} \xi_1[R(t)]^{\xi_2} & \text{for } 0.359\,mm \le D_k \le 1.506\,mm \\ \xi_1[R(t)]^b + \xi_2 & \text{for } 1.665\,mm \le D_k \le 3.544\,mm \\ \xi_1[R(t)]^{\xi_2} & \text{for } 3.916\,mm \le D_k \le 5.373\,mm \end{cases}$$

These values correspond to the functions given in Tables G-1 to G-6 of this appendix. They are obtained by regression fitting techniques.

Table G-1: Parameters showing the fitted values for each disdrometer bin for the function in Pietermaritzburg and Cape Town.

Diameter (mm)	PIETERMARITZBURG $\xi(t) = \xi_1 R(t)^{\xi_2}$			CAPE TOWN $\xi(t) = \xi_1 R(t)^{\xi_2}$		
	ξ_1	ξ_2	b	ξ_1	ξ_2	b
0.359	831.9023	0.1428		812.2984	0.2492	
0.455	223.0294	0.4406		207.2064	0.7689	
0.551	103.4007	0.7038		91.9346	1.2281	
0.656	38.9770	0.8409		33.8703	1.4674	
0.771	20.2994	0.8827		17.5171	1.5404	
0.913	4.7955	0.9465		8.3632	1.6518	
1.116	4.5863	1.0118		3.8733	1.7657	
1.331	2.3909	1.0123		2.0190	1.7666	
1.506	1.9583	0.9237		1.6783	1.6119	
1.665	0.4724	4.4458	1.2899	0.3808	4.4458	2.2510
1.912	0.3018	-0.1790	1.2899	0.2433	-0.1790	2.2510
2.259	0.1497	-1.2751	1.2899	0.1206	-1.2751	2.2510
2.584	0.0763	-0.5428	1.2899	0.0615	-0.5428	2.2510
2.869	0.0489	-0.6245	1.2899	0.0394	-0.6245	2.2510
3.198	0.0221	0.3508	1.2899	0.0178	0.3508	2.2510
3.544	0.0103	0.9418	1.2899	0.0083	0.9418	2.2510
3.916	0.3336	0.3908		0.3116	0.6821	
4.35	0.3866	0.3133		0.3669	0.5468	
4.859	0.2648	0.3458		0.25	0.6035	
5.373	0.0769	0.8197		0.0662	1.4305	

Table G-2: Parameters showing the fitted values for each disdrometer bin for the function at East London and Richards Bay

Diameter (mm)	EAST LONDON $\xi(t) = \xi_1 R(t)^{\xi_2}$			RICHARDS BAY $\xi(t) = \xi_1 R(t)^{\xi_2}$		
	ξ_1	ξ_2	b	ξ_1	ξ_2	b
0.359	761.4502	0.1981		630.1961	0.2094	
0.455	169.7351	0.6112		94.6723	0.6463	
0.551	66.8516	0.9762		26.3116	1.0323	
0.656	23.1469	1.1664		7.5968	1.2334	
0.771	11.7468	1.2243		3.6476	1.2947	
0.913	5.4485	1.3129		1.5546	1.3883	
1.116	2.4499	1.4034		0.6411	1.4841	
1.331	1.2767	1.4042		0.3339	1.4848	
1.506	1.1048	1.2812		0.3249	1.3549	
1.665	0.2124	4.4458	1.7892	0.0384	4.4458	1.8920
1.912	0.1357	-0.1790	1.7892	0.0246	-0.1790	1.8920
2.259	0.0673	-1.2751	1.7892	0.0122	-1.2751	1.8920
2.584	0.0343	-0.5428	1.7892	0.0062	-0.5428	1.8920
2.869	0.0220	-0.6245	1.7892	0.0040	-0.6245	1.8920
3.198	0.01	0.3508	1.7892	0.0018	0.3508	1.8920
3.544	0.0046	0.9418	1.7892	0.0008	0.9418	1.8920
3.916	0.2611	0.5421		0.1555	0.5733	
4.35	0.3184	0.4346		0.2102	0.4596	
4.859	0.2138	0.4797		0.1352	0.5072	
5.373	0.0459	1.1370		0.0159	1.2024	

Table G-3: Parameters showing the fitted values for each disdrometer bin for the function at Pretoria and Brandvlei

Diameter (mm)	PRETORIA $\xi(t) = \xi_1 R(t)^{\xi_2}$			BRANDVLEI $\xi(t) = \xi_1 R(t)^{\xi_2}$		
	ξ_1	ξ_2	b	ξ_1	ξ_2	b
0.359	754.2818	0.1960		1105.1	0.1011	
0.455	164.8524	0.6408		535.7	0.3119	
0.551	63.8066	0.9660		419.1	0.4982	
0.656	21.8929	1.1542		207.5	0.5952	
0.771	11.0797	1.2116		117.4	0.6248	
0.913	5.1174	1.2992		64.3	0.6700	
1.116	2.911	1.3888		34.3	0.7162	
1.331	1.1939	1.3895		17.9	0.7166	
1.506	1.0392	1.2679		12.3	0.6539	
1.665	0.1950	4.4458	1.7705	6.1	4.4458	0.9131
1.912	0.1246	-0.1790	1.7705	3.9	-0.1790	0.9131
2.259	0.0618	-1.2751	1.7705	1.9	-1.2751	0.9131
2.584	0.0315	-0.5428	1.7705	1	-0.5428	0.9131
2.869	0.0202	-0.6245	1.7705	0.6	-0.6245	0.9131
3.198	0.0091	0.3508	1.7705	0.3	0.3508	0.9131
3.544	0.0042	0.9418	1.7705	0.1	0.9418	0.9131
3.916	0.2544	0.5365		0.7	0.2767	
4.35	0.3118	0.4301		0.7	0.2218	
4.859	0.2089	0.4747		0.5	0.2448	
5.373	0.0432	1.1252		0.4	0.5803	

Table G-4: Parameters showing the fitted values for each disdrometer bin for the function at Vryheid

Diameter (mm)	$\xi(t) = \xi_1 R(t)^{\xi_2}$		
	ξ_1	ξ_2	*b*
0.359	974.3783	0.1318	
0.455	363.2619	0.4068	
0.551	225.3723	0.6498	
0.656	98.8807	0.7763	
0.771	53.9364	0.8149	
0.913	27.9333	0.8739	
1.116	14.0586	0.9341	
1.331	7.3330	0.9346	
1.506	5.4450	0.8528	
1.665	1.97	4.4458	1.909
1.912	1.2585	-0.1790	1.909
2.259	0.6241	-1.2751	1.909
2.584	0.3182	-0.5428	1.909
2.869	0.2038	-0.6245	1.909
3.198	0.0923	0.3508	1.909
3.544	0.0429	0.9418	1.909
3.916	0.5127	0.3608	
4.35	0.5469	0.2893	
4.859	0.3884	0.3193	
5.373	0.1880	0.7598	

Appendix H

Predicted Specific Attenuation for Selected Locations in South Africa at 20 ^{O}C

Table H-1: Computed specific attenuation results for selected locations at 4 mm/h

Frequency (GHz)	DBN	CPT	PMB	ELN	RBY	PTA	VRY	BRV
2	0.000992	0.00041	0.000236	0.000224	0.000123	0.000218	0.000451	0.000697
4	0.008361	0.003665	0.002202	0.002102	0.001201	0.002036	0.004009	0.005997
6	0.051552	0.024054	0.014973	0.014331	0.008404	0.013821	0.026147	0.03789
10	0.253182	0.119407	0.074714	0.071533	0.042079	0.068945	0.129665	0.186936
12	0.365457	0.171189	0.106764	0.102199	0.060004	0.09854	0.186014	0.26905
15	0.560084	0.260102	0.161518	0.154574	0.090514	0.149114	0.282863	0.410847
19.5	0.876563	0.401974	0.247978	0.237218	0.138299	0.229013	0.437696	0.639701
20	0.909692	0.4165	0.256718	0.245565	0.143079	0.237095	0.453585	0.663452
30	1.393544	0.613962	0.370069	0.353432	0.202417	0.342142	0.671335	1.001456
40	1.692849	0.718021	0.421984	0.402194	0.225183	0.390583	0.788503	1.200392
50	1.925848	0.791496	0.454217	0.431996	0.236086	0.420883	0.872517	1.35186
60	2.126393	0.853777	0.480352	0.455962	0.243661	0.445538	0.944005	1.482616
70	2.305543	0.91127	0.505072	0.478648	0.251054	0.468852	1.009747	1.60122
90	2.638075	1.027682	0.560005	0.529557	0.271152	0.520451	1.14128	1.828072
100	2.796847	1.087666	0.590563	0.55811	0.284012	0.549059	1.208362	1.939133

Table H-2: Computed specific attenuation results for selected locations at 9 mm/h

Frequency (GHz)	DBN	CPT	PMB	ELN	RBY	PTA	VRY	BRV
2	0.001766	0.001291	0.000395	0.000465	0.000221	0.000448	0.000811	0.001141
4	0.014438	0.010722	0.003548	0.00412	0.002074	0.003938	0.00692	0.009528
6	0.085651	0.064931	0.023354	0.026806	0.014147	0.025484	0.043302	0.058178
10	0.417506	0.317803	0.115987	0.132886	0.07062	0.126238	0.213241	0.285249
12	0.605558	0.459739	0.166233	0.19068	0.10089	0.181225	0.307275	0.412181
15	0.933561	0.706487	0.252472	0.290044	0.15258	0.275834	0.469906	0.632543
19.5	1.473285	1.109945	0.389956	0.449005	0.234129	0.427425	0.733169	0.991925
20	1.530539	1.152443	0.404017	0.465332	0.242363	0.443024	0.760585	1.029672
30	2.399503	1.784709	0.594494	0.689685	0.348659	0.658921	1.154734	1.58686
40	2.97405	2.189127	0.694011	0.811237	0.396536	0.778373	1.391132	1.939049
50	3.433267	2.50852	0.763908	0.898822	0.425675	0.866165	1.572371	2.216599
60	3.826641	2.783048	0.823168	0.973438	0.449067	0.941756	1.728286	2.456158
70	4.171166	3.026054	0.878059	1.041977	0.471226	1.011374	1.868565	2.669614
90	4.78599	3.468621	0.989923	1.178601	0.521107	1.149248	2.13325	3.062218
100	5.069627	3.676437	1.047844	1.248056	0.54915	1.218758	2.261474	3.247964

Table H-3: Computed specific attenuation results for selected locations at 25 mm/h

Frequency (GHz)	DBN	CPT	PMB	ELN	RBY	PTA	VRY	BRV
2	0.00391	0.007923	0.000872	0.001523	0.000605	0.001432	0.001905	0.002261
4	0.031038	0.061821	0.007408	0.012542	0.00526	0.011683	0.015536	0.018279
6	0.175901	0.339258	0.046128	0.075122	0.03359	0.069539	0.091812	0.10683
10	0.849026	1.625058	0.226962	0.366893	0.166001	0.339367	0.447179	0.51922
12	1.239283	2.383776	0.327224	0.531487	0.238665	0.491842	0.648929	0.7545
15	1.925168	3.724657	0.500757	0.818126	0.36395	0.757592	1.001047	1.165862
19.5	3.069922	5.985253	0.782088	1.28839	0.565514	1.194339	1.581152	1.845855
20	3.193241	6.231364	0.811436	1.338111	0.586355	1.240611	1.642771	1.918354
30	5.142406	10.22198	1.235705	2.085834	0.879232	1.941822	2.581407	3.034545
40	6.50854	13.10486	1.49323	2.572874	1.046572	2.40777	3.205504	3.790226
50	7.615727	15.44384	1.692192	2.960139	1.171444	2.785111	3.705046	4.399922
60	8.551472	17.39211	1.863828	3.292446	1.278589	3.11306	4.132385	4.921727
70	9.350193	19.01977	2.018229	3.584925	1.376041	3.403986	4.505679	5.375987
90	10.71395	21.707	2.308519	4.111761	1.564837	3.929083	5.168887	6.176078
100	11.31974	22.86733	2.448592	4.356789	1.658437	4.172589	5.473708	6.540703

Table H-4: Computed specific attenuation results for selected locations at 75 mm/h

Frequency (GHz)	DBN	PMB	ELN	RBY	PTA	VRY	BRV
2	0.009838	0.002413	0.00725	0.002578	0.006577	0.005381	0.005038
4	0.076463	0.019478	0.056671	0.020747	0.050913	0.042379	0.039683
6	0.416104	0.113458	0.312137	0.120253	0.278593	0.236748	0.222191
10	1.988976	0.55097	1.496489	0.58333	1.334753	1.1389	1.069647
12	2.921585	0.801074	2.193901	0.84872	1.957608	1.666	1.563951
15	4.57221	1.238611	3.425645	1.313391	3.058582	2.594675	2.434454
19.5	7.362341	1.962649	5.499861	2.083528	4.915788	4.151633	3.892767
20	7.666928	2.039933	5.725411	2.16587	5.118142	4.320155	4.050491
30	12.6366	3.23301	9.372388	3.442563	8.41444	7.015012	6.569351
40	16.25021	4.043173	11.99881	4.314447	10.83254	8.930705	8.36049
50	19.17943	4.696663	14.12995	5.017881	12.83072	10.48428	9.817706
60	21.60803	5.255084	15.90826	5.617132	14.52418	11.78846	11.04606
70	23.62412	5.740369	17.39773	6.135543	15.96088	12.89058	12.08853
90	26.92075	6.593306	19.86657	7.04045	18.36665	14.74326	13.84946
100	28.3328	6.981488	20.93618	7.450001	19.41253	15.55557	14.62401